# Design and Application of Novel Biodegradable Chain Extenders and Surface-Tuneable Hyperbranched Chain Terminating Agents in Thermoplastic Polyurethane Elastomers

**Zoe J. Roberts**

**A Thesis Submitted for the Degree of Doctor of Philosophy**

**Department of Chemistry**

**October 2017**

# Table of Contents

# List of Figures

# List of Schemes

# List of Tables

# List of Abbreviations

$\delta$ - Chemical shift (nuclear magnetic resonance spectroscopy)

$\delta$ - Phase angle (dynamic mechanical analysis)

$\varepsilon$ - Strain

$\sigma$ - Stress

%HS - Percentage hard segment

2K-PCL - Poly(ε-caprolactone) with a molecular weight of 2,000 g $mol^{-1}$

BDI - 1,4-butane diisocyanate

BDO - 1,4-butanediol

BnOH – Benzyl alcohol

BPUE – Biodegradable polyurethane elastomer

CASE – Coating, adhesive, sealant and elastomer

$^{13}C$ NMR - Carbon-13 nuclear magnetic resonance spectroscopy

CBC – Carbonylbiscaprolactam

CBC-AHCTA - Hyperbranched chain terminating agent derived from CBC, with aromatic chain ends

CDI - 1,1'-Carbonyldiimidazole

CDI-AHCTA - Hyperbranched chain terminating agent derived from CDI with aromatic chain ends

CDI-FHCTA - Hyperbranched chain terminating agent derived from CDI with fluorinated chain ends

CDI-HCTA - Hyperbranched chain terminating agent derived from CDI

ε-CL - ε-Caprolactone

ε-CLM - ε-Caprolactam

DBU - 1,8-Diazabicyclo[5.4.0]undec-7-ene

DKP - Diketopiperazine

$Đ_M$ - Dispersity

DMAP - 4-dimethylaminopyridine

DMF - *N,N*-dimethylformamide

DMF-$d_7$ - Deuterated *N,N*-dimethylformamide

DMSO - Dimethyl sulfoxide

DMSO-$d_6$ - Deuterated dimethyl sulfoxide

DMA - Dynamic mechanical analysis

DSC - Differential scanning calorimetry

E - Young's modulus

E' - Storage modulus

E'' - Loss modulus

EDC - 1-ethyl-3-(3-dimethylaminopropyl)carbodiimide

EGDMA - Ethylene glycol dimethyl methacrylate

$^{19}$F DOSY NMR –Fluorine-19 diffusion ordered nuclear magnetic resonance spectroscopy

$^{19}$F NMR - Fluorine-19 nuclear magnetic resonance spectroscopy

FT-IR - Fourier-transform infrared spectroscopy

GC-MS – Gas chromatography mass spectrometry

GDKP - 3,3'-((2*S*,5*S*)-3,6-dioxopiperazine-2,5-diyl)dipropionic acid (glutamic acid diketopiperazine)

GDKPAA - 3,3'-((2*S*,5*S*)-3,6-dioxopiperazine-2,5-diyl)bisN-4-hydroxymethylbenzyl propanamide (GDKP with an aromatic amide)

GDKPAA-TPUE - Thermoplastic polyurethane with GDKPAA chain extenders

GDKPAA-TPUE30 – GDKPAA-TPUE with a targeted 30 %HS (observed 13 %HS)

GDKPAA-TPUE45 – GDKPAA-TPUE with a targeted 45 %HS (observed 16 %HS)

GDKPAE - bis4-hydroxymethylbenzyl-3,3'-((2*S*,5*S*)-3,6-dioxopiperazine-2,5-diyl) dipropionate (GDKP with an aromatic ester)

GDKPAE-TPUE - Thermoplastic polyurethane with GDKPAE chain extenders

GDKPAE-TPUE30 – GDKPAE-TPUE with a targeted 30 %HS (observed 15 %HS)

GDKPAE-TPUE45 – GDKPAE-TPUE with a targeted 45 %HS (observed 16 %HS)

GDKPAE-TPUE60 – GDKPAE-TPUE with a targeted 60 %HS (observed 20 %HS)

GDKPAE/GDKPAA-TPUE - Thermoplastic polyurethane with a blend of GDKPAE and GDKPAA chain extenders

GDKPAE/GDKPAA-TPUE30 – GDKPAE/GDHPAA-TPUE with a targeted 30 %HS (observed 18 %HS) and a targeted 50:50 molar blend (observed 56:44 molar blend)

ESI-MS – High resolution electron spray ionisation mass spectrometry

$H_{12}$MDI - 4,4'-methylenebis(cyclohexyl isocyanate)

HBP - Hyperbranched Polymer

HCTA – Hyperbranched chain terminating agent

HDI - Hexamethylene diisocyanate

$^{1}$H DOSY NMR –Hydrogen-1 diffusion ordered nuclear magnetic resonance spectroscopy

$^{1}$H NMR - Hydrogen-1 nuclear magnetic resonance spectroscopy

HMPA - 2-hydroypropyl methacrylate

HSQC 2D NMR - Heteronuclear single quantum correlation 2D NMR spectroscopy

IPDI - Isophorone diisocyanate

$LiAlH_4$ – Lithium aluminium hydride

*L*-LDI – *L*-Lysine ethyl ester diisocyanate

$M_n$ – Number-average molecular weight

$M_w$ – Weight-average molecular weight

MDI - Methylene diphenyl diisocyanate

N - Number of molecules present in the system after time including unreacted monomers

$N_o$ - Number of molecules initially present in the systems

$N_{oA}$ - Number of unreacted functional groups of an A-A monomer

$N_{oB}$ - Number of unreacted functional groups of a B-B monomer

NCO% – Percentage isocyanate chain ends in a TPU

$NEt_3$ – Triethylamine

NHS - *N*-hydroxysuccinimde

p – Extent of reaction

$P_2O_5$ - Phosphorus pentoxide

PCL - Poly(ε-caprolactone)

PDKP - 1,7-diazatricyclo[7.3.0.0]dodecane-2,6,8,12-tetrone (pyroglutamic diketopiperazine)

PEG - Polyethylene glycol

PTFE - Polytetrafluoroethylene

PU - Polyurethane

r - Stoichiometric ratio of reactants

R - Ratio of diisocyanate to polyol

RI – Refractive index

$Sn(Oct)_2$ - Tin(II) 2-ethylhexanoate

$T_c$ - Crystallisation temperature

$T_g$ - Glass transition temperature

$T_m$ - Melting transition temperature

TDI - Toluene diisocyanate

TDKP - 3,6-bis(4-hydroxybenzyl)piperazine-2,5-dione

TDKP-TPUE – Thermoplastic polyurethane with tyrosine chain extenders

TGA - Thermogravimetric analysis

THF – Tetrahydrofuran

TPU - Thermoplastic polyurethane

TPUE - Thermoplastic polyurethane elastomer

UTS - Ultimate tensile strength

UV – Ultraviolet

$X_n$ – Degree of polymerisation

# Acknowledgements

First, I would like to thank my PhD supervisor Professor Andrew Dove for the opportunity to conduct my PhD in his group. Your support, guidance, constructive criticism and belief in me throughout have been invaluable and I am a significantly better scientist because of it. Thanks also to The Lubrizol Corporation for my PhD studentship and collaboration and for the fantastic opportunity to work in Montmeló. The members of the Dove and O'Reilly Groups all deserve a medal for putting up with me for 3.5 years! Conducting my PhD in the company of you all has made the journey so much fun, even if I did consume copious amounts of cake and coffee in that time! Thanks for humouring my Croydonisms, bad days and terrible jokes! A special thanks to Annette and Laura for picking me up on the tough days and celebrating with me on the great days and to Anaïs for all your proof reading!

A big thank you to my Jubilee crew for your intentional provision over the years, that includes you Small Talk! From hiking around Mont Blanc to the parties we had at Catalyst, you have been top class. A special mention to Tanya for providing some much-needed PhD solidarity and cooking delicious food; to Amanda for taking every opportunity to fuel my studies with Warwickshire's finest cream teas and to Matthew for making sure I made it to each airport healthy! Thanks also to the netball girls for the de-stress; keep socking it to the opposition, oh wait, that's who we are! Don't all rush at once for the centre bib!

My family has played a crucial part in every challenge I've set myself and my PhD is no exception. Sadly, Maldwyn, Douglas and Monty, are not here to see the completion of my studies, I miss them dearly, but I know they would be very proud of what I have achieved. Thank you to my parents, Meurig and Christine, and my brothers, Luke and Samuel, for your steadfast love and encouragement throughout my PhD, always taking every opportunity to champion me along the journey and humouring me about what my research has encompassed; even if our mutual friends think I spend my time watching paint dry and stretching elastic bands!

# Declaration of Authorship

This thesis is submitted to the University of Warwick in support of my application for the degree of Doctor of Philosophy. It has been composed by myself and has not been submitted in any previous application for any degree.

The work presented (including data generated and data analysis) was carried out by the author except in the cases outlined below:

- The elemental analyses in chapters 2 and 4 were conducted by Exeter Analytical (Warwick Analytical Service);
- The ESI-MS analyses in chapters 2, 4 and 5 and the GC-MS analyses in chapter 2 were conducted by Dr Lijiang Song and Mr Phillip Aston at University of Warwick;
- The $^{1}H$, $^{13}C$, and $^{19}F$ NMR spectroscopies and the $^{1}H$ and $^{19}F$ DOSY NMR spectroscopies in chapters 4 and 5 were conducted by Dr Ivan Prokes and Mr Robert Perry at University of Warwick.

# Abstract

This thesis is in two distinct sections.

In the first section, novel diketopiperazines are synthesised and incorporated as chain extenders into thermoplastic polyurethane elastomers and the resulting mechanical, thermal and degradative properties are analysed.

In the second section, hyperbranched chain terminating agents are synthesised from 1,1'-carbonyldiimidazole in a one-pot process and the potential applications of fluorinated hyperbranched chain terminating agents are investigated.

Chapter 1 has three parts. First, the synthesis and applications of polyurethanes are introduced and the current market trends and growth projections are discussed. Secondly, an overview of current literature covering biodegradable polymers focusing on the incorporation of amino acids into polyurethanes and their potential applications is presented. Thirdly, hyperbranched polymers are introduced and a focus is made on the synthesis of isocyanate and non-isocyanate polyurethanes and polyureas.

In chapter 2, the use of the dipeptides of tyrosine and glutamic acid as chain extenders in polyurethane synthesis is explored. The dipeptide of glutamic acid is modified to incorporate a higher content of ester and amide degradable linkages with aromatic character that form comparable chain extenders to tyrosine dipeptide. Their use in the organocatalysed step-growth polymerisation of novel thermoplastic polyurethane elastomers is described.

In chapter 3, the resulting tyrosine and glutamic acid-derived thermoplastic polyurethane elastomers are utilised to explore the variation of thermal, mechanical and degradative properties of a range of polymer compositions.

In chapter 4, the synthesis of novel hyperbranched materials polymerised in a one-pot, temperature-controlled sequential synthesis incorporating aromatic or

fluorinated functional chain ends from both carbonylbiscaprolactam and 1,1'-carbonyldiimidazole precursors is described.

In chapter 5, 1,1'-carbonyldiimidazole derived hyperbranched polymers are incorporated into an existing thermoplastic polyurethane formulation and the surface properties are studied by varying polymer composition.

In chapter 6, the significant findings and conclusions are summarised.

In chapter 7, the experimental methods used are set out.

# Chapter 1

# Introduction

# 1.1 Introduction to and Applications of Polyurethanes

## 1.1.1 History of polyurethanes

Ever since their discovery by Otto Bayer in 1937[1], polyurethanes (PUs) have been a crucial class of material in society. Bayer observed the reaction between a polyol and a diisocyanate, which formed a polymer with repeated urethane links. PUs enhance a wide variety of everyday objects, from the soles of shoes to car components and in 2012 contributed 7% of the 47 million tons of plastic that was produced in Europe.[2] **(Figure 1.1 left)** Specifically, PUs can be found in four main markets: rigid and flexible foams; elastomers; coatings; and adhesives, binders and sealants.[3] **(Figure 1.1 right)**

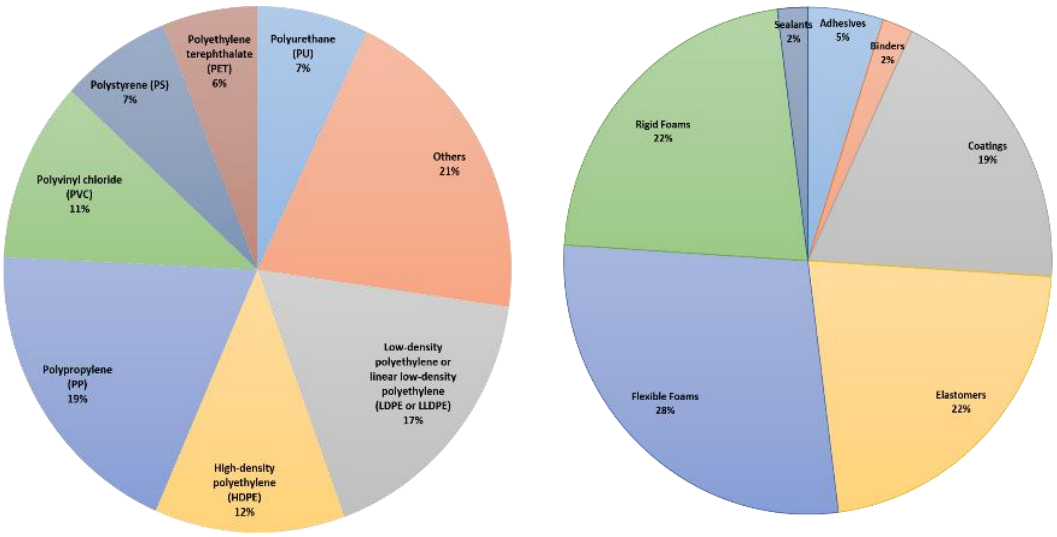


**Figure 1.1 European plastic production (left) and main PU markets (right) in 2012.**

From the outset, PUs have offered a cheap, highly versatile and industrially scalable alternative chemistry for producing high class performance materials. PUs were first used during World War II, where they were employed as a replacement for rubber that at that time was in short supply and consequently very expensive.[4] The use of PUs quickly advanced and throughout the war period they were used to provide corrosion resistant coatings for aeroplanes and chemical resistant coatings for specialist clothing.[5] The use of PUs continued to gain momentum and by the 1950s

they were used in coatings, adhesives, sealants and elastomers (CASE) products and foams.[6] By the 1970s PUs had been recognised as suitable materials for use in orthopaedic and medical applications.[7] A significant discovery was the invention of the SynCardia total artificial heart, which had PU ventricles.[8] **(Figure 1.2)**

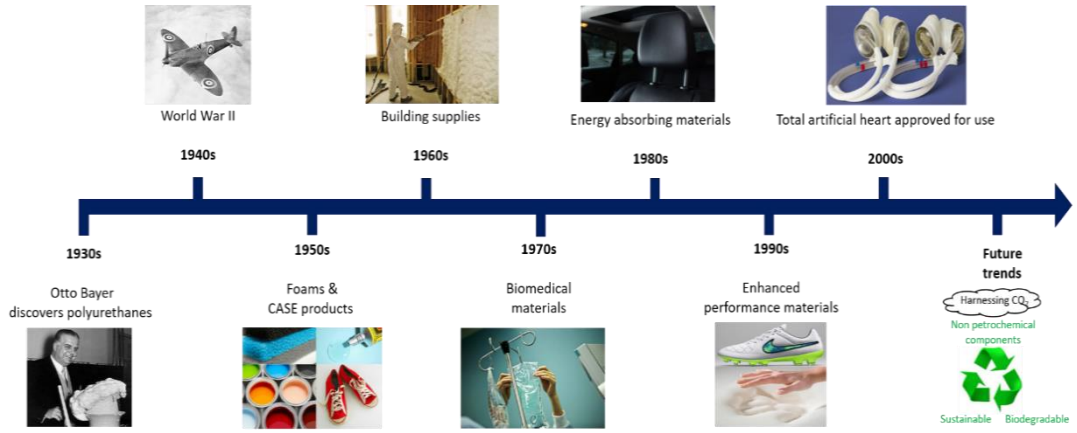


**Figure 1.2 Timeline of new uses of PUs.**

Since Bayer's initial breakthrough, PUs have enhanced the scope of performance materials and impact every aspect of life today. In 2016, 18 million tonnes were produced and they ranked 6$^{th}$ in the total global production of plastics. It is anticipated that between 2017 and 2023 there will be a 5% compound annual growth in the production of PUs, which will be driven by the desire for higher efficiency materials and the need to reduce harmful emissions.[9] The biggest growth is forecast to be in the construction industry with increasing infrastructure building coupled with the need for superior performance and highly energy efficient, lightweight materials.[10] Other major areas of growth will be the use of PU elastomers to replace natural rubber and the production of bio-based PUs from sustainable resources. It is forecast that the global production of bio-based PUs will increase from 1,600 tonnes in 2013 to 2,600 tonnes in 2020.[11]

### 1.1.2 Structure and applications of polyurethanes

PUs can take many forms from traditional linear polymers to ones with branched and crosslinked architectures. This is possible because PUs have a segmented

architecture, which fundamentally consists of three main components: a diisocyanate, a polyol and a small molecule diol or chain extender. PU chemistry is based around a family of chemicals called diisocyanates, which form urethane bonds when combined with an alcohol and urea bonds when combined with an amine, in the presence of a catalyst or with ultraviolet (UV) radiation.[12] The easily modifiable structure of PUs opens the possibility of a versatile set of materials which in turn can create almost any structure or application that is desired, whilst their fundamental chemistry remains the same.

Diisocyanates, which are known respiratory irritants or sensitisers, can be grouped into two main categories: aliphatic and aromatic. Commercially available aliphatic diisocyanates such as 1,4-butane diisocyanate (BDI), hexamethylene diisocyanate (HDI), 4,4'-methylenebis(cyclohexyl isocyanate) ($H_{12}$MDI) and isophorone diisocyanate (IPDI) are primarily used to form colour-stable, durable coatings or contact adhesives as they aid heat and moisture resistance and can adhere to oily substrates.[7,13] Aliphatic diisocyanates can also be found in elastomers as they provide high abrasion and UV-resistant properties.[14] However, they make up only 5% of the overall consumption of diisocyanates.[15] This low usage level is primarily because they tend to be toxic liquids and have higher vapour pressures than other diisocyanates. Nevertheless, the introduction of monitored handling protocols and education programmes has resulted in a decrease in asthma related cases.[16] Aromatic diisocyanates such as methylene diphenyl diisocyanate (MDI) and toluene-2,4-diisocyanate (TDI) are much more widely used in industry as, with the exception of TDI, they tend to be solids and consequently produce lower concentrations of airborne toxins.[17,18] TDI is most commonly used in the automotive industry to reduce the weight of components and MDI is often used in the formation of rigid foams in the insulation industry.[19,20] One potential negative feature of aromatic diisocyanates is that they are known to darken after prolonged exposure to light.[21] **(Figure 1.3)**

**Aliphatic** **Aromatic**

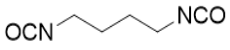


1,4-Butane diisocyanate (BDI)

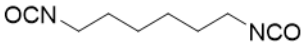


Hexamethylene diisocyanate (HDI)

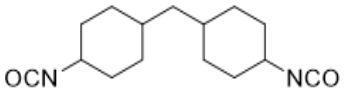


4,4'-Methylenebis(cyclohexyl isocyanate) ($H_{12}$MDI)

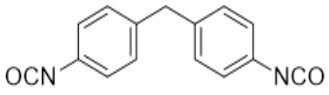


4,4'-Methylene diphenyl diisocyanate (MDI)

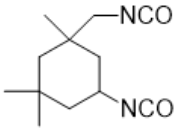


Isophorone diisocyanate (IPDI)

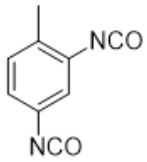


Toluene-2,4-diisocyanate (TDI)

**Figure 1.3 Commercially available aliphatic and aromatic diisocyanates.**

### 1.1.3 Thermoplastic polyurethanes

Thermoplastic polyurethanes (TPUs) encompass an array of varied materials with unique mechanical and thermal properties and are often water-insoluble, non-ionic and inert. TPUs are often referred to as segmented copolymers as they possess a soft segment with at least one low glass-transition temperature ($T_g$) and a hard segment with at least one high $T_g$. Because of this segmented composition, a range of TPUs with a variety of hard and soft segments can be synthesised. The easily modifiable structural architecture is a platform for the manufacture of a very diverse range of materials. Different percentages of hard segment (%HS), traditionally 15, 30, 45 or 60% are used in the TPU composition to tune the resulting properties. The higher the %HS the tougher and more brittle the TPU is, whilst increasing the percentage of soft segment results in a softer and more flexible TPU. However, there is a lower limit of

hardness where TPUs begin to lose their physical properties and become viscous. Consequently, these TPUs become challenging to process and this prevents the production of ''ultra-soft'' varieties. The incorporation of a plasticiser in the structure has been reported to lower the hardness of TPUs, however, such plasticisers are often toxic and, thus, their incorporation into a TPU is not acceptable for many applications.[22] There is a constant need for TPUs that are not sensitive to changes in processing conditions and can easily be processed *via* industrial methods, such as continuous reactive extruding.[23] The choice of hard segment component is important to the mechanical properties of TPUs. The hard segments of such TPUs form non-covalent interactions such as hydrogen bonding. These non-covalent interactions act as crosslinks between the phase-separated hard segments of TPUs. These crosslinks produce the toughness and elasticity properties of the resulting TPUs and enable them to be melt processed. Such hard segments are immobile and rigid whereas soft segments are mobile and free-flowing[24], which results in both high tensile strength and elongation at break.[25] By contrast, thermoset PUs have covalent bonds from an additional crosslink component between the layers of hard segments that determine their mechanical properties but also make them non-remouldable and incapable of being processed by heat.[26] **(Figure 1.4)**

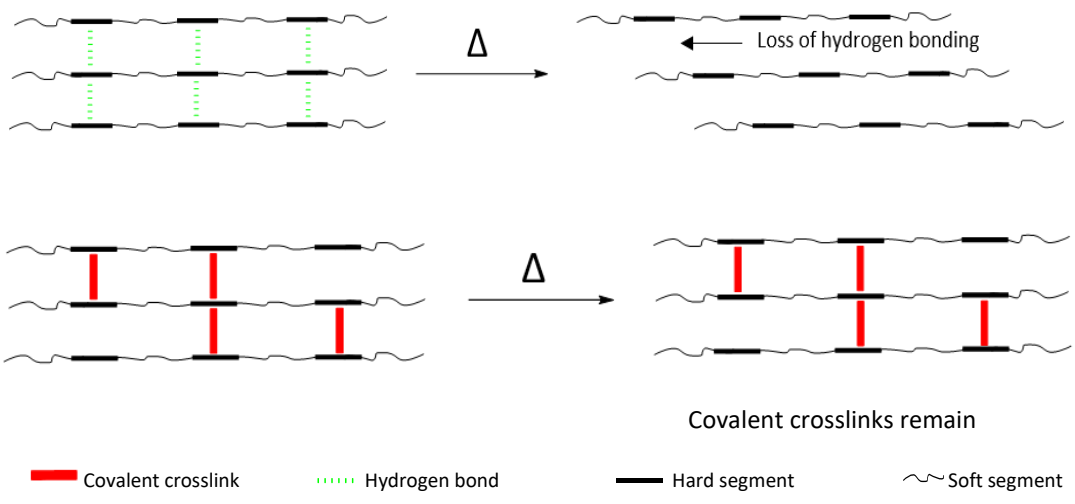


**Figure 1.4 The effect of heat on thermoplastic and thermoset structures.**

The chain extender component of TPUs has traditionally been petroleum based, for example the aliphatic 1,4-butanediol (BDO) however, because of environmental concerns and the high-energy costs associated with the manufacture of petroleum, it is becoming increasingly important to manufacture sustainable and green TPUs.[27]

The choice of polyol can also affect the resulting properties of TPUs. Soft elastic TPUs have flexible long polyols whilst highly crosslinked polyols produce rigid, tough TPUs. In addition, polyols with long chains and high degrees of crosslinking are ideal for making foams. TPUs with polyether polyols have superior hydrolytic stability but perform less well in oxidative and flammability studies.[28-30] Those with aliphatic polyester polyols are oxidatively stable but hydrolytically unstable whilst those with aromatic polyester polyols make effective flame retardants.[31,32] TPUs with polycarbonate polyols are a strong, hydrolytically stable alternative to those with polyester polyols, however, they are often extremely viscous at room temperature.[7] TPUs with acrylic polyols are both hydrolytically and oxidatively stable but are hard and brittle and those with polybutadiene polyols are flexible at low temperatures and resistant to solvent effects but are thermally oxidable because of the unsaturated structure.[33,34]

### 1.1.4 Step-growth polymerisation

Step-growth polymerisation is commonly either a self-condensing reaction of an A-B monomer or a condensation reaction between A-A and B-B difunctional monomers. Examples of these include the hydroxyl and carboxylic acid groups for esterification and isocyanate and alcohol for urethane formation. **(Scheme 1.1)**

$$_n\text{A-B} \longrightarrow \text{-(-A-B-A-B-)}_n\text{-}$$

$$_n\text{A-A} + {}_n\text{B-B} \longrightarrow \text{-(-A-A-B-B-A-A-B-B-)}_n\text{-}$$

**Scheme 1.1: Step-growth polymerisation of A-B and A-A/B-B monomer systems.**

The reactions proceed in a step wise fashion where the monomers react together to form a dimer. This dimer then reacts with either another monomer or dimer to form a trimer or tetramer respectively. As the reaction proceeds, polymers with increasing molecular weight are produced. The original monomers are consumed in the initial stages of the reaction before any high molecular weight $M_w$ polymers are formed. Assuming all functional groups to be equally reactive, irrespective of the size or mobility of the chain to which they are attached, it is possible to calculate the degree of polymerisation of the reaction mixture, defined as $X_n$. This can be demonstrated by comparing the consumption of functional groups with the average length of the chains. The consumption of functional groups can reach high percentages when $X_n$ remains low. For example, when $X_n$ = 2, half of the functional groups have been consumed but the reaction mixture is still predominantly dimers and trimers. At 75% functional group consumption, $X_n$ is only 4. Therefore, for high molecular weight polymers to be produced the reaction must proceed almost to completion, ideally > 99% functional group consumption. [35-37] **(Figure 1.5)**

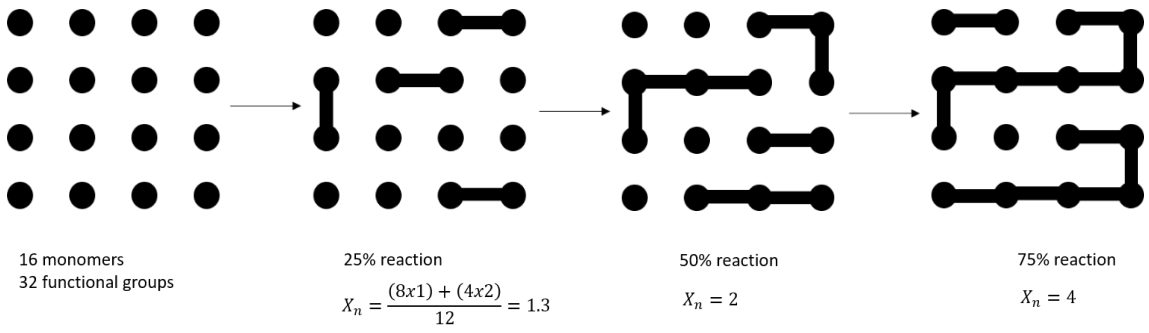


**Figure 1.5 The evolution of molecular weight in step-growth polymerisation of functional groups and molecular weight as a function of the degree of polymerisation.**

### 1.1.4.1 Molecular weight of a polymer

#### 1.1.4.1.1 Equivalent monomers

Building on the principles of step-growth polymerisation discussed above, the Carothers equation can be used to determine $X_n$ at a defined fraction of monomer conversion or extent of reaction (p).

p is defined using the following equation where $N_o$ is the number of monomers initially present, N is the number of molecules, including unreacted monomers, present after time *t* and f is the average functionality per monomer present in the system. Assuming no side reactions occur, $2(N_o - N)$ represents the number of functional groups of either A or B that have reacted at any given time.

$$p = \frac{2(N_o - N)}{N_o f} \quad (1.1)$$

Therefore:

$$N = N_o \frac{(2 - fp)}{2} \quad (1.2)$$

Since:

$$X_n = \frac{N_o}{N} \quad (1.3)$$

Then:

$$X_n = \frac{2}{2 - fp} \quad (1.4)$$

Therefore as

$$X_n = \frac{M_n}{M_o} \quad (1.5)$$

$$M_n = \frac{2M_o}{2 - fp} \quad (1.6)$$

Assuming a functionality of 2, then:

$$X_n = \frac{1}{1 - p} \quad (1.7)$$

And:

$$M_n = \frac{M_o}{1 - p} \quad (1.8)$$

Therefore, this demonstrates that a high degree of monomer conversion is required to produce high molecular weight polymers. For example, a p of 0.95 is required for an $X_n$ of 20 and a p of 0.99 is required for an $X_n$ of 100. The control of molecular weight is important as a low value results in waxy materials with low tensile properties whereas with an extremely high value the material becomes challenging to solubilise and process for mechanical testing. [38-40] **(Table 1.1)**

**Table 1.1 Degree of polymerisation at selected % reaction points per the Carothers equation.** [39]

| % reaction | $X_n$ | $M_n$ |
|---|---|---|
| **50** | 2 | 200 |
| **75** | 4 | 400 |
| **90** | 10 | 1,000 |
| **95** | 20 | 2,000 |
| **99** | 100 | 10,000 |
| **99.5** | 200 | 20,000 |
| **99.95** | 2,000 | 200,000 |

#### 1.1.4.1.2 One monomer in excess

The control of molecular weight by stoichiometric imbalances, with one monomer in excess in an A-A or B-B system, where the stoichiometric ratio of reactants, r, is less than 1 limits the molecular weight of the polymer. Therefore, when one monomer is present in stoichiometric excess the Carothers equation becomes:

$$X_n = \frac{1+r}{1+r-2rp} \qquad (1.9)$$

$$r = \frac{N_{0A-A}}{N_{0B-B}} = \frac{N_{0A}}{N_{0B}} \qquad (1.10)$$

Where $N_{0A\text{-}A}$ and $N_{0B\text{-}B}$ are the number of A-A and B-B monomer molecules initially present in the system and $N_{0A}$ and $N_{0B}$ are the number of unreacted functional groups of each type of monomer. The monomer or functional group in excess should be the denominator of the fraction and hence r < 1. If neither monomer is in excess, then r = 1 and therefore can be cancelled out leaving:

$$X_n = \frac{1}{1-p} \qquad (1.11)$$

The effect of the excess reactant is to reduce the degree of polymerisation for a given value of p. For a quantitative reaction, p tends towards 1 as the reaction proceeds. Therefore, the equation can be re written as:

$$X_n \longrightarrow \frac{1+r}{1-r} \qquad (1.12)$$

The consequences of a 5% molar excess are shown in the table below where r decreases from 1.000 to 0.952 and $X_n$ reduces from 1,000 to 41. [41-44] **(Table 1.2)**

**Table 1.2 Effect on r and $X_n$ of a 5% molar excess of monomer $N_{0B-B}$.**

| $N_{0A-A}$ | $N_{0B-B}$ | r | $X_n$ |
|---|---|---|---|
| 1.00 | 1.00 | 1.000 | 1,000 |
| 1.00 | 1.05 | 0.952 | 41 |

### 1.1.4.2 Reaction kinetics

The rate of step-growth polymerisation is expressed in terms of the concentration of each reactive group. A polyesterification is an equilibrium reaction where, both reactive groups are in equal concentrations. An example is shown by the following scheme of a reaction between a carboxylic acid and an alcohol to form an ester with water as a by-product. **(Scheme 1.2)**

$$RCOOH + OH \longrightarrow COOR + H_2O$$

**Scheme 1.2..Reaction of a carboxylic acid and an alcohol.**

For this reaction to proceed a catalyst is required. The kinetics can be either self-catalysed from the acid group itself or from the addition of a different acid catalyst.

A self-catalysed system proceeds by the following equation for polymerisation rate, R. The reaction is third order overall with a second order dependence on the carboxylic acid concentration (one for the catalyst and one for the reactant). [45]

$$R = -\frac{d[COOH]}{dt} = k[COOH]^2[OH] \quad (1.13)$$

Where k is the rate constant for the reaction.

In the instance where [COOH] = [OH] ⟶ concentration c then:

$$R = -\frac{dc}{dt} = kc^3 \quad (1.14)$$

Integration of this equation with an initial concentration of $c_0$ gives:

$$2kt = \frac{1}{c^2} - \frac{1}{c_0^2} \quad (1.15)$$

The Carothers equation can be expressed as a function of concentration:

$$X_n = \frac{c_o}{c} = \frac{1}{1-p} \quad (1.16)$$

And therefore:

$$c = c_o(1-p) \quad (1.17)$$

If the equation for c is substituted into the equation for 2kt, then:

$$2c_0^2kt + 1 = \left[\frac{1}{(1-p)^2}\right] \quad (1.18)$$

And:

$$X_n = \sqrt{2c_0^2kt + 1} \quad (1.19)$$

For a system catalysed by a separate acid with polymerisation rate R' and a rate constant k'. [46]

$$R' = -\frac{d[COOH]}{dt} = k'[COOH][OH] \quad (1.20)$$

$$R' = -\frac{dc}{dt} = k'c^2 \quad (1.21)$$

$$k't = \frac{1}{c} - \frac{1}{c_0} \quad (1.22)$$

$$c_o k' t = \frac{1}{(1-p)} - 1 \qquad (1.23)$$

And:

$$X_n = 1 + c_o k' t \qquad (1.24)$$

Plotting $X_n$ against time for both catalysation methods shows a straight-line trend with a y intercept of 1. When $X_n$ = 1 all the molecules are monomers. The most significant difference between the two plots is the steepness of the gradient. In the case of the addition of a separate acid catalyst the gradient is steeper showing that this is the more efficient kinetic method to form high molecular weight polymers. [47-49]

### 1.1.4.3 Size distributions

The degree of polymerisation distribution can be defined by the following equation that can be used to calculate the probability P(x) of producing a polymer comprising x units, which is also known as a mole fraction.

$$P(x) = \frac{N_x}{N} = \frac{\text{Number of x-mers}}{\text{Total number of molecules}} \qquad (1.25)$$

In any given system, polymers have (x-1) interunit links, an A functional group at one end and a B functional group at the other end. **(Scheme 1.3)**

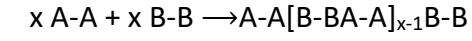


**Scheme 1.3..Conversion of monomers to polymers via A and B functional groups.**

If the probability of a random monomer reacting independently of other monomers with the same functional group is p, then:

$$P_x = p^{x-1}(1-p) \qquad (1.26)$$

Substituting for $P_{(x)}$ :

$$\frac{N_x}{N} = p^{x-1}(1-p) \longrightarrow N_x = Np^{x-1}(1-p) \quad (1.27)$$

Substituting for N:

$$N_x = N_0 p^{x-1}(1-p)^2 \quad (1.28)$$

Substituting $w_x/x$ for $N_x/N_o$, where $w_x$ is the weight fraction of polymers at length x:

$$w_x = xp^{x-1}(1-p)^2 \quad (1.29)$$

From the Carothers equation it is possible to calculate theoretical values for molecular weight averages and the polydispersity of the polymer as a function of p for a step-growth polymer.

$$X_n = \frac{M_n}{M_o} = \frac{1}{1-p} \quad (1.30)$$

$$M_n = \frac{M_o}{1-p} \quad (1.31)$$

$$M_w = \frac{M_o(1+p)}{(1-p)} \quad (1.32)$$

$$Đ_M = \frac{M_w}{M_n} = 1 + p \quad (1.33)$$

Where $M_n$ is the number average molecular weight, $M_w$ is the weight average molecular weight, $M_0$ is the molecular weight of the repeating monomer unit and $Đ_M$ is the polydispersity index.

As the reaction proceeds p⟶1, therefore the maximum $Đ_M$ value for a step-growth polymerisation is 2, which occurs at 100% monomer conversion or p=1. However, in practise this can be affected by monomer purity, the presence of side reactions and the viscosity of the polymer. [50-52]

Polyurethane elastomer synthesis consists of an A-A, B-B and C-C system, where A-A and C-C are diols and B-B is the diisocyanate. The molar ratio of the A-A, B-B and C-C reactants is 1:2:1 so the overall NCO to OH ratio is 1. These reactions are usually conducted by reacting A-A with B-B, which is in excess, and the product of that

reaction, B-B-A-A-B-B, reacts with C-C as well as any excess B-B to form $[C\text{-}C\text{-}B\text{-}B\text{-}A\text{-}A\text{-}B\text{-}B\text{-}C\text{-}C]_n$. This method results in a copolymer being formed with controlled segments. [53-55] PUs can be referred to as block copolymers, which can be synthesised by either a two pre-polymer or one prepolymer method. . In the former method of synthesising a polyester-*block*-PU, two prepolymers are made. The first a mixture of diol and diacid with the diol in excess and the second a diol and a diisocyanate with the diisocyanate in excess. These prepolymers, referred to as a macrodiol and a macrodiisocyanate respectively, are then combined to form a block copolymer. The block lengths can be determined by varying r and consequently the length of the polymer created. In the one prepolymer synthesis method a macrodiol and a diisocyanate that is in excess are combined. This macrodiisocyanate is then combined with a chain extender (small diol) to increase the molecular weight. Both methods in theory can yield identical polymers, however, a lower dispersity is achieved with the two prepolymer method.[56]

These PU copolymers, also known as thermoplastic elastomers, have hard and soft blocks. They are used extensively in the chemical industry as they are able to form physical crosslinks between like blocks and hence provide materials with elasticity akin to rubber that can easily be manipulated with heat.[57]

### 1.1.5 Synthesis of polyurethanes

As discussed in the precious section, PU synthesis is conducted by step-growth polymerisation. This method of polymerisation relies on three main factors to achieve high molecular weight linear polymers:

- The efficiency of the underpinning chemical reaction: for PUs this is the alcohol and diisocyanate reaction;
- The purity of the monomers: as impurities cap the chain ends preventing further polymerisation; and
- The correct stoichiometric ratios of the monomers: another consequence of impure monomers as this would cause an offset.

In step-growth polymerisation the chain is built by difunctional monomers forming dimers that are then converted into oligomers and then high molecular weight molecules. More specifically in PU synthesis the reaction proceeds by the addition of a diisocyanate to a polyol to form a macrodiisocyanate that only slightly increases the molecular weight of the chain. Upon the addition of the low molecular weight diol, the molecular weight rises significantly over a short period as the macrodiisocyanate chain is extended by the low molecular weight diol, hence the term chain extender.[58] **(Figure 1.6)**

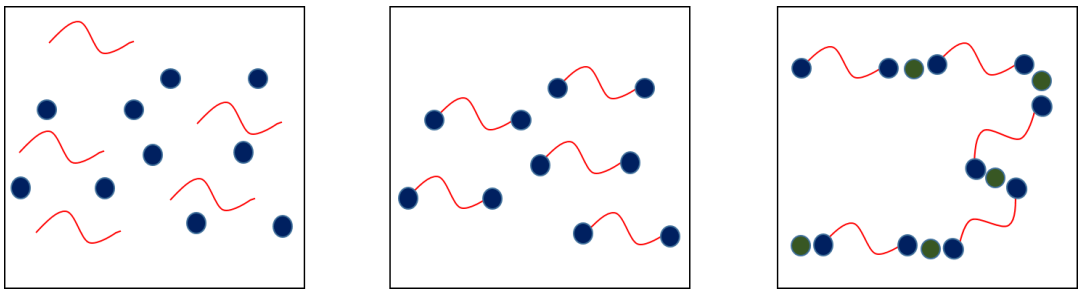

**Figure 1.6 The growth of a polyurethane polymer 1) A diisocyanate and polyol are charged in the presence of a catalyst 2) A macrodiisocyanate is formed 3) A small molecular weight diol chain extends the macrodiisocyanate to form a linear polyurethane.**

Step-growth polymerisation differs from chain-growth polymerisation an example of which is ring opening polymerisation of cyclic monomers, in a variety of ways:

- Step-growth polymerisation relies on one reaction unlike chain-growth polymerisation that requires multiple different reactions;
- The growth of the chain in chain-growth polymerisation occurs by a steady addition of one monomer to the end of the chain resulting in linear growth whereas step-growth polymerisation proceeds by minimal chain growth until the chain extender is added, which causes a sharp rise in molecular weight;
- The consumption of the monomers in step-growth polymerisation happens in the initial stages of the process whereas in chain-growth polymerisation the monomer concentration steadily decreases during the reaction;

- Step-growth polymerisation yields a broad distribution of polymers that should not contain residual monomers unlike in chain-growth polymerisation where 100% conversion is not normally achieved. [58] **(Figure 1.7)**

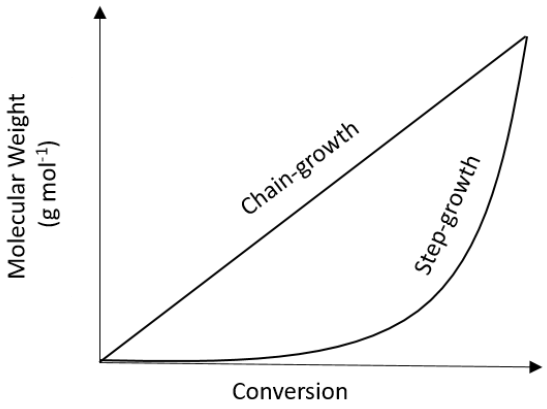


**Figure 1.7 Chart to compare the evolution of molecular weight by chain-growth and step-growth polymerisation methods.**

PUs can be synthesised by two main methods; the all-in-one method and the prepolymer method. The all-in-one method involves charging all the reactants into one pot at the same time. It is very popular in industrial manufacturing as it is a simple method with minimal steps but produces a very uncontrolled distribution of the hard and soft segments of the resulting PUs. Conversely, the prepolymer method provides an extra degree of control over the reaction and produces a more even distribution of hard and soft segments. In this method the diisocyanate and the polyol are combined in the presence of a catalyst or are exposed to UV radiation to form a prepolymer to which the chain extender is then added.[59] **(Figure 1.8)**

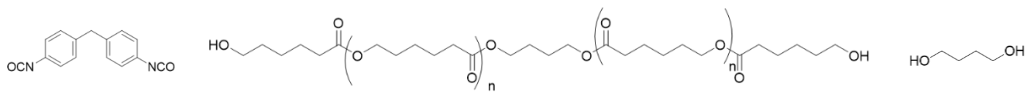


Diisocyanate Polyol Chain Extender

**Figure 1.8 Components of a PU.**

There are multiple methods for calculating stoichiometry for a desired PU. The stoichiometry is governed by the desired %HS, which is formed by the isocyanate and the low molecular weight diol. A method that is popular with industrial manufacturers of PUs is simply dividing the combined weight of the hard segment components by the total weight of the system. This method is very easily modifiable to include additives within the formulations such as end cappers.

$$\%\mathrm{HS} = \frac{100(\text{wt of diisocynate+wt of chain extender})}{\text{total wt of (diisocyanate+chain extender+polyol)}} \qquad (1.34)$$

Whilst this is an effective and versatile method for determining the stoichiometry of a PU, the following equation takes the NCO/OH ratio (*R*) into account:

$$\%\mathrm{HS} = \frac{100(R-1)(M_{\mathrm{ce}}+M_{\mathrm{di}})}{(M_{\mathrm{po}}+R(M_{\mathrm{di}})+(R-1)(M_{\mathrm{ce}}))} \qquad (1.35)$$

where $M_{\mathrm{ce}}$, $M_{\mathrm{di}}$ and $M_{\mathrm{po}}$ are the mole average molecular weights of the chain extender, diisocyanate and polyol respectively. It is generally considered that this equation best represents the material residing in the hard segment of the PU as it includes the portion of the isocyanate that reacts with the alcohol, that creates the urethane content as described by Flory. [60,61]

### 1.1.6 Catalysts for polyurethane synthesis

Catalysts play a vital role in the synthesis of polyurethanes as they control the reaction kinetics resulting in milder conditions. The reaction between an isocyanate and an alcohol at room temperature is slow. Some have hypothesised that this is because of the phase incompatibility between the dense non-polar bonds in the isocyanate and the less dense polar bonds in the alcohol.[62] Therefore, for such reactions to proceed in a reasonable time frame a catalyst is required. There are two main groups of catalysts that have an affinity for such isocyanate and alcohol reactions: transition metals and tertiary amines or amidines, which are generally considered to have different catalytic mechanisms.[63] **(Scheme 1.4)**

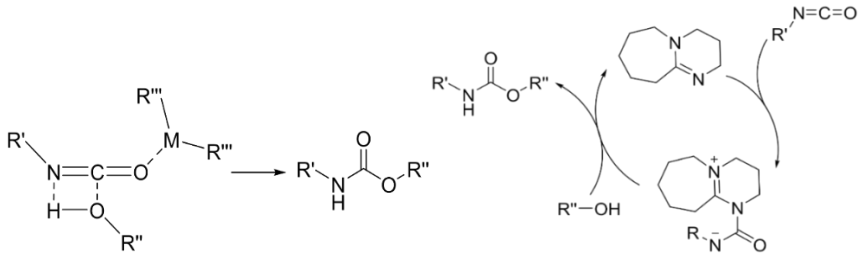

**Scheme 1.4 Organometallic catalysis (left) and organocatalysis (right) of urethane synthesis.**

Transition metals act as Lewis acids in the organometallic catalytic mechanism of urethane synthesis.[64] The most common metal used is tin in the two different compounds, tin(II) 2-ethylhexanoate ($Sn(Oct)_2$) and dibutyltin dilaurate. Zirconium and bismuth complexes can also act as catalysts in urethane synthesis and are much less toxic than tin but are more expensive.[65,66] Many experiments have been conducted to understand the organometallic catalytic mechanism of such transition metals and it is generally considered that either the nitrogen or oxygen atom in the bonds in the isocyanate are polarised leaving the carbon atom electropositive and therefore susceptible to nucleophilic attack by the alcohol in the polyol or chain extender.[67] This is consistent with the non-catalytic mechanism of urethane synthesis.

Because of the toxicity of certain organometallic catalysts and their presence in the final polymer causing an aging affect, organocatalysts have become of great interest to circumvent these shortfalls.[68,69] Tertiary amines such as 1,4-diazabicyclo[2.2.2]octane (DABCO), 2,2'-bis(dimethylaminoethylether) (BDMAEE) or amidines such as 1,8-diazabicyclo[5.4.0] undec-7-ene (DBU) have been shown to be effective in reducing reaction times with good selectivity because of higher reaction rates. [70] DBU has also been found to be non-toxic *in vivo* which is ideal for use in the synthesis of biomaterials.[71] They also have a different catalytic mechanism, nucleophilic catalysis, which involves the addition of the catalyst to the isocyanate group followed by the subsequent addition of the alcohol.[72] The mechanism for amidines is understood to differ from that of tertiary amines as they

utilise a general base catalysis, which involves the activation of the alcohol to the isocyanate but this mechanism is still being studied.[73]

Whilst isocyanates are effective in urethane synthesis, they can also participate in several side reactions depending on the conditions. Irreversible side reactions include the trimerisation by highly polar catalysts of the isocyanate to an isocyanurate and the formation of a urea from the combination of isocyanate and water.[74] Reversible side reactions can also occur in urethane synthesis, most notably allophanate formation when an isocyanate and a urethane combine. Allophanate formation can result from elevated temperatures and an excess of isocyanate and is reversible at temperatures between 100 and 150 °C, dependant on the functional group.[75-77] Further reversible side reactions include the formation of biuret from the combination of an isocyanate and a urea and the formation of the dimer of isocyanate, uretdione, which can form at room temperature and dissociate between 80 and 100 °C, dependant on the functional group.[62,72] **(Scheme 1.5)**

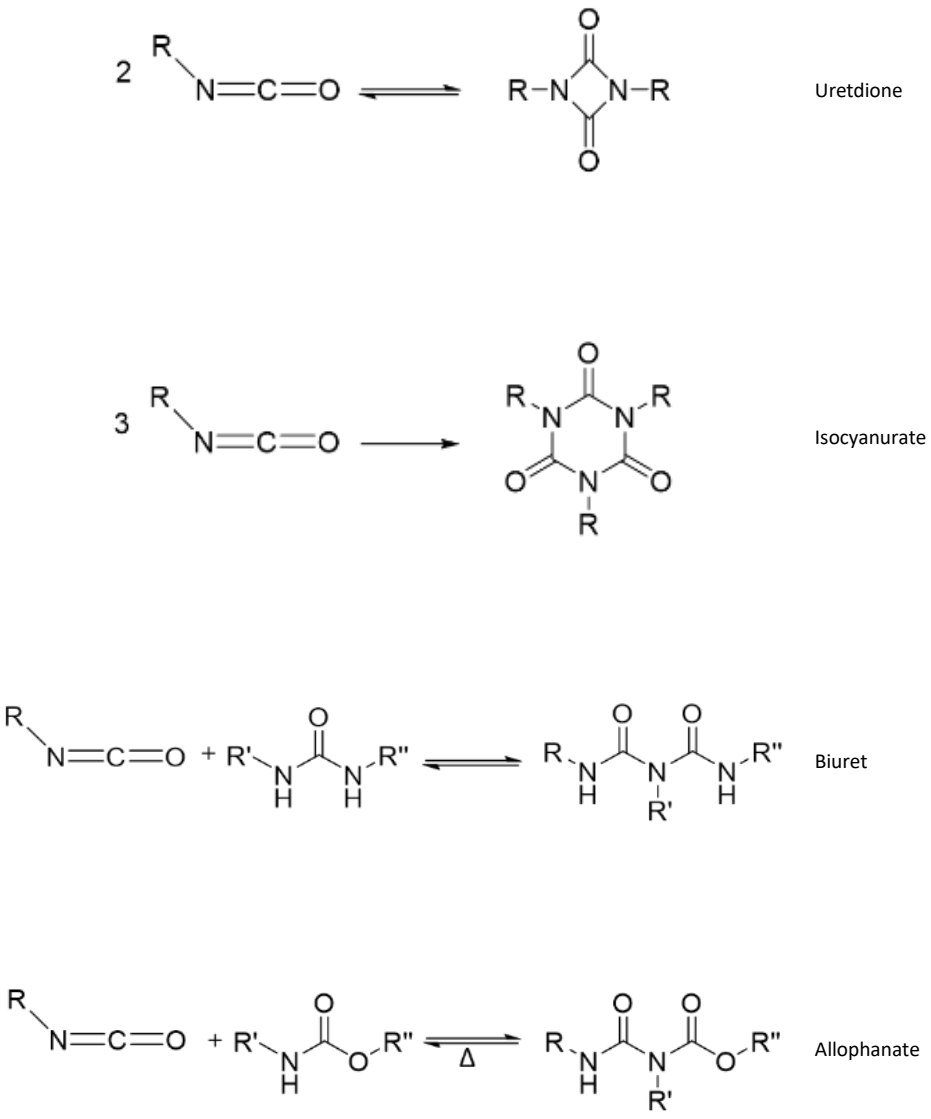


**Scheme 1.5 Side reactions of isocyanates.**

## 1.2 Biodegradable Thermoplastic Polyurethane Elastomers

### 1.2.1 Hard and soft segment chemistry of biodegradable thermoplastic polyurethane elastomers

Biodegradable polyurethane elastomers (BPUEs) contain hard segments comprising diisocyanates and di-functional chain extenders, which are highly polar small molecules, and soft segments, which are polyols that consist of either a polyester, a polyether or a polycarbonate.

Variation in the hard segment chemistry opens up greater control over the degradation and mechanical properties. Bio-based diisocyanates such as BDI and *L*-Lysine ethyl ester diisocyanate (*L*-LDI), which degrade into putrescine and lysine respectively and are non-toxic to the human body, have been investigated.[78] Cystamine diisocyanate has also been studied which benefits from the disulfide degradable link.[79] In addition, IPDI and $H_{12}$MDI have been shown to lead to BPUEs that display superior mechanical and physical properties. Studies have shown that BPUEs that contain the trans-trans isomer of $H_{12}$MDI have particularly enhanced mechanical properties.[80] Commercially available aromatic diisocyanates, such as, MDI and TDI degrade into carcinogenic and mutagenic aromatic amines that are not suitable for biomedical applications.[81,82] More recently, tailored aromatic diisocyanates, based on glycolic acid, have been shown to have significantly superior material properties to their aliphatic counterparts, whilst producing comparable cytocompatibility results.[83] A particular study compared HDI (aliphatic), TDI (aromatic) and IPDI (cycloaliphatic). HDI was found to produce a crystalline BPUE but TDI and IPDI produced amorphous BPUEs. TDI and IPDI produced BPUEs with a high elongation at break and a low Young's Modulus, but the physical crosslinks of the crystalline domains of HDI enhanced the Young's modulus and reduced the elongation at break.[84] **(Figure 1.9)**

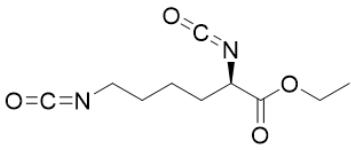

*L*-Lysine ethyl ester diisocyanate

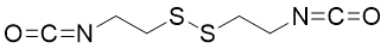

Cystamine diisocyanate

**Figure 1.9 Examples of amino acid-based isocyanates.**

The chain extenders in the hard segments were traditionally low molecular weight diamines or diols, such as BDO, that form urea and urethane bonds respectively when combined with a diisocyanate.[85] However, thiol chain extenders have also been used.[86] A major disadvantage of such chain extenders is that they do not possess any hydrolytically or enzymatically degradable bonds. Because of their susceptibility to degradation, which enables greater control over the breakdown of BPUEs and because of their non-toxic by-products, amino acid-based chain extenders have been investigated.[87] Further as a consequence of their highly polar structure, amino acid-based chain extenders have amide bonds that can act as hydrogen bond acceptors and donor sites. These intermolecular interactions aid the crystallisation of the hard segment of the polyurethane and affect their resulting physical properties.[88] A variety of such amino acid-based chain extenders have been reported including single amino acids such as *L*-arginine, *L*-glycine and *L*-aspartic acid,[89] a range of diester diamines such as *L*-phenylalanine and *L*-glycine-*L*-leucine on a 2:1 ratio with 1,4-cyclohexanedimethanol with HDI and *L*-LDI and soft segments of poly(ε-caprolactone) (PCL) and polyethylene glycol (PEG),[90,91] di-*L*-phenylalanine[92,93] or *L*-glycine-*L*-leucine coupled with cyclohexyl diisocyanate[90] and ethyl esters of *L*-lysine and *L*-ornithine.[94] Peptide sequences of amino acid residues,[95] such as *L*-alanine-*L*-alanine-*L*-lysine, which is susceptible to degradation by elastase,[96] and tripeptides such as *L*-glutathione, which is made up of *L*-glutamic acid, *L*-cysteine, *L*-glycine[97,98] and *L*-phenylalanine-*L*-lysine ethyl ester-*L*-phenylalanine, which has been shown to be very sensitive to enzymatic degradation.[99] Other amino acid-based hard segments have included *L*-tyrosine ethyl ester and *L*-tyramine precursors on a

1:2 ratio with BDI or *L*-LDI.[100] It should also be noted that chain extenders with a blend of amino acids can be used to fine tune the properties of BPUEs.[101] **(Figure 1.10)**

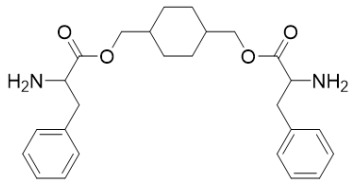

*L*-Phenylalanine based chain extender

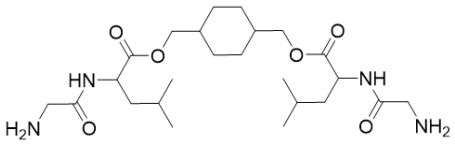

*L*-Glycine-*L*-leucine based chain extender

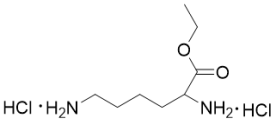

*L*-Lysine ethyl ester based chain extender

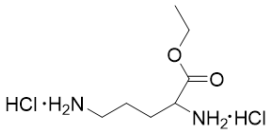

*L*-Ornithine ethyl ester based chain extender

**Figure 1.10 Examples of amino acid-based chain extenders.**

The soft segments have a low $T_g$, are the primary source of elasticity in BPUEs and have a molecular weight ranging from 1,000 to 2,000 g mol$^{-1}$. Initially, ester, amide, ether and carbonate functional polymers were used for the soft segment of BPUEs. An example of this was PCL, a semi-crystalline and hydrophobic polyester, which was used because of its low toxicity and slow degradation rate that allowed it to remain *in vivo* for up to two years. PEG-based BPUEs are hydrophilic and amorphous but are weaker than PCL-based BPUEs that are semi-crystalline, hydrophobic, strong and elastomeric.[102-105] Whilst the soft segment chemistry has been extensively studied recently He *et al.* used the amino acids *L*-arginine-*L*-leucine in their soft segment which resulted in the biodegradable nanoparticles which were found to be an good nanocarrier for doxorubicin.[106] **(Figure 1.11)**

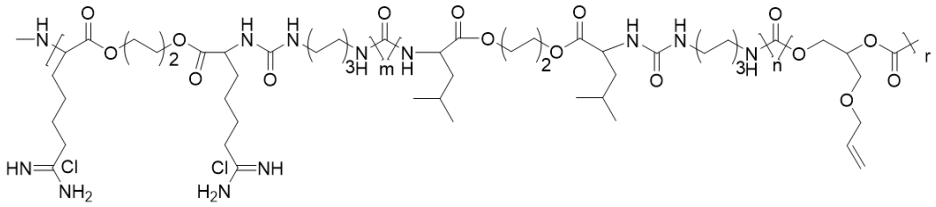

*L*-Arginine diester-*L*-leucine diester soft segment

**Figure 1.11 An example of an amino acid-based soft segment.**

### 1.2.2 Applications of biodegradable thermoplastic polyurethane elastomers

Biomaterials that occur in nature such as polysaccharides,[107] polyesters, such as poly(hydroxybutyrate)[108] and poly(hydroxybutyrate-co-hydroxyvalerate)[109] (which is the copolymer of butyric acid and valeric acid)[110] and collagens[111] initially provided a low cost, biocompatible variety but ultimately their poor amenability to processing and the demand for site-specific mechanical and degradative specifications has curtailed their development and use.[112] Synthetic biomaterials have also been used. These have been synthesised by ring opening polymerisation of cyclic esters from naturally derived monomers such as lactic acid, which is a slow degrading, brittle material, and glycolic acid that has a rapid degradation rate. Further, copolymers of these monomers have aided the tuning of the resulting biomaterials for specific application requirements.[113] Biomaterials containing PCL also cover a large segment of the biomaterials market as PCL is hydrophilic because of the combination of the five-methylene alkyl unit between the ester links. However, such hydrophilicity is not so extreme as to prevent hydrolytic degradation of the ester links.[114] As a consequence of a shallow monomer pool, a current focus in this area is on monomer functionalisation to create pendant groups on the resulting linear polymer and thereby gain further functionalisation or a handle for post polymerisation reactions[115], but often requires extensive syntheses and purification steps to achieve this.

Initially TPUs were not designed as biodegradable materials, but instead were used in implants because of their biocompatibility and their desirable mechanical

properties.[116,117] It was later discovered that they are susceptible to degradation by enzymes and hydrolysis.[118] However, these initial shortcomings are of interest when designing intentionally degradable elastomeric materials. BPUEs have been shown to have excellent mechanical properties and chemical versatility, which promote the growth of cells and tissue but also provide an intermediate material and scaffold whilst regeneration occurs.[92] They have slower degradation rates, are more elastic, and are less brittle than traditional biomaterials.[119,120] They can also be designed to have a function for a predetermined period of time and then degrade *in vivo* and subsequently be absorbed by the body making them ideal for use in a range of biomedical applications from tissue scaffolds to drug delivery.[121-123] This also eliminates potential long term complications arising from the effects of a foreign material in the body and circumvents the need for multiple invasive surgeries.[124,125] In addition, it is easier to tune the mechanical, thermal and biodegradative properties of BPUEs compared with natural monomer polymerisations because of their versatile 3-component system.

### 1.2.3 Degradation of biodegradable thermoplastic polyurethane elastomers

Biomaterials that are placed *in vivo* are exposed to several forms of degradation, which include mechanical degradation through wear and tear as the material stretches and regains its shape continuously throughout its lifetime, oxidative degradation, whereby inflammatory cells, such as leukocytes and macrophages, react against foreign materials by producing highly reactive oxygen species, as well as hydrolytic and enzymatic degradation. *In vivo* degradation of BPUEs includes all the above forms but the focus of this chapter is on hydrolytic and enzymatic degradation only.

Key properties of biomaterials are the way they degrade in different environments and the subsequent toxicity of their degradation products. The rate of degradation is dependent on their thermal properties and physical characteristics such as composition and crystallinity. Their hydrophilic or hydrophobic nature and the number of hydrolysable bonds they contain are also key factors. For example, PCL,

an aliphatic polyester is commonly used in biomaterials because of its low toxicity and melting point and can take up to two years to degrade *in vivo* because of its semi-crystalline and hydrophobic properties.[103-105]

Hydrolytic degradation occurs by hydrolysis of susceptible bonds within the structure of biomaterials resulting in mass loss and breakdown over time. Hydrolytic degradation can be more classified as bulk degradation and/or surface erosion.[126,127] Bulk degradation, which is typically exhibited by polyesters[128], proceeds by a non-linear mass loss profile after an initial increase in mass of the biomaterials. This profile occurs when the rate of diffusion of water through the biomaterial is faster than the rate of hydrolysis. Furthermore, accumulated degradation products within biomaterials can also increase the degradation rate and therefore accelerate the loss of their structural integrity.[104,116,129] On the other hand, surface erosion characterised by a linear mass loss profile predominates as the primary degradation pathway when the rate of hydrolysis is faster than the rate of water diffusion through the biomaterial. Bulk degradation and surface erosion are not necessarily independent of each other and most degradation profiles involve a complex mixture of the two processes.[130] **(Figure 1.12)**

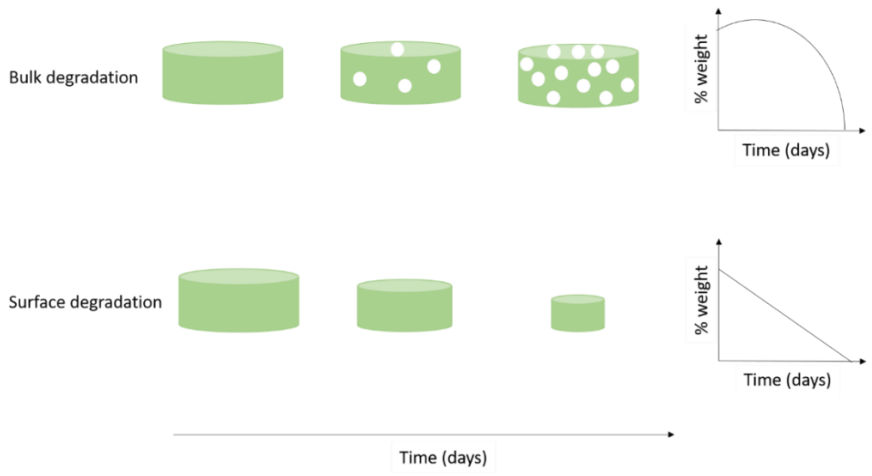


**Figure 1.12 Pictograms and charts of bulk and surface degradation.**

Enzymatic degradation occurs when enzymes, which occur in different concentrations throughout the body, cleave certain bonds within biomaterials .[126,127] Enzymes are often referred to as biological catalysts because they increase the rate of reaction and find their optimal efficacy at 37 °C (body temperature). Hydrolases such as proteases, esterases, glucosides and phosphates often catalyse the hydrolysis reaction.[131] A key enzyme in the breakdown of BPUEs is cholesterol esterase, which is an enzyme that typically catalyses the breakdown of ester bonds to an alcohol and an acid, has been shown to increase the degradation rate of BPUEs by a factor of 10 compared to a phosphate buffer solution.[132] This example highlights that the specific location of a biomaterial in the body is vital to fully understand the mechanism by which it will degrade. Furthermore, α-chymotrypsin, which is a digestive enzyme that is involved in the proteolysis of proteins and peptides and as such, preferentially cleaves peptide amide bonds. Such proteolysis is particularly prevalent in amino acids such as tyrosine, tryptophan and phenylalanine that are large and hydrophobic in nature.[133] As previously discussed the use of amino acids within BPUEs can be used to tune their biodegradative properties by incorporating peptide sequences that are known to be degraded by a specific enzyme. As an example of this, *L*-alanine-*L*-alanine-*L*-lysine has been incorporated into BPUEs because of its susceptibility to degradation by elastase that specifically cleaves peptide bonds on small hydrophobic molecules such as *L*-glycine, *L*-alanine and *L*-valine. [96,100]

# 1.3 Hyperbranched Polyurethanes

## 1.3.1 Structure and properties of hyperbranched polymers

Hyperbranched polymers (HBPs) began to appear 60 years after Herman Staudinger first named linear polymers, macromolecules. 'Hyperbranched' is a generic term for any polymer that has branched substituents across a 3D network with a vast number of end groups. These can take many forms such as grafted, hyperbranched, multi-arm star and dendrimer. Except for dendrimers that have a complete branched star-like morphology, these structures have irregular or incomplete branching. A hyperbranched structure allows a superior degree of functionalisation compared to their linear analogues and consequently HBPs are becoming increasingly important for a wide range of applications from coatings to biomaterials.[134-137] Another advantage that HBPs have over their linear analogues is that, despite their less well-defined structures, they present improved chemical and physical properties, most notably their different viscosity characteristics, as they form gel-free up to three branch. The viscosity of a linear polymer is dependent on its molecular weight increasing as the chain grows, but in HBPs, although viscosity also increases as the length of the chain grows, it does so at a much slower rate. [138-140] **(Figure 1.13)**

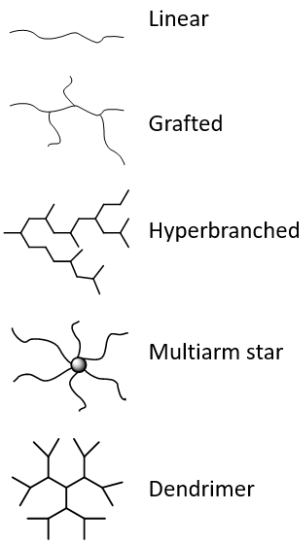


**Figure 1.13 Examples of polymer structures.**

### 1.3.2 Synthesis of hyperbranched polymers

One of the many attractions of HBPs is that they can be synthesised in a one-pot process unlike their structure perfect analogues, dendrimers, which involve long and involved synthetic procedures with multiple purification steps. HBPs can be synthesised from either an $AB_2$ monomer or a combination of $A_2$ and $B_3$ monomers, where A and B are functional groups. HBPs have been reported not to gel like their linear analogues for at least three branches of branching and possess high degrees of chain end functionality.[141-143] A range of functional HBPs can be synthesised through a variety of methods but in this chapter the review is limited to the synthesis of hyperbranched polyurethanes, with and without isocyanates, and polyureas both using a combination of $A_2$ and $B_3$ monomers and $AB_2$ monomers.

#### 1.3.2.1 Hyperbranched polyurethanes from isocyanates

Many $A_2$ and $B_3$ monomers are commercially available but can result in gelation if the stoichiometry is not carefully controlled. T. Long and co-workers have shown $A_2$ and $B_3$ monomers such as oligomeric polyols and polyisocyanates can yield elastomeric materials that can be tuned according to the monomer functionality, whilst gelation and cyclisation were avoided by careful stoichiometric control.[144] A variation on this was a reaction of a diisocyanate with an amino alcohol forming a urea intermediate, which then proceeded to form an HBP. [145-149] The introduction of hyperbranched polyols and polyisocyanates that can be tuned according to the desired characteristics has aided the synthesis of HBPs by a combination of $A_2$ and $B_3$ monomers.[150] These HBPs showed a significantly lower viscosity compared to their linear analogues. [151,152]

In 1993, Spindler and Fréchet were the first to synthesise HBPs from $AB_2$ monomers, using a phenol-capped 3,5-diisocyanatobenzyl alcohol monomer and by thermally deblocking the isocyanate groups forming an $AB_2$ monomer *in situ* prior to polyurethane synthesis.[153] Vanjinathan *et al.* later added ester and amide links within the alcohol terminated side chain[154] and unlike $A_2$ and $B_3$ monomers, there are a limited number of commercially available $AB_2$ monomers,[155-159] the most studied of which is 2,2-dimethylolpropionic acid because it is commercially available.[160] Also

Bruchmann *et al.* used commercially available diisocyanates such as TDI with trimethylolpropane to form an $AB_2$ type system.[161] Synthetic procedures have been reported to produce $AB_2$ monomers, however, they require multiple steps and extensive purification. Crucially $AB_2$ monomers have been reported to form gel free HBPs up to three branches.[162,163]

#### 1.3.2.2 Hyperbranched polyurethanes *via* isocyanate free chemistry

The synthesis of HBPs from isocyanates currently remains the method of choice because of the low cost and abundance of raw materials as well as its desirable atom economy, despite the need for a catalyst[6,72] However, because such HBPs are petroleum-based, water-sensitive and toxic, most notably to the respiratory system and skin, there has recently been an attempt to utilise a safer, greener and more sustainable approach to the synthesis of HBPs.[164,165] The main driving factor for this change is the increasing imposition of restrictive regulatory controls and guidelines for their use across the globe.[17,18,166,167] A new class of HBPs called non-isocyanate HBPs (NIPUs) has been created with the aminolysis of cyclic carbonates looking to be the most promising synthetic method.[164,168-170] Torkelson and co-workers have shown recently that segmented NIPUs can be synthesised by this method and they have formed a structure-function relationship by investigating each of the chain extenders[171], soft segments[172], hydroxyl groups[173] and amide groups.[174,175] Nai-Shang Liou and co-workers have taken this greener approach further by harnessing the use of $CO_2$ to introduce cyclic carbonates along a Jatropha Curcas oil backbone, which has resulted in two NIPU isomer products that are solvent and chemical resistant.[176] **(Figure 1.14)**

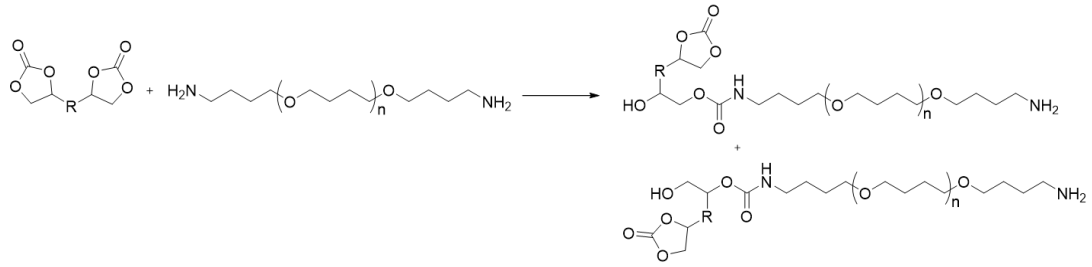

**Figure 1.14 Carbonate amine NIPU formation.**

In the same year that Spindler and Fréchet reported their isocyanate-based HBPs, Kumar and Ramakrishnan reported their non-isocyanate route to HBP formation, through the Curtius rearrangement of azides, which can form an $AB_2$ monomer and subsequently react with an alcohol to form an HBP.[177] **(Figure 1.15)**

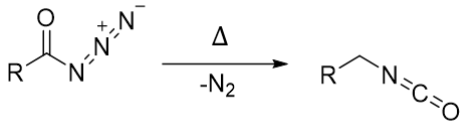

**Figure 1.15 Curtius rearrangement of azides.**

This chemistry was expanded to the use of oligomeric azides that allowed greater control over the size of the links between branching points.[178] Tang *et al* found that using oligomeric azides aided the formation of conducting HBPs.[179] S. Rannard *et al*. reported the sequential reactivity of 1,1'-carbonyldiimidazole (CDI) with N-(3-aminopropyl)triethanolamine. The imidazole end group was thermally removed to yield an *in situ* $AB_2$ type intermediate, which formed an HBP *via* the free alcohol chain ends.[180]

Rannard and Davis continued to develop the scope of the selectivity of CDI, firstly with primary, secondary and tertiary alcohols [181] and then with primary and secondary amines. In this work they identified that imidazole carboxylic esters could be formed from CDI and secondary or tertiary amines. These precursors were reacted selectively with primary alcohols, within a molecule containing mixtures of primary,

secondary and tertiary alcohols. Building on from this, the imidazole carboxylic esters combined with polyamines. Selectivity was observed at the primary amine site affording a carbamate. The selectivity of these reactions was suggested to be a consequence of which specific alcohol was on the imidazole carboxylic ester.[182] This work was subsequently extended to aliphatic polyamides and polycarbonate dendrimers. [183,184] A further study was undertaken where a secondary or tertiary imidazole carboxylic ester was selectively reacted with the primary alcohol on 1-[N,N-bis(2-hydroxyethyl)amino]-2-propanol to form dendritic polycarbonates. It was found that this reaction, which was successfully conducted in a one-pot vessel, was completely selective and no side reactions on the secondary alcohol or cyclic species were observed. [184]

Aliphatic polyurethane homodendrimers were synthesised *via* a convergent approach to yield high $M_w$ using a selective reactivity mechanism. This involved reacting CDI with a tertiary alcohol followed by a triamine to form a di-protected triamine that was further reacted with propylene oxide to achieve a secondary alcohol functionality. Using this intermediate, the diamino alcohol 1-[bis(2-aminoethyl)-amino]-2-propanol was produced by deprotecting the tertiary alcohol and then subsequently adding this to the di-protected triamine to form a polyurethane dendrimer, all in a one-pot selective procedure. [185] This work was then developed using CDI with the selective activation of unprotected $AB_2$ monomers producing water-soluble hyperbranched polyurethanes. This demonstrated the high selectivity of the carboxamide with a primary amine of the amino diol leaving the primary alcohol groups unreacted. This work was further developed using benzoic acid groups. This is an effective method to produce aliphatic homodendrimers through the selective activation of the A functionality but no reaction was reported at the B functional site of the unprotected $AB_2$ monomer.[186] **(Scheme 1.6)**

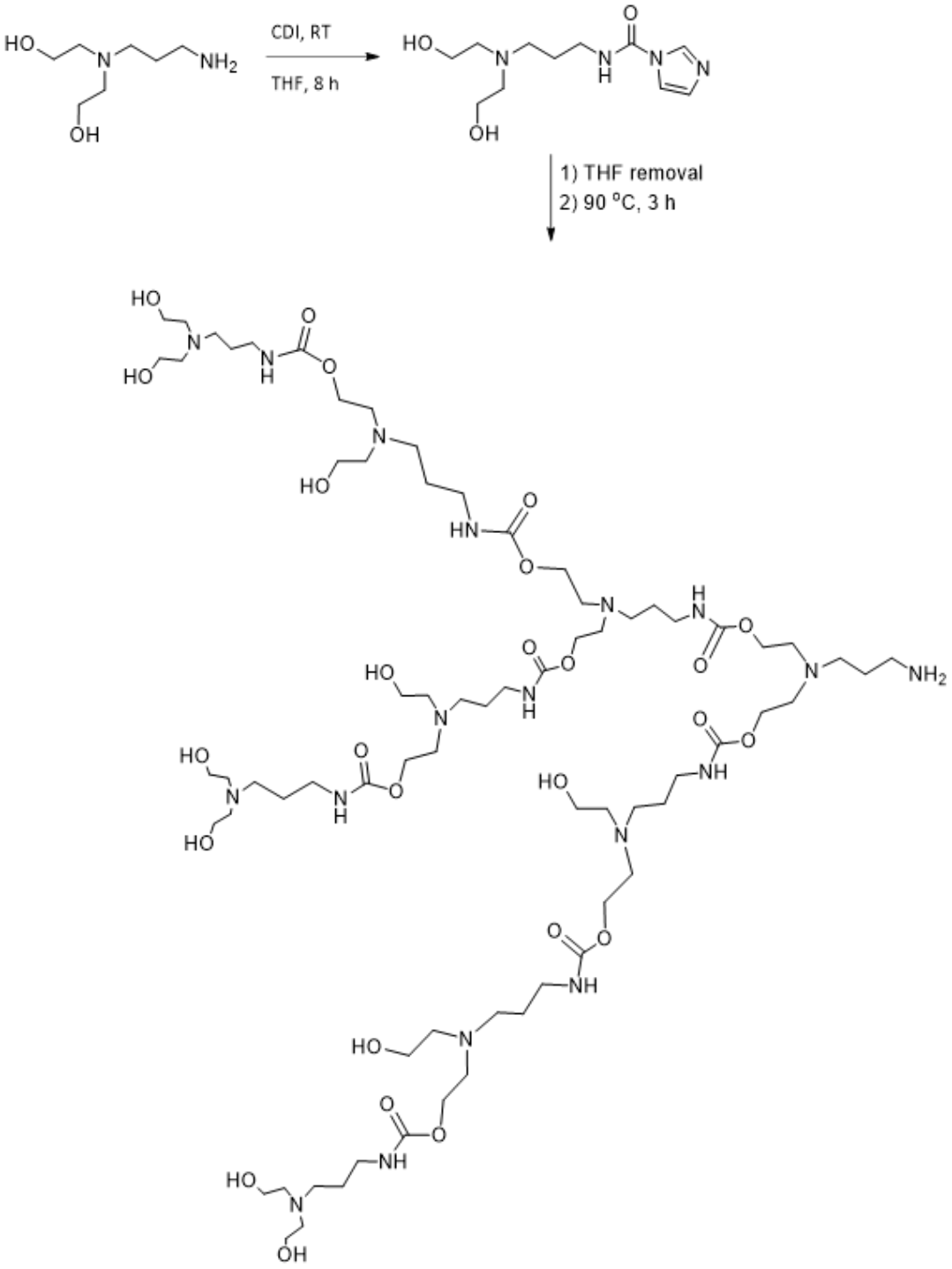


**Scheme 1.6..Selective activation of an unprotected $AB_2$ monomer producing a hyperbranched polyurethane.**

Further modification of these polyurethane dimers was then used to create polydendrons. The secondary amines focal point was converted to a secondary

amine and consequently a tertiary bromo group acceptable for atom transfer radical polymerisation. Copper catalysed ATRP synthesis was used to create a variety of architectures including a linear dendritic hybrid, a dendritic linear dendritic hybrid, a hyperbranched polydendron and a dendronized linear polymer using 2-hydroypropyl methacrylate (HMPA) and ethylene glycol dimethyl methacrylate (EGDMA). **(Schemes 1.7 and 1.8)**

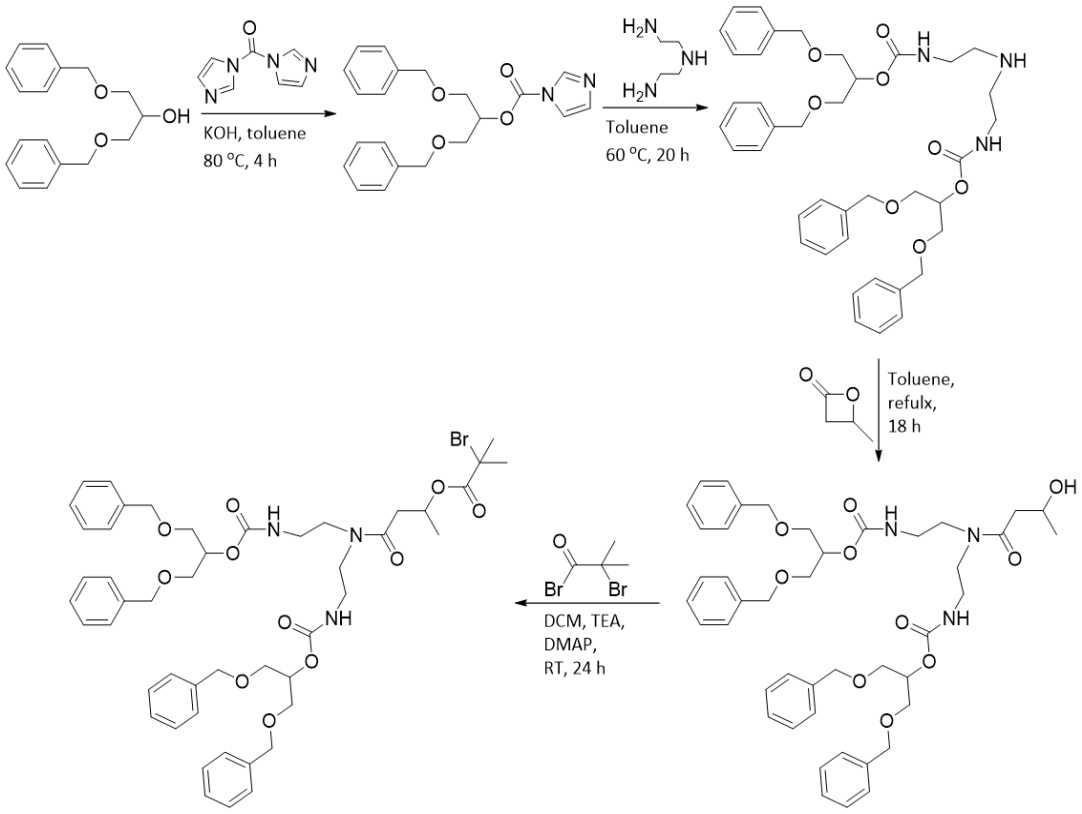


**Scheme 1.7..Preparation of hyperbranched polyurethanes for copper-catalysed ATRP synthesis.**

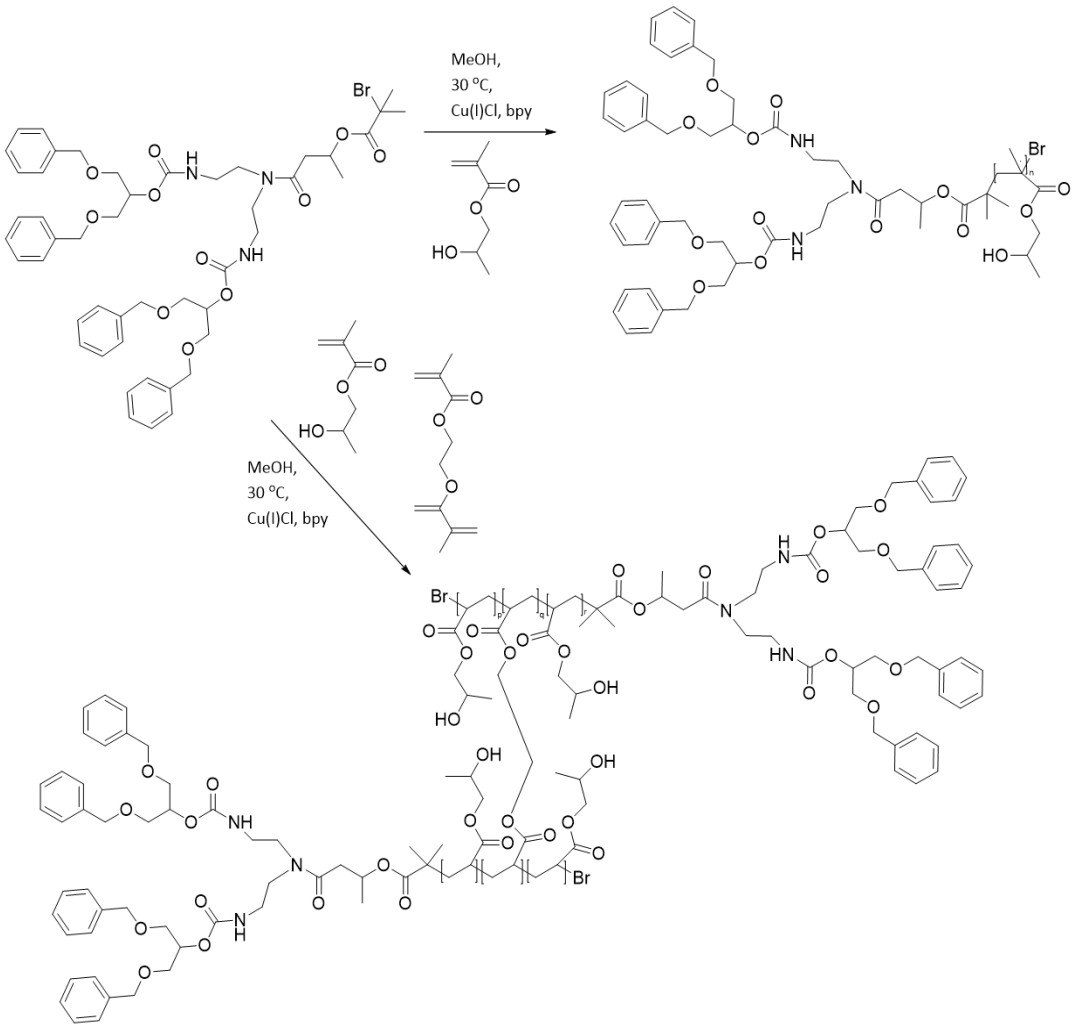


**Scheme 1.8 ATRP synthesis of hyperbranched polyurethanes with HMPA and EGDMA to form linear-dendritic and dendritic-linear-dendritic hybrids.**

Following the synthesis of polydendrons it was discovered that they assembled depending on the solvent in which they were placed. This provided an effective route to the creation of a wide variety of nanoparticles, which are forecast to be applied to molecule loading and biological interaction with cells. [187]

### 1.3.2.3 Hyperbranched polyureas

The study of hyperbranched polyureas has only begun to gain momentum in recent years. There are only a few studies of hyperbranched polyureas synthesised from a combination of $A_2$ and $B_3$ monomers[144,145,188] and even fewer studies of hyperbranched polyureas synthesised from $AB_2$ monomers.[154,189-191] Dendritic

polyureas have recently been reported to be biodegradable and other studies have explored the possibility of hyperbranched polyureas also being biodegradable. Such hyperbranched polyureas could provide easily synthesisable biomaterials with potential *inter alia* as drug delivery mechanisms.[192]

The challenge is to create an $AB_2$ monomer with secondary and primary amino groups in the A and B positions respectively and the ability to selectively react each component whilst in a one-pot process. Kumar and Meijer were the first to begin to tackle this challenge by employing the Curtius rearrangement of benzoyl azide [190] and Vanjinathan *et al*. introduced the concept of using blocked isocyanates (BIs) to control the reaction sequence.[162] These initial studies proved a good starting basis but required multiple step synthetic procedures and purification steps and consisted of aromatic $AB_2$ monomers as they were less prone to form cyclic structures but proved difficult to process.

Building on this early work, T. Loontjens *et al*. have recently shown that carbonylbiscaprolactam (CBC) can form HBPs by selectively reacting with primary and secondary amine groups on a six-membered triamine according to the reaction temperature and using BIs for branching control.[193-195] This selectivity, has been exploited to make $AB_2$ monomers in a one-pot process.[196] It has further been reported that self-condensation of $AB_2$ monomers by un-blocking the BIs resulted in the production of HBPs, where no gelation was observed up to a third generation of branching.[197] Post-polymerisation modification of such HBPs was performed in the same pot, by unblocking the ε-caprolactam (ε-CLM) BI chain termini, with monomethoxy poly(ethylene glycol)s forming urethane chain ends.[198]

## 1.4 Conclusions

PUs provide a commercially and industrially viable range of a highly diverse group of performance materials across the foams, elastomers, coatings, adhesives, binders and sealants markets which all stem from a simple but very effective synthetic route. The choice of diisocyanate plays a significant role in the application of TPUs whilst there is an increasing priority to remove tin catalysts and move towards organic bases to catalyse urethane bond formation. It is forecast that the future trend in PU production will be aimed at a greener and more sustainable synthesis by capturing $CO_2$. As the production of petroleum-based PUs decreases so the manufacture of biodegradable materials and light weight, energy efficient building materials will increase.

The chain extenders of PUs are a largely understudied area but has recently been used to successfully tune the mechanical, thermal and biodegradative properties of the resulting PUs. It has been shown that the use of naturally occurring products are ideal candidates for this as they are biocompatible, susceptible to degradation by hydrolysis and enzymes and produce non-toxic degradation products.

On the other hand, HBPs present a unique set of chemical and physical properties compared to their linear analogues despite their irregular 3D structure and can be made in a one-pot process circumventing the need for extensive purification steps required in dendrimer synthesis. Isocyanates currently provide an effective, versatile and industrially approved route to produce HBPs but recently there is a new focus on utilising greener and more sustainable method that do not require phosgene and its derivatives such as isocyanates. Hyperbranched polyureas have been a relatively under studied area but recently breakthroughs in the control of their synthesis and potential application as drug delivery mechanisms has prompted further study.

## 1.5 References


1. O. Bayer, *Angew. Chem.*, 1947, **59**, 257-288.

2. *Plastics – the Facts 2012. An analysis of European plastics production, demand and waste data for 2011*, Plastics Europe - Association of Plastics Manufacturers, Brussels, Belgium, 2012.

3. *Europe Polyurethanes Market Segmented by Application, Industry and Geography Trends and Forecasts (2016 - 2021)*, Mordor Intelligence, Hyderabad, India, 2016.

4. R. B. Seymour and G. B. Kauffman, *J. Chem. Educ.*, 1992, **69**, 909-910.

5. Z. S. Petrovic and J. Ferguson, *Prog. Polym. Sci.*, 1991, **16**, 695-836.

6. D. K. Chattopadhyay and K. V. S. N. Raju, *Prog. Polym. Sci.*, 2007, **32**, 352-418.

7. J. O. Akindoyo, M. D. H. Beg, S. Ghazali, M. R. Islam, N. Jeyaratnam and A. R. Yuvaraj, *RSC Adv.*, 2016, **6**, 114453-114482.

8. *SynCardia Systems Inc. CardioWest Total Artificial Heart (TAH) - Directions for use*, SynCardia Systems, LLC, Tucson, AZ, USA.

9. *Polyurethanes (PU) Market Size By Product (Flexible Foams, Rigid Foam, Adhesives & Sealants, Elastomers, Coatings), By Application (Construction, Automotive, Furniture & Interiors, Electronics, Footwear, Packaging), Industry Analysis Report, Regional Outlook (U.S., Germany, Italy, UK, China, India, Japan, Indonesia, Brazil, Saudi Arabia), Bio-based PU Application Potential, Price Trends, Competitive Market Share & Forecast, 2016 – 2023*, Global Market Insights, Inc., Ocean View, DE, USA, 2016.

10. *The Economic Benefits of the U.S. Polyurethanes Industry 2015*, The American Chemistry Council, Washington, D.C., USA, 2016.

11. *Bio-Based Polyurethane (PU) Market Analysis By Product (Rigid Foams, Flexible Foams, CASE), By End-Use (Furniture & Interiors, Construction, Automotive, Footwear) And Segment Forecasts To 2020*, Grand View Research, Inc., San Francisco, CA, USA, 2015.

12. E. Delebecq, J.-P. Pascault, B. Boutevin and F. Ganachaud, *Chem. Rev.*, 2013, **113**, 80-118.

13. D.-K. Lee and H.-B. Tsai, *J. Appl. Polym. Sci.*, 2000, **75**, 167-174.

14. C. R. Coleman, *USA Pat.,* 4,731,289, 1988.

15. *2014 End-Use Market Survey on the Polyurethanes Industry in the United States, Canada and Mexico*, Center for the Polyurethanes Industry, The American Chemistry Council, Washington, D.C., USA, 2015.

16. Responsible Care® Safety Related Performance Measures, https://responsiblecare.americanchemistry.com/ResponsibleCare/Performance-Results/Safety/, Accessed 29/06/2017.

17. *Toluene Diisocyanate (TDI) Action Plan*, U.S. Environmental Protection Agency, Washington, D.C., USA, 2011.

18. *Methylene Diphenyl Isocyanate (MDI) and Related Compounds Action Plan*, U.S. Environmental Protection Agency, Washington, D.C., USA, 2011.

19. I. Boustead, *Eco-profiles of the European Plastics Industry - Polyurethane Rigid Foam*, Plastics Europe - Association of Plastics Manufacturers, Brussels, Belgium, 2005.

20. D. R. Hartter, in *Toxicity of Nitroaromatic Compounds*, ed. D. E. Rickert, Hemisphere Publishing, USA, 1985, ch. 1, pp. 1-14.

21. C. Hepburn, *Polyurethane Elastomers*, Elsevier, USA, 2nd edn., 1992, ch. 12, p. 341.

22. A. S. Wilson, *Plasticisers: Selection, Applications and Implications*, Rapra Technology, UK, 1997, ch. 5, pp. 26-28.

23. U. G. Makal, B. W. Steinmetz, Q. Lu and R. W. Day, *USA Pat.,* 9,546,242, 2017.

24. M.Charlon, B.Heinrich, Y.Matter, E.Couzigné, B.Donnio and L.Avérous, *Eur. Polym. J.*, 2014, **61**, 197-205.

25. J. Blackwell and K. H. Gardner, *Polymer*, 1979, **20**, 13-17.

26. J. P. Pascault, H. Sautereau, J. Verdu and R. J. J. Williams, *Thermosetting Polymers*, Marcel Dekker, USA, 2002, ch. 1, pp. 1-4.

27. H. Gang, D. Lee, K.-Y. Choi, H.-N. Kim, H. Ryu, D.-S. Lee and B.-G. Kim, *ACS Sustain. Chem. Eng.*, 2017, **5**, 4582-4588.

28. P. Król, *Prog. Mater Sci.*, 2007, **52**, 915-1015.

29. M. Rutkowska, K. Krasowska, A. Heimowska, I. Steinka and H. Janik, *Polym. Degrad. Stab.*, 2002, **76**, 233-239.

30. Y. D. Kim and S. C. Kim, *Polym. Degrad. Stab.*, 1998, **62**, 343-352.

31. M. Ionescu, *Chemistry and Technology of Polyols for Polyurethane*, Rapra Technology, UK, 1st edn., 2005, ch. 21, pp. 535-550.

32. P. Parcheta and J. Datta, *J. Therm. Anal. Calorim.*, 2017, **130**, 197-206.

33. H.-W. Engels, H.-G. Pirkl, R. Albers, R. W. Albach, J. Krause, A. Hoffmann, H. Casselmann and J. Dormish, *Angew. Chem. Int. Ed.*, 2013, **52**, 9422-9441.

34. M. Ionescu, *Chemistry and Technology of Polyols for Polyurethane*, Rapra Technology, UK, 1st edn., 2005, ch. 9-10, pp. 295-309.

35. B. M. Mandal, *Fundamentals of Polymerization*, World Scientific Publishing Co. Pte. Ltd., Singapore, 2012, ch. 2, pp. 37-38.

36. D. Braun, H. Cherdron, M. Rehahn, H. Ritter and B. Voit, *Polymer Synthesis: Theory and Practice*, Springer-Verlag, Germany, 5th edn., 2013, ch. 4, pp. 259-260.

37. G. Odian, *Principles of Polymerization*, John Wiley & Sons, Inc., USA, 4th edn., 2004, ch. 2, pp. 39-40.

38. B. M. Mandal, *Fundamentals of Polymerization*, World Scientific Publishing Co. Pte. Ltd., Singapore, 2012, ch. 2, pp. 47-49.

39. D. Braun, H. Cherdron, M. Rehahn, H. Ritter and B. Voit, *Polymer Synthesis: Theory and Practice*, Springer-Verlag, Germany, 5th edn., 2013, ch. 4, pp. 260-261.

40. G. Odian, *Principles of Polymerization*, John Wiley & Sons, Inc., USA, 4th edn., 2004, ch. 2, pp. 105-106.

41. B. M. Mandal, *Fundamentals of Polymerization*, World Scientific Publishing Co. Pte. Ltd., Singapore, 2012, ch. 2, pp. 47-52.

42. D. Braun, H. Cherdron, M. Rehahn, H. Ritter and B. Voit, *Polymer Synthesis: Theory and Practice*, Springer-Verlag, Germany, 5th edn., 2013, ch. 4, pp. 261-262.

43. G. Odian, *Principles of Polymerization*, John Wiley & Sons, Inc., USA, 4th edn., 2004, ch. 2, pp. 74-79.

44. G. Odian, *Principles of Polymerization*, John Wiley & Sons, Inc., USA, 4th edn., 2004, ch. 2, pp. 106-108.

45. G. Odian, *Principles of Polymerization*, John Wiley & Sons, Inc., USA, 4th edn., 2004, ch. 2, pp. 44-48.

46. G. Odian, *Principles of Polymerization*, John Wiley & Sons, Inc., USA, 4th edn., 2004, ch. 2, pp. 51-53.

47. B. M. Mandal, *Fundamentals of Polymerization*, World Scientific Publishing Co. Pte. Ltd., Singapore, 2012, ch. 2, pp. 38-41.

48. G. Odian, *Principles of Polymerization*, John Wiley & Sons, Inc., USA, 4th edn., 2004, ch. 2, pp. 40-41.

49. G. Odian, *Principles of Polymerization*, John Wiley & Sons, Inc., USA, 4th edn., 2004, ch. 2, pp. 53-54.

50. B. M. Mandal, *Fundamentals of Polymerization*, World Scientific Publishing Co. Pte. Ltd., Singapore, 2012, ch. 2, pp. 52-56.

51. G. Odian, *Principles of Polymerization*, John Wiley & Sons, Inc., USA, 4th edn., 2004, ch. 2, pp. 50-51.

52. G. Odian, *Principles of Polymerization*, John Wiley & Sons, Inc., USA, 4th edn., 2004, ch. 2, pp. 80-83.

53. B. M. Mandal, *Fundamentals of Polymerization*, World Scientific Publishing Co. Pte. Ltd., Singapore, 2012, ch. 2, pp. 67-69.

54. D. Braun, H. Cherdron, M. Rehahn, H. Ritter and B. Voit, *Polymer Synthesis: Theory and Practice*, Springer-Verlag, Germany, 5th edn., 2013, ch. 4, pp. 313-316.

55. G. Odian, *Principles of Polymerization*, John Wiley & Sons, Inc., USA, 4th edn., 2004, ch. 2, pp. 130-132.

56. G. Odian, *Principles of Polymerization*, John Wiley & Sons, Inc., USA, 4th edn., 2004, ch. 2, pp. 139-140.

57. G. Odian, *Principles of Polymerization*, John Wiley & Sons, Inc., USA, 4th edn., 2004, ch. 2, pp. 142-143.

58. J. K. Stille, *J. Chem. Educ.*, 1981, **58**, 862.

59. M. Ionescu, *Chemistry and Technology of Polyols for Polyurethane*, Rapra Technology, UK, 1st edn., 2005, ch. 2, pp. 23-25.

60. C. S. Paik Sung, C. B. Hu and C. S. Wu, *Macromolecules*, 1980, **13**, 111-116.

61. M. J. O'Sickey, B. D. Lawrey and G. L. Wilkes, *J. Appl. Polym. Sci.*, 2002, **84**, 229-243.

62. M. F. Sonnenschein, *Polyurethanes: Science, Technology, Markets, and Trends*, Wiley-Blackwell, USA, 1st edn., 2014, ch. 3, pp. 105-123.

63. M. Soto, R. M. Sebastián and J. Marquet, *J. Org. Chem.*, 2014, **79**, 5019-5027.

64. R. Devendra, N. R. Edmonds and T. Söhnel, *J. Mol. Catal. A: Chem.*, 2013, **366**, 126-139.

65. H. Sardon, L. Irusta and M. J. Fernández-Berridi, *Prog. Org. Coat.*, 2009, **66**, 291-295.

66. A. R. Leckart and H. V. Hansen, *USA Pat.,* 4,584,362, 1986.

67. A. J. Bloodworth and A. G. Davies, *J. Chem. Soc.*, 1965, **0**, 5238-5244.

68. H. Sardon, A. Pascual, D. Mecerreyes, D. Taton, H. Cramail and J. L. Hedrick, *Macromolecules*, 2015, **48**, 3153-3165.

69. D. J. Coady, H. W. Horn, G. O. Jones, H. Sardon, A. C. Engler, R. M. Waymouth, J. E. Rice, Y. Y. Yang and J. L. Hedrick, *ACS Macro Letters*, 2013, **2**, 306-312.

70. S. Dworakowska, D. Bogdał, F. Zaccheria and N. Ravasio, *Catal. Today*, 2014, **223**, 148-156.

71. J. B. Havla, A. S. Lotz, E. Richter, K. Froelich, R. Hagen, R. Staudenmaier and N. H. Kleinsasser, *Toxicol. Vitro*, 2010, **24**, 849-853.

72. A. L. Silva and J. C. Bordado, *Catal. Rev.: Sci. Eng.*, 2004, **46**, 31-51.

73. J. Alsarraf, Y. A. Ammar, F. Robert, E. Cloutet, H. Cramail and Y. Landais, *Macromolecules*, 2012, **45**, 2249-2256.

74. G. Raspoet, M. T. Nguyen, M. McGarraghy and A. F. Hegarty, *J. Org. Chem.*, 1998, **63**, 6867-6877.

75. L. Okrasa, P. Czech, G. Boiteux, F. Méchin and J. Ulanski, *Polymer*, 2008, **49**, 2662-2668.

76. P. F. Yang, X. W. Zhu, J. Y. Li, Y. M. Xia and T. D. Li, *J. Appl. Polym. Sci.*, 2010, **117**, 1095-1099.

77. A. Lapprand, F. Boisson, F. Delolme, F. Méchin and J. P. Pascault, *Polym. Degrad. Stab.*, 2005, **90**, 363-373.

78. Y. Higaki, K. Suzuki, Y. Oniki, K. L. White, N. Ohta and A. Takahara, *Polymer*, 2015, **78**, 173-179.

79. X. Wang, J. Zhang, R. Cheng, F. Meng, C. Deng and Z. Zhong, *Biomacromolecules*, 2016, **17**, 882-890.

80. A. Saralegui, A. Etxeberria, B. F. d. A. Bidegain, I. Mondragon, A. Eceiza and M. A. Corcuera, *Polym. Bull.*, 2013, **70**, 2193-2210.

81. R. E. Marchant, Q. Zhao, J. M. Anderson and A. Hiltner, *Polymer*, 1987, **28**, 2032-2039.

82. R. G. Heijkants, R. V. van Calck, T. G. van Tienen, J. H. de Groot, P. Buma, A. J. Pennings, R. P. Veth and A. J. Schouten, *Biomaterials*, 2005, **26**, 4219-4228.

83. D. K. Dempsey, J. L. Robinson, A. V. Iyer, J. P. Parakka, R. S. Bezwada and E. M. Cosgriff-Hernandez, *J. Biomater. Sci., Polym. Ed.*, 2014, **25**, 535-554.

84. W. Panwiriyarat, V. Tanrattanakul, J. F. Pilard, P. Pasetto and C. Khaokong, *J. Appl. Polym. Sci.*, 2013, **130**, 453-462.

85. C. Hepburn, *Polyurethane Elastomers*, Elsevier, USA, 1st edn., 1982, ch. 3, pp. 74-75.

86. L. H. Chan-Chan, R. S. Solis-Correa, R. F. Vargas-Coronado, J. M. Cervantes-Uc, J. V. Cauich-Rodríguez, P. Quintana and P. Bartolo-Pérez, *Acta Biomaterialia*, 2010, **6**, 2035–2044.

87. A. Rodríguez-Galán, L. Fuentes and J. Puiggalí, *Polymer*, 2000, **41**, 5967-5970.

88. P. J. Woodward, D. Hermida Merino, B. W. Greenland, I. W. Hamley, Z. Light, A. T. Slark and W. Hayes, *Macromolecules*, 2010, **43**, 2512-2517.

89. L. H. Chan-Chan, C. Tkaczyk, R. F. Vargas-Coronado, J. M. Cervantes-Uc, M. Tabrizian and J. V. Cauich-Rodriguez, *J. Mater. Sci. - Mater. Med.*, 2013, **24**, 1733-1744.

90. I. C. Parrag and K. A. Woodhouse, *J. Biomater. Sci., Polym. Ed.*, 2010, **21**, 843-862.

91. G. A. Skarja and K. A. Woodhouse, *J. Appl. Polym. Sci.*, 2000, **75**, 1522-1534.

92. G. A. Skarja and K. A. Woodhouse, *J. Biomater. Sci., Polym. Ed.*, 1998, **9**, 271-295.

93. G. A. Skarja and K. A. Woodhouse, *J. Biomater. Sci., Polym. Ed.*, 2001, **12**, 851-873.

94. A. Marcos-Fernández, G. A. Abraham, J. L. Valentín and J. S. Román, *Polymer*, 2006, **47**, 785-798.

95. J. L. West and J. A. Hubbell, *Macromolecules*, 1999, **32**, 241-244.

96. J. Guan and W. R. Wagner, *Biomacromolecules*, 2005, **6**, 2833-2842.

97. J. L. A. Perales-Alcacio, J. Santa-Olalla Tapia, C. Mojica-Cardoso, R. F. Vargas-Coronado, L. H. Chan-Chan, D. M. Headen, A. J. García, J. M. Cervantes-Uc and J. V. Cauich-Rodríguez, *J. Biomater. Sci., Polym. Ed.*, 2013, **24**, 1601-1617.

98. J. Wang, Z. Zheng, L. Chen, X. Tu and X. Wang, *J. Biomater. Sci., Polym. Ed.*, 2013, **24**, 831-848.

99. F. Wang, Z. Zheng, W. Wang, Z. Gu, J. Wang and X. Wang, *Polym. Degrad. Stab.*, 2014, **100**, 86–92.

100. S. A. Guelcher, K. M. Gallagher, J. E. Didier, D. B. Klinedinst, J. S. Doctor, A. S. Goldstein, G. L. Wilkes, E. J. Beckman and J. O. Hollinger, *Acta Biomaterialia*, 2005, **1**, 471–484.

101. J. D. Fromstein and K. A. Woodhouse, *J. Biomater. Sci., Polym. Ed.*, 2002, **13**, 391-406.

102. C. Hepburn, *Polyurethane Elastomers*, Elsevier, USA, 1st edn., 1982, ch. 1, pp. 19-20.

103. W. J. Lin, *J. Biomed. Mater. Res. Part A*, 1999, **47**, 420-423.

104. G. G. Pitt, M. M. Gratzl, G. L. Kimmel, J. Surles and A. Sohindler, *Biomaterials*, 1981, **2**, 215-220.

105. S. Y. Lin, K. S. Chen, H. H. Teng and M. J. Li, *J. Microencapsulation*, 2000, **17**, 577-586.

106. M. He, A. Potuck, J. C. Kohn, K. Fung, C. A. Reinhart-King and C.-C. Chu, *Biomacromolecules*, 2016, **17**, 523-537.

107. M. G. Cascone, N. Barbani, C. Cristallini, P. Giusti, G. Ciardelli and L. Lazzeri, *J. Biomater. Sci., Polym. Ed.*, 2001, **12**, 267-281.

108. T. Freier, C. Kunze, C. Nischan, S. Kramer, K. Sternberg, M. Saß, U. T. Hopt and K.-P. Schmitz, *Biomaterials*, 2002, **23**, 2649-2657.

109. G. T. Köse, H. Kenar, N. Hasırcı and V. Hasırcı, *Biomaterials*, 2003, **24**, 1949-1958.

110. M. R. Timmins, R. W. Lenz and R. Clinton Fuller, *Polymer*, 1997, **38**, 551-562.

111. C. H. Lee, A. Singla and Y. Lee, *Int. J. Pharm.*, 2001, **221**, 1-22.

112. N. Goonoo, A. Bhaw-Luximon, G. L. Bowlin and D. Jhurry, *Polym. Int.*, 2013, **62**, 523-533.

113. R. P. Brannigan and A. P. Dove, *Biomaterials Science*, 2017, **5**, 9-21.

114. L. S. Nair and C. T. Laurencin, *Prog. Polym. Sci.*, 2007, **32**, 762-798.

115. F. Sinclair, L. Chen, B. W. Greenland and M. P. Shaver, *Macromolecules*, 2016, **49**, 6826-6834.

116. A. Göpferich, *Biomaterials*, 1996, **17**, 103-114.

117. V. Tangpasuthadol, S. M. Pendharkar and J. Kohn, *Biomaterials*, 2000, **21**, 2371-2378.

118. J. P. Santerre, K. Woodhouse, G. Laroche and R. S. Labow, *Biomaterials*, 2005, **26**, 7457-7470.

119. I. Engelberg and J. Kohn, *Biomaterials*, 1991, **12**, 292-304.

120. Z. You and Y. Wang, in *Biomaterials for Tissue Engineering Applications: A Review of the Past and Future Trends*, eds. J. A. Burdick and R. L. Mauck, Springer, Austria, 2011, ch. 4, pp. 75-118.

121. R. J. Zdrahala and I. J. Zdrahala, *J. Biomater. Appl.*, 1999, **14**, 67-90.

122. R. S. Moglia, J. L. Robinson, A. D. Muschenborn, T. J. Touchet, D. J. Maitland and E. Cosgriff-Hernandez, *Polymer*, 2014, **55**, 426–434.

123. G. T. Howard, *Int. Biodeterior. Biodegrad.*, 2002, **49**, 245–252.

124. J. R. Lentino, *Clin Infect Dis*, 2003, **36**, 1157-1161.

125. A. van Ooij, S. M. Kurtz, F. Stessels, H. Noten and L. van Rhijn, *Spine*, 2007, **32**, 223-229.

126. L. M. Orozco-Castellanos, A. Marcos-Fernández and A. Martínez-Richa, *Polym. Adv. Technol.*, 2009, **22**, 430-436.

127. I. Castilla-Cortázar, J. Más-Estellés, J. M. Meseguer-Dueñas, J. L. Escobar Ivirico and B. Marí, Vidaurre, A., *Polym. Degrad. Stab.*, 2012, **97**, 1241-1248.

128. D. S. Katti, S. Lakshmi, R. Langer and C. T. Laurencin, *Adv Drug Deliv Rev*, 2002, **54**, 933-961.

129. S. Lyu and D. Untereker, *Int. J. Mol. Sci.*, 2009, **10**, 4033-4065.

130. K. E. Uhrich, S. M. Cannizzaro, R. S. Langer and K. M. Shakesheff, *Chem. Rev.*, 1999, **99**, 3181-3198.

131. S. W. Shalaby and K. Park, in *Biomedical Polymers. Designed-to-Degrade Systems.*, ed. S. W. Shalaby, Hanser Publishers, Germany, 1994, ch. 9, pp. 214-250.

132. J. P. Santerre, R. S. Labow, D. G. Duguay, D. Erfle and G. A. Adams, *J. Biomed. Mater. Res.*, 1994, **28**, 1187-1199.

133. L. Gráf, L. Szilágyi and I. Venekei, in *Handbook of Proteolytic Enzymes*, ed. G. Salvesen, Academic Press, 2013, vol. 3, ch. 582, pp. 2626-2633.

134. F. Xiang, L. Asri, O. Ivashenko, P. Rudolf and T. Loontjens, *Langmuir*, 2015, **31**, 2761-2769.

135. J. Yin, J. Wildeman and T. Loontjens, *J. Polym. Sci., Part A: Polym. Chem.*, 2015, **53**, 2036-2049.

136. G. Cheng, B. W. Greenland, C. Lampard, N. Williams, M. S. Bahra and W. Hayes, *J. Polym. Sci., Part A: Polym. Chem.*, 2013, **51**, 3964-3974.

137. G. Cheng, B. W. Greenland, C. Lampard, N. Williams, M. S. Bahra and W. Hayes, *React. Funct. Polym.*, 2013, **73**, 619-623.

138. T. H. Mourey, S. R. Turner, M. Rubinstein, J. M. J. Frechet, C. J. Hawker and K. L. Wooley, *Macromolecules*, 1992, **25**, 2401-2406.

139. S. R. Turner, B. I. Voit and T. H. Mourey, *Macromolecules*, 1993, **26**, 4617-4623.

140. S. R. Turner, F. Walter, B. I. Voit and T. H. Mourey, *Macromolecules*, 1994, **27**, 1611-1616.

141. T. Emrick, H.-T. Chang and J. M. J. Fréchet, *Macromolecules*, 1999, **32**, 6380-6382.

142. M. Smet, Y. Fu, X. Zhang, E. H. Schacht and W. Dehaen, *Macromol. Rapid Commun.*, 2005, **26**, 1458-1463.

143. C. Sivakumar and A. S. Nasar, *Eur. Polym. J.*, 2009, **45**, 2329–2337.

144. S. Unal, I. Yilgor, E. Yilgor, J. P. Sheth, G. L. Wilkes and T. E. Long, *Macromolecules*, 2004, **37**, 7081-7084.

145. C. Gao and D. Yan, *Macromolecules*, 2003, **36**, 613-620.

146. M. Abdelrehim, H. Komber, J. Langenwalter, B. Voit and B. Bruchmann, *J. Polym. Sci., Part A: Polym. Chem.*, 2004, **42**, 3062-3081.

147. K. Sahre, M. H. Abd Elrehim, K.-J. Eichhorn and B. Voit, *Macromol. Mater. Eng.*, 2006, **291**, 470-476.

148. K. Sahre, U. Schulze, T. Hoffmann, M. A. Elrehim, K.-J. Eichhorn, D. Pospiech, D. Fischer and B. Voit, *J. Appl. Polym. Sci.*, 2006, **101**, 1374-1380.

149. M. A. Elrehim, B. Voit, B. Bruchmann, K.-J. Eichhorn, K. Grundke and C. Bellmann, *J. Polym. Sci., Part A: Polym. Chem.*, 2005, **43**, 3376-3393.

150. B. Bruchmann, U. Ehe, F. Wingerter, K. Stiefenhofer and U. Treuling, *USA Pat.,* 6,376,637, 2002.

151. J. P. Sheth, S. Unal, E. Yilgor, I. Yilgor, F. L. Beyer, T. E. Long and G. L. Wilkes, *Polymer*, 2005, **46**, 10180-10190.

152. A. R. Fornof, T. E. Glass and T. E. Long, *Macromol. Chem. Phys.*, 2006, **207**, 1197-1206.

153. R. Spindler and J. M. J. Frechet, *Macromolecules*, 1993, **26**, 4809-4813.

154. M. Vanjinathan, A. Shanavas, A. Raghavan and A. S. Nasar, *J. Polym. Sci., Part A: Polym. Chem.*, 2007, **45**, 3877-3893.

155. Y. H. Kim, *J. Polym. Sci., Part A: Polym. Chem.*, 1998, **36**, 1685-1698.

156. M. Jikei and M. A. Kakimoto, *J. Polym. Sci., Part A: Polym. Chem.*, 2004, **42**, 1293-1309.

157. C. R. Yates and W. Hayes, *Eur. Polym. J.*, 2004, **40**, 1257-1281.

158. B. Voit, *J. Polym. Sci., Part A: Polym. Chem.*, 2000, **38**, 2505-2525.

159. B. Voit, *J. Polym. Sci., Part A: Polym. Chem.*, 2005, **43**, 2679-2699.

160. J. W. Bartels, P. M. Imbesi, J. A. Finlay, C. Fidge, J. Ma, J. E. Seppala, A. M. Nystrom, M. E. Mackay, J. A. Callow, M. E. Callow and K. L. Wooley, *Appl. Mater. Interfaces*, 2011, **3**, 2118-2129.

161. B. Bruchmann, F. Wingerter, H. Graf and S. Wolff, *USA Pat.,* 5,981,684, 1999.

162. M. Vanjinathan, A. Raghavan and A. Sultan Nasar, *J. Polym. Sci., Part A: Polym. Chem.*, 2007, **45**, 2959-2977.

163. T. Shanmugam and A. S. Nasar, *Macromol. Chem. Phys.*, 2008, **209**, 651-665.

164. H. Blattmann, M. Fleischer, M. Bähr and R. Mülhaupt, *Macromol. Rapid Commun.*, 2014, **35**, 1238-1254.

165. B. Nohra, L. Candy, J.-F. Blanco, C. Guerin, Y. Raoul and Z. Mouloungui, *Macromolecules*, 2013, **46**, 3771-3792.

166. *Regulation (EC) No 552/2009 amending Regulation (EC) No 1907/2006 of the European Parliament and of the Council on the Registration, Evaluation, Authorisation and Restriction of Chemicals (REACH) as regards Annex XVII*, 2009.

167. EPA Proposes Rule to Protect Customers from Harmful Chemicals Found in Homes and Schools, Enviromental Protection Agency Press Release, 8/1/2015

168. M. S. Kathalewar, P. B. Joshi, A. S. Sabnis and V. C. Malshe, *RSC Adv.*, 2013, **3**, 4110-4129.

169. L. Maisonneuve, O. Lamarzelle, E. Rix, E. Grau and H. Cramail, *Chem. Rev.*, 2015, **115**, 12407-12439.

170. A. Cornille, R. Auvergne, O. Figovsky, B. Boutevin and S. Caillol, *Eur. Polym. J.*, 2017, **87**, 535-552.

171. G. Beniah, W. H. Heath, J. Jeon and J. M. Torkelson, *J. Appl. Polym. Sci.*, 2017, **134**, 44942.

172. G. Beniah, X. Chen, B. E. Uno, K. Liu, E. K. Leitsch, J. Jeon, W. H. Heath, K. A. Scheidt and J. M. Torkelson, *Macromolecules*, 2017, **50**, 3193-3203.

173. E. K. Leitsch, G. Beniah, K. Liu, T. Lan, W. H. Heath, K. A. Scheidt and J. M. Torkelson, *ACS Macro Letters*, 2016, **5**, 424-429.

174. G. Beniah, K. Liu, W. H. Heath, M. D. Miller, K. A. Scheidt and J. M. Torkelson, *Eur. Polym. J.*, 2016, **84**, 770-783.

175. G. Beniah, D. J. Fortman, W. H. Heath, W. R. Dichtel and J. M. Torkelson, *Macromolecules*, 2017, **50**, 4425-4434.

176. M. A. C. M. Haniffa, Y. C. Ching, C. H. Chuah, Y. C. Kuan, D.-S. Liu and N.-S. Liou, *Polymers*, 2017, **9**, 162.

177. A. Kumar and S. Ramakrishnan, *J. Chem. Soc., Chem. Commun.*, 1993, **18**, 1453-1454.

178. A. Kumar and S. Ramakrishnan, *J. Polym. Sci., Part A: Polym. Chem.*, 1996, **34**, 839-848.

179. L. Hong, Y. Cui, X. Wang and X. Tang, *J. Polym. Sci., Part A: Polym. Chem.*, 2002, **40**, 344-350.

180. N. J. Davis and S. P. Rannard, *WO Pat.,* 050453, 1998.

181. S. P. Rannard and N. J. Davis, *Org. Lett.*, 1999, **1**, 933-936.

182. S. P. Rannard and N. J. Davis, *Org. Lett.*, 2000, **2**, 2117-2120.

183. S. Rannard, N. Davis and H. McFarland, *Polym. Int.*, 2000, **49**, 1002-1006.

184. S. P. Rannard and N. J. Davis, *J. Am. Chem. Soc.*, 2000, **122**, 11729-11730.

185. W. J. Feast, S. P. Rannard and A. Stoddart, *Macromolecules*, 2003, **36**, 9704-9706.

186. S. P. Rannard, N. J. Davis and I. Herbert, *Macromolecules*, 2004, **37**, 9418-9430.

187. F. L. Hatton, P. Chambon, T. O. McDonald, A. Owen and S. P. Rannard, *Chem. Sci.*, 2014, **5**, 1844-1853.

188. A. Kyritsis, K. Raftopoulos, M. A. Rehim, S. S. Shabaan, A. Ghoneim and G. Turky, *Polymer*, 2009, **50**, 4039-4047.

189. A. V. Ambade and A. Kumar, *J. Polym. Sci., Part A: Polym. Chem.*, 2004, **42**, 5134-5145.

190. A. Kumar and E. W. Meijer, *Chem. Commun.*, 1998, **16**, 1629-1630.

191. A. V. Ambade and A. Kumar, *J. Polym. Sci., Part A: Polym. Chem.*, 2001, **39**, 1295-1304.

192. R. B. Restani, P. I. Morgado, M. P. Ribeiro, I. J. Correia, A. Aguiar-Ricardo and V. D. B. Bonifácio, *Angew. Chem. Int. Ed.*, 2012, **51**, 5162-5165.

193. O. Persenaire, M. Alexandre, P. Degée and P. Dubois, *Macromol. Mater. Eng.*, 2008, **293**, 581-588.

194. S. Maier, T. Loontjens, B. Scholtens and R. Mülhaupt, *Macromolecules*, 2003, **36**, 4727-4734.

195. S. Maier, T. Loontjens, B. Scholtens and R. Mülhaupt, *Angew. Chem. Int. Ed.*, 2003, **42**, 5094-5097.

196. T. Loontjens, *J. Polym. Sci., Part A: Polym. Chem.*, 2003, **41**, 3198-3205.

197. F. Xiang, T. Loontjens, E. Geladé and J. Vorenkamp, *Macromol. Chem. Phys.*, 2012, **213**, 1841-1850.

198. F. Xiang, M. Stuart, J. Vorenkamp, S. Roest, H. Timmer-Bosscha, M. C. Stuart, R. Fokkink and T. Loontjens, *Macromolecules*, 2013, **46**, 4418-4425.

# Chapter 2

# The Preparation and Characterisation of Novel Diketopiperazines and Their Use as Chain Extenders in Thermoplastic Polyurethane Elastomers

## 2.1 Introduction

Polyurethanes (PUs) have, for some time, been used in implants because of their compatibility with the human tissue and their desirable mechanical properties but have been susceptible to premature failure. It was discovered that the reason for such premature failure was their susceptibility to degradation by enzymes and hydrolysis.[1] Recent research has focussed on utilising this apparent susceptibility to design intentionally degradable elastomeric materials.[2-8]

As previously discussed, PUs have an easily modifiable segmented structure that can be tuned to a desired application. They are synthesised by the reaction of a polyol, a diisocyanate and a low molecular weight diol known as a chain extender, *via* step-growth polymerisation. Originally, functional polymers such as esters, amides, ethers and carbonates were used in the soft segment. An example of this was using poly(ε-caprolactone) (PCL), a semi-crystalline and hydrophobic polyester, as a biomaterial because of its low toxicity and reported degradation of between one and two years *in vivo*.[9-12] Furthermore, the use of more bio-based chain extenders, rather than a traditional petroleum derived 1,4-butanediol (BDO) chain extender, that does not possess any hydrolytically or enzymatically degradable bonds, gives further control over the breakdown of the material. The use of amino acid-based chain extenders has been of great interest because of their increased susceptibility to degradation and their non-toxic by-products. A variety of amino acid-based chain extenders have been reported including: single amino acids,[13] tripeptides,[14-16] diesters,[17] diamines[18] and peptide sequences of amino acid residues.[19] Efforts have also been made to tune peptide sequences to a specific enzyme, such as elastase, by, for instance, incorporating *L*-alanine-*L*-alanine-*L*-lysine into the chain extender.[20,21] It has also been reported that blending amino acid-based PUs opens up greater control over the degradative and mechanical properties of the final material.[22]

The cyclic dipeptides of amino acids, known as diketopiperazines (DKPs), are small, constrained heterocyclic molecules that possess two chiral centres and stereochemistry through multiple conformations. DKPs have two *cis*-amide bonds

that present two hydrogen bond acceptors and two hydrogen bond donor sites. These intermolecular interactions aid the crystallisation of the hard segment of the polyurethane and affect their physical properties[23]. DKPs have also been shown to have a large array of biological activity such as antibacterial and antiviral properties, thus rendering them ideal candidates for use in biomaterials.[24,25] However, the low-solubility and the need for protecting group chemistries required to access the DKPs can result in multi-step syntheses. Some DKPs can be produced through dehydration cyclisation reactions such as *L*-phenylalanine and *L*-tyrosine. **(Scheme 2.1)** The incorporation of tyrosine diketopiperazine (TDKP) into a thermoplastic polyurethane elastomer (TPUE), resulted in an elastomeric and degradable biomaterial with a high glass transition ($T_g$) for the hard segment (195 °C as determined by DMA).[26]

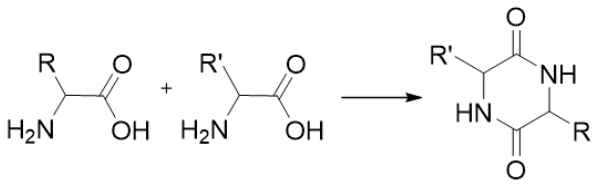


**Scheme 2.1 Formation of TDKP by dehydration cyclisation.**

Alternatively, post-cyclisation functionalisation can provide an alternative route to bio-based chain extenders and open-up greater control over mechanical, thermal and degradative properties, simply by varying the hard segment composition. Further coupling reactions should allow increased degradable links and functionality within the chain extender to be incorporated in the hard segment of the polyurethane. This chapter sets out the synthesis and post-cyclisation functionalisation of glutamic acid DKP, in chain extenders of TPUEs, which was directly compared to a TDKP-based TPUE. Further to this, a blend material was synthesised with a view to opening-up greater control over the mechanical, thermal and degradative properties by combining the characteristics from each homopolymer TPUE. Such materials were studied to gain further understanding of the structure-function relationship of the family of DKP-based TPUEs.

## 2.2 Results and Discussion

Each chain extender required the formation of a DKP and subsequent coupling reactions were used to introduce more degradable links and chosen functionality, apart from in the TDKP. The TPUEs were synthesised *via* a one-pot, two-step prepolymer method to ensure a relatively controlled hard and soft segment distribution within the polymer chain. **(Scheme 2.2)**

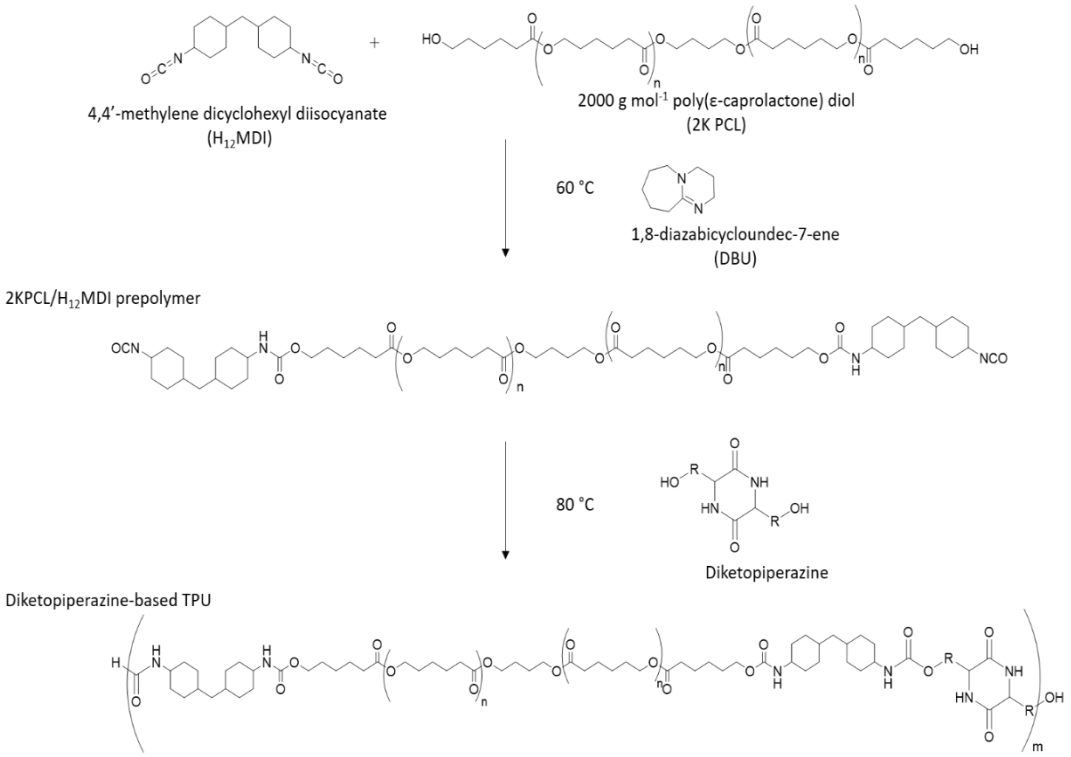


**Scheme 2.2 PU synthesis *via* a one-pot two-step prepolymer method.**

### 2.2.1 Synthesis of (3*S*,6*S*)-3,6-bis(4-hydroxybenzyl)piperazine-2,5-dione

(3*S*,6*S*)-3,6-bis(4-hydroxybenzyl)piperazine-2,5-dione (tyrosine diketopiperazine, TDKP) can be formed by microwave radiation.[27] The cyclisation reactions of amino acids often result in both symmetrical and unsymmetrical products, side reactions and low yields. However, Stevenson and Moye-Sherman demonstrated in their patent that phosphorus pentoxide ($P_2O_5$) was effective at catalysing the dehydrative cyclocondensation reaction to form the DKP of *L*-phenylalanine, in *m*-cresol solvent,

with a yield up to 80%.[28] These conditions were applied to *L*-tyrosine and were found to be effective in forming TDKP, by simply increasing the reaction time. **(Scheme 2.3)**

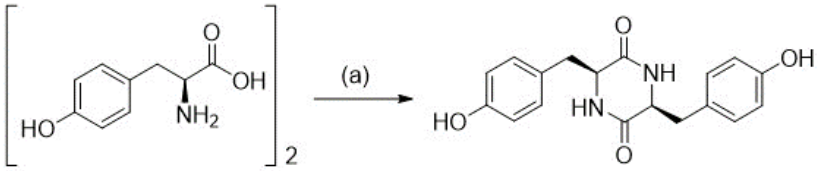


(a) m-cresol, $P_2O_5$, 200 °C, 8 h, 85% yield.

**Scheme 2.3 Formation of TDKP.**

The progress of the cyclisation reaction was monitored by *in situ* $^1$H NMR spectroscopy experiments. In the 3 h *in situ* $^1$H NMR spectrum a mixture of linear and cyclic DKPs co-existed. This was observed by two sets of aromatic resonances and bridging methylene resonances next to the aromatic ring. By 8 h the cyclisation was complete and confirmed by the *in situ* $^1$H NMR spectrum, which showed discrete aromatic resonances between $\delta$ = 6.94 ppm and 6.55 ppm and a single amide resonance at $\delta$ = 7.94 ppm. In addition, a single tertiary methine resonance was detected at $\delta$ = 3.30 ppm together with a single bridging methylene resonance, with a large multiplet, between $\delta$ = 2.97 ppm and 2.55 ppm. The reaction products were isolated by being washed with water and methanol (50:50 mixture) and were then dissolved in deuterated dimethyl sulfoxide (DMSO-$d_6$) for the $^1$H NMR spectroscopic experiments. **(Figure 2.1)**

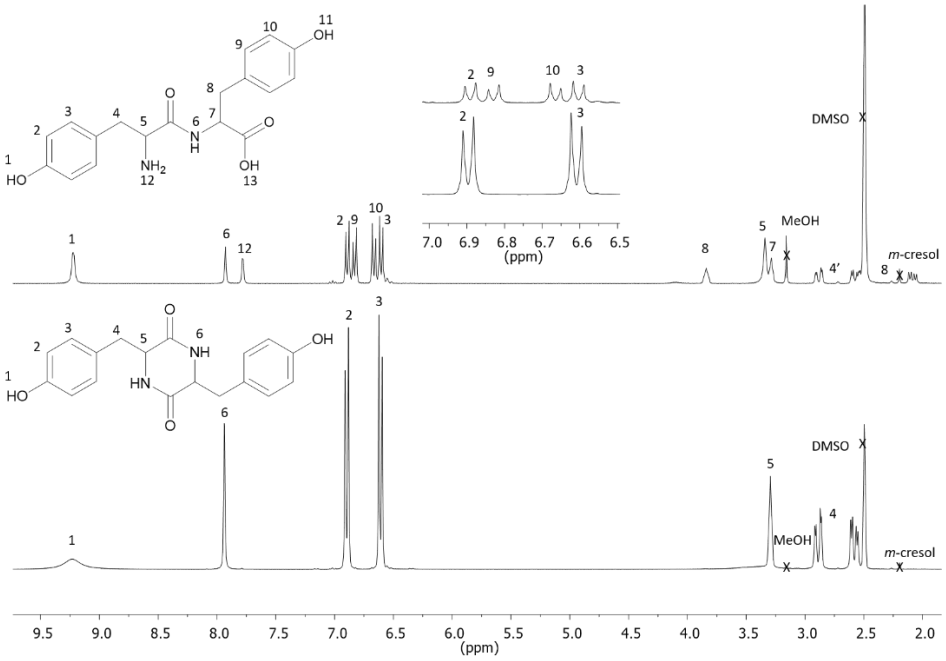


**Figure 2.1** ***In situ*** **$^1$H NMR spectra for the cyclisation reaction of TDKP after 3 h (top) and 8 h (bottom) (400 MHz, 298 K, DMSO-$d_6$).**

## 2.2.2 Synthesis of 3,3'-((2*S*,5*S*)-3,6-dioxopiperazine-2,5-diyl)dipropionic acid

3,3'-((2*S*,5*S*)-3,6-dioxopiperazine-2,5-diyl)dipropionic acid (glutamic acid diketopiperazine, GDKP) was chosen to further extend the family of DKP chain extenders, as it can be accessed without protecting group chemistry. It also has two free carboxylic acid functional groups that remain after cyclisation, which can facilitate further coupling reactions to increase degradable links and functionalisation in the chain extender. Parrish and Mathias[29] reported that to obtain GDKP, the synthesis required adding *S*-pyroglutamic acid to a refluxing mixture of acetic anhydride and pyridine to form the tricyclic structure of 1,7-diazatricyclo[7.3.0.0]dodecane-2,6,8,12-tetrone (pyroglutamic diketopiperazine, PDKP). PDKP was subsequently ring opened by sulfuric acid and water to yield GDKP. **(Scheme 2.4)**

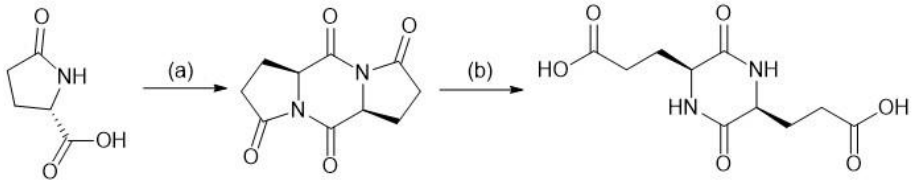


(a) acetic anhydride, pyridine, 110 °C, 1 h, 43% yield; (b) $H_2SO_4$, $H_2O$, 0 °C, 1 h, 89% yield.

**Scheme 2.4 Formation of GDKP.**

The $^1$H NMR spectra showed a large multiplet for each of the methylene resonances for all the cyclic structures and these were retained throughout the synthetic procedure. This was because of the chirality within the ring structures. The formation of PDKP from *s*-pyroglutamic acid was observed by the shift of the tertiary methine resonance from $\delta$ = 4.01 ppm to 4.85 ppm, the loss of the carboxylic acid resonance at $\delta$ = 12.75 ppm and the loss of the lactam amide resonance at $\delta$ = 7.90 ppm. The $^1$H NMR spectrum of GDKP showed a shift of the tertiary methine peak from $\delta$ = 4.85 ppm to 3.85 ppm and the reformation of the carboxylic acid and lactam amide peaks at $\delta$ = 12.15 ppm and $\delta$ = 8.20 ppm respectively. **(Figure 2.2)**

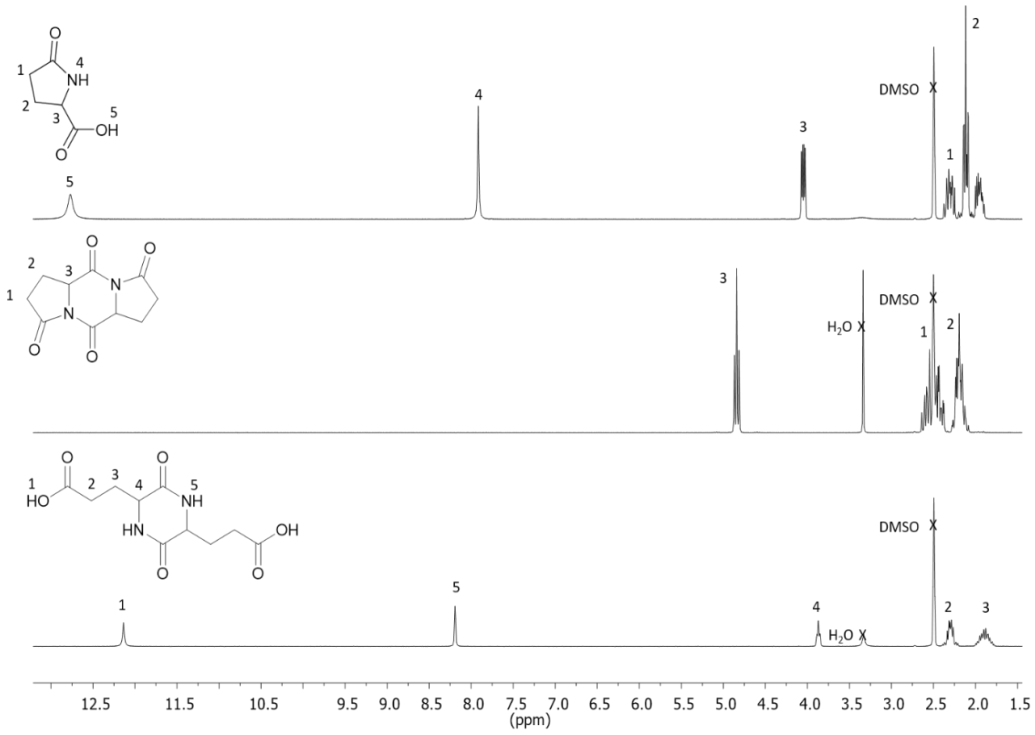


**Figure 2.2 $^1$H NMR spectra for *s*-pyroglutamic acid (top) PDKP (middle) and GDKP (bottom) (400 MHz, 298 K, DMSO-$d_6$).**

### 2.2.3 Synthesis of bis4-hydroxymethylbenzyl-3,3'-((2*S*,5*S*) -3,6-dioxopiperazine-2,5-diyl) dipropionate

As outlined previously, TDKP was the initial benchmark TPUE for this work.[26] To introduce more degradable links into the chain extender, the first target was to increase the ester content in the hard segment of the TPUE as ester links are very susceptible to hydrolytic and enzymatic degradation making them ideal candidates for biodegradable materials.

#### 2.2.3.1 Synthesis of 4-(chloromethyl)benzyl alcohol

4-(chloromethyl)benzyl alcohol is the ideal precursor required for esterification of GDKP. This molecule was accessed by the selective chlorination of 1,4-benzenedimethanol by charging a 1.1 molar equivalent of thionyl chloride in chloroform.[30] **(Scheme 2.5)**

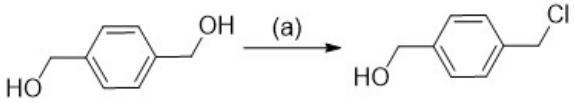


(a) thionyl chloride, chloroform, 0 °C, 2 h, 94% yield.

**Scheme 2.5 Formation of 4-(chloromethyl)benzyl alcohol.**

The $^{1}$H NMR spectrum of 4-(chloromethyl)benzyl alcohol showed the same alcohol resonance as 1,4-benzenedimethanol at $\delta$ = 5.22 ppm. However, most notably, a new singlet methylene resonance appeared at $\delta$ = 4.75 ppm alongside the existing doublet methylene resonance at $\delta$ = 4.47 ppm. This new resonance corresponds to the methylene next to the new chloro-group. **(Figure 2.3)**

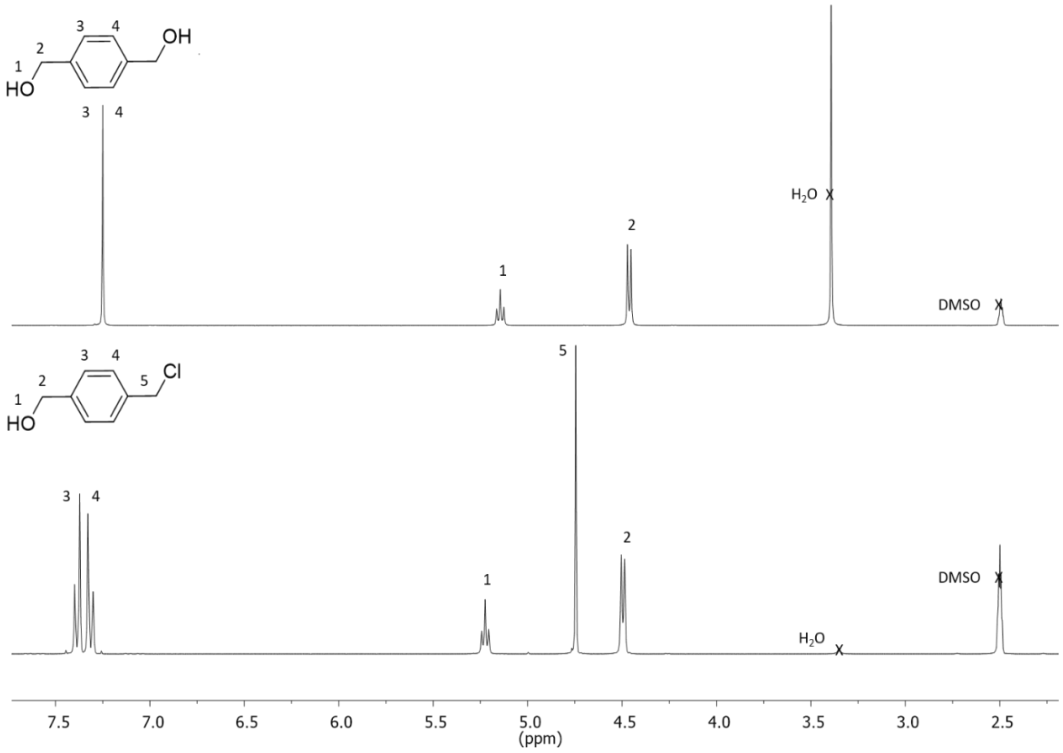


**Figure 2.3 $^{1}$H NMR spectra for 1,4-benzenedimethanol (top) and 4-(chloromethyl)benzyl alcohol (bottom) (400 MHz, 298 K, DMSO-$d_6$).**

4-(chloromethyl)benzyl alcohol was then used for the base catalysed esterification of GDKP. A variety of different bases were screened including potassium carbonate, potassium hydroxide, 4-dimethylaminopyridine (DMAP) and triethylamine ($NEt_3$). $NEt_3$ was the only base to effectively catalyse the reaction, which yielded bis4-hydroxymethylbenzyl-3,3'-((2*S*,5*S*)-3,6-dioxopiperazine-2,5-diyl)dipropionate (GDKP with an aromatic ester, GDKPAE). **(Scheme 2.6)**

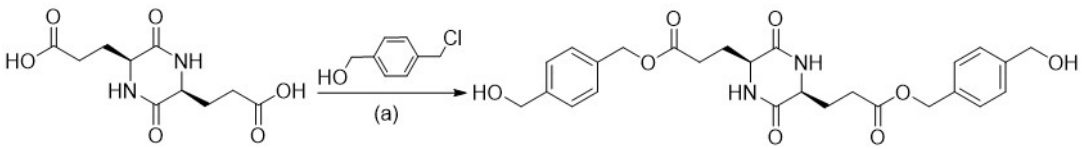


(a) $NEt_3$, DMF, 80 °C, 47% yield.

**Scheme 2.6 Formation of GDKPAE.**

The formation of GDKPAE was confirmed by the $^{1}H$ NMR spectrum, which showed the loss of the carboxylic acid resonance of GDKP at $\delta$ = 12.15 ppm, the formation of an aromatic resonance at $\delta$ = 7.31 ppm, the terminating hydroxyl triplet resonance at $\delta$ = 5.19 ppm and two methylene resonances, a singlet and doublet, at $\delta$ = 5.06 ppm and 4.49 ppm respectively. Further to this the $^{13}C$ NMR spectrum showed the formation of an ester carbonyl resonance at $\delta$ = 173 ppm, the evolution of two methylene resonances at $\delta$ = 66 ppm and 63 ppm and four aromatic resonances at $\delta$ = 143 ppm, 135 ppm, 128 ppm and 127 ppm. **(Figure 2.4)**

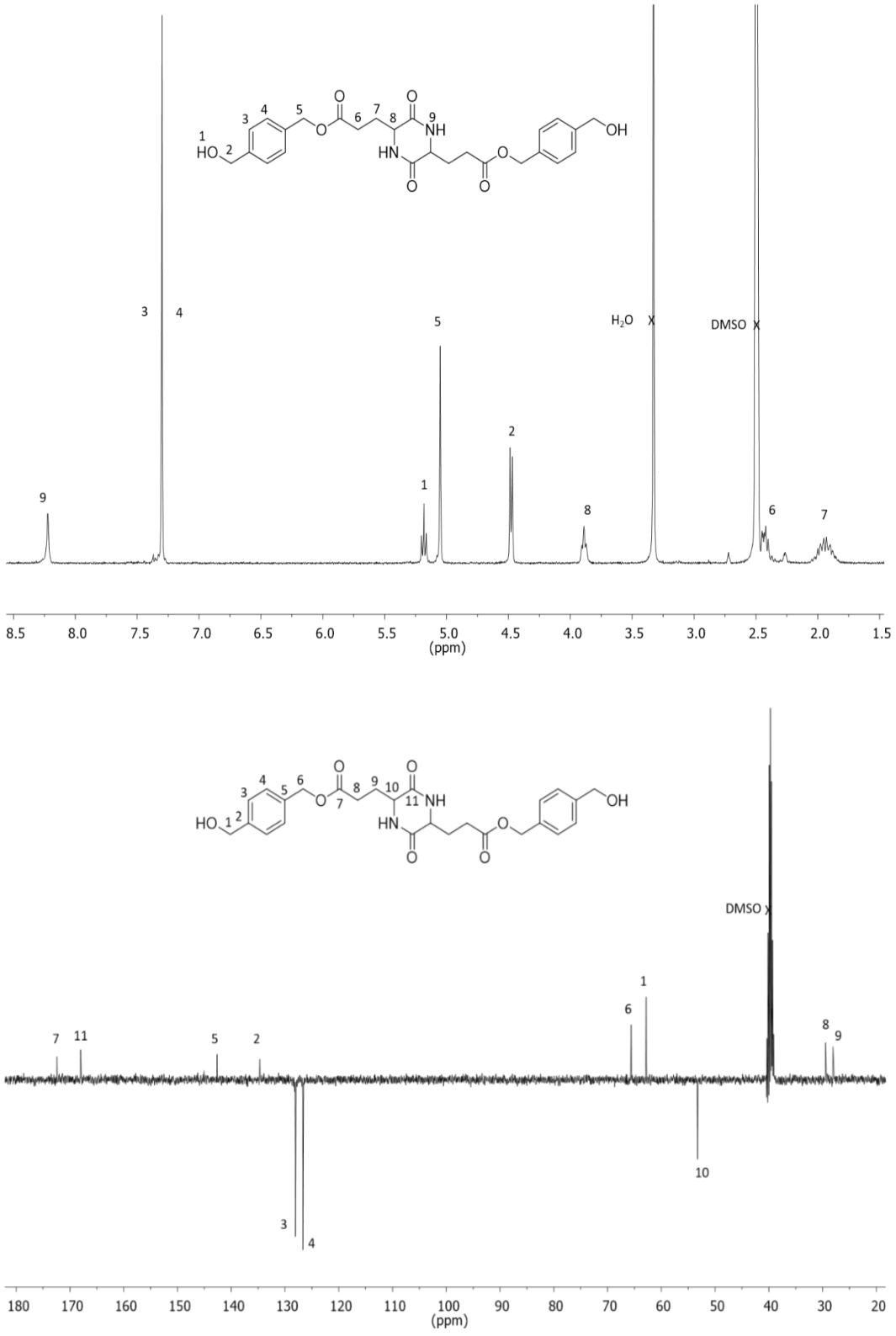


**Figure 2.4 $^{1}$H (*top*) and $^{13}$C (*bottom*) NMR spectra of GDKPAE (400 and 125 MHz, 298 K, DMSO-$d_6$).**

### 2.2.4 Synthesis of 3,3'-((2*S*,5*S*)-3,6-dioxopiperazine-2,5-diyl)bisN-4 -hydroxymethylbenzyl propanamide

3,3'-((2*S*,5*S*)-3,6-dioxopiperazine-2,5-diyl)bisN-4-hydroxymethylbenzyl propanamide (GDKP with an aromatic amide, GDKPAA) was then targeted to compare the effect of increased amide content on mechanical properties, the rate of degradation and to allow access to a broader range of materials. It was hypothesised that GDKPAA-based TPUEs would be stronger, because of the increased hydrogen bonding sites, and less susceptible to hydrolytic degradation relative to GDKPAE-based TPUEs.

#### 2.2.4.1 Synthesis of 4-(aminomethyl)benzyl alcohol

The precursor required for amidation of GDKP is 4-(aminomethyl)benzyl alcohol. Two synthetic pathways were considered for 4-(aminomethyl)benzyl alcohol. The first pathway was by reduction by lithium aluminium hydride ($LiAlH_4$) in tetrahydrofuran (THF) of the commercially available methyl 4-cyanobenzoate to 4-(aminomethyl)benzyl alcohol as reported by Dogan *et al*.[31] It was noted that methyl 4-cyanobenzoate is an expensive precursor, thus a second synthetic pathway with an inexpensive commercially available precursor of 4-(aminomethyl)benzoic acid was investigated. This second pathway involved the esterification of the carboxylic group on the 4-(aminomethyl)benzoic acid by combining it with thionyl chloride and methanol, which resulted in a near-quantitative yield of methyl 4-(aminomethyl)benzoate and this was subsequently reduced by $LiAlH_4$ in THF to produce 4-(aminomethyl)benzyl alcohol. **(Scheme 2.7)**

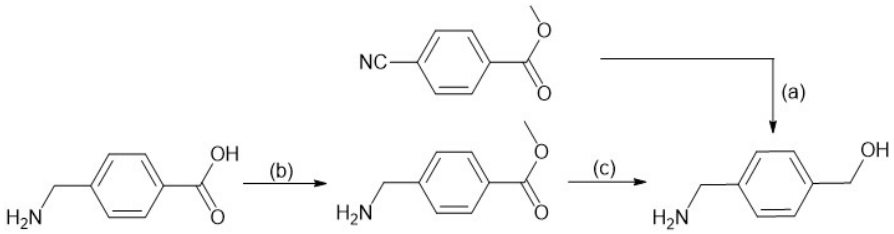


(a) $LiAlH_4$, THF, 0 °C, 85% yield. (b) $SOCl_2$, methanol, 98% yield; (c) $LiAlH_4$, THF, 0 °C, 55% yield.

**Scheme 2.7 Formation of 4-(aminomethyl)benzyl alcohol.**

The first pathway of converting methyl 4-cyanobenzoate to 4-(aminomethyl)benzyl alcohol was tracked by $^1H$ NMR spectroscopy and Fourier-Transform infrared

spectroscopy (FT-IR). The $^{1}$H NMR spectrum showed the loss of the methyl ester resonance at $\delta$ = 3.90 ppm, the formation of two methylene resonances at $\delta$ = 4.47 ppm and 3.68 ppm and the formation of broad amine and alcohol resonances at $\delta$ = 3.10 ppm and 4.10 ppm respectively. **(Figure 2.5)**

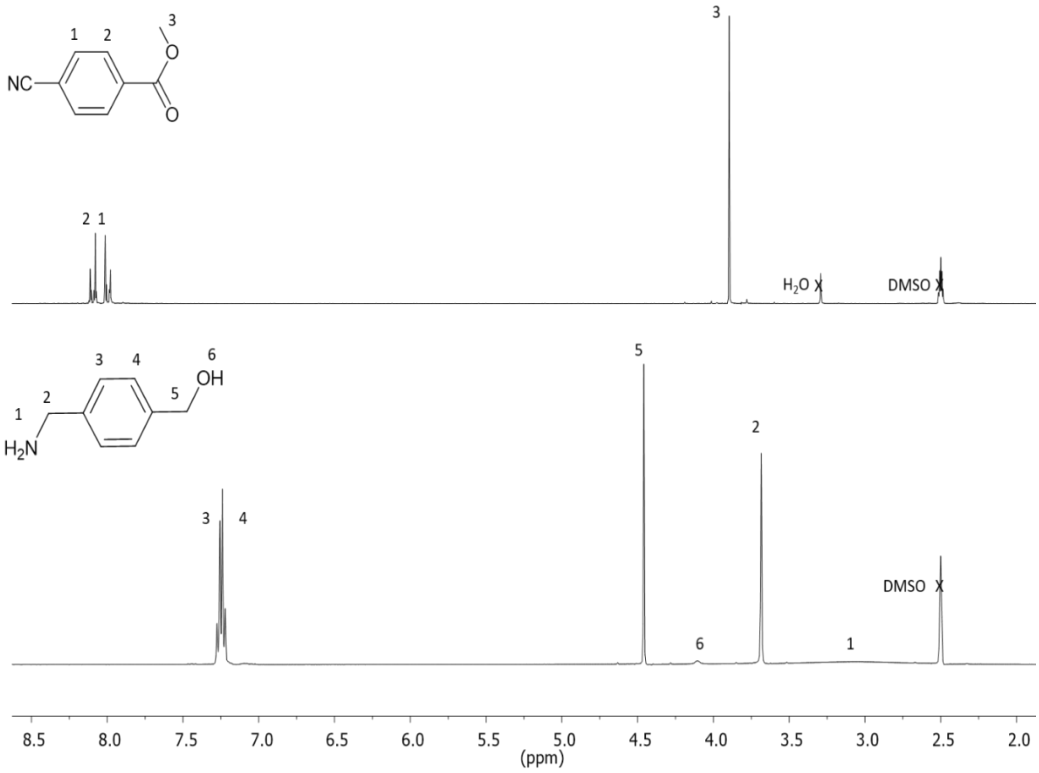


**Figure 2.5 $^{1}$H NMR spectra of methyl 4-cyanobenzoate (*top*) and 4-(aminomethyl)benzyl alcohol (*bottom*) (400 MHz, 298 K, DMSO-$d_6$).**

The FT-IR spectrum also showed the change in the functionality. For 4-(aminomethyl)benzyl alcohol the nitrile and carbonyl absorption peaks for methyl 4-cyanobenzoate at *c.a.* $\nu$ = 2,200 cm$^{-1}$ and *c.a.* $\nu$ = 1,700 cm$^{-1}$ receded, amine absorption peaks appeared at *c.a.* $\nu$ = 3,300 cm$^{-1}$ and *c.a.* $\nu$ = 1,600 cm$^{-1}$ and an alcohol absorption peak appeared at *c.a.* $\nu$ = 3,400 cm$^{-1}$. **(Figure 2.6)**

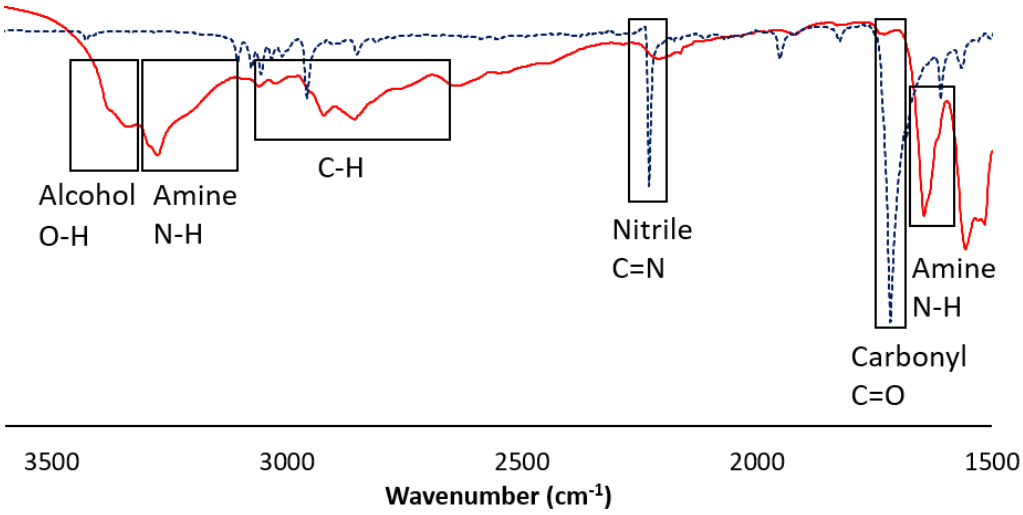


**Figure 2.6 FT-IR spectra of methyl 4-cyanobenzoate (*blue*) and 4-(aminomethyl)benzyl alcohol (*red*).**

The second pathway of converting of 4-(aminomethyl)benzoic acid to 4-(aminomethyl)benzyl alcohol was also observed using $^{1}$H NMR spectroscopy and the formation of a methyl group on the ester resonance at $\delta$ = 4.12 ppm was noted. The methyl 4-(aminomethyl)benzoate was then reduced under the same conditions as the methyl 4-cyanobenzoate and significant changes were observed in the $^{1}$H NMR spectrum. A methylene resonance was observed at $\delta$ = 4.54 ppm next to an alcohol resonance at $\delta$ = 4.10 ppm. **(Figure 2.7)**

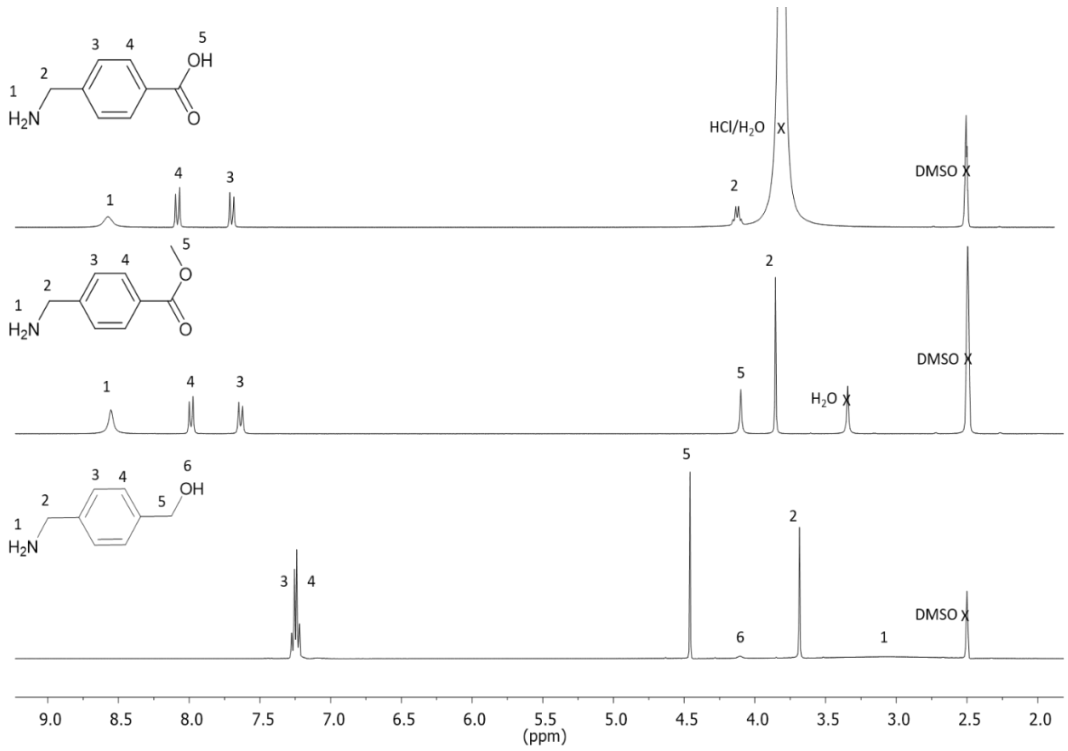


**Figure 2.7 $^{1}$H NMR spectra of 4-(aminomethyl)benzoic acid (*top*), methyl 4-(aminomethyl)benzoate (*middle*) and 4-(aminomethyl)benzyl alcohol (*bottom*) (400 MHz, 298 K, DMSO-$d_6$).**

An activated ester was formed by reacting GDKP with *N*-hydroxysuccinimde (NHS), using DMAP as a catalytic base in *N,N'*-dimethylformamide (DMF). The reaction then proceeded with the addition of 1-ethyl-3-(3-dimethylaminopropyl)carbodiimide (EDC) and 4-(aminomethyl)benzyl alcohol, which yielded GDKPAA. **(Scheme 2.8)**

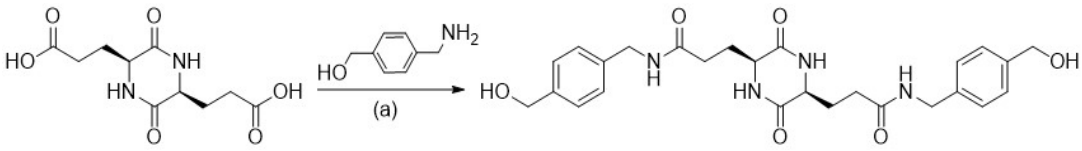


(a) NHS, EDC, DMAP, DMF, R.T, 50% yield.

**Scheme 2.8 Formation of GDKPAA.**

$^{1}$H NMR spectroscopy was used to confirm the formation of GDKPAA with the loss of the carboxylic acid proton resonance of GDKP at $\delta$ = 12.15 ppm, the formation of the amide resonance at $\delta$ = 8.30 ppm, the evolution of an aromatic proton resonance range at $\delta$ = 7.35 ppm to 7.21 ppm and a terminal hydroxyl triplet resonance at $\delta$ = 5.12 ppm. In addition, the two methylene resonances were observed to shift upfield to $\delta$ = 4.45 ppm and 4.22 ppm respectively; a characteristic of amide bond formation. The $^{13}$C NMR spectrum further complimented the characterisation of GDKPAA showing two carbonyl resonances at $\delta$ = 172 ppm and 168 ppm and two methylene resonances either side of the aromatic ring at $\delta$ = 63 ppm and 42 ppm. **(Figure 2.8)**

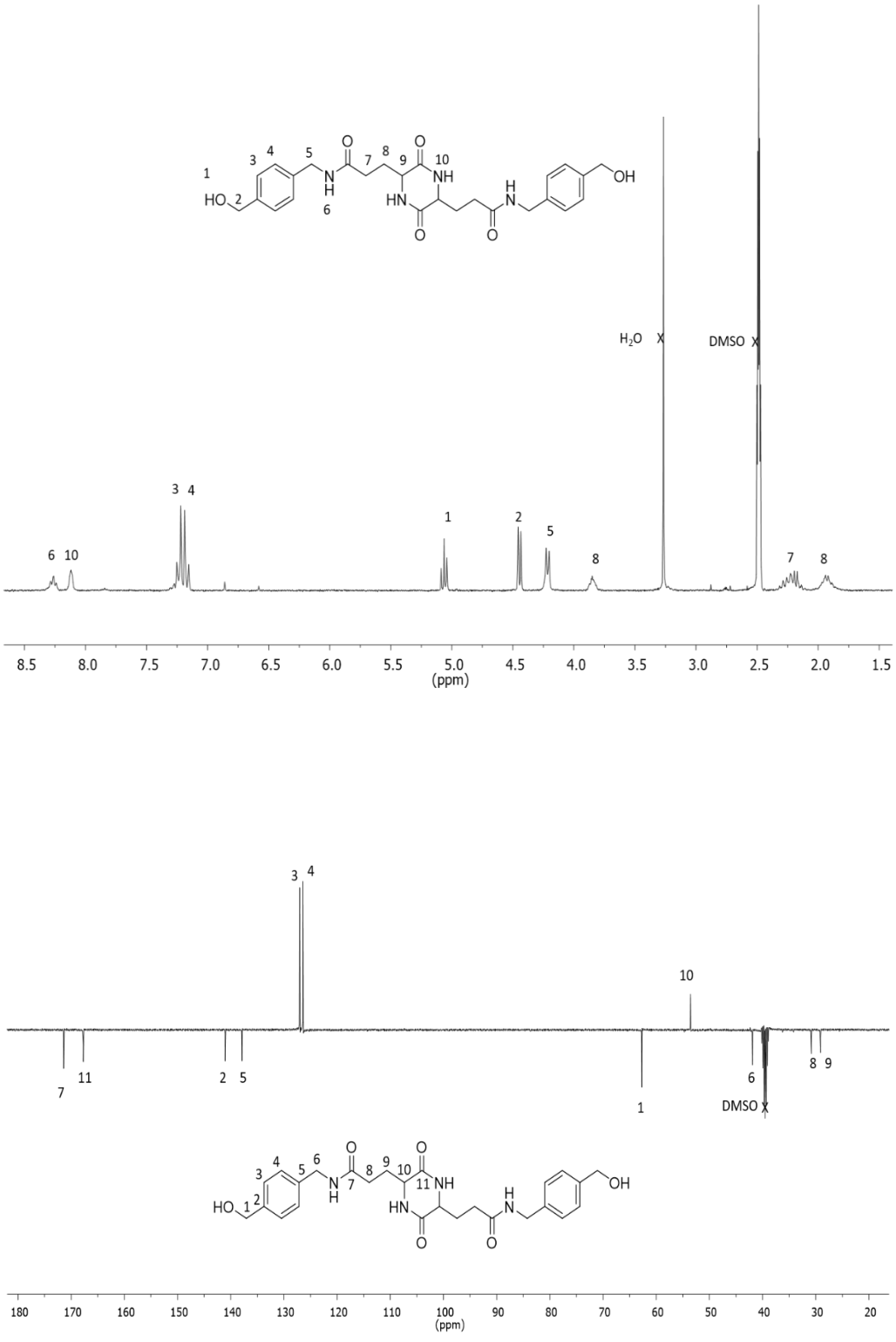


**Figure 2.8 $^{1}$H NMR(*top*) and $^{13}$C NMR (*bottom*) spectra of GDKPAA (400 and 125 MHz, 298 K, DMSO-$d_6$).**

### 2.2.5 Organocatalysed step-growth polymerisation of novel diketopiperazines as chain extenders in thermoplastic polyurethane elastomers

It is possible to produce relatively controlled segmented TPUEs by the one-pot, two-step prepolymer method. This synthetic route involved the formation of a prepolymer using a PCL diol with a $M_w$ = 2,000 gmol$^{-1}$ as determined by SEC (2K-PCL) and 4,4'-methylenebis(cyclohexyl isocyanate) ($H_{12}$MDI). The 2K-PCL/$H_{12}$MDI prepolymer was then added to the chain extender to form the TPUE. **(Scheme 2.9)**

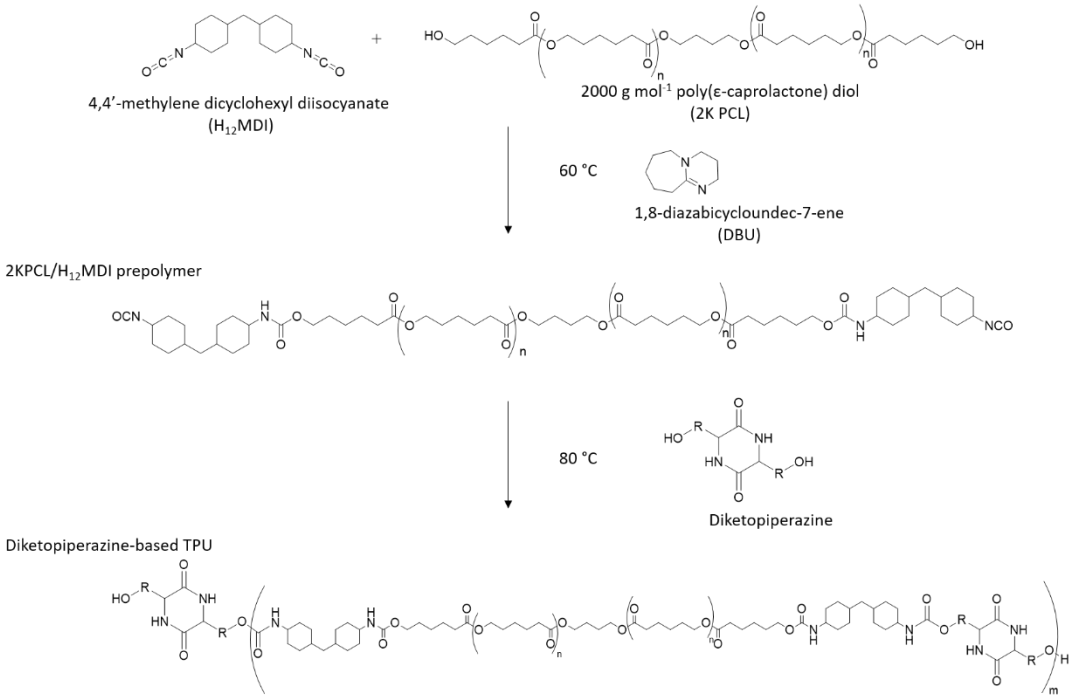


**Scheme 2.9 One-pot, two-step, organocatalysed step-growth polymerisation using DKPs.**

The mole ratio (R) of $H_{12}$MDI to 2K-PCL was calculated for TPUEs with targeted hard segment percentages (%HS) of 30, 45 and 60 using equation **(2.1 below)**[32] as set out below, where $M_{ce}$, $M_{di}$ and $M_{po}$ are the mole average molecular weights of the DKP chain extender, $H_{12}$MDI and 2K-PCL respectively.

$$\%\mathrm{HS} = \frac{100(\mathrm{R}-1)(M_{\mathrm{ce}}+M_{\mathrm{di}})}{(M_{\mathrm{po}}+\mathrm{R}(M_{\mathrm{di}})+(\mathrm{R}-1)(M_{\mathrm{ce}}))} \qquad (2.1)$$

A range of mechanical, thermal and degradative properties were achieved by varying the level of %HS and the type of DKP chain extender in the TPUEs. Owing to its inherently low toxicity *in vivo* in comparison to conventional tin-based catalysts, 1,8-diazabicyclo[5.4.0]undec-7-ene (DBU)[33] was employed for the step-growth polymerisation at 5 mol% according to the 2K-PCL component. The polymerisation of a TPUE with GDKPAE chain extenders (GDKPAE-TPUE) was effectively monitored by FT-IR spectroscopy showing the peak at, corresponding to the NCO group within the $H_{12}$MDI had reduced to *c.a.* $\nu$ = 2,200 $cm^{-1}$, the loss of the alcohol peak at *c.a.* $\nu$ = 3,600 $cm^{-1}$ and the formation of a (C=O) urethane peak at *c.a.* $\nu$ =1,650 $cm^{-1}$ and (N-H) peaks at *c.a.* $\nu$ =3,300 $cm^{-1}$ and 1,600 $cm^{-1}$. **(Figure 2.9)**

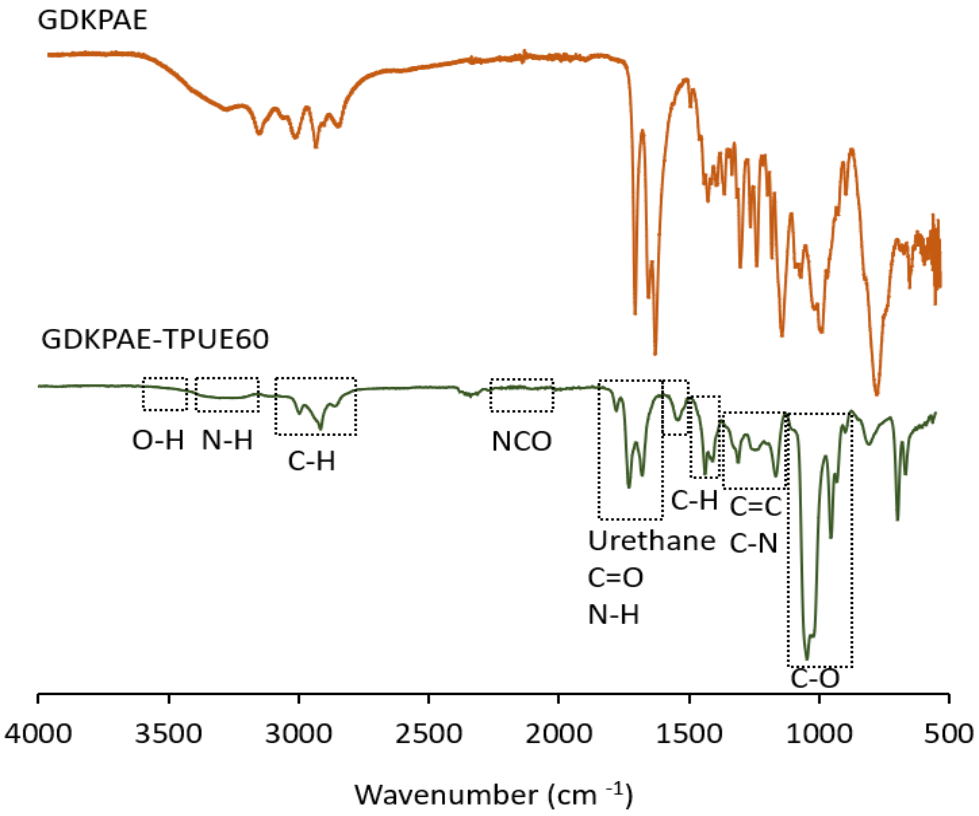


**Figure 2.9 FT-IR spectra of GDKPAE (*top*) and a GDKPAE-TPUE (*bottom*).**

The resulting GDKPAE-TPUEs were analysed by size exclusion chromatography (SEC) that showed them to have $M_w$ of 30,000 g mol$^{-1}$, 39,000 g mol$^{-1}$ and 12,300 g mol$^{-1}$ for a GDKPAE-TPUE with targeted 30%HS (GDKPAE-TPUE30), a GDKPAE-TPUE with targeted 45%HS (GDKPAE-TPUE45) and a GDKPAE-TPUE with targeted 60%HS (GDKPAE-TPUE60) respectively. **(Table 2.1)** The $Đ_M$ values for these TPUEs are higher than expected ($Đ_M$ = 2.75, 3.42 and 3.16 respectively), which was a result of an incomplete polymerisation as some residual PCL remained in all the experiments. This PCL species is likely an $H_{12}$MDI-PCL-$H_{12}$MDI polymer as its $M_w$ of 2,500 g mol$^{-1}$ is larger than the $M_w$ of 2,000 g mol$^{-1}$ of the 2K-PCL diol starting material and the alcohol chain ends of the 2K-PCL diol are not visible on the $^1$H NMR spectra of the TPUEs. Furthermore, it was noted that the $Đ_M$ of the GDKPAE-TPUEs increased, while the $M_w$ decreased with increasing %HS. Because of adding more high polarity GDKPAE chain extenders to increase the %HS of the GDKPAE-TPUEs the viscosity of the solution was raised, thereby hindering its linear growth. Following the incorporation of GDKPAE at different %HS, TPUEs with GDKPAA chain extenders (GDKPAA-TPUEs) with targeted 30 %HS (GDKPAA-TPUE30) and targeted 45 %HS (GDKPAA-TPUE45) were synthesised by the same method. Through SEC analysis it was observed that the resulting TPUEs had a $M_w$ of 31,000 g mol$^{-1}$ and 66,000 g mol$^{-1}$ and $Đ_M$ = 3.07 and 5.67 respectively. Further to this, a TPUE with a blend of GDKPAE and GDKPAA chain extenders with a targeted 50:50 molar blend a 30 %HS was also produced (GDKPAE/GDKPAA-TPUE30), which combined the two chain extenders at the point of synthesis and the resulting TPUE had a molecular weight of 16,000 g mol$^{-1}$ and $Đ_M$ = 2.58. This blend material is expected to open up greater control over the mechanical, thermal and degradative properties, combining the material properties from the GDKPAE and the GDKPAA homo-TPUEs. **(Figure 2.10 and Table 2.1)**

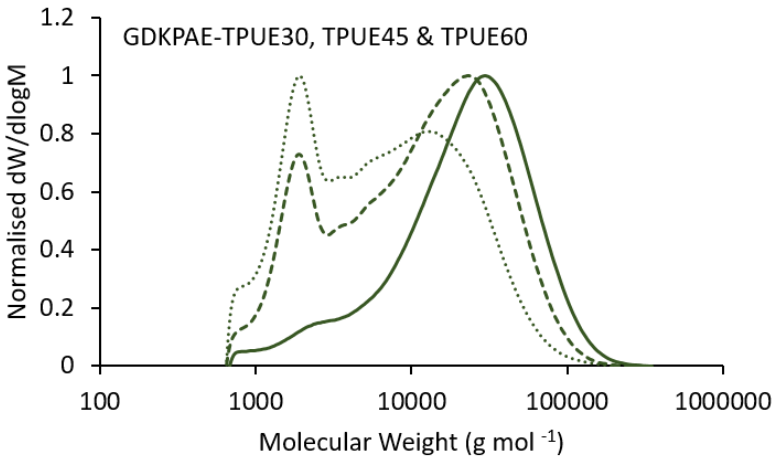


GDKPAE-TPUE30 (solid), GDKPAE-TPUE45 (dashed) and GDKPAE-TPUE60 (dotted)

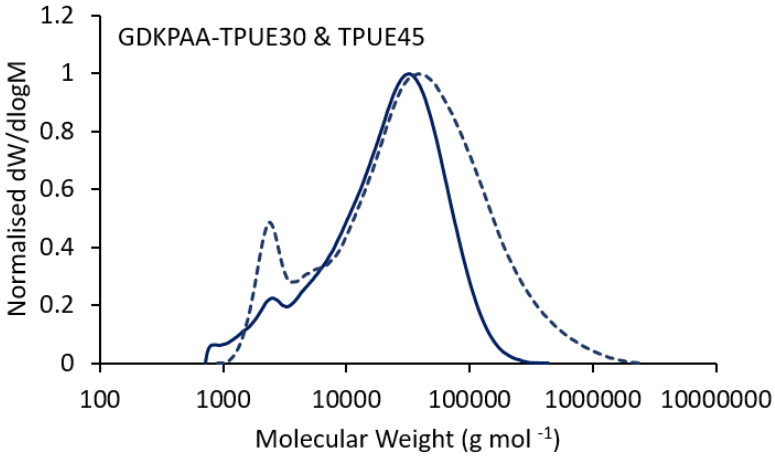


GDKPAA-TPUE30 (solid), GDKPAA-TPUE45 (dashed)

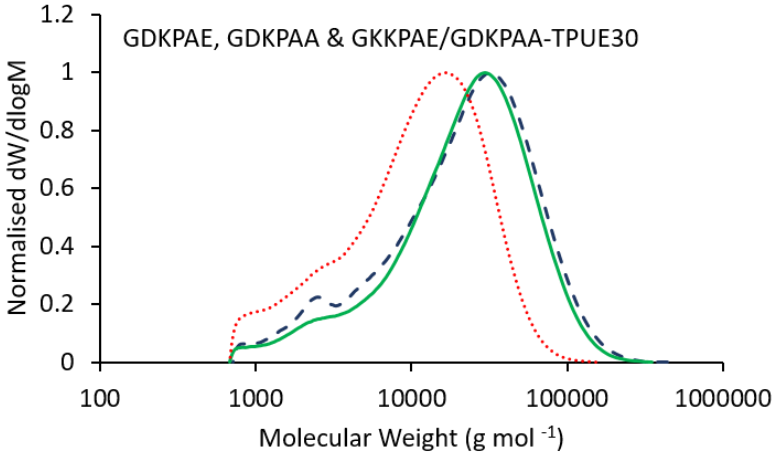


GDKPAE-TPUE30 (solid), GDKPAA-TPUE30 (dashed) and GDKPAE/GDKPAA-TPUE30 (dotted)

**Figure 2.10 SEC chromatograms of GDKPAE-TPUEs (*top*), GDKPAA-TPUEs (*middle*) and comparing GDKPAE, GDKPAA and GDKPAE/GDKPAA-TPUE30s (*bottom*) in DMF against PMMA standards.**

**Table 2.1 SEC data for GDKPAE-TPUEs, GDKPAA-TPUEs and a GDKPAE/GDKPAA-TPUE30.**

| Polymer | Targeted %HS | *Observed %HS*[a] | 2K-PCL/ $H_{12}$MDI ratio (R)[b] | $M_w$ (g $mol^{-1}$)[c] | $M_n$ (g $mol^{-1}$)[c] | $Đ_M$[b] |
|---|---|---|---|---|---|---|
| GDKPAE-TPUE30 | 30 | 15 | 2.27 | 30,400 | 11,100 | 2.75 |
| GDKPAE-TPUE45 | 45 | 16 | 3.43 | 39,000 | 19,000 | 3.42 |
| GDKPAE-TPUE60 | 60 | 20 | 5.46 | 12,300 | 3,900 | 3.16 |
| GDKPAA-TPUE30 | 30 | 13 | 2.28 | 31,000 | 10,100 | 3.07 |
| GDKPAA-TPUE45 | 45 | 16 | 3.44 | 66,400 | 12,000 | 5.67 |
| GDKPAE/ GDKPAA-TPUE30 | 30 | 18 (10/8) | 2.28 | 16,000 | 6,200 | 2.58 |
| TDKP TPUE30 | 30 | 15 | 2.65 | 31,000 | 14,000 | 7.62 |

a) Determined by $^1$HNMR analysis b) Determined by equation 2.1 c) Determined by SEC analysis in DMF against poly(methyl methacrylate) (PMMA) standard

The final composition of the GDKPAE-TPUEs was confirmed using $^1$H NMR and FT-IR spectroscopy. It was found by $^1$H NMR spectroscopy that the resonances of the 2K-PCL soft segment were at $\delta$ = 3.97 ppm, 2.26 ppm, 1.55 ppm and 1.29 ppm and it was noted that these decreased as the hard segment increased. At the same time, the amide resonance of the chain extender at $\delta$ = 8.31 ppm was observed to increase when the %HS was raised, which indicated a greater incorporation of chain extenders into the final TPUEs. It was also noted that the methylene resonance at $\delta$ = 4.50 ppm and the resonance for the alcohol end group on the monomer at $\delta$ = 5.20 ppm remained in reduced amounts alongside the resonance for the methylene next to the urethane bond in the polymer at $\delta$ = 4.90 ppm, which suggests an incomplete polymerisation that is consistent with the SEC analysis. By relative integration of the reacted and unreacted residual monomer methylene peaks next to the alcohol on GDKPAE (denoted 23 and 23' respectively) it was observed that the actual %HSs were 15 % for the GDKPAE-TPUE30 (targeted 30 %) 16 % for the GDKPAE-TPUE45 (targeted 45 %) and 20 % for the GDKPAE-TPUE60 (targeted 60 %). **(Figure 2.11)**

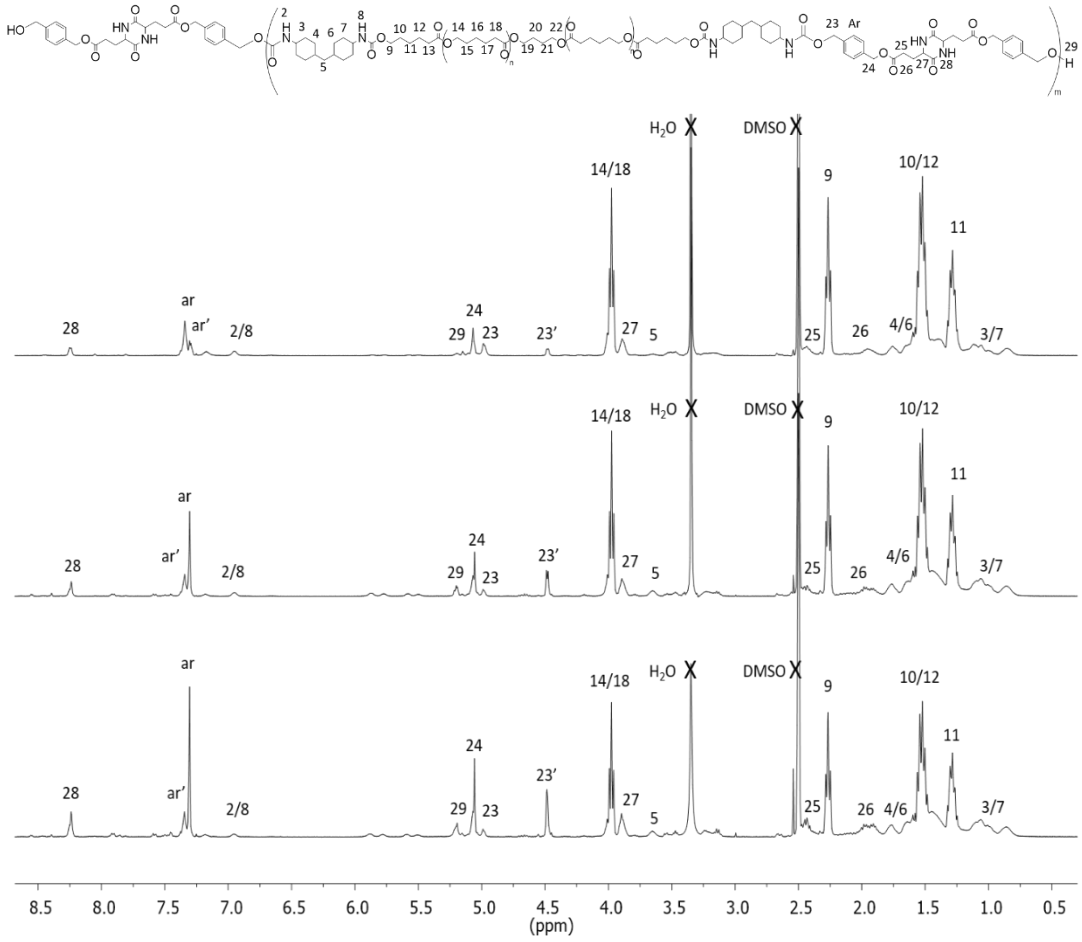


**Figure 2.11 $^{1}$H NMR spectra of GDKPAE-TPUE30 (*top*), GDKPAE-TPUE45 (*middle*) and GDKPAE-TPUE60 (*bottom*) (400 MHz, 298 K, DMSO-$d_6$).**

FT-IR spectroscopy of the GDKPAE-TPUEs showed a (C=O) urethane peak at *c.a.* $\nu$ = 1,650 cm$^{-1}$ and (N-H) peaks at *c.a.* $\nu$ = 3,300 cm$^{-1}$ and 1,600 cm$^{-1}$ respectively, as well as ester carbonyl and C-O peaks at *c.a.* $\nu$ = 1,700 cm$^{-1}$ and *c.a.* $\nu$ = 1,100 cm$^{-1}$ respectively. A comparable trend to the $^{1}$H NMR spectra was observed; it was found that the peaks corresponding to the GDKPAE chain extender increased with higher %HS. **(Figure 2.12)**

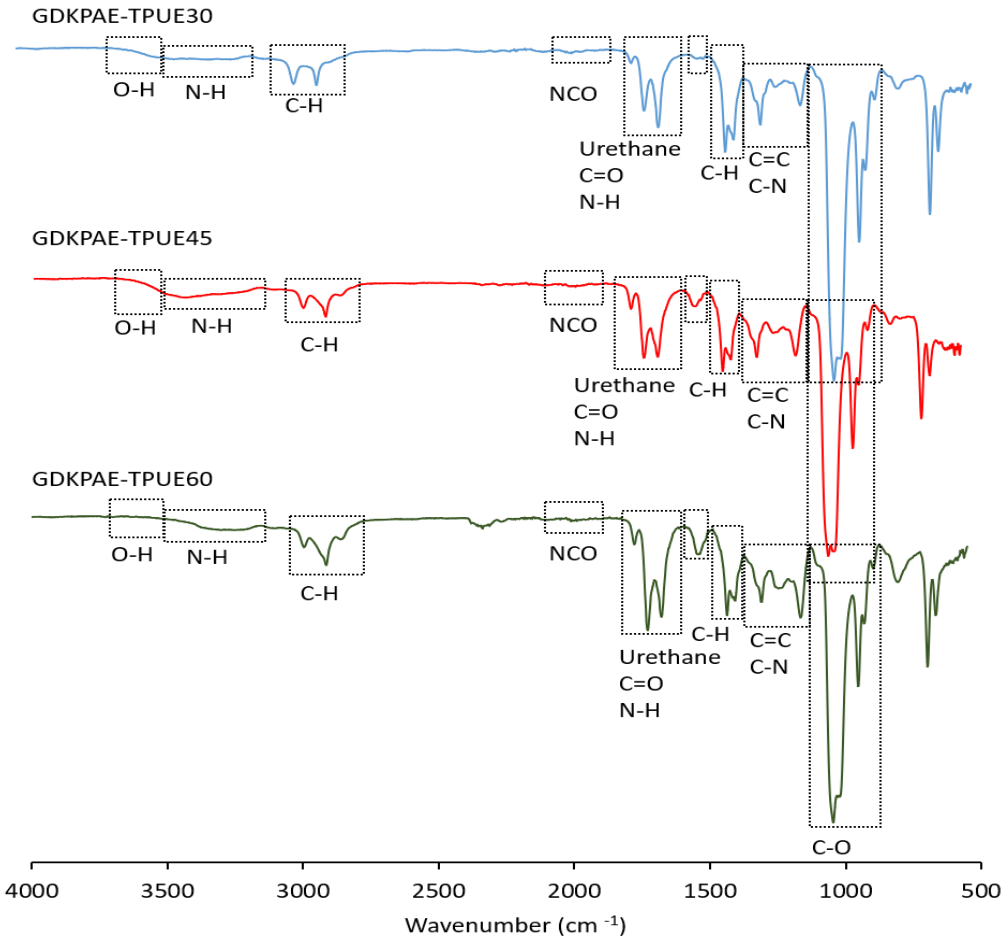


**Figure 2.12 FT-IR spectra of GDKPAE-TPUE30 (*top*), GDKPAE-TPUE45 (*middle*) and GDKPAE-TPUE60 (*bottom*).**

This trend was also observed for the GDKPAA-TPUEs, however, an additional amide resonance was observed in the $^{1}$H NMR spectrum at $\delta$ = 8.31 ppm, which corresponds to the bridging amide proton resonance that also was observed to increase with a higher %HS. As with the GDKPAE-TPUEs, the methylene resonance at $\delta$ = 4.50 ppm and resonance for the alcohol end group on the monomer at $\delta$ = 5.20 ppm remained in reduced amounts alongside the resonance for the methylene next to the urethane bond in the polymer at $\delta$ = 4.90 ppm, which again suggests an incomplete polymerisation that is consistent with the SEC analysis. By relative integration of the reacted and unreacted residual monomer methylene peaks next to the alcohol on GDKPAA (denoted 23 and 23' respectively) it was observed that the actual %HSs were

13 % for the GDKPAA-TPUE30 (targeted 30 %) and 16 % for the GDKPAA-TPUE45 (targeted 45 %). **(Figure 2.13)**

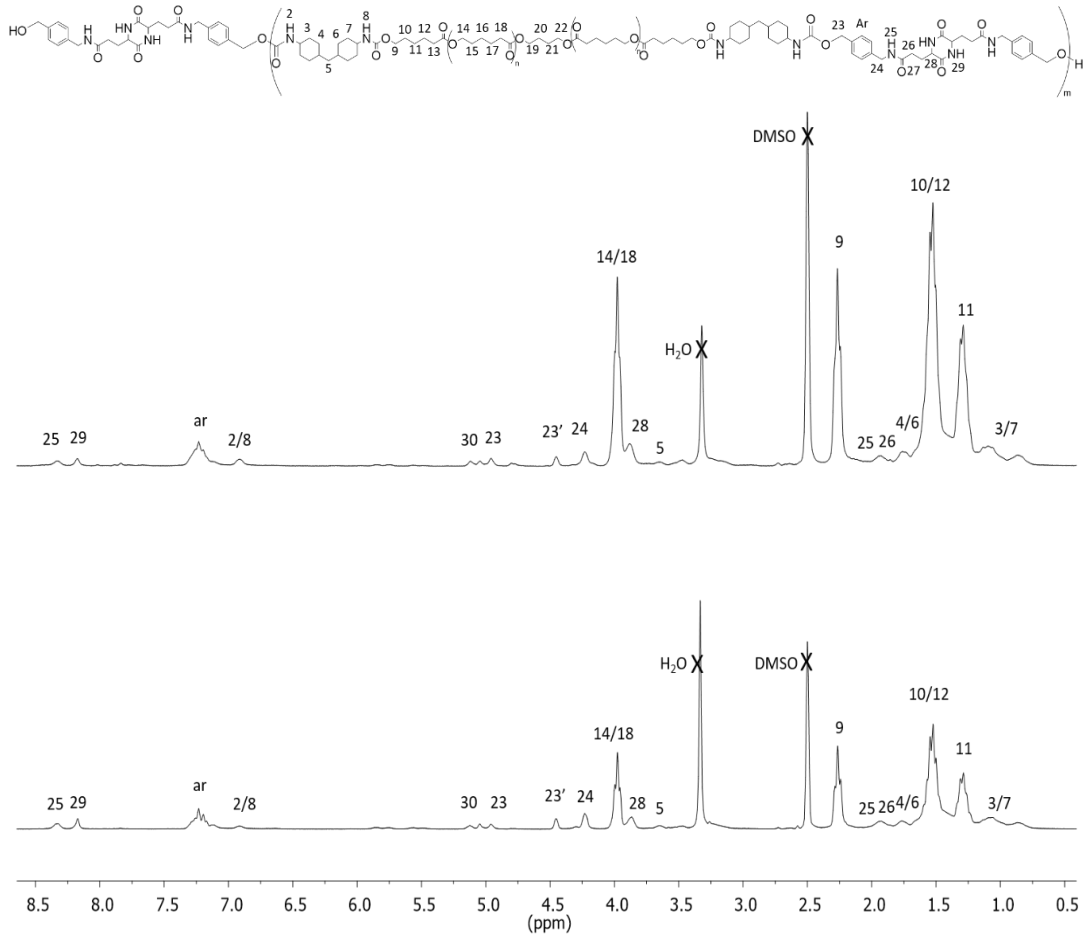


**Figure 2.13 $^{1}$H NMR spectra of GDKPAA-TPUE30 (*top*) and GDKPAA-TPUE45 (*bottom*) (400 MHz, 298 K, DMSO-$d_6$).**

Additionally, the FT-IR spectrum of the GDKPAA-TPUEs revealed urethane peaks at *c.a.* $\tilde{\nu}$ = 1,650 cm$^{-1}$ and *c.a.* $\tilde{\nu}$ = 1,600 cm$^{-1}$ respectively, alongside amide peaks at *c.a.* $\tilde{\nu}$ = 3,300 cm$^{-1}$, *c.a.* $\tilde{\nu}$ = 1,650 cm$^{-1}$ and *c.a.* $\tilde{\nu}$ = 1,600 cm$^{-1}$ respectively. As with the GDKPAE-TPUEs the GDKPAA peaks increased with increasing %HS. **(Figure 2.14)**

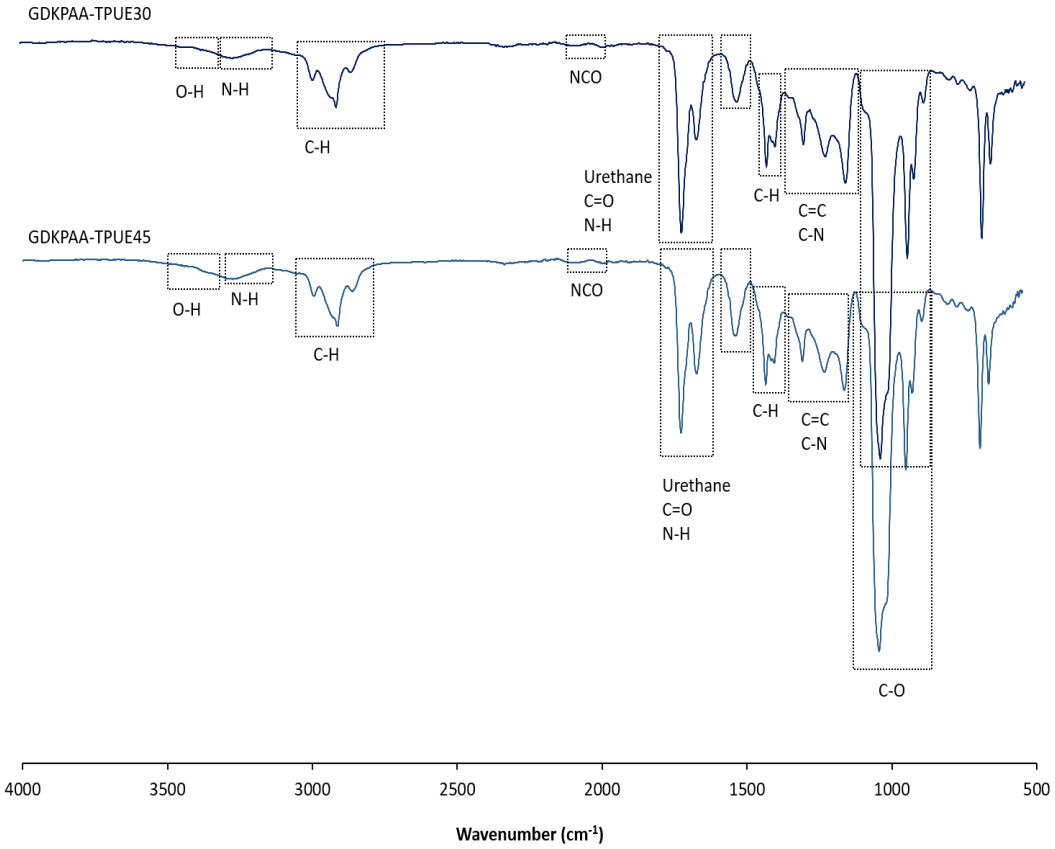


**Figure 2.14 FT-IR of GDKPAA-TPUE30 (*top*) and GDKPAA-TPUE45 (*bottom*).**

For the blend material, combined ester and amide functional handles were used to observe the incorporation of both GDKPAE and GDKPAA. The $^{1}$H NMR spectrum showed resonances at $\delta$ = 8.35 ppm and 8.19 ppm, which correspond to the lactam and bridging amide for both the ester and amide chain extenders. Moreover, methylene resonances were also observed at $\delta$ = 4.23 ppm and 4.98 ppm for GDKPAE and $\delta$ = 4.46 ppm and 4.48 ppm for GDKPAA. By relative integration of the reacted and unreacted residual monomer methylene peaks next to the alcohol on GDKPAE (denoted 23 and 23' respectively) it was observed that the actual %HS was 18 % for the GDKPAE/GDKPAA-TPUE30 (targeted 30 %), comprising 10% % from GDKPAE and 8 % from GDKPAA.**(Figure 2.15)** As with the GDKPAE and GDKPAA-TPUEs, it was also observed that for the GDKPAE/GDKPAA-TPUE the methylene resonances at $\delta$ = 4.50 ppm and the resonance for the alcohol end group on the monomers at

$\delta$ = 5.20 ppm remained in reduced amounts alongside the resonance for the methylenes next to the urethane groups at $\delta$ = 4.90 ppm, which also suggests an incomplete polymerisation that is consistent with the SEC analysis. Further to this, the FT-IR spectrum of the GDKPAE/GDKPAA-TPUE displayed peaks for the ester at *c.a.* $\nu$ = 1,700 $cm^{-1}$ and *c.a.* $\nu$ = 1,100 $cm^{-1}$ and the amide peaks at *c.a.* $\nu$ = 3,300 $cm^{-1}$, *c.a.* $\nu$ = 1,650 $cm^{-1}$ and *c.a.* $\nu$ = 1,600 $cm^{-1}$, along with the urethane peaks at *c.a.* $\nu$ = 1,650 $cm^{-1}$ and *c.a.* $\nu$ = 1,600 $cm^{-1}$.

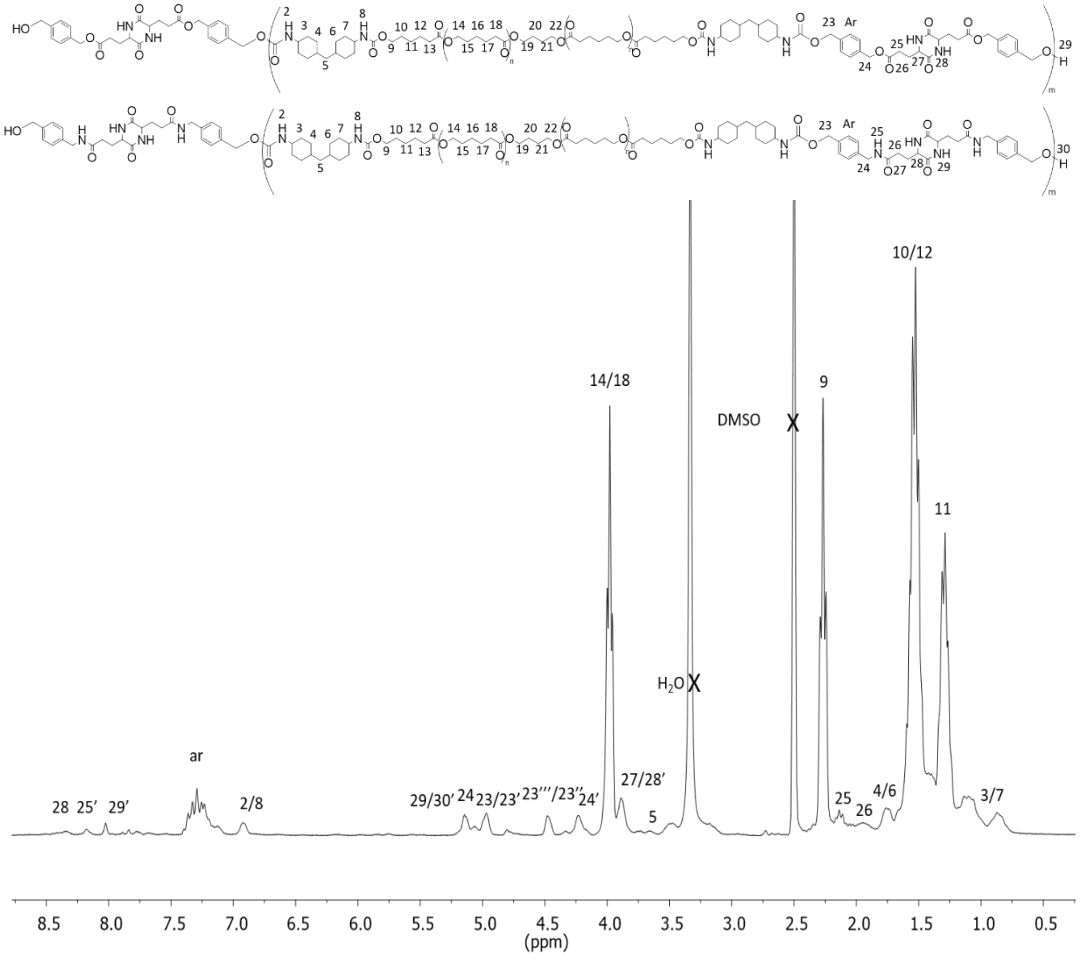


**Figure 2.15 $^{1}$H NMR spectrum of a GDKPAE/GDKPAA-TPUE30 (400 MHz, 298 K, DMSO-$d_6$).**

Elastomers find their optimal properties at a $M_w$ of 100,000 g $mol^{-1}$ and, as is clear from the data described in the latter half of this chapter, this was consistently not observed across the entire range of %HS TPUEs. As previously discussed, the synthesis of PUs was conducted under step-growth polymerisation conditions and

there are a variety of factors that could have hindered the $M_w$ of each TPUE reaching 100,000 g $mol^{-1}$.

First, it is key to have high purity reagents and this was demonstrated by the clean NMR data that was complimented by the elemental analysis, which was within the accepted 0.5% error limit.

Secondly, as it was previously discussed, isocyanates degrade in the presence of water. To make every effort to remove any residual water content from the reagents, the chain extenders were heated at 105 °C under vacuum overnight, the diisocyanate was distilled over $CaH_2$, the polyol was heated over 100 °C for 1 h prior to synthesis and the DMSO was dried over 3A sieves.

Thirdly, since every practical effort was made to target high $M_w$ PUs, the next area to analyse to find the source of the low $M_w$ results is the practical set up of the experiment. These experiments were initially conducted in vials with a flea stirrer, a $N_2$ blanket and a stopper, which was successful for the formation of the prepolymer but shortly after the addition of the chain extender the system became extremely viscous and stirring was significantly reduced/ceased. Subsequently, a closed round bottom flask with an overhead stirrer and a $N_2$ blanket was used but similar results ensued. Variations in the solvent quantity and temperature appeared not to alleviate the system significantly. This high viscosity is considered a factor that in the resulting lower $M_w$s produced as the chain ends were not able to fully react with the next monomer or other chain ends. A further factor to consider was the addition of the chain extender and the prepolymer reaction. The chain extender was only soluble in DMSO at 80 °C and therefore the only practical way to introduce the two components was to add the prepolymer to the chain extender as the chain extender would crystallise out of the DMSO upon addition to the prepolymer. As discussed previously, per the Carothers equation, this process has the potential to cause a stoichiometric imbalance resulting in a lower $M_w$ TPUE.

Focussing on the reactions at the molecular level. As the diisocyanate and the polyol were charged on a 2.27: 1 molar ratio to form dimers and trimers of PCL and $H_{12}$MDI known as a macrodiisocyanates, where the amount of diisocyanate was considerably in excess of the polyol, thereby limiting the growth of the chain and ensuring the diisocyanate was on the chain end, which resulted in a prepolymer with a low $M_w$ of 2,500 $gmol^{-1}$. At this stage of the reaction, the level of NCO at 2,200 $cm^{-1}$ was monitored over time by IR to ensure that the reaction was progressing and all the NCO was not consumed. The successful addition of the chain extender brought the total initial molar ratio of NCO/OH to 1:1. This prepolymer method was chosen as it provided much more defined segments by only allowing the diisocyanate and the polyol to form soft segments. The subsequent addition of the chain extender then allowed the controlled formation of hard segments. [34] At this point of the reaction the dimers and trimers combined with the chain extender and the $M_w$ increased exponentially as this process continued until the reaction was quenched.

Taking the GDKPAE-TPUE30 as an example; it was observed to have an $M_n$ of 11,100 $gmol^{-1}$, which is about 5 repeat units, and hence per Table 1.1 a p of about 99%. This shows that a significant proportion of the reactive groups had been used up but not sufficient enough to produce a high molecular weight TPUE.

Considering the entire process, potential reasons for the low $M_w$ of the TPUEs are:

- a stoichiometric imbalance [35] caused because of the poor solubility of the chain extender in DMSO;
- the inhomogeneity of the reaction mixture because of its high viscosity, therefore making it challenging for the chain to grow as reactive groups become harder to find as the reactive groups become inaccessible to each other; [36]
- the diffusion mobility of the growing chains and their collision rate being insufficient to extend the TPUE chain;

- the three monomers had very different reactivities, therefore the desired high $M_w$ TPUEs were not formed in a traditional time frame; and
- the polarity difference between the chain extender and the prepolymer being sizeable and therefore making it difficult to increase significantly the %HS in the polymer chain.

## 2.3 Conclusions

It was demonstrated that tyrosine and glutamic acid derived cyclic dipeptides offer a viable route to bio-based chain extenders for the synthesis of TPUEs. GDKP was modified to incorporate additional ester and amide functionality and was consequently incorporated into TPUEs with different %HS. Finally, a blend material of ester and amide chain extenders was produced. This method provides a simple way to incorporate desired functionality into the chain extender component and it is projected that the resulting TPUEs will result in a range of thermal, mechanical and degradative properties and aid the formation of a structure-function relationship.

## 2.4 References


1. J. P. Santerre, K. Woodhouse, G. Laroche and R. S. Labow, *Biomaterials*, 2005, **26**, 7457-7470.

2. R. J. Zdrahala and I. J. Zdrahala, *J. Biomater. Appl.*, 1999, **14**, 67-90.

3. R. S. Moglia, J. L. Robinson, A. D. Muschenborn, T. J. Touchet, D. J. Maitland and E. Cosgriff-Hernandez, *Polymer*, 2014, **55**, 426–434.

4. G. T. Howard, *Int. Biodeterior. Biodegrad.*, 2002, **49**, 245–252.

5. I. Engelberg and J. Kohn, *Biomaterials*, 1991, **12**, 292-304.

6. Z. You and Y. Wang, in *Biomaterials for Tissue Engineering Applications: A Review of the Past and Future Trends*, eds. J. A. Burdick and R. L. Mauck, Springer, Austria, 2011, ch. 4, pp. 75-118.

7. C. Hepburn, *Polyurethane Elastomers*, Elsevier, USA, 1st edn., 1982, ch. 3, pp. 74-75.

8. L. H. Chan-Chan, R. S. Solis-Correa, R. F. Vargas-Coronado, J. M. Cervantes-Uc, J. V. Cauich-Rodríguez, P. Quintana and P. Bartolo-Pérez, *Acta Biomaterialia*, 2010, **6**, 2035–2044.

9. C. Hepburn, *Polyurethane Elastomers*, Elsevier, USA, 1st edn., 1982, ch. 1, pp. 19-20.

10. W. J. Lin, *J. Biomed. Mater. Res. Part A*, 1999, **47**, 420-423.

11. G. G. Pitt, M. M. Gratzl, G. L. Kimmel, J. Surles and A. Sohindler, *Biomaterials*, 1981, **2**, 215-220.

12. S. Y. Lin, K. S. Chen, H. H. Teng and M. J. Li, *J. Microencapsulation*, 2000, **17**, 577-586.

13. L. H. Chan-Chan, C. Tkaczyk, R. F. Vargas-Coronado, J. M. Cervantes-Uc, M. Tabrizian and J. V. Cauich-Rodriguez, *J. Mater. Sci. - Mater. Med.*, 2013, **24**, 1733-1744.

14. J. L. A. Perales-Alcacio, J. Santa-Olalla Tapia, C. Mojica-Cardoso, R. F. Vargas-Coronado, L. H. Chan-Chan, D. M. Headen, A. J. García, J. M. Cervantes-Uc and J. V. Cauich-Rodríguez, *J. Biomater. Sci., Polym. Ed.*, 2013, **24**, 1601-1617.

15. J. Wang, Z. Zheng, L. Chen, X. Tu and X. Wang, *J. Biomater. Sci., Polym. Ed.*, 2013, **24**, 831-848.

16. F. Wang, Z. Zheng, W. Wang, Z. Gu, J. Wang and X. Wang, *Polym. Degrad. Stab.*, 2014, **100**, 86–92.

17. I. C. Parrag and K. A. Woodhouse, *J. Biomater. Sci., Polym. Ed.*, 2010, **21**, 843-862.

18. G. A. Skarja and K. A. Woodhouse, *J. Appl. Polym. Sci.*, 2000, **75**, 1522-1534.

19. J. L. West and J. A. Hubbell, *Macromolecules*, 1999, **32**, 241-244.

20. J. Guan and W. R. Wagner, *Biomacromolecules*, 2005, **6**, 2833-2842.

21. S. A. Guelcher, K. M. Gallagher, J. E. Didier, D. B. Klinedinst, J. S. Doctor, A. S. Goldstein, G. L. Wilkes, E. J. Beckman and J. O. Hollinger, *Acta Biomaterialia*, 2005, **1**, 471-484.

22. J. D. Fromstein and K. A. Woodhouse, *J. Biomater. Sci., Polym. Ed.*, 2002, **13**, 391-406.

23. P. J. Woodward, D. Hermida Merino, B. W. Greenland, I. W. Hamley, Z. Light, A. T. Slark and W. Hayes, *Macromolecules*, 2010, **43**, 2512-2517.

24. A. D. Borthwick, *Chem. Rev.*, 2012, **112**, 3641-3716.

25. M. B. Martins and I. Carvalho, *Tetrahedron*, 2007, **63**, 9923-9932.

26. C. G. Kirchhoefer, A. P. Dove and A. J. Walder, *WO Pat.,* 173202, 2017.

27. Nonappa, K. Ahonen, M. Lahtinen and E. Kolehmainen, *Green Chem.*, 2011, **13**, 1203-1209.

28. J. J. Stevenson and D. Moye-Sherman, *USA Pat.,* 7,709,639, 2010.

29. D. A. Parrish and L. J. Mathias, *J. Org. Chem.*, 2002, **67**, 1820-1826.

30. M. E. Pierce, G. D. Harris, Q. Islam, L. A. Radesca, L. Storace, R. E. Waltermire, E. Wat, P. K. Jadhav and G. C. Emmett, *J. Org. Chem.*, 1996, **61**, 444-450.

31. Z. Dogan, R. Paulini, J. A. Rojas-Stütz, S. Narayanan and C. Richert, *J. Am. Chem. Soc.*, 2004, **126**, 4762-4763.

32. M. J. O'Sickey, B. D. Lawrey and G. L. Wilkes, *J. Appl. Polym. Sci.*, 2002, **84**, 229-243.

33. J. Alsarraf, Y. A. Ammar, F. Robert, E. Cloutet, H. Cramail and Y. Landais, *Macromolecules*, 2012, **45**, 2249-2256.

34. G. Odian, *Principles of Polymerization*, John Wiley & Sons, Inc., USA, 4th edn., 2004, ch. 2, pp. 139-140.

35. G. Odian, *Principles of Polymerization*, John Wiley & Sons, Inc., USA, 4th edn., 2004, ch. 2, pp. 79-80.

36. G. Odian, *Principles of Polymerization*, John Wiley & Sons, Inc., USA, 4th edn., 2004, ch. 2, pp. 63-65.

# Chapter 3

# Mechanical, Thermal and Degradation Analysis of Thermoplastic Polyurethane Elastomers with Novel Diketopiperazine Chain Extenders

## 3.1 Introduction

Bioabsorbable polymers are materials that degrade *in vivo* and are absorbed by the body after the material has been broken down, thus making them ideal materials for use in a range of biomedical applications from tissue scaffolds to drug delivery.[1,2] Such polymers have three significant advantages over natural biomaterials:

- the ability to tailor the degradation rate of the material to match the formation of new tissue or the desired rate of drug release;
- the ability to modulus match with the surrounding tissues; and
- the autonomous clearance of the material from the body.

Polymers that exhibit mechanical properties akin to the strength of the tissue that they are surrounded by, as well as durable elasticity, have been shown to promote cell function and tissue development. In addition, polymers that are used in soft tissue engineering are placed in a mechanically-demanding environment, requiring them to stretch and regain their original shape whilst causing minimal disturbance to the surrounding structures. If a polymer is weak or brittle it may result in premature failure and potentially the need to repair the injury with a second operation. Equally, a polymer that is too strong may result in damage and swelling of the surrounding tissue. Therefore, it is very important to carefully tune a polymer's mechanical properties to encourage synergy between it and human tissue.

The way such polymers break down in different environments and the subsequent toxicity of the degradation products is key. The degradation rate is dependent on the thermal and physical properties of the polymer, such as composition and crystallinity. For example, poly(ε-caprolactone) (PCL), an aliphatic polyester that is commonly used in biomaterials because of its low toxicity and low melting point, can take up to two years to degrade *in vivo* because of its semi-crystalline and hydrophobic properties.[3-5] *In vivo* degradation pathways are generally a result of hydrolytic or enzymatic degradation.

Hydrolytic degradation occurs by hydrolysis of the cleavable bonds within the polymer structure, resulting in mass loss and the breakdown of the material over time. Heteroatomic bonds (*e.g*. C-O and C-N) are more easily cleaved than homoatomic bonds (*e.g*. C-C) as the associated dissociation energies are generally lower**. (Scheme 3.1)**

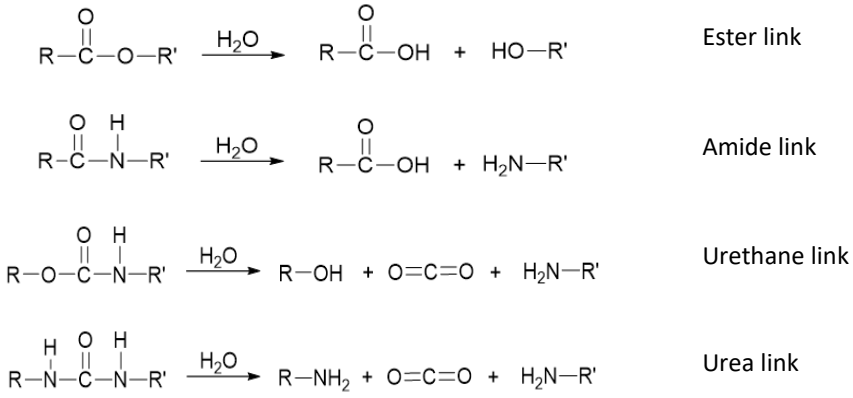


**Scheme 3.1 Examples of the hydrolytic cleavage of ester, amide urethane and urea links.**

Hydrolytic degradation can be further sub-categorised as bulk degradation and/or surface erosion. Bulk degradation, which is typically exhibited by polyesters, proceeds by a non-linear mass loss profile after an initial increase in mass. This profile typically occurs when the rate of diffusion of water through the material is faster than the rate of hydrolysis. In addition, accumulated degradation products within the polymer network can promote accelerated degradation resulting in loss of structural integrity.[4,6,7] Conversely, surface erosion, which is characterised by a linear mass loss profile, is the primary degradation pathway when the rate of hydrolysis is faster than the rate of diffusion of water through the material. Bulk degradation and surface erosion are not necessarily independent of each other and most degradation profiles involve a complex mixture of the two processes.[8]

Enzymatic degradation of a polymer is caused by the action of an enzyme, such as elastase, cleaving certain bonds within the material's structure.[9,10] Polymers can be tuned to incorporate peptide sequences that are known to be susceptible to degradation by a specific enzyme, such as *L*-alanine-*L*-alanine-*L*-lysine, which is

degraded by elastase that preferentially cleaves peptide bonds in small hydrophobic molecules such as *L*-alanine.[11,12]

Mechanical, thermal and degradative studies were undertaken on tyrosine and glutamic acid-based thermoplastic polyurethane elastomers (TPUEs) synthesised and characterised in chapter 2, to assess their potential application as biomaterials. A comparison between the effect of increased ester and/or amide glutamic acid-based dipeptides as chain extenders in TPUEs and with tyrosine dipeptide was made over a range of hard segment percentage (%HS) analogues. Finally, the hypothesis that a blend of increased ester and amide glutamic acid based-dipeptides as chain extenders should allow greater control over the mechanical and degradative properties of the resulting material was tested.

## 3.2 Results and Discussion

To assess the effect of different dipeptide-based chain extenders, increased ester and amide content in the hard segment, increasing the %HS, and the effect of blending ester and amide chain extenders on the material properties of the various TPUEs, mechanical, thermal and degradative studies were conducted.

The family of dipeptide-based TPUEs examined (defined in **(Table 2.1)** were as follows:

- A TPUE with a tyrosine-based chain extender (used as a comparative material) (TDKP-TPUE30);
- TPUEs with a glutamic acid-based chain extender with additional ester links with a variety of hard segment percentage (%HS) (GDKPAE-TPUE30, GDKPAE-TPUE45 and GDKPAE-TPUE60);
- TPUEs with a glutamic acid-based chain extender with additional amide links with a variety of %HS (GDKPAA-TPUE30 and GDKPAA-TPUE45);
- A TPUE with a 50:50 molar blend of ester and amide glutamic acid-based chain extenders (GDKPAE/GDKPAA-TPUE30).

### 3.2.1 Mechanical analysis of thermoplastic polyurethane elastomers with novel diketopiperazine chain extenders

The mechanical properties of a biomaterial are crucial in matching a material to an application. To assess the mechanical properties of the dipeptide-based TPUEs, tensile analysis was conducted to observe the differences between the chain extenders and the effect of increasing the %HS. Prior to analysis the TPUEs were compression moulded into ‘‘dog-bones’’ in a polytetrafluoroethylene (PTFE) mould and annealed for 7 days in an incubator at 25 °C so that they would more completely phase separate. It should be noted that the processing temperatures of the GDKPAE, GDKPAA and GDKPAE/GDKPAA-TPUEs were significantly lower (40 to 80 °C) in comparison to the TDKP-TPUE (280 to 300 °C).

Initial tensile experiments were conducted to compare the effect of the different chain extenders on the mechanical properties of the TPUE30s. The GDKPAE-TPUE30 was observed to have soft and elastic characteristics; ultimate tensile strength (UTS) of 0.7 MPa, elongation at break of 560% and a Young's modulus of 1.2 MPa. By comparison, the GDKPAA-TPUE30 showed it to be a tougher material but it remained similarly elastic with the following characteristics: UTS of 14.6 MPa, elongation at break of 550% and a Young's modulus of 12.7 MPa. The GDKPAE/GDKPAA-TPUE30, which was synthesised to provide greater control over the mechanical properties, was observed to have the following characteristics: UTS of 6.9 MPa, elongation at break of 110% and a Young's modulus of 44.3 MPa. All the glutamic acid-based TPUEs were compared to the TDKP-TPUE30, which was observed to have a UTS of 5.2 MPa, elongation at break of 480% and a Young's modulus of 3.3 MPa. This data set showed that by varying the composition of the hard segment through modifying the chain extender a range of TPUEs could be accessed and GDKPAE/GDKPAA provided further ability to tune the TPUE properties. The GDKPAA-TPUEs are tougher materials than the GDKPAE-TPUEs because they have more amide groups that are both hydrogen bond donors and acceptors. The toughness of the TDKP-TPUE30 lies between the toughness of the GDKPAE-TPUE30 and the GDKPAA-TPUE30 and has elastic properties because of the uniform π-π stacking interactions in the hard segment. The GDKPAE/GDKPAA-TPUE30 combined the properties of the ester and amide chain extenders, however, further analysis of the phase separation behaviour of such blended TPUEs needs to be conducted. **(Figures 3.1 and 3.2)**

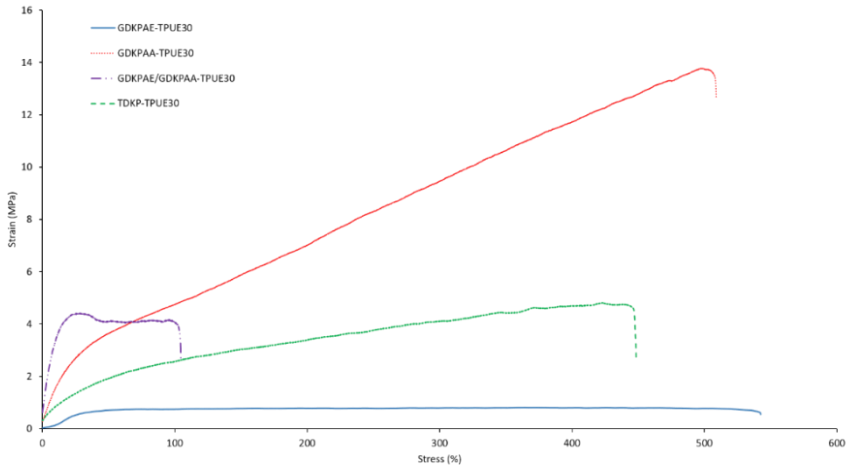


**Figure 3.1 Exemplar stress vs strain curves for GDKPAE, GDKPAA, GDKPAE/GDKPAA and TDKP-TPUE30s. Experiments were conducted at ambient temperature (~20 °C) at an elongation rate of 5 mm min$^{-1}$ until failure.**

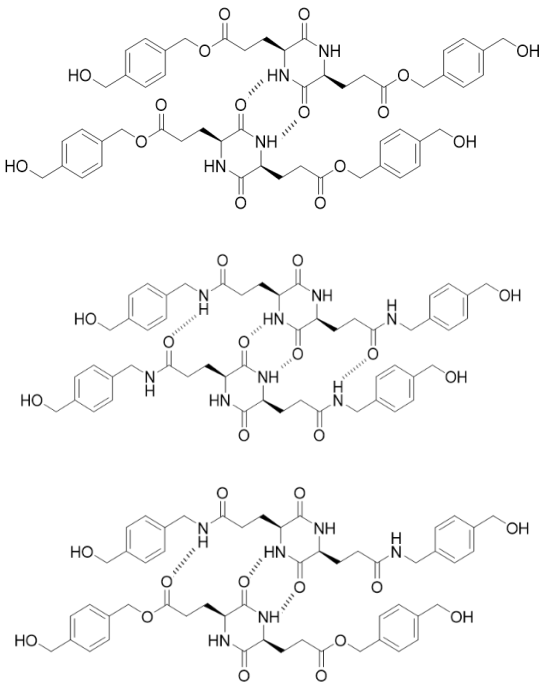

Ester-ester non-covalent interactions

Amide-amide non-covalent interactions

Ester-amide non-covalent interactions

**Figure 3.2 Hydrogen bonding between ester-ester (top), amide-amide (middle) and ester-amide (bottom) hard segments.**

A further set of comparative tensile analyses were conducted to compare the effect of increasing the %HS on the mechanical properties of the TPUEs. As previously discussed the GDKPAE-TPUE30 was a very soft but elastic material (UTS of 0.7 MPa, elongation at break of 560% and a Young's modulus of 1.2 MPa). It was observed that the GDKPAE-TPUE45 had an increased UTS of 9.4 MPa, an increased Young's modulus of 5.7 MPa but the elongation at break remained at 560%. Interestingly, the GDKPAE-TPUE60 had an elongation at break of 150%, which is unusually elastic compared to equivalent TPUE60 counterparts, a Young's modulus of 13.9 MPa and contrary to the trend a UTS of 3.1 MPa. This trend was also observed with the GDKPAA-TPUEs. The GDKPAA-TPUE45 was observed to have an increased UTS of 32.6 MPa, an elongation at break of 120% and a Young's modulus of 54.8 MPa. This set of data showed that when the %HS of the TPUE was increased, the resulting material became significantly tougher because of the increased hydrogen bonding interactions between the hard segments within the TPUE. **(Table 3.1 and Figure 3.3)**

**Table 3.1 Comparison of the tensile properties of GDKPAE-TPUEs, GDKPAA-TPUEs, a GDKPAE/GDKPAA-TPUE30 and a TDKP-TPUE30.**

| Polymer | Targeted %HS | Observed %HS[a] | Ultimate Tensile Strength (MPa)[b] | Elongation at Break (%)[b] | Young's Modulus (MPa)[b] |
|---|---|---|---|---|---|
| **GDKPAE-TPUE30** | 30 | 15 | 0.7 ± 0.2 | 560 ± 95 | 1.2 ± 0.1 |
| **GDKPAE-TPUE45** | 45 | 16 | 9.4 ± 1.2 | 560 ± 60 | 5.7 ± 3.5 |
| **GDKPAE-TPUE60** | 60 | 20 | 3.1 ± 0.5 | 150 ± 35 | 13.9 ± 6.5 |
| **GDKPAA-TPUE30** | 30 | 13 | 14.6 ± 1.1 | 550 ± 45 | 12.7 ± 0.6 |
| **GDKPAA-TPUE45** | 45 | 16 | 32.6 ± 1.1 | 120 ± 25 | 54.8 ± 6.4 |
| **GDKPAE/GDKPAA-TPUE30** | 30 | 18 (10/8) | 6.9 ± 3.9 | 110 ± 3 | 44.3 ± 7.7 |
| **TDKP-TPUE30** | 30 | 15 | 5.2 ± 0.6 | 480 ± 50 | 3.3 ± 0.9 |

a) Determined by $^{1}$HNMR analysis b) Determined by tensile analysis (average of 6 samples)

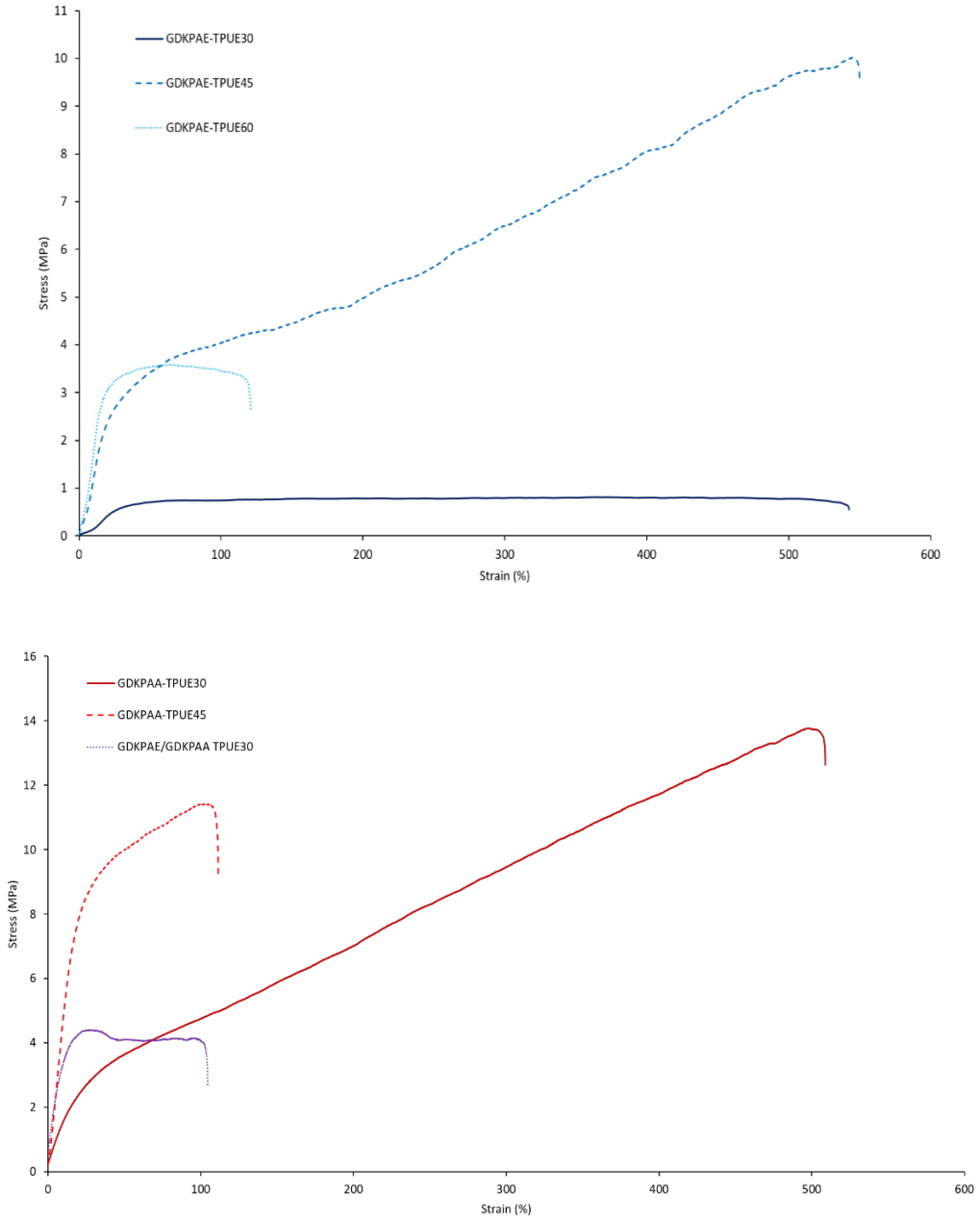


**Figure 3.3 Exemplar stress *vs* strain curves for a GDKPAE-TPUE30, TPUE45 and TPUE60 (*top*), a GDKPAA-TPUE30 and TPUE45 and a GDKPAE/GDKPAA-TPUE30 (*bottom*). Experiments were conducted at ambient temperature (~20 °C) at an elongation rate of 5 mm min$^{-1}$ until failure.**

The GDKPAE-TPUE60 and the GDKPAE/GDKPAA TPUE30 were observed to have reduced $M_n$ values compared to the other TPUEs. Therefore, the mechanical data reported is used as a guide only, but it is anticipated that it should be possible to increase the $M_n$ values, and hence the mechanical properties, of the TPUEs. A potential reason for the low $M_n$ values for the GDKPAE/GDKPAA TPUE30 was the difference in reactivity between the GDKPAE and GDKPAA chain extenders. However, the deficiency in $M_n$ for the GDKPAE-TPUE60 was more likely a combination of:

- a stoichiometric imbalance [13] caused by the increasingly poor solubility of the chain extender in DMSO;
- the inhomogeneity of the reaction mixture because of its extremely high viscosity, therefore making it challenging for the chain to grow as the reactive groups become inaccessible to each other; [14]
- the diffusion mobility of the growing chains and their collision rate being insufficient to extend the TPUE chain;
- the three monomers had very different reactivities, therefore the desired high $M_w$ TPUEs were not formed in a traditional time frame; and
- the polarity difference between the chain extender and the prepolymer being sizeable and therefore making it difficult to increase significantly the %HS in the polymer chain.

### 3.2.2 Thermal analysis of thermoplastic polyurethane elastomers with novel diketopiperazine chain extenders

Differential scanning calorimetry (DSC), thermogravimetric analysis (TGA) and dynamic mechanical analysis (DMA) were employed to investigate the thermal properties of the TPUEs.

#### 3.2.2.1 Differential scanning calorimetry

Each TPUE was subjected to three heating and cooling cycles across a temperature range from -80°C to 100 °C. For the GDKPAE-TPUE30 the heating run of the first DSC

cycle showed a soft segment melting temperature ($T_m$) of 48 °C. The heating sections of the second and third cycles both revealed a soft segment glass-transition temperature ($T_g$) of -55 °C and a hard segment $T_g$ of 64 °C. Comparable DSC analysis of the GDKPAE-TPUE45 and the GDKPAE-TPUE60 showed the same soft segment $T_g$ of -55 °C. No $T_m$ for both the soft and hard segments was observed in the subsequent cycles It is considered that this was because the time between cycles did not allow enough time for the TPUEs to recrystallise and then melt again. The GDKPAA-TPUEs were subjected to the same heat and cooling cycles as the GDKPAE-TPUEs and it was observed that the GDKPAA-TPUE30 had a hard segment $T_g$ of 64 °C and the GDKPAA-TPUE45 had a hard segment $T_g$ of 66 °C; both similar to the equivalent GDKPAE-TPUE. It was also noted that at *c.a*. 70 °C there was an endothermic transition. This is likely a phase change with respect to the hard segment because of the preceding $T_m$. This trend was observed across all the TPUEs and all %HS. **(Figure 3.4)**

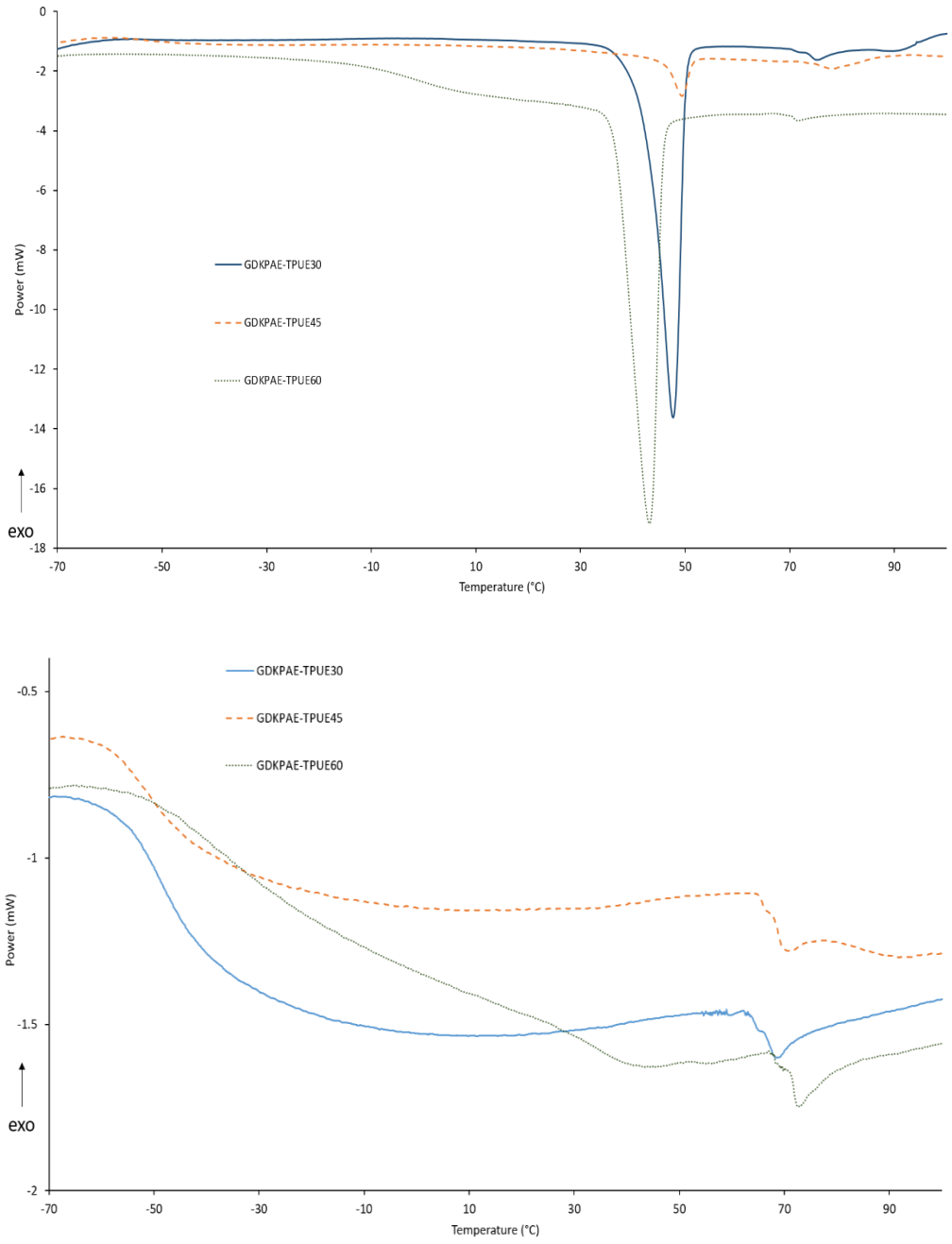


**Figure 3.4 DSC thermograms of the first (*top*) and second (*bottom*) heating runs of a GDKPAE-TPUE30, TPUE45 and TPUE60. Experiments were conducted at a heating rate of 5 K min$^{-1}$.**

The heating run of the first cycle for the GDKPAE/GDKPAA-TPUE30 showed a soft segment $T_m$ of 45 °C and a $T_m$ for both the GDKPAE and the GDKPAA-TPUEs at 72 °C. The heating run of the second cycle revealed a $T_g$ for both the GDKPAE and GDKPAA-TPUEs' hard segment at 64 °C, which indicated proportions of the mixture

are homopolymers of the GDKPAE and GDKPAA-TPUEs. Further to this a second hard segment $T_g$ peak was observed at 35 °C, which is considered to be a $T_g$ of the copolymer of the GDKPAE and GDKPAA chain extenders. **(Figure 3.5 and Table 3.2)**

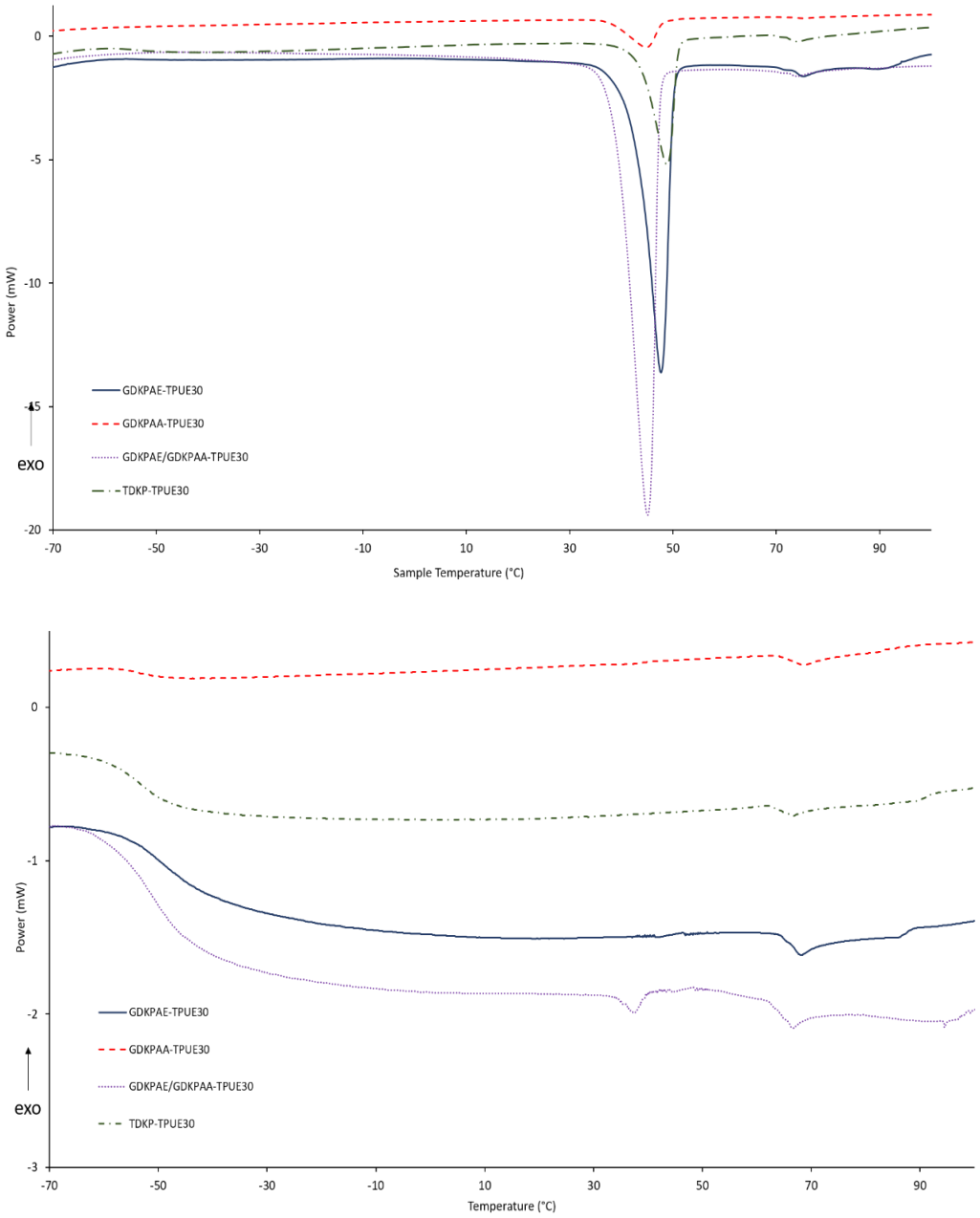


**Figure 3.5 DSC thermograms of the first (*top*) and second (*bottom*) heating runs of GDKPAE, GDKPAA, GDKPAE/GDKPAA and TDKP-TPUE30s. Experiments were conducted at a heating rate of 5 K min$^{-1}$.**

**Table 3.2 Comparison of melt and glass transition temperatures of a GDKPAE-TPUE30, TPUE45 and TPUE60, a GDKPAA-TPUE30 and TPUE45, a GDKPAE/GDKPAA-TPUE30 and a TDKP-TPUE30.**

| Polymer | Hard Segment $T_g$ (°C) | Soft Segment $T_m$ (°C) | Soft Segment $T_g$ (°C) |
|---|---|---|---|
| GDKPAE-TPUE30 | 64 | 48 | -55 |
| GDKPAE-TPUE45 | 67 | 49 | -55 |
| GDKPAE-TPUE60 | 70 | 43 | -55 |
| GDKPAA-TPUE30 | 64 | 45 | -56 |
| GDKPAA-TPUE45 | 66 | 46 | -58 |
| GDKPAE/GDKPAA-TPUE30 | 64 and 35 | 45 | -59 |
| TDKP-TPUE30 | 63 | 49 | -61 |

### 3.2.2.2 Thermogravimetric analysis

Thermogravimetric analysis (TGA) of the TPUEs was conducted to observe the effect of the various hard segment compositions and the range of %HS on the rate of thermal degradation. The thermograms showed the onset of degradation for the soft segment at *c.a*. 300 °C across all the TPUEs. A series of trends were observed by comparing the thermograms of the TPUE30s. It was noted that the GDKPAE-TPUE30 began degrading at a lower temperature than the GDKPAA-TPUE30 and the GDKPAE/GDKPAA-TPUE30 began to degrade at a temperature between the two homopolymers. In addition, it was observed that by increasing the %HS of the TPUEs the temperature at which degradation began increased, when compared to the PCL homopolymer thermogram **(Figure 3.6)**

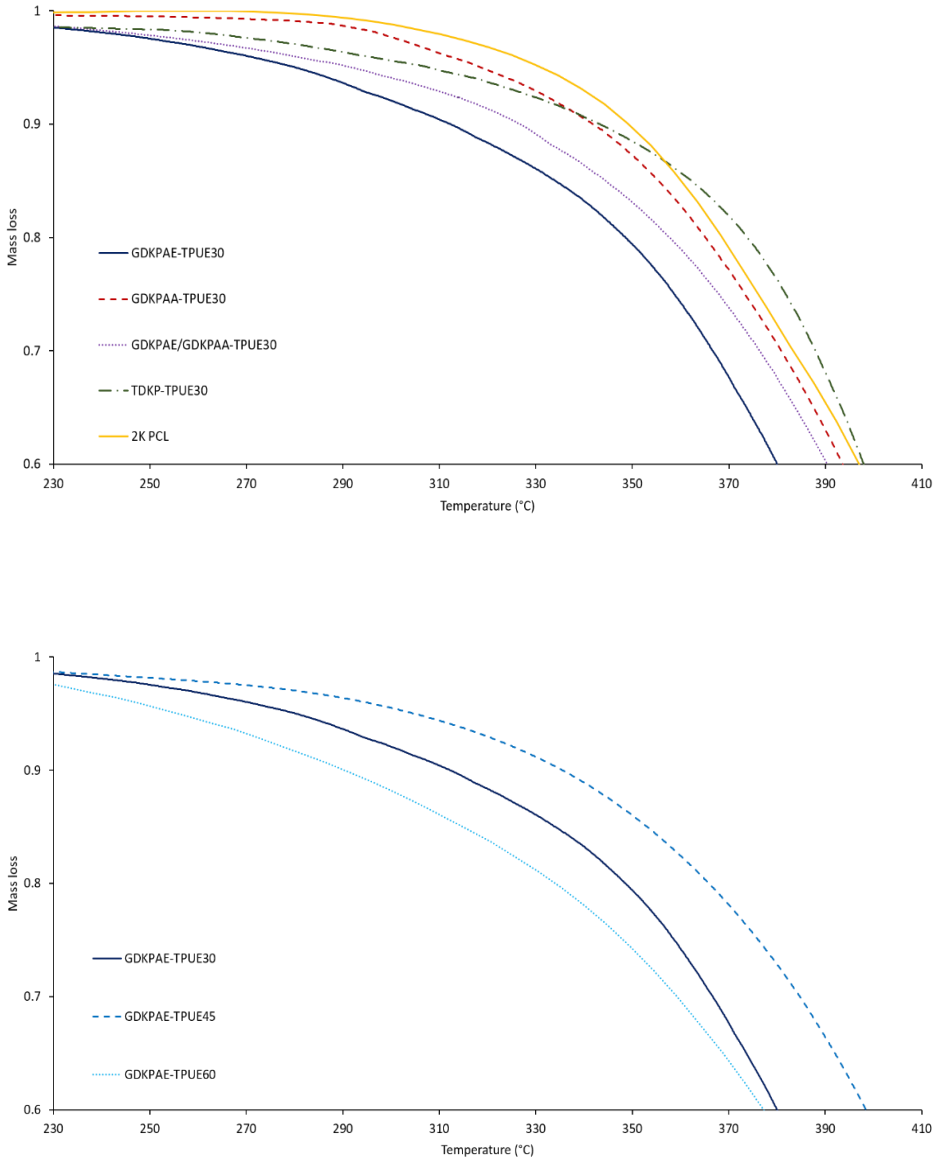


**Figure 3.6 TGA thermograms for GDKPAE, GDKPAA, GDKPAE/GDKPAA and TDKP-TPUE30s and 2K-PCL (*top*) and a GDKPAE-TPUE30, TPUE45 and TPUE60 (*bottom*), Experiments were conducted at a heating rate of 10 K min$^{-1}$.**

### 3.2.2.3 Dynamic mechanical analysis

Dynamic mechanical analysis (DMA) was conducted on the TPUEs as it is a more sensitive analysis technique than DSC, particularly for $T_g$ measurements and can probe further the thermomechanical properties of viscoelastic materials. For a sample that is not completely elastic the strain ($\varepsilon$) is delayed behind the stress ($\sigma$)

resulting in a phase angle ($\delta$) and the peak stress and the peak strain give the complex modulus ($M^*$). $M^*$ consists of the in-phase storage modulus ($M'$) that is proportional to the mechanical energy stored in the sample, and the out-of-phase loss modulus ($M''$) that is the energy dissipated from the sample as heat. The ratio of $M'$ to $M''$ is known as the loss factor or damping factor (tan $\delta$) and the elasticity of the sample is inversely proportional to value of tan $\delta$.[15] **(Figure 3.7)**

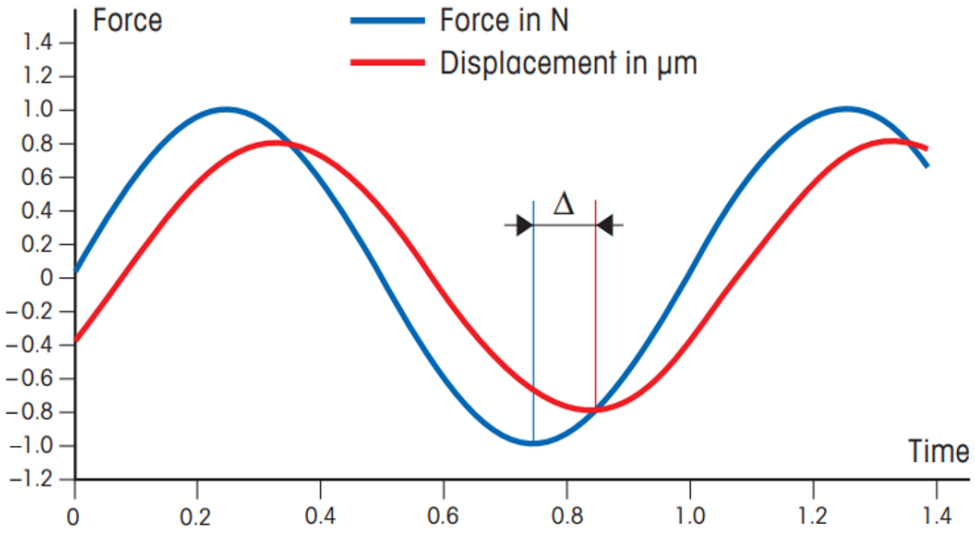


**Figure 3.7 Chart of force and displacement against time showing time delay.**

Using DMA, it is also possible to determine the temperature at which thermal events such as $T_g$ take place as a function of the elastic moduli; the storage modulus ($E'$) as defined in equation **(3.1 below)**, the loss modulus ($E''$) as defined in equation **(3.2 below)** and thereby tan $\delta$ as defined in equation **(3.3 below).** For example, the occurrence of a $T_g$ can be characterised as a drop of several decades (powers of 10) in the $E'$ trendline and peak maxima in the $E''$ and tan $\delta$ trendlines. Also, it is possible to calculate each modulus at different temperatures and thereby deduce a material's properties at a chosen application temperature; for example, at 37 °C, which is body temperature.

$$E' = \frac{\sigma_0}{\varepsilon_0} cos\,\delta \quad \{3.1\}$$

$$E'' = \frac{\sigma_0}{\varepsilon_0} sin\,\delta \quad \{3.2\}$$

$$tan\,\delta = \frac{E'}{E''} \quad \{3.3\}$$

Prior to the DMA, the TPUEs were compression moulded into cuboids in a PTFE mould and annealed for 7 days at 25 °C in an incubator to allow the materials to more completely phase separate. The TPUEs were tested under the following specifications:

- in tension mode (preload 1 N);
- at two frequencies (0.5 Hz and 5.0 Hz);
- with a displacement of 20 µm;
- with a temperature range of-80 °C to 200 °C; and
- a heating rate of 5 K $min^{-1}$.

Several trends were observed from this analysis. First, the GDKPAE-TPUE30, the GDKPAA-TPUE30, the GDKPAE/GDKPAA-TPUE30 and the TDKP-TPUE30 were subjected to DMA to observe the effect of the chain extender in the hard segment. It was observed that all the homopolymers had a soft segment $T_g$ of -30 °C. In addition, the elasticity of each TPUE was measured based on the tan $\delta$ maximum of the soft segment $T_g$. The GDKPAE-TPUE30 was the most elastic with tan $\delta$ value of 0.05, the TDKP-TPUE30 had a tan $\delta$ value of 0.13, the GDKPAE/GDKPAA-TPUE30 had a tan $\delta$ value of 0.15, and the GDKPAA-TPUE30 was the least elastic with a tan $\delta$ value of 0.5. The homopolymers also had a hard segment $T_g$. the GDKPAE-TPUE30 had a hard segment $T_g$ of 70 °C and then melted at a $T_m$ of 80 °C. This was characterised by the steep elevation of the tan $\delta$ trendline, which is characteristic of a solid to liquid transition. The GDKPAA-TPUE30 had a higher hard segment $T_g$ of 95 °C and then melted at a $T_m$ of 200 °C, again characterised by a steep elevation in the tan $\delta$ trendline. The TDKP-TPUE30 had a significantly higher hard segment $T_g$ of 195 °C but

no $T_m$ was observed because the experiment was stopped before the TPUE could melt. The GDKPAE/GDKPAA-TPUE30 had a slightly elevated soft segment $T_g$ of -20 °C and a bi-modal hard segment $T_g$ of 70 °C and 95 °C, which corresponds to the GDKPAE and GDKPAA hard segments. It is considered that the third tan $\delta$ peak observed in the thermogram of the GDKPAE/GDKPAA-TPUE30 at 180 °C is the copolymer of GDKPAE and GDKPAA that is also present in the DSC thermogram **(Figure 3.5)**. The GDKPAE/GDKPAA-TPUE30 was then observed to melt immediately after the final $T_g$ at a $T_m$ of 190 °C, once again characterised by a steep elevation in the tan $\delta$ trendline. **(Figure 3.8)**

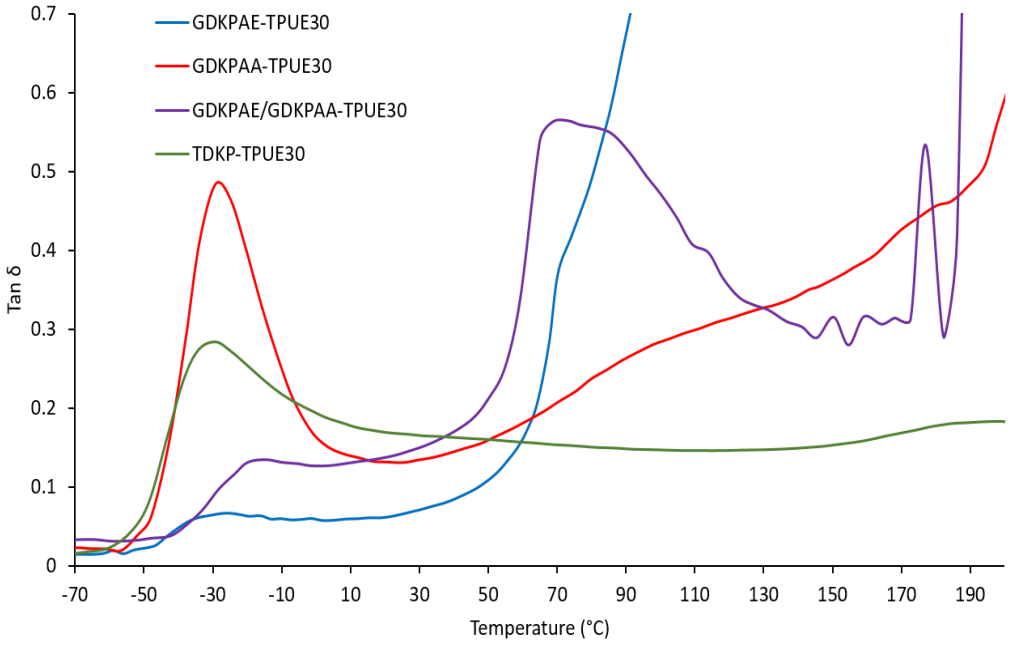


**Figure 3.8 DMA thermograms for GDKPAE, GDKPAA, GDKPAE/GDKPAA and TDKP-TPUE30s. Experiments were conducted in tension mode (preload 1 N) with a displacement of 20 µm and a frequency of 5 Hz across a temperature range of -80 °C to 250 °C with a heating rate 5 K min$^{-1}$.**

Further analysis was conducted to observe the effect of increasing the %HS on the thermal properties of the TPUEs. Each of the tan $\delta$ thermograms for the GDKPAE-TPUEs showed a soft segment $T_g$ of -30 °C. The hard segment $T_g$ reduced as the %HS increased; the GDKPAE-TPUE30 and the GDKPAE-TPUE60 had a hard segment $T_g$ of 70 °C and 50 °C respectively. It was observed that an increased %HS resulted in an increased magnitude of the tan $\delta$ peak maxima; the GDKPAE-TPUE30

was the most elastic with a tan $\delta$ peak maximum value of 0.50 and the GDKPAE-TPUE60 was the least elastic with a tan $\delta$ peak maximum value of 0.40. It was noted that the GDKPAE-TPUE45 had a hard segment $T_g$ of 40 °C with a tan $\delta$ peak maximum value of 0.20 but did not show a soft segment $T_g$ of the same a tan $\delta$ maximum value of the GDKPAE-TPUE30 and the GDKPAE-TPUE45. This may have resulted from the material not fully phase separating before the analysis was conducted. An inverse trend was observed in the thermograms for the GDKPAA-TPUE30 and the GDKPAA-TPUE45. Each of the tan $\delta$ thermograms for the GDKPAA-TPUEs also had a soft segment $T_g$ of -30 °C but the hard segment $T_g$ increased as the %HS increased. The GDKPAA-TPUE30 and the GDKPAA-TPUE45 had a hard segment $T_g$ of 95 °C and 130 °C respectively. It is considered that this is because of an increase in the number of hydrogen bonding sites between the hard segment domains. It was observed that an increase in the %HS resulted in a decrease in the magnitude of the peak maximum values of tan $\delta$; the GDKPAA-TPUE30 was the least elastic with a tan $\delta$ peak maximum value of 0.30 and the GDKPAE-TPUE45 was the most elastic with a tan $\delta$ peak maximum value of 0.20 according to the hard segment $T_g$. Finally, the GDKPAE/GDKPAA-TPUE30 was shown to be the most inelastic TPUE with a tan $\delta$ peak maximum value of 0.60 according to the hard segment $T_g$. **(Figures 3.9 and 3.10)**

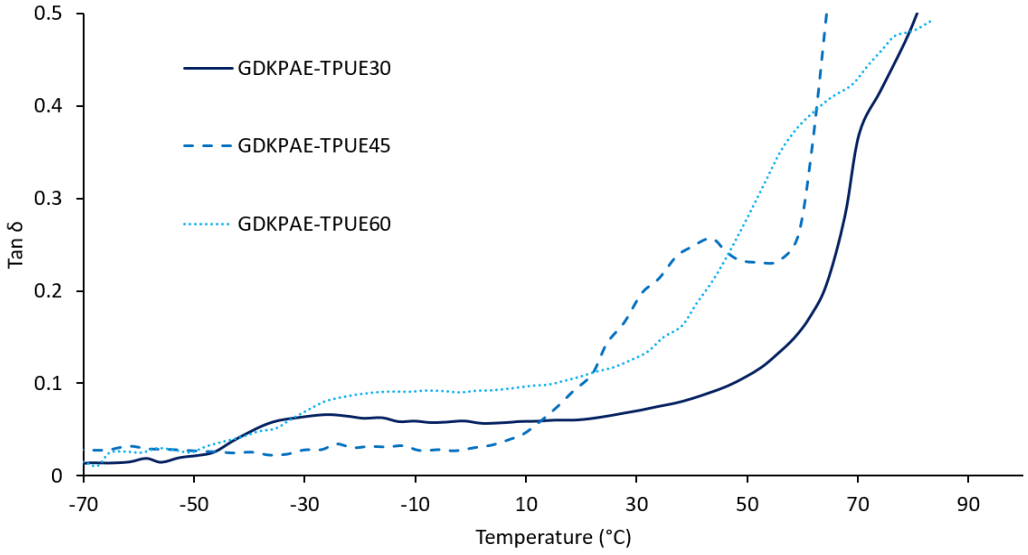


**Figure 3.9 DMA thermograms of tan *δ* for a GDKPAE-TPUE30, TPUE45, and TPUE60. Experiments were conducted in tension mode (preload 1 N) with a displacement of 20 µm and a frequency of 5 Hz across a temperature range of-80 °C to 200 °C with a heating rate of 5 K min$^{-1}$.**

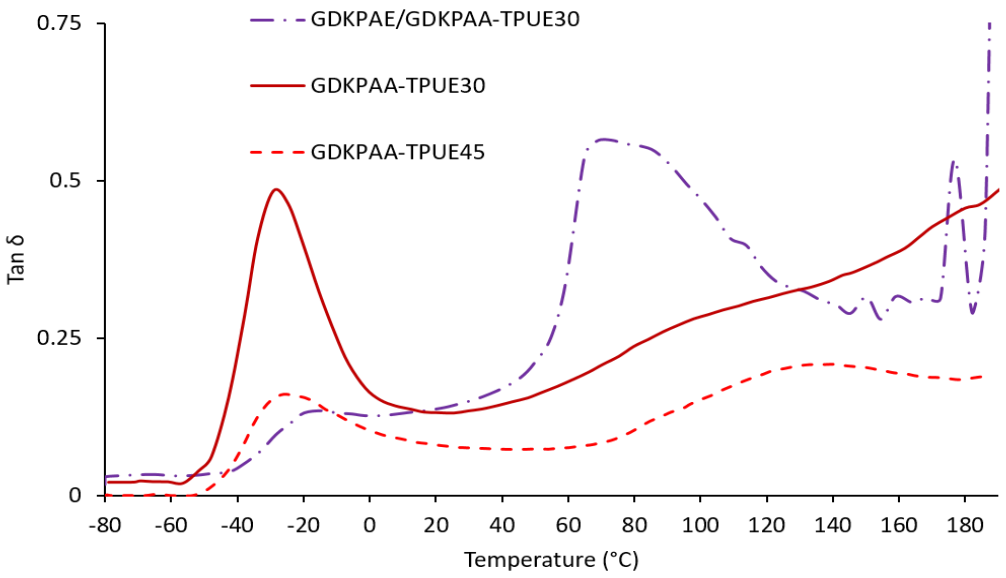


**Figure 3.10 DMA thermograms of tan *δ* for a GDKPAA-TPUE30 and TPUE45 and a GDKPAE/GDKPAA-TPUE30. Experiments were conducted in tension mode (preload 1 N) with a displacement of 20 µm and a frequency of 5 Hz across a temperature range of-80 °C to 200 °C with a heating rate of 5 K min$^{-1}$.**

As previously discussed, using DMA it is possible to observe *E'* and *E''* as a function of temperature and the thermomechanical properties of the GDKPAE-TPUEs could be deduced. E' exhibits a steep, multiple decade decrease across all %HS as a result of a glass transition. The most severe reduction of E' was observed in the GDKPAE-TPUE60, which transitioned from 13,000 MPa to 0 MPa between --80 °C and 70 °C with only a minimal plateau at 40 °C between thermal events. This severe decrease in E' is because of the soft and hard segment glass transitions of the GDKPAE-TPUE60. When E' reached 0 MPa the TPUE was no longer a self-supporting solid material but instead was a free-flowing liquid and hence the experiment was terminated.

As these materials are expected to be applied to *in vivo* applications it is of interest to gain an understanding of their properties at body temperature. First, the E' values, which show the energy stored in the material, were observed to increase with increased %HS in both the GDKPAE and the GDKPAA-TPUEs. This increased E' is a result of an increase in the number of hydrogen bonding sites between the hard segment domains and the stacking of the ring structures in the chain extender. The E' of the GDKPAE/GDKPAA-TPUE30 was observed to be similar in magnitude to that of the GDKPAA-TPUE30 at 38 MPa at 37 °C. It was noted that the GDKPAE-TPUE45 dissipated a substantial proportion of its stored energy rapidly after the onset of the hard segment $T_g$. Secondly, E'' values, which show the energy dissipated as heat, were observed to have two peak maxima for all %HS. These peak maxima correspond to the $T_g$ of the hard and soft segments. The E'' readings were observed to increase with increased %HS in both the GDKPAE and GDKPAA-TPUEs. The GDKPAE/GDKPAA-TPUE30 was observed to have an E'' of a similar magnitude to the GDKPAE-TPUE30 of 34 MPa at 37 °C which differs to the E' character. **(Figures 3.11 and 3.12 and Table 3.3)**

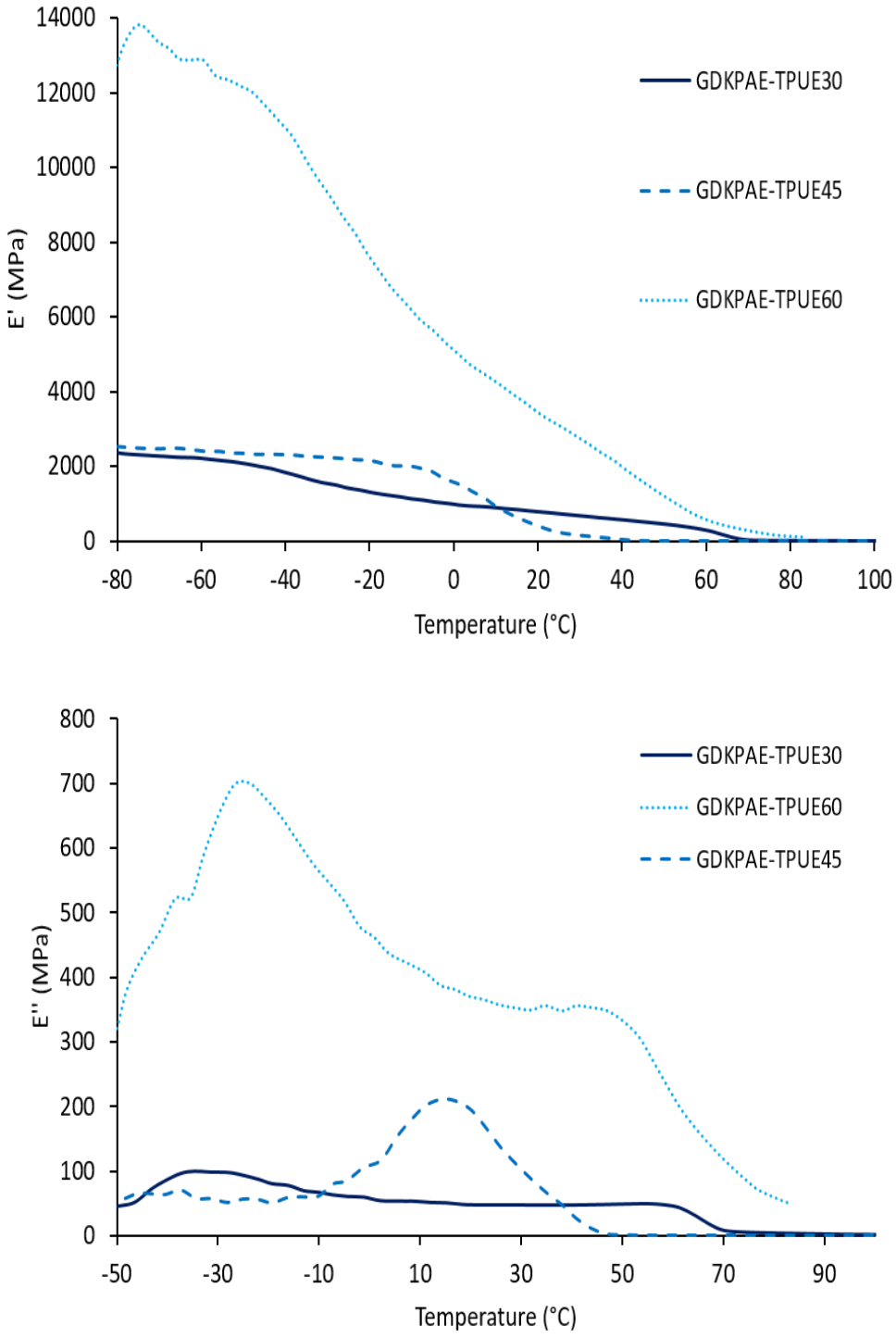


**Figure 3.11 DMA thermograms of E' (*top*) and E'' (*bottom*) for a GDKPAE-TPUE30, TPUE45, and TPUE60. Experiments were conducted in tension mode (preload 1 N) with a displacement of 20 µm and a frequency of5 Hz across a temperature range of -80 °C to 200 °C with a heating rate of 5 K min$^{-1}$.**

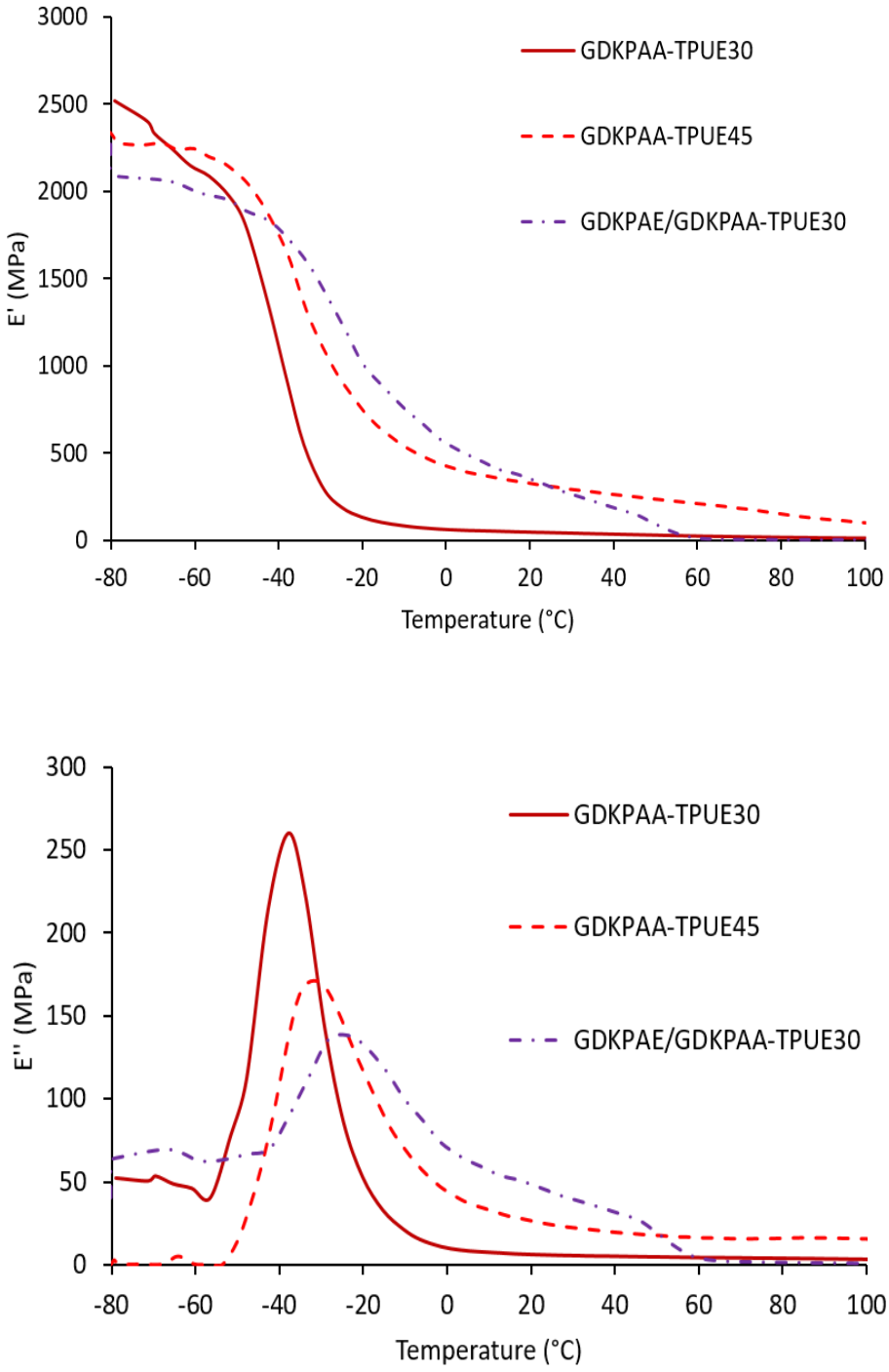


**Figure 3.12 DMA thermograms of E' (*top*) and E'' (*bottom*) for a GDKPAA-TPUE30 and TPUE45 and a GDKPAE/GDKPAA-TPUE30. Experiments were conducted in tension mode (preload 1 N) with a displacement of 20 µm and a frequency of5 Hz across a temperature range of -80 °C to 200 °C with a heating rate of 5 K $min^{-1}$.**

**Table 3.3 Comparison of the mechanical and thermal properties of a GDKPAE-TPUE30, TPUE45, TPUE60, GDKPAA, GDKPAE/GDKPAA and TDKP TPUEs.**

| Polymer | E'' (MPa at 37°C) | E' (MPa at 37°C) | Hard Segment Tan δ | Soft Segment Tan δ | Hard Segment $T_m$ (°C) | Hard Segment $T_g$ (°C) | Soft Segment $T_g$ (°C) |
|---|---|---|---|---|---|---|---|
| GDKPAE-TPUE30 | 47 | 594 | 0.50 | 0.05 | 80 | 70 | -30 |
| GDKPAE-TPUE45 | 47 | 47 | 0.20 | 0.01 | 60 | 40 | -30 |
| GDKPAE-TPUE60 | 348 | 2,137 | 0.40 | 0.13 | 80 | 50 | -30 |
| GDKPAA-TPUE30 | 5 | 34 | 0.30 | 0.50 | 200 | 95 | -30 |
| GDKPAA-TPUE45 | 20 | 267 | 0.20 | 0.20 | No data | 130 | -30 |
| GDKPAE/GDKAA-TPUE30 | 34 | 38 | 0.60 | 0.15 | 190 | 70,95,180 | -20 |
| TDKP-TPUE30 | 9 | 57 | 0.20 | 0.13 | No data | 195 | -30 |

### 3.2.3 Degradation analysis of thermoplastic polyurethane elastomers with novel diketopiperazine chain extenders

The way these TPUEs interact with water and subsequently degrade under hydrolytic conditions are key properties, which were investigated with static contact angle analysis with water and hydrolytic degradation analysis.

#### 3.2.3.1 Static contact angle analysis

To study the effect of different %HS on the surface interaction of the TPUEs with water, solutions at 5 wt.% in DMF of each of the TPUEs were layered to make thin films on glass slides on a heated plate at 60 °C, to evaporate the DMF. The slides were then heated for 6 h and allowed to cool to ambient temperature. Static water contact angle measurements were conducted on each TPUE after the thin films had annealed for 7 days in an incubator at 25 °C. This process was repeated ten times and the error between samples was calculated; using standard deviation.

For the GDKPAE-TPUE30, TPUE45 and TPUE60 the static water contact angles decreased with increasing %HS at 98.7 ° ± 3.2, 90.4 ° ± 8.4 and 84.6 ° ± 6.4 respectively **(Figure 3.13 top)**. This was because of an increase in the hydrophilicity of the chain extenders within the TPUE network resulting from more hydrogen bonding sites in the dipeptide structure caused by the increased %HS. The static water contact angles of 97.3 ° ± 6.6 for the GDKPAE-TPUE30, 97.4 ° ± 2.9 for the GDKPAA-TPUE30,

99.1 ° ± 6.4 for the GDKPAE/GDKPAA-TPUE30 and 102.6 ° ± 0.7 for the TDKP-TPUE30, were all within the error range. This result suggests that the hard segment of the TPUEs did not significantly affect the surface properties of the TPUE. **(Figure 3.13 bottom)**

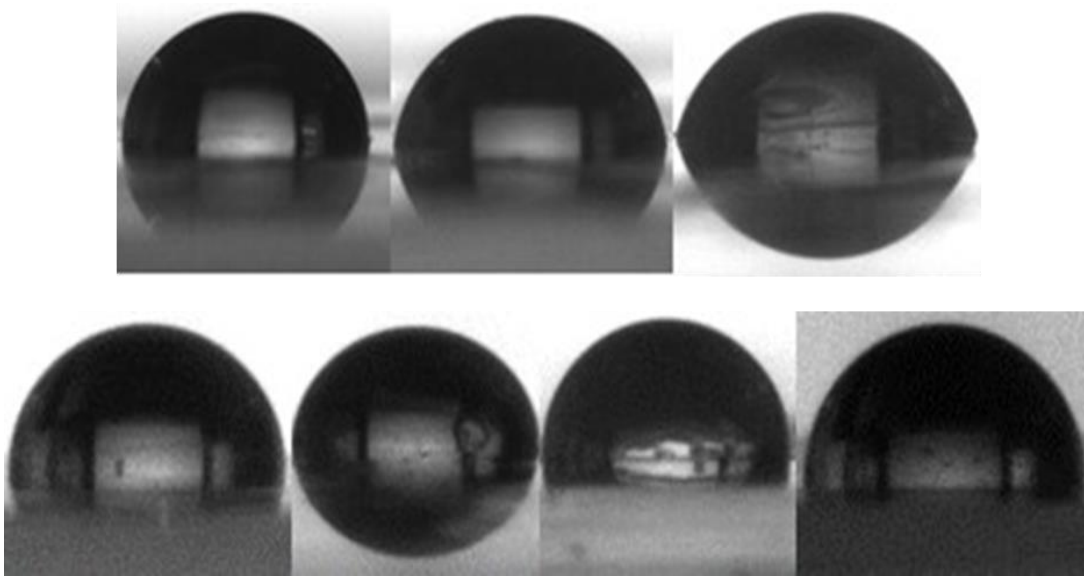

**Figure 3.13 Static water contact angle measurements for (*top*) a GDKPAE-TPUE30 (*left*), TPUE45 (*middle*) and TPUE60 (*right*) and (*bottom*) a GDKPAE-TPUE30 (*left*), a GDKPAA-TPUE30 (*centre, left*), a GDKPAE/GDKPAA-TPUE30 (*centre, right*) and a TDKP-TPUE30 (*right*).**

### 3.2.3.2 Hydrolytic degradation analysis

Following the static contact angle analysis with water, a set of experiments were conducted to assess the hydrolytic degradability of the GDKPAE, GDKPAA, GDKPAE/GDKPAA and TDKP-TPUE30s. Each of these TPUEs was compression moulded into 3 discs, placed in individual vials and submerged in 5 M KOH solution. The vials were stored in an incubator at 37 °C that was stirred at 60 rpm. For each TPUE the experiment was conducted three times and the mass was measured at predetermined time intervals until the sample became unrecoverable.

To assess the effect of increasing the %HS on the rate of hydrolytic degradation, a first set of experiments was conducted on samples of the GDKPAE-TPUE30, TPUE45 and TPUE60. It was observed that the GDKPAE-TPUE45 and TPUE60 initially had a mass gain in the first 24 h of 119% and 123% respectively. This was followed by rapid

degradation over the following 75 h. By contrast, the GDKPAE-TPUE30, which is predominately PCL, had a mass gain of 102% at 4 h and then degraded over 475 h. **(Figure 3.14)** This quicker rate of hydrolytic degradation is because of the superior hydrophilicity of the chain extenders as a result of more hydrogen bonding sites in the dipeptide structure caused by the enhanced %HS . The increased %HS enabled a more rapid diffusion of the degradation solution through the disc, which ultimately resulted in the rapid break down of the ester links within the hard and the soft segments.

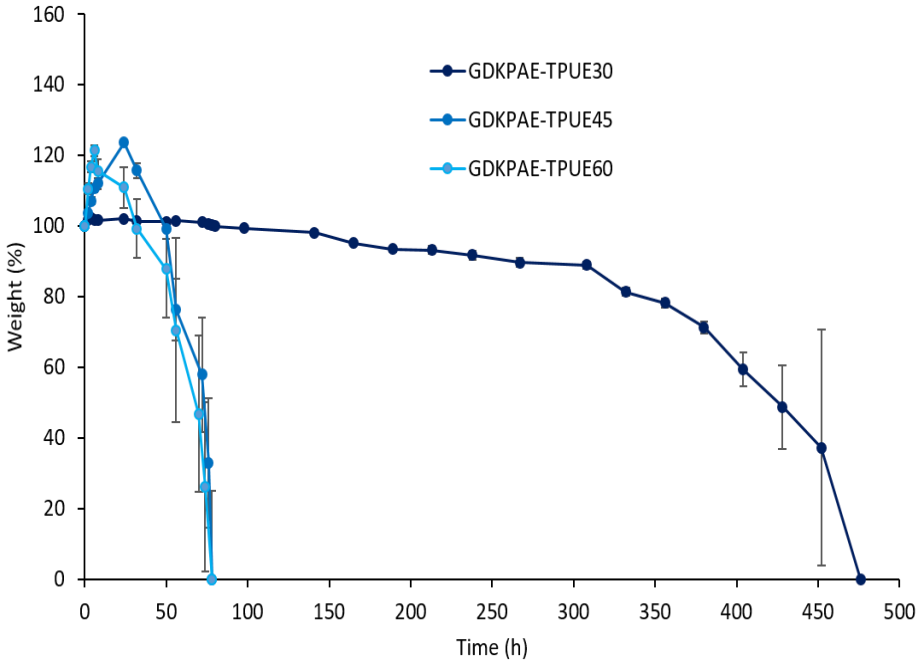


**Figure 3.14 A chart of % mass loss against time for a GDKPAE-TPUE30, TPUE45 and TPUE60: average of 3 samples, in a 5 M KOH solution at 37 °C and 60 rpm.**

A second set of experiments was conducted to observe the different hydrolytic degradation rates of the GDKPAE-TPUE30, the GDKPAA-TPUE30, the TDKP-TPUE30 and the GDKPAA/GDKPAA-TPUE30. The GDKPAE-TPUE30 degraded over 35 days, the GDKPAA-TPUE30 degraded over 19 days, the TDKP-TPUE30 had a mass gain of 139% and then degraded rapidly over 5 days and the GDKPAE/GDKPAA-TPUE30 degraded rapidly over 5 days. In the case of the GDKPAE-TPUE30, both the hard and soft segments contributed to the its breakdown. The PCL content of the soft segment

degraded first followed by the ester links in the hard segment, resulting in its complete breakdown. Conversely the GDKPAA-TPUE30 was observed to be more hydrophilic, which was characterised by a more rapid degradation of the PCL content of the soft segment but the amide links in the hard segment did not degrade under these conditions and ultimately it became unrecoverable after 19 days. The TDKP-TPUE30 showed even more hydrophilicity than the GDKPAA-TPUE30, which was characterised by the initial 139% mass gain followed by rapid degradation over 5 days. The rapid degradation of the GDKPAE/GDKPAA-TPUE30 was because of the combined effect of the complete breakdown of the PCL content of the soft segment and the ester component in the hard segment. This degradation was further accelerated by the increased hydrophilicity of the non-degrading amide components in the hard segment. **(Figure 3.15)**

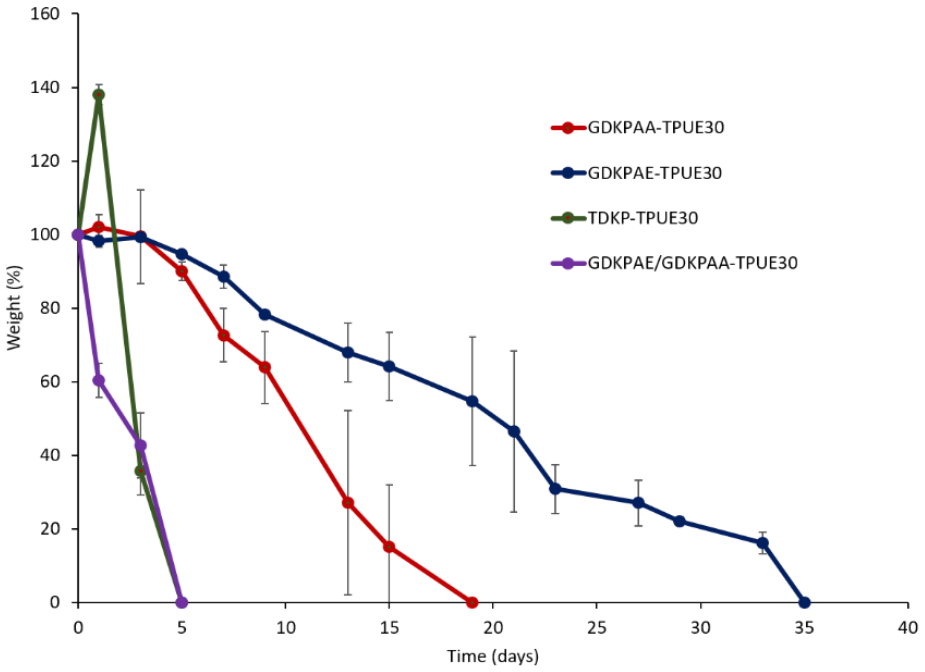


**Figure 3.15 A chart of % mass loss against time for a GDKPAE, a GDKPAA, a GDKPAE/GDKPAA and a TDKP-TPUE30: average of 3 samples in a 5 M KOH solution at 37 °C and 60 rpm.**

After studying the effect of the different hard segments on the rate of degradation, a further focus was made to analyse more closely the effect of the increased %HS on the degradation rate between the GDKPAE-TPUEs and the GDKPAA-TPUEs. As

previously stated, the GDKPAE-TPUE30, which fully degraded over 15 days, showed an increased degradation rate when the %HS was increased to 45%. This is because of the increased ester content in the hard segment, which contributed to a more complete and controlled breakdown of the TPUE. Conversely, the GDKPAA-TPUE30, which degraded over 19 days because of the rapid breakdown of the PCL component of the soft segment, showed a reduced degradation rate when the %HS was increased to 45%. This was because of the increased hydrophilicity of the amide content compared to the ester content in the relevant hard segments, which was characterised by a mass gain of 120% followed by the rapid breakdown of the PCL soft segment. However, as the soft segment decreased with increasing %HS there was less PCL to break down. The amide content in the hard segment did not appear to contribute to the more complete degradation of the TPUE that was characterised by a reduced rate of degradation between 23 and 50 days at which point it was unrecoverable. **(Figures 3.16 and 3.17)**

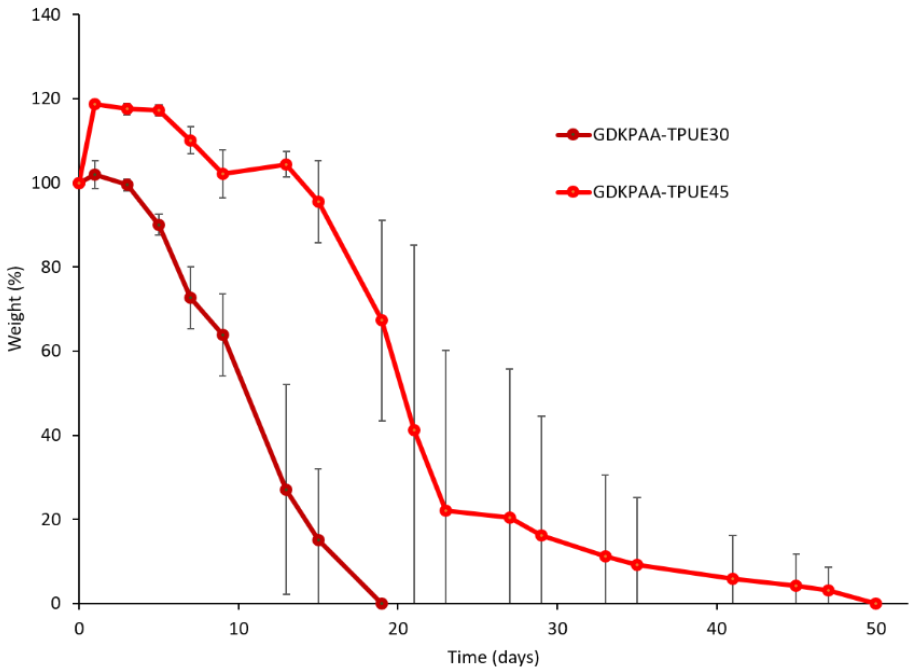


**Figure 3.16 A chart of % mass loss against time for a GDKPAE-TPUE30 and TPUE45: average of 3 samples in a 5 M KOH solution at 37 °C and 60 rpm.**

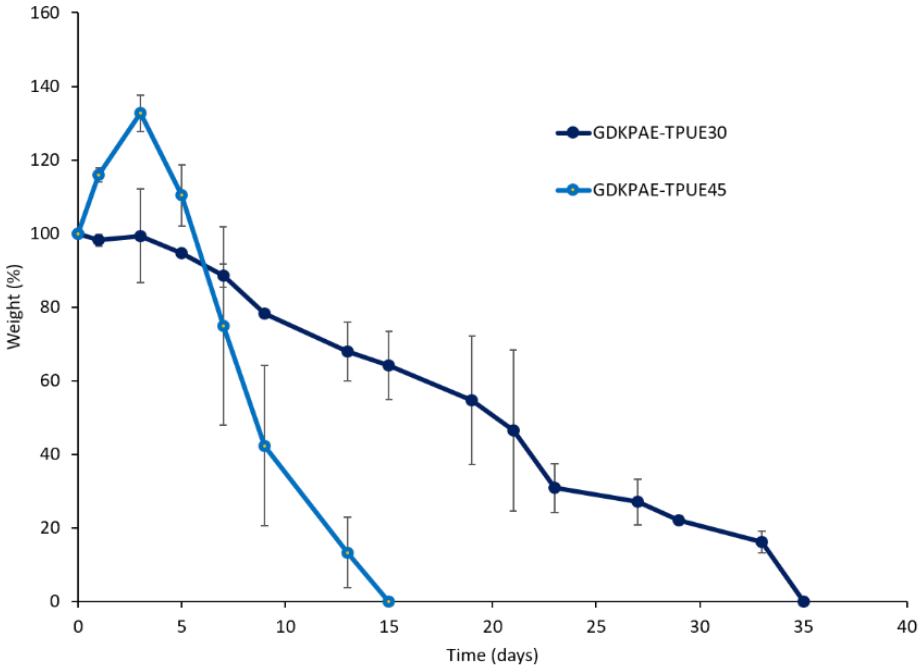


**Figure 3.17 A chart of % mass loss against time for a GDKPAA-TPUE30 and TPUE45: average of 3 samples in a 5 M KOH solution at 37 °C and 60 rpm.**

### 3.2.4 Further research directions for DKP-based thermoplastic polyurethane elastomers

In chapters 2 and 3 the concept of using DKPs in TPUEs has been developed and how the amount and variety of DKP alters the mechanical, thermal and degradative properties of the resulting TPUEs has been explored. Future areas of interest could include:

- different links and functionality of the coupling molecule using symmetrical and non-symmetric DKPs;
- variation of the stereochemistry;
- non-alcohol DKPs such a *L*-tryptophan and *L*-cysteine; and
- degradative drug release systems.

## 3.3 Conclusions

The use of DKPs as chain extenders provides a simple and effective method of tuning the mechanical, thermal and degradative properties of TPUEs.

Using tensile analysis, a trend was observed whereby with increasing quantities of DKP-based chain extender the TPUEs became tougher and displayed a reduction in their elastomeric properties. Further to this, the GDKPAE-TPUEs were soft and elastic materials by comparison to the GDKPAA-TPUEs that were tough and elastic. The GDKPAE/GDKPAA-TPUE combined properties of both the GDKPAE and GDKPAA homopolymers. Using DMA, the storage and loss moduli were observed to reduce with lower amounts of DKP--based chain extender at 37 °C.

Under accelerated hydrolytic degradation conditions, the GDKPAE-TPUEs were observed to exhibit an increased degradation rate as the %HS increased and resulted in a more complete breakdown of the hard segment. Conversely, it was observed that the GDKPAA-TPUEs degraded more slowly as the %HS increased because of the incomplete breakdown of the hard segment. Again, the GDKPAE/GDKPAA-TPUE30 was observed to combine characteristics from both the GDKPAE and GDKPAA homopolymers, which resulted in rapid degradation over 7 days.

Finally, the structure-function relationship of this family of TDKP and GDKP-based TPUEs has been further understood and they have been shown to provide an encouraging platform by which TPUEs can be tuned and tailored to a desired application, simply by modifying their hard segment structure or content.

## 3.4 References


1. R. J. Zdrahala and I. J. Zdrahala, *J. Biomater. Appl.*, 1999, **14**, 67-90.

2. R. S. Moglia, J. L. Robinson, A. D. Muschenborn, T. J. Touchet, D. J. Maitland and E. Cosgriff-Hernandez, *Polymer*, 2014, **55**, 426–434.

3. W. J. Lin, *J. Biomed. Mater. Res. Part A*, 1999, **47**, 420-423.

4. G. G. Pitt, M. M. Gratzl, G. L. Kimmel, J. Surles and A. Sohindler, *Biomaterials*, 1981, **2**, 215-220.

5. S. Y. Lin, K. S. Chen, H. H. Teng and M. J. Li, *J. Microencapsulation*, 2000, **17**, 577-586.

6. A. Göpferich, *Biomaterials*, 1996, **17**, 103-114.

7. S. Lyu and D. Untereker, *Int. J. Mol. Sci.*, 2009, **10**, 4033-4065.

8. K. E. Uhrich, S. M. Cannizzaro, R. S. Langer and K. M. Shakesheff, *Chem. Rev.*, 1999, **99**, 3181-3198.

9. L. M. Orozco-Castellanos, A. Marcos-Fernández and A. Martínez-Richa, *Polym. Adv. Technol.*, 2009, **22**, 430-436.

10. I. Castilla-Cortázar, J. Más-Estellés, J. M. Meseguer-Dueñas, J. L. Escobar Ivirico and B. Marí, Vidaurre, A., *Polym. Degrad. Stab.*, 2012, **97**, 1241-1248.

11. J. Guan and W. R. Wagner, *Biomacromolecules*, 2005, **6**, 2833-2842.

12. S. A. Guelcher, K. M. Gallagher, J. E. Didier, D. B. Klinedinst, J. S. Doctor, A. S. Goldstein, G. L. Wilkes, E. J. Beckman and J. O. Hollinger, *Acta Biomaterialia*, 2005, **1**, 471-484.

13. G. Odian, *Principles of Polymerization*, John Wiley & Sons, Inc., USA, 4th edn., 2004, ch. 2, pp. 79-80.

14. G. Odian, *Principles of Polymerization*, John Wiley & Sons, Inc., USA, 4th edn., 2004, ch. 2, pp. 63-65.

15. Dynamic Mechanical Analysis - Comprehensive Materials Characterization, https://www.mt.com/dam/Analytical/ThermalAnalysi/TA-PDF/DMA1_Brochure_en_30129289A_V02.16.pdf, Accessed 20/8/17.

# Chapter 4

# The Preparation of Hyperbranched Chain Terminating Agents from 1,1’-Carbonyldiimidazole in a One-Pot Process.

## 4.1 Introduction

Hyperbranched polymers (HBPs) possess several noteworthy chemical and physical properties, most particularly their viscosity characteristics, as they are capable of remaining gel-free for up to three branches unlike their linear analogues. As a result, they are becoming increasingly utilised in a wide range of applications from coatings to biomaterials.[1,2]. One of the main advantages of HBPs is that, despite their less well-defined structures, they can be synthesised in a one-pot process from either an $AB_2$ monomer or a combination of $A_2$ and $B_3$ monomers.[3-5] However, unlike $A_2$ and $B_3$ monomers, there are a limited number of commercially available $AB_2$ monomers for polymerisation.[6-10] The most studied of these is 2,2-dimethylolpropionic acid.[11] Synthetic procedures have been reported to produce $AB_2$ monomers, however, these require multiple steps and extensive purification.[12,13]

Carbonylbiscaprolactam (CBC) is a non-toxic precursor, which was first prepared by Meyer[14] and was, until recently, commercially available from Koninklijke DSM N.V.(DSM). CBC has been reported to react with a nucleophile *via* two mechanisms; ring-opening and ring-elimination of ε-caprolactam (ε-CLM). **(Scheme 4.1[15])**[16,17] Furthermore, it has recently been shown that CBC selectively reacts with a primary amine, even in the presence of a secondary amine, when the temperature is maintained at 80 °C. This is because secondary amines do not react below 145 °C. This selectivity, has been exploited to make $AB_2$ monomers in a one-pot process; 'A' being a secondary amine functionality and 'B' being an ε-CLM terminus.[18] It has further been reported that self-condensation of the $AB_2$ monomer resulted in the production of an HBP, where no gelation of the material was observed up to a third generation of branching.[19] Post-polymerisation modification of this HBP was performed in the same pot, by unblocking the ε-CLM chain termini, with monomethoxy poly(ethylene glycol)s forming urethane chain ends.[20]

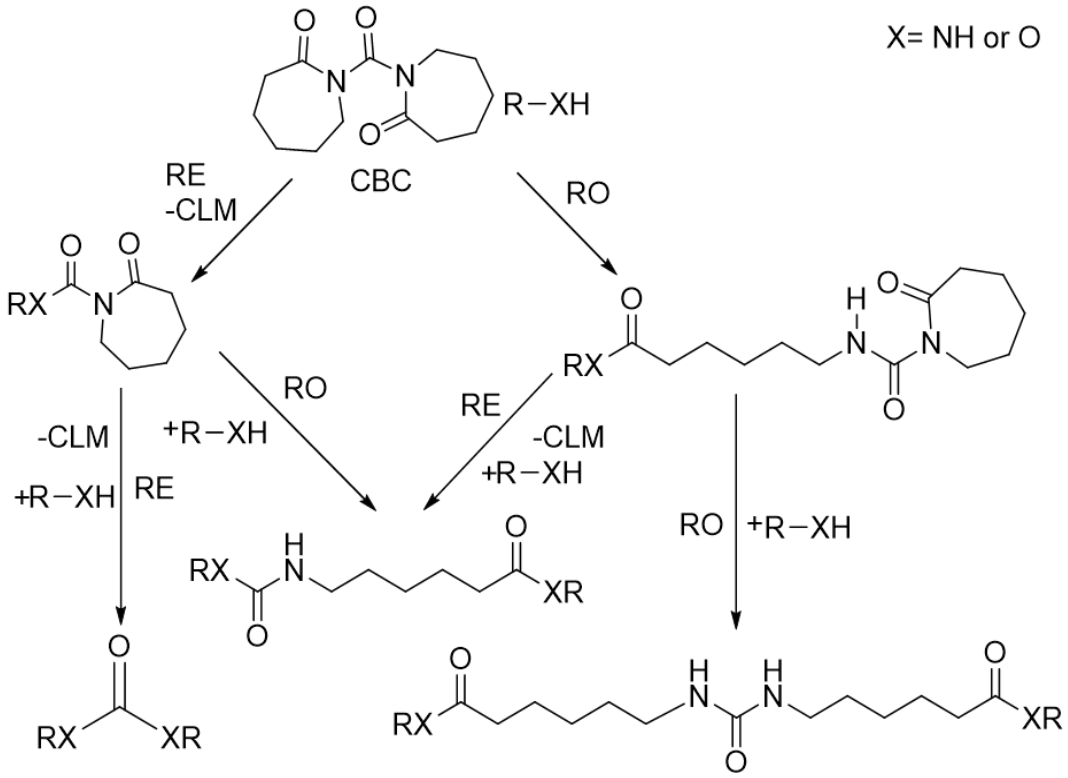


(Scheme reproduced from reference 15).

**Scheme 4.1 The ring-opening (RO) and ring-elimination (RE) reaction pathways of ε-CLM on CBC.**

An alternative synthesis method was developed by Rannard and co-workers to form aliphatic polyurethane (PU) homodendrimers by reacting CDI with a tertiary alcohol followed by a triamine to form a di-protected triamine that was then further reacted with propylene oxide to achieve a secondary alcohol functionality. Using this intermediate, the diamino alcohol 1-[bis(2-aminoethyl)-amino]-2-propanol was produced by deprotecting the tertiary alcohol and then subsequently adding this to the di-protected triamine to form a PU dendrimer, all in a one-pot selective procedure. [21] This work was then developed using CDI with the selective activation of unprotected $AB_2$ monomers producing water-soluble hyperbranched PUs. This is an effective method to produce aliphatic homodendrimers through the selective activation of the A functionality but no reaction was reported at the B functional site of the unprotected $AB_2$ monomer as shown in **(Scheme 1.6)**.

Herein is described the synthesis of HBPs, using the literature-reported synthetic route, from CBC and the post-polymerisation chain end modification with aromatic chain ends of the HBP. Furthermore, the synthesis of multi-branched HBPs, with low

dispersities, from 1,1'-carbonyldiimidazole (CDI), utilising a versatile one-pot, catalyst free, hyperbranching process and with the one-pot, temperature-controlled sequential synthesis of primary and secondary amines, with aromatic or fluorinated chain ends, is reported.

## 4.2 Results and Discussion

### 4.2.1 Hyperbranched chain terminating agents derived from carbonylbiscaprolactam

#### 4.2.1.1 Synthesis of carbonylbiscaprolactam

As mentioned in the introduction to this chapter, CBC was until recently commercially available from DSM, however, because of a fall in supply and concerns over the safety of the reaction on an industrial scale this is no longer the case. Fortunately, there are a variety of literature reports that describe the synthesis of CBC.[22] It was decided to synthesise CBC using triphosgene in the carbonylation of two molar equivalents of ε-CLM with *N,N*-diisopropylethylamine (DIPEA) as a hydrochloric acid scavenger. **(Scheme 4.2)**

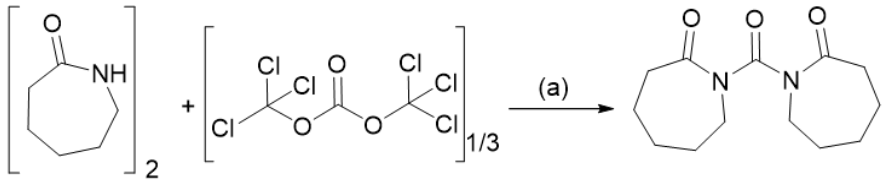


(a) DIPEA, toluene, 40 °C, 4 h, 63% yield.

**Scheme 4.2 The synthesis of CBC from triphosgene and ε-CLM.**

The synthesis of CBC was confirmed by $^{1}$H NMR spectroscopy that showed the loss of the ε-CLM amide resonance at $\delta$ = 6.91 ppm and that the resonances of the ε-CLM methylenes had shifted downfield. Most notably the resonance of the methylene next to the nitrogen atom had shifted from $\delta$ = 3.16 ppm to 3.80 ppm. Also, the resonances observed in the CBC $^{1}$H NMR spectrum were very broad unlike the resonances in the ε-CLM $^{1}$H NMR spectrum that had large multiplets. It is considered that this is because of the free rotation of the carbonyl-bridged ε-CLMs. In addition, $^{13}$C NMR spectroscopy confirmed the formation of a bridging carbonyl resonance at $\delta$ = 157 ppm. **(Figures 4.1 and 4.2)**

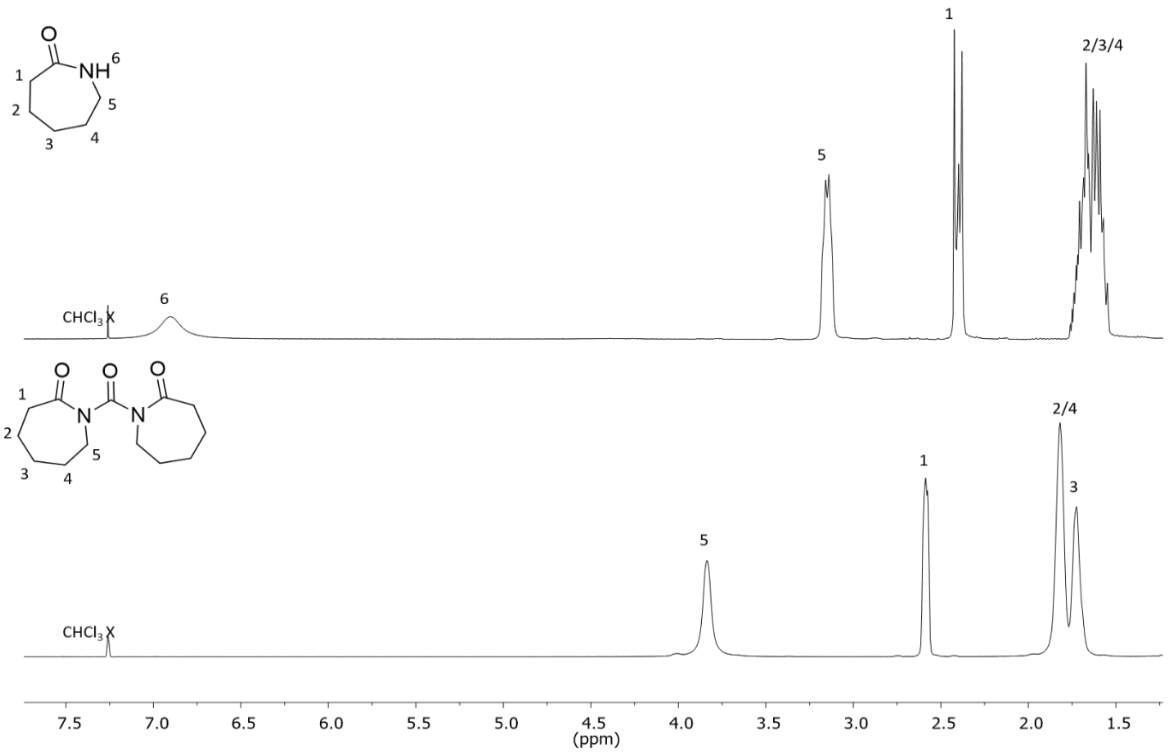


**Figure 4.1 $^{1}$H NMR spectra of ε-CLM (top) and CBC (bottom) (400 MHz, 298 K, $CDCl_3$).**

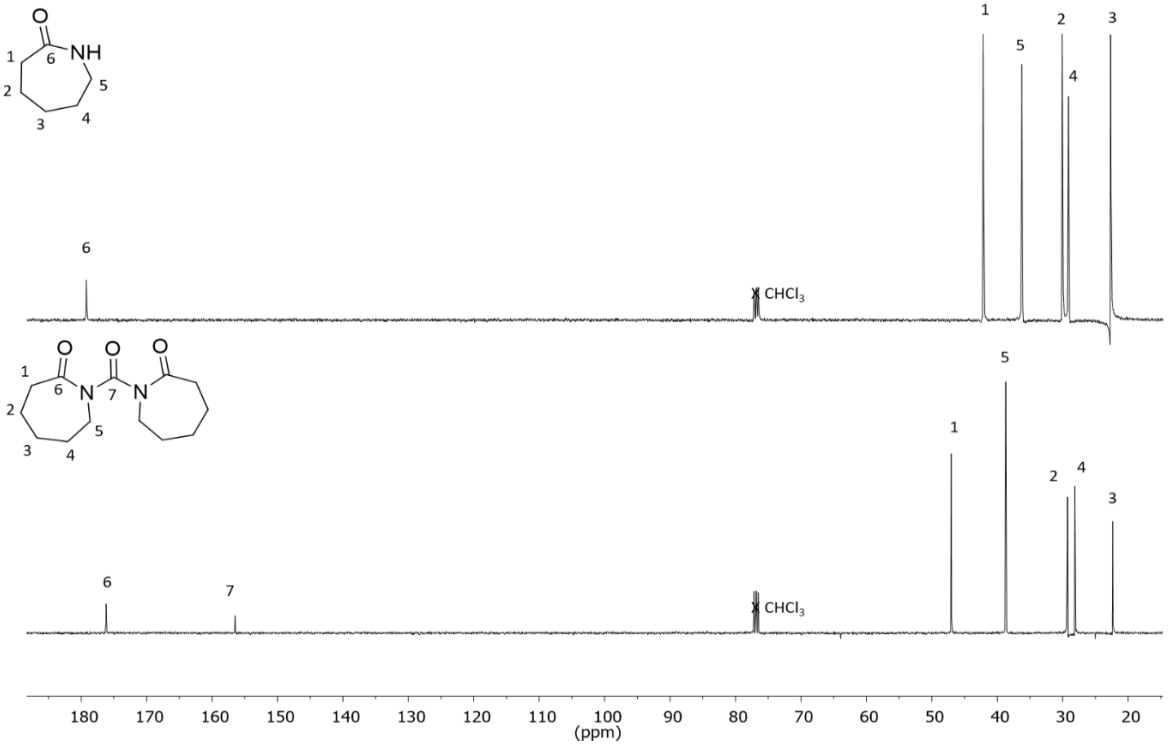


**Figure 4.2 $^{13}$C NMR spectra of ε-CLM (top) and CBC (bottom) (125 MHz, 298 K, $CDCl_3$).**

### 4.2.1.2 Synthesis of an $AB_2$ monomer from carbonylbiscaprolactam

As previously described, it has been reported that CBC exhibits selectivity towards primary amines, even in the presence of secondary amines, when the reaction temperature is maintained at 80°C. Initial control experiments were performed to confirm these reports. First, CBC and hexylamine (1:1 molar equivalents) were combined for 8 h at 80 °C to yield a mono-substituted urea product, *N*-hexyl-2-oxoazepane-1-carboxamide **(Scheme 4.3).** *In situ* $^1$H NMR spectroscopy confirmed the free ε-CLM (by-product of the reaction) resonances at $\delta$ = 6.25 ppm, 3.20 ppm, 2.44 ppm and 1.70 ppm and the urea proton resonance at $\delta$ = 9.25 ppm. **(Figure 4.3)**

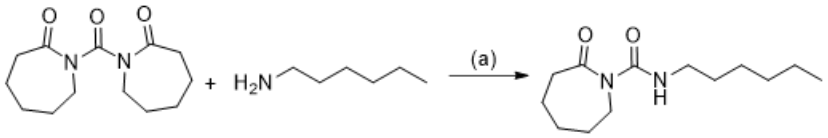


(a) toluene, 80 °C, 8 h, 94% yield.

**Scheme 4.3 The synthesis of *N*-hexyl-2-oxoazepane-1-carboxamide from CBC and hexylamine.**

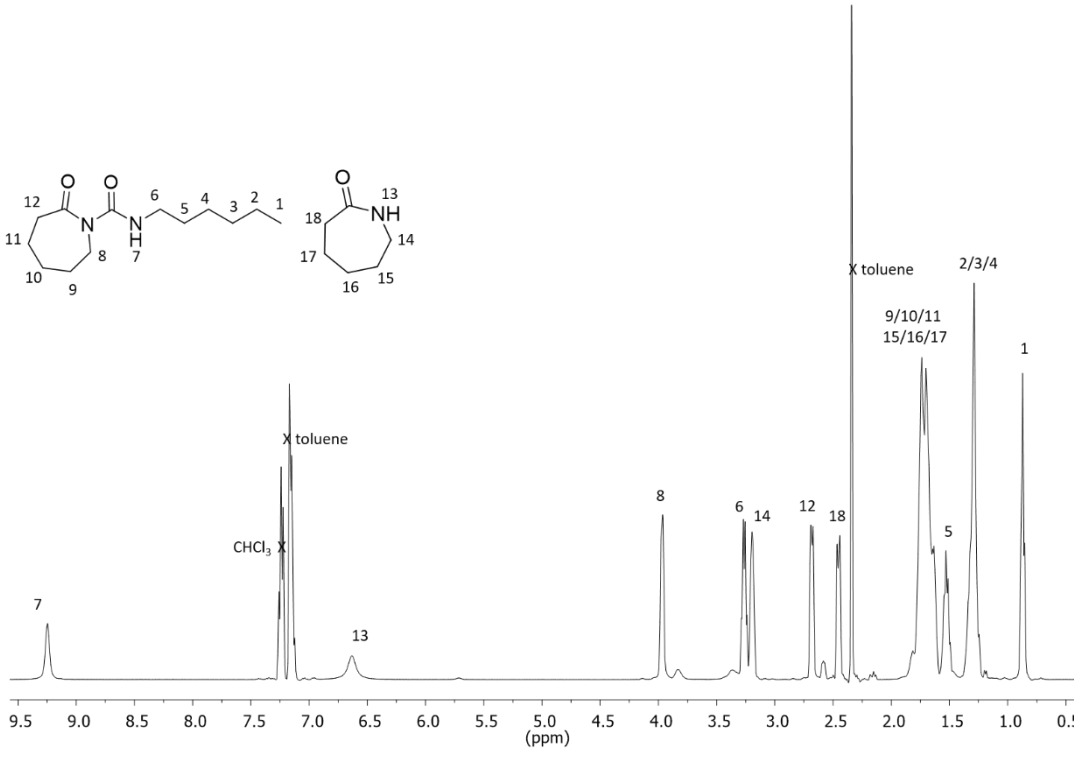


**Figure 4.3 *In situ* $^1$H NMR spectrum, after 8 h at 80 °C, of the reaction mixture of CBC and hexylamine (400 MHz, 298 K, $CDCl_3$).**

Secondly, CBC was combined with dihexylamine (1:1 molar equivalents) for 8 h at 80 °C and no reaction occurred **(Scheme 4.4).** *In situ* $^{1}$H NMR spectroscopy confirmed no chemical shifts of the methylene resonances and no appearance of free ε-CLM resonances. **(Figure 4.4)**

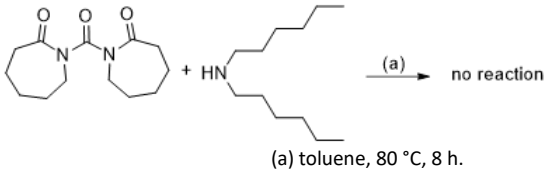


**Scheme 4.4 The non-reaction of CBC with dihexylamine.**

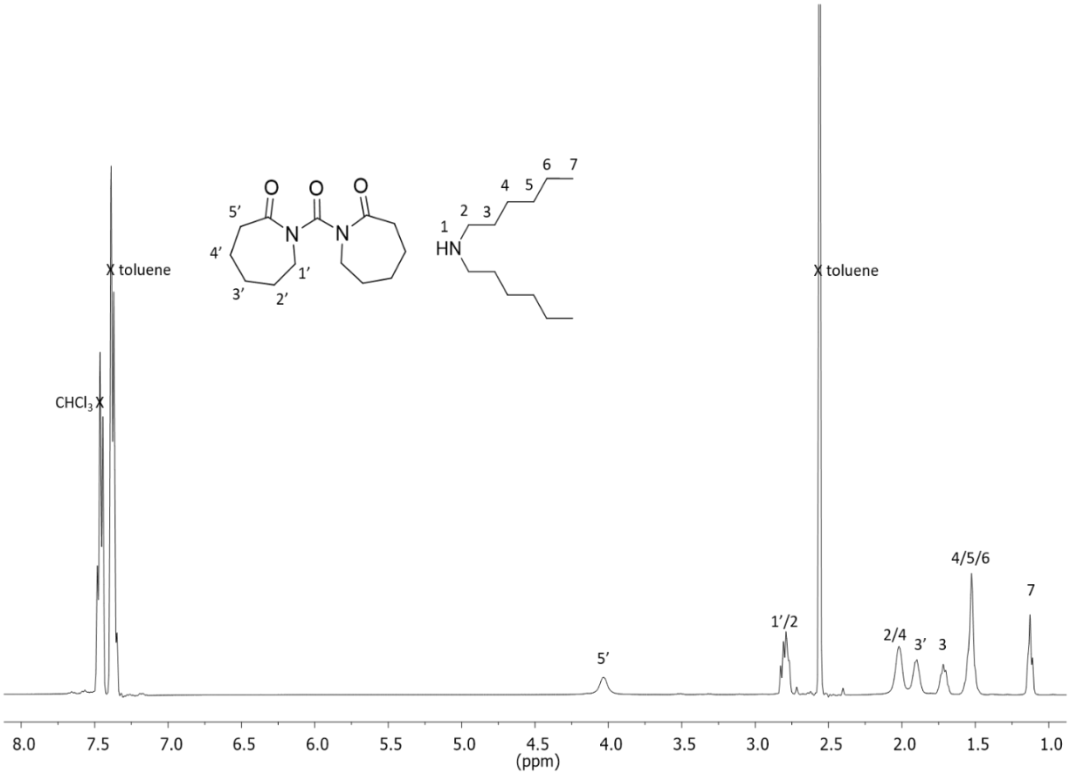


**Figure 4.4 *In situ* $^{1}$H NMR spectrum, after 8 h at 80 °C, of the non-reaction of CBC and dihexylamine (400 MHz, 298 K, $CDCl_3$).**

The previous small molecule experiments suggest that combining CBC with bis(hexamethylene)triamine (BHMTA) (2:1 molar equivalents) for 8 h at 80 °C will produce the $AB_2$ monomer *N,N'*-(azanediylbishexane-6,1-diyl)bis(2-oxoazepane-1-carboxamide) (CBC-$AB_2$), which is consistent with reports.[19] **(Scheme 4.5)**

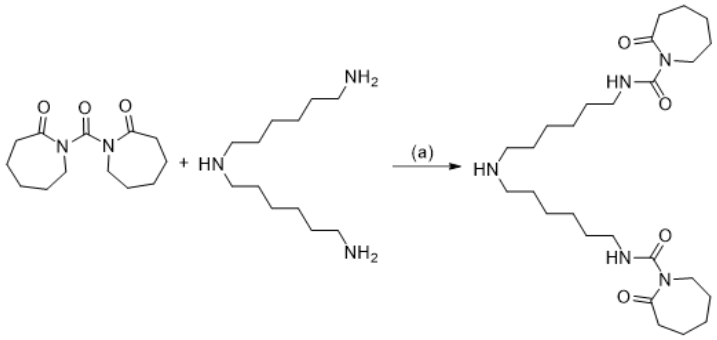


(a) toluene, 80 °C 8 h, 14% yield.

**Scheme 4.5 The one-pot, temperature-controlled sequential synthesis of a CBC-AB$_2$ from CBC and BHMTA.**

*In situ* $^1$H NMR spectroscopy showed the formation of a urea proton resonance at $\delta$ = 9.20 ppm and the formation of free ε-CLM (by-product of the reaction) resonances at $\delta$ = 6.75 ppm, 3.15 ppm, 2.45 ppm and 1.74 ppm. This by-product was removed by washing with a saturated $CaCl_2$ solution, as shown by its absence in the pure $^1$H NMR spectrum of purified CBC-AB$_2$. **(Figure 4.5)**

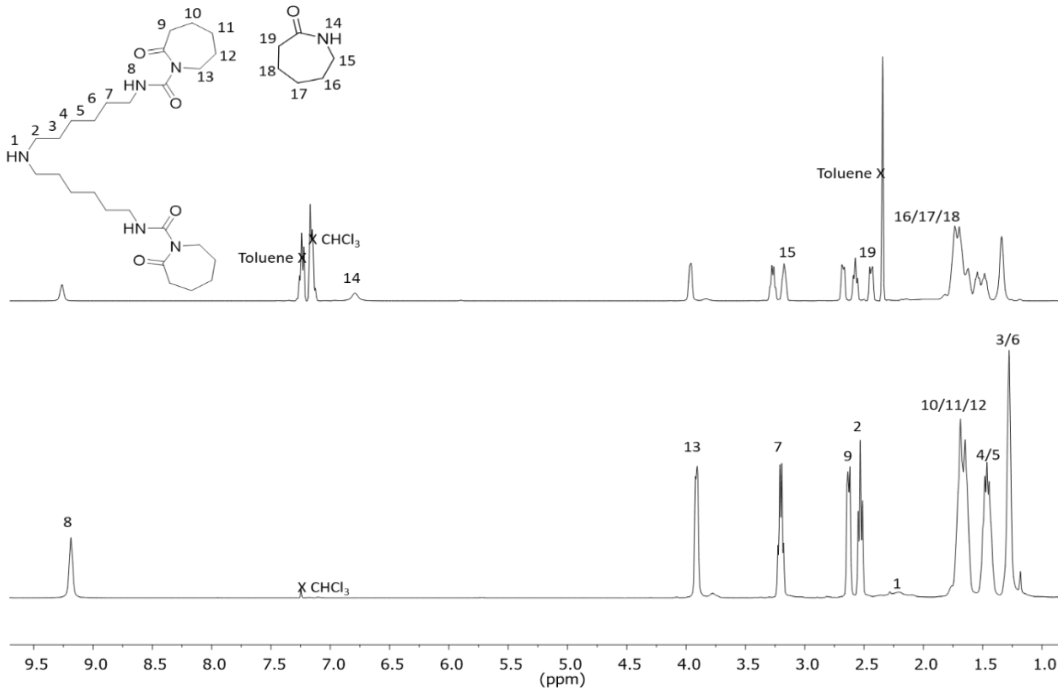


**Figure 4.5 *In situ* $^1$H HMR spectrum, after 8 h at 80 °C, of the reaction mixture of CBC and BHMTA (top) and $^1$H HMR spectrum of the purified CBC-AB$_2$ (bottom) (400 MHz, 298 K, $CDCl_3$).**

### 4.2.1.3 Synthesis of hyperbranched chain terminating agents from carbonylbiscaprolactam and bis(hexamethylene)triamine

Following the successful formation of CBC-$AB_2$, the temperature of the reaction was elevated to 145 °C, in the same pot, without the removal of the liberated ε-CLM, which produced hyperbranched *N,N'*-(azanediylbishexane-6,1-diyl)bis(2-oxoazepane-1-carboxamide) *via* the secondary amine focal point. **(Scheme 4.6)**

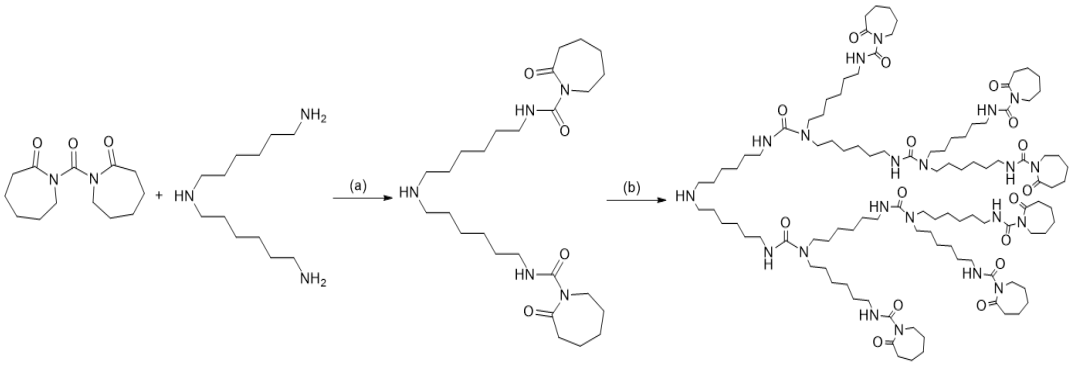


(a) DMF, 80 °C, 8 h; (b) DMF, 145 °C, 24 h, 13% yield.

**Scheme 4.6 The synthesis of hyperbranched *N,N'*-(azanediylbishexane-6,1-diyl)bis(2-oxoazepane-1-carboxamide) from a CBC-$AB_2$ using the one-pot, temperature-controlled sequential synthesis from CBC and BHMTA.**

The synthesis of hyperbranched N,N'-(azanediylbishexane-6,1-diyl)bis(2-oxoazepane-1-carboxamide) was confirmed by $^1$H NMR spectroscopy that showed the evolution of proton resonances for the methylene next to the urea between $\delta$ = 3.23 ppm and 2.92 ppm, a resonance at $\delta$ = 9.15 ppm for the urea at the chain end, a resonance at $\delta$ = 7.95 ppm for the mid chain urea and the free ε-CLM (by-product of the reaction) resonances at $\delta$ = 2.25 ppm, 1.75 ppm and 1.50 ppm. (**Figure 4.6)**

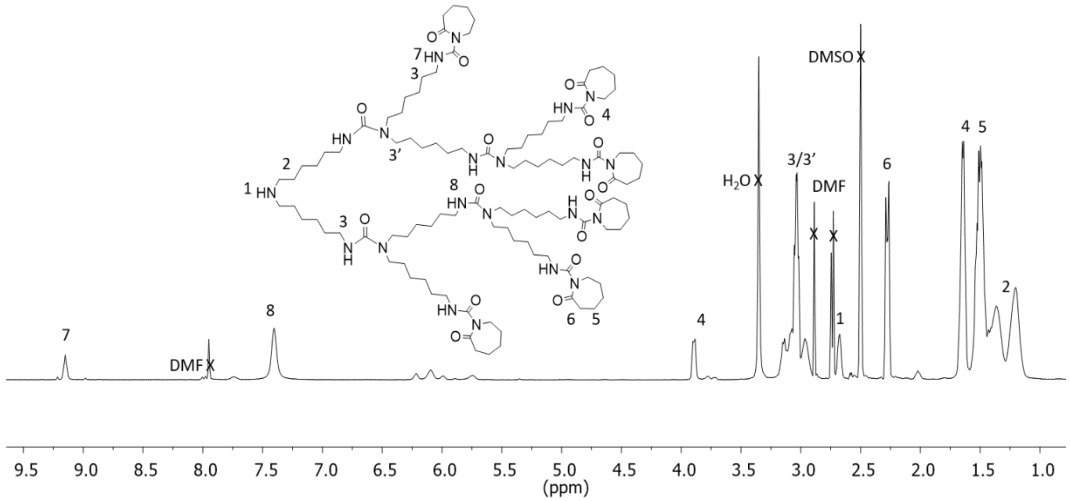


**Figure 4.6 $^{1}$H NMR spectrum of hyperbranched *N,N'*-(azanediylbishexane-6,1-diyl)bis(2-oxoazepane-1-carboxamide) synthesised from a CBC-AB$_2$ using the one-pot, temperature-controlled sequential synthesis from CBC and BHMTA (400 MHz, 298 K, DMSO-*d*$_6$).**

Post-polymerisation chain end modification of the hyperbranched ,N'-(azanediylbishexane-6,1-diyl)bis(2-oxoazepane-1-carboxamide) was then conducted, in the same pot, at a lowered temperature of 125 °C after the addition of benzyl alcohol (BnOH) and using tin(II) 2-ethylhexanoate (Sn(Oct)$_2$) as a catalyst, which was reported by Loontjens *et al* to effectively catalyse the ring-elimination and ring-opening reactions of ε-CLM by an alcohol. **(Scheme 4.7)**

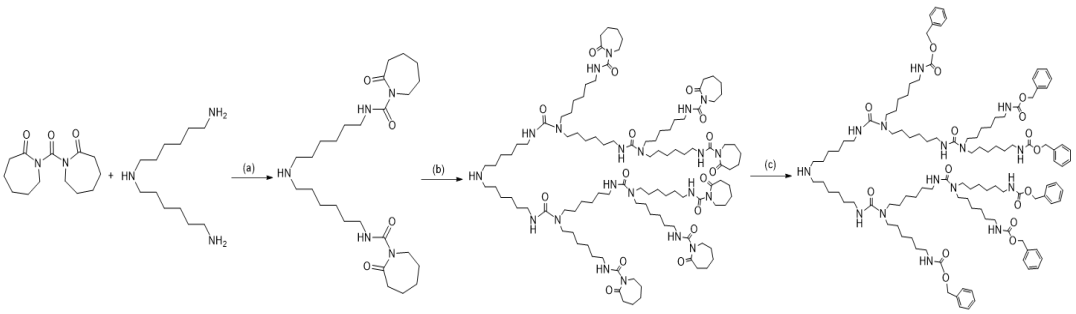


(a) DMF, 80 °C, 8 h; (b) DMF, 145 °C, 24 h; (c) BnOH, 125 °C, Sn(Oct)$_2$, DMF, 72 h, 10% yield.

**Scheme 4.7 The post-polymerisation chain end modification, with BnOH, of a CBC-AHCTA synthesised from a CBC-AB$_2$ using the one-pot, temperature-controlled sequential synthesis from CBC and BHMTA.**

After 72 h, the reaction mixture was precipitated into ethyl acetate to yield a hyperbranched N,N'-(azanediylbishexane-6,1-diyl)bis(2-oxoazepane-1-carboxamide) with aromatic BnOH chain ends (CBC-AHCTA). This was confirmed by $^{1}$H NMR spectroscopy showing the addition of an aromatic BnOH resonance at $\delta$ = 7.30 ppm and the resonance of the methylene on the BnOH end group at $\delta$ = 5.00 ppm. It was noted that not every chain end was aromatised with BnOH as the free ε-CLM (by-product of the reaction) resonances remained at $\delta$ = 2.35 ppm, 1.75 ppm and 1.50 ppm. **(Figure 4.7)**

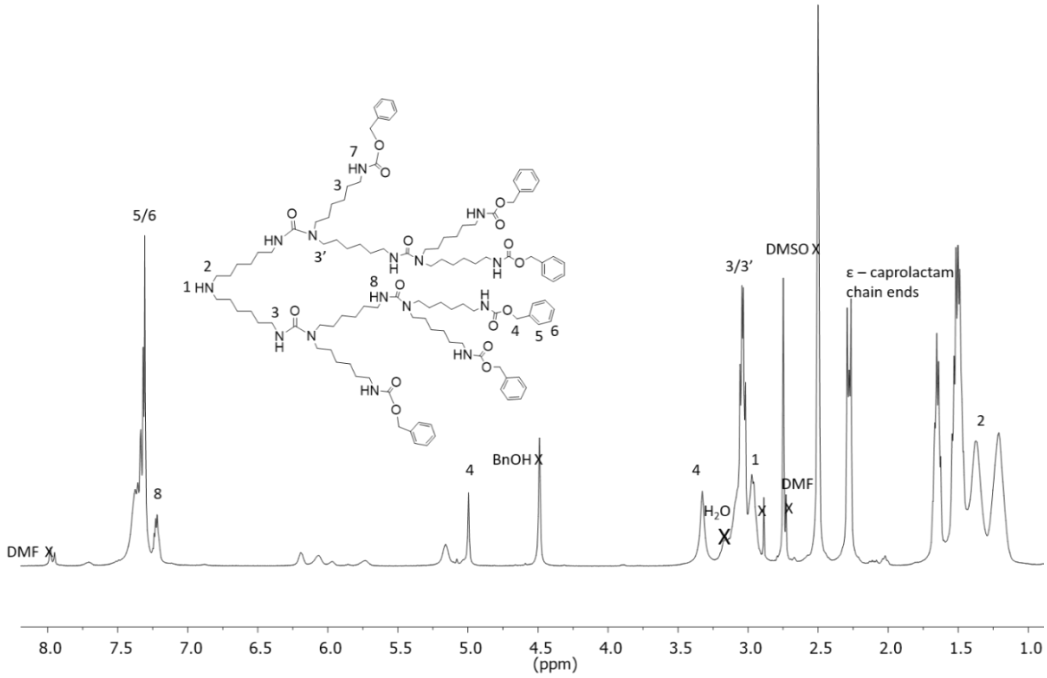


**Figure 4.7 $^{1}$H NMR spectrum of a CBC-AHCTA synthesised from a CBC-AB$_2$ produced from CBC and BHMTA (400 MHz, 298 K, DMSO-$d_6$).**

Size exclusion chromatography (SEC) of the CBC-AHCTA showed a unimodal distribution with a $M_n$ = 2,900 g mol$^{-1}$, $M_w$ = 7,100 g mol$^{-1}$ and $Đ_M$ = 2.50. **(Table 4.1)** After post-polymerisation chain end modification, the CBC-AHCTA showed an increase in molecular weight and dispersity at $M_n$ = 7,400 g mol$^{-1}$, $M_w$ = 3,000 g mol$^{-1}$, and $Đ_M$ = 2.51. **(Figure 4.8)**

**Table 4.1 Size exclusion chromatography data for a CBC-HCTA with and without aromatic BnOH chain ends synthesised from a CBC-$AB_2$ produced from CBC and BHMTA.**

| Sample | $M_n$ (g mol$^{-1}$)[a] | $M_w$ (g mol$^{-1}$)[a] | $Đ_M$[a] |
|---|---|---|---|
| Without aromatic chain ends | 2,900 | 7,100 | 2.50 |
| With aromatic chain ends | 3,000 | 7,400 | 2.51 |

a) Determined by SEC analysis in DMF against PMMA standards.

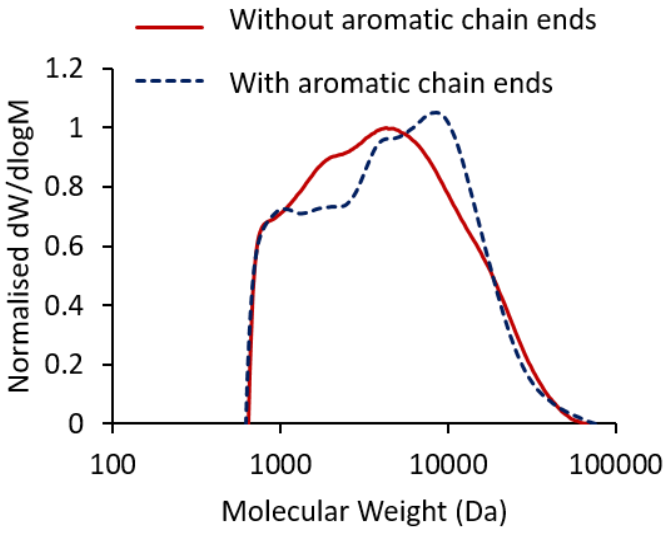


**Figure 4.8 SEC chromatograms of CBC-HCTAs with and without aromatic BnOH chain ends in DMF against PMMA standards.**

The advantage of this process is that it can be conducted in the same pot and the production of ε-CLM does not hinder each reaction step and this ε-CLM can easily be removed by precipitation in the last step. However, the scarce supply of CBC presented a problem for subsequent scale-up experiments for testing in various applications. It is also noted that, although the selectivity of CBC, with primary and secondary amines, is easily controlled by temperature, the branching and post-polymerisation reactions require heating between 125 °C and 145 °C for extended periods of time. In addition, post polymerisation modification requires a metal catalyst to aid the reaction process, which has been reported to be toxic in a range of applications.

## 4.2.2 Hyperbranched chain terminating agents derived from 1,1'-carbonyldiimidazole

### 4.2.2.1 Selectivity of 1,1'-carbonyldiimidazole with primary and secondary amines

Whilst the synthesis of CBC was being trialled, CDI was investigated as an alternative precursor for hyperbranched chain terminating agents (CDI-HCTAs). CDI was considered promising because it is commercially available and, compared to CBC, is relatively inexpensive. Both CBC and CDI possess similar chemical structures and can liberate their respective ε-CLM or imidazole leaving group under different conditions. However, unlike CBC, CDI is significantly more reactive towards nucleophiles because of the greater stability of imidazole compared to ε-CLM.

It has been reported that CDI is not controlled by either primary or secondary amines under the same conditions as CBC.[23-26] To confirm these reports, initial control experiments were conducted in which CDI and hexylamine (1:1 molar equivalents at room temperature, in bulk) were combined and yielded a mixture of the single and double addition urea products, *N*-hexyl-1*H*-imidazole-1-carboxamide and 1,3-dihexylurea **(Scheme 4.8).**

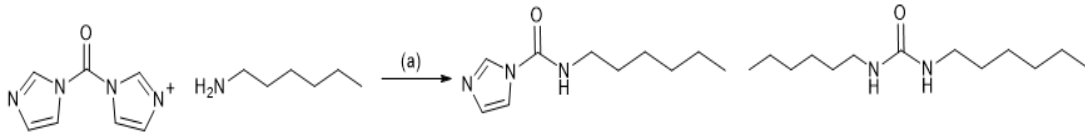


(a) in bulk at room temperature, 50% yield.

**Scheme 4.8 The synthesis of *N*-hexyl-1*H*-imidazole-1-carboxamide and 1,3-dihexylurea from CDI and hexylamine.**

$^{1}$H NMR spectroscopy confirmed the synthesis of both single and double addition products. The single addition product had methylene resonances at $\delta$ = 3.37 ppm, 1.69 ppm, 1.49 ppm and 1.09 ppm, a urea resonance at $\delta$ = 9.16 ppm and methine resonances at $\delta$ = 8.58 ppm, 8.44 ppm and 7.77 ppm corresponding to the pendant imidazole. The double addition product had methylene resonances at $\delta$ = 3.62 ppm, 1.69 ppm, 1.49 ppm and 1.09 ppm, a urea resonance at $\delta$ = 5.57 ppm and no imidazole methine resonances. Moreover, $^{13}$C NMR spectroscopy showed two carbonyl resonances, one at $\delta$ = 151 ppm relating to the double addition product and

the other at $\delta$ = 149 ppm relating to the single addition product. **(Figure 4.9)** It is considered that this mixture of single and double addition products was produced because of the exothermic heat resulting from the rapid addition of the amine to CDI and the sequential liberation of imidazole. This produced sufficient energy to activate the double addition, which is consistent with previous reports, as the double addition is only possible at higher temperatures.

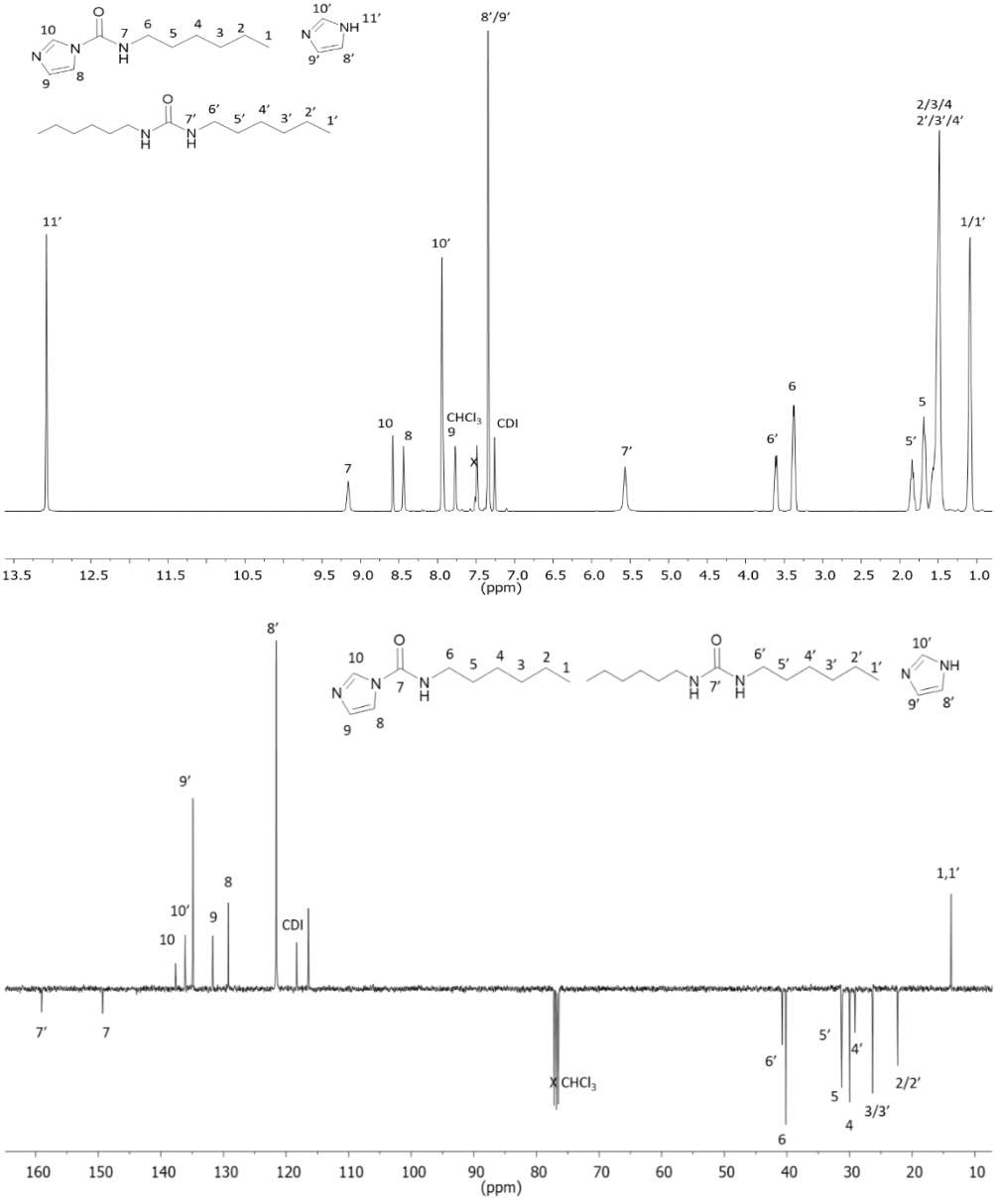


**Figure 4.9** ***In situ*** **$^{1}$H NMR (top) and $^{13}$C NMR (bottom) spectra, after 30 min, of the single and double addition urea products, *N*-hexyl-1*H*-imidazole-1-carboxamide and 1,3-dihexylurea, synthesised from CDI and hexylamine, in bulk at room temperature (400 MHz and 125 MHz, 298 K, $CDCl_3$).**

Subsequently, CDI and dihexylamine (1:1 molar equivalents at room temperature, in bulk) were combined and yielded only a single addition urea product, *N*,*N*-dihexyl-1*H*-imidazole-1-carboxamide. **(Scheme 4.9)** This was confirmed by $^{1}$H NMR spectroscopy that showed a resonance of the methylene next to the nitrogen atom at $\delta$ = 3.53 ppm, which had shifted downfield from the dihexylamine starting material together with the formation of methine proton resonances of the pendant imidazole at $\delta$ = 8.05 pm, 7.39 ppm and 7.26 ppm. $^{13}$C NMR spectroscopy showed a single carbonyl resonance at $\delta$ = 152 ppm. This result was consistent with literature as it has been reported that steric hindrance prevents the double addition of the secondary amine even at elevated temperatures **(Figure 4.10).**

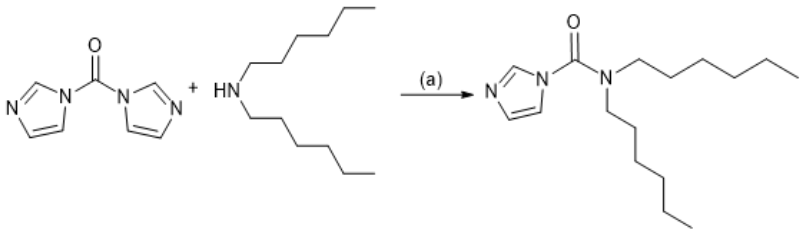


(a) in bulk at room temperature, 25% yield.

**Scheme 4.9 The synthesis of *N*,*N*-dihexyl-1*H*-imidazole-1-carboxamide from CDI and dihexylamine.**

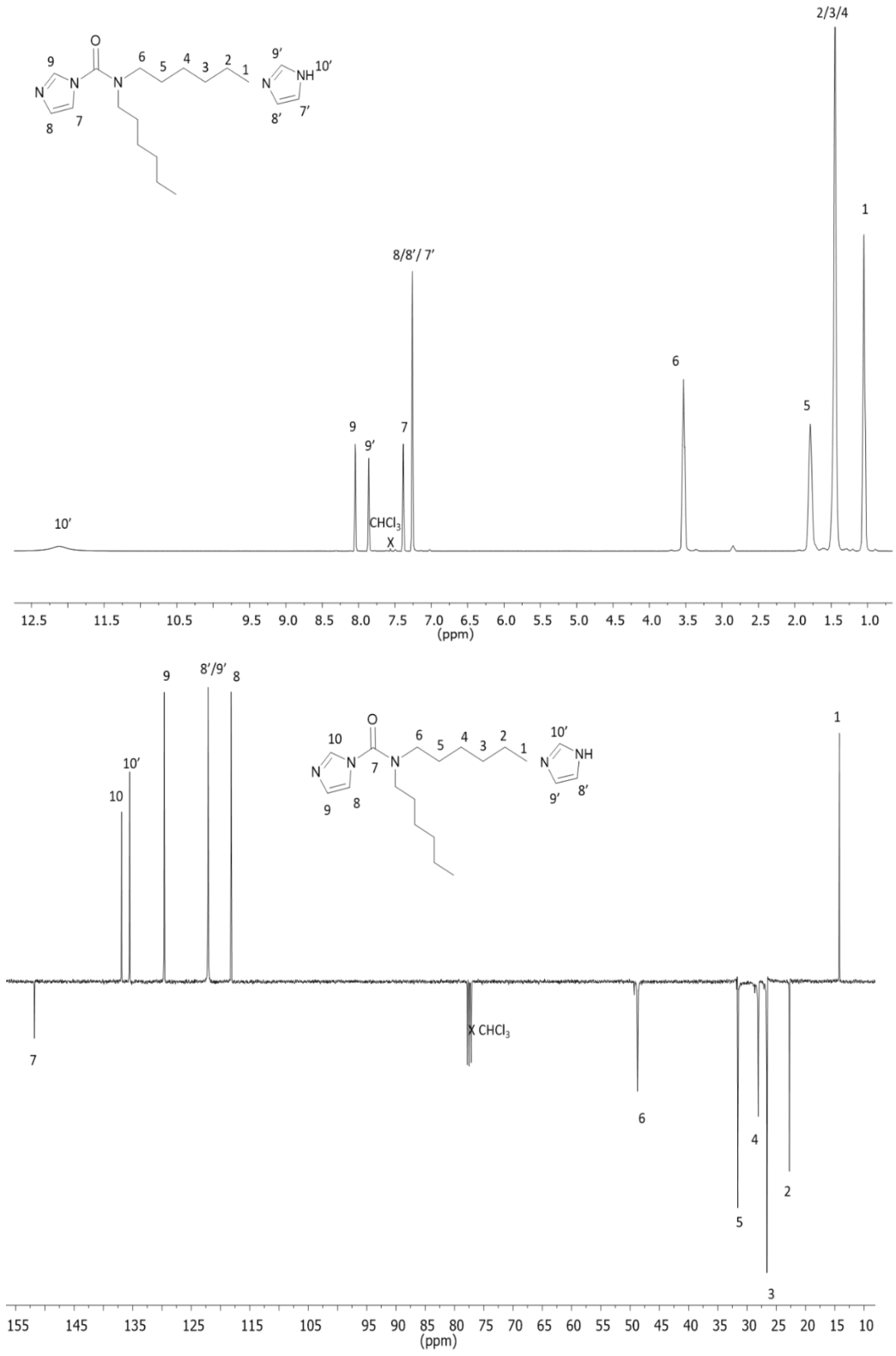


**Figure 4.10** ***In situ*** **$^{1}$H NMR (top) and $^{13}$C NMR (bottom) spectra, after 30 min, of the single urea product *N*,*N*-dihexyl-1*H*-imidazole-1-carboxamide synthesised from CDI and dihexylamine, in bulk at room temperature (400 MHz and 125 MHz, 298 K, $CDCl_3$).**

Because of the results of the previous small molecule experiments, it is considered that it will not be possible to produce an $AB_2$ monomer by combining CDI and BHMTA at room temperature. There is limited literature on the scope and control of the selectivity of CDI towards primary amines over secondary amines, but it is hypothesised that to create CDI-HCTAs the reaction conditions need to be controlled so that the primary amine reacts completely with the CDI before the secondary amine is consumed. To investigate this further, experiments were performed where CDI was initially combined with hexylamine (1:1 molar equivalents at -78 °C), then stirred for 2 h, whilst maintaining the temperature at -78 °C, at which point dihexylamine was charged to the reaction mixture that was then allowed to warm to room temperature. **(Scheme 4.10)**

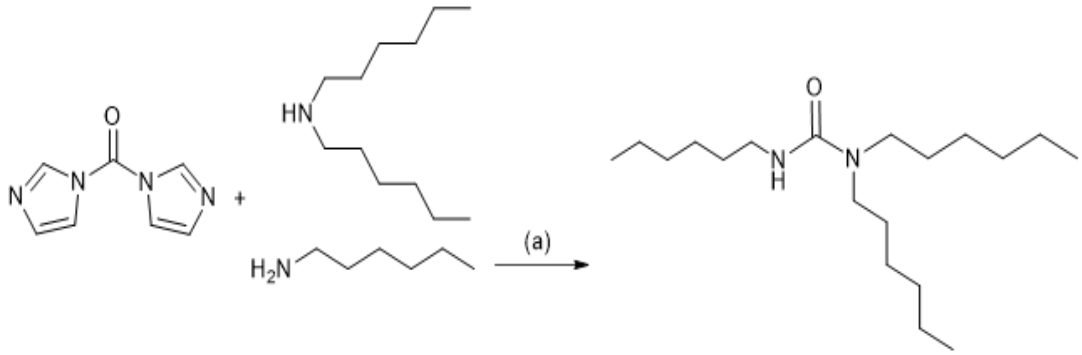


(a) -78 °C, toluene, dihexylamine charged after 2 h just before warming to room temperature, 10% yield.

**Scheme 4.10 The synthesis of 1,1,3-trihexylurea obtained by the sequential charging of hexylamine and dihexylamine to CDI.**

$^1$H NMR spectroscopy of the reaction mixture showed the presence of two different overlapping methylene resonances at $\delta$ = 3.13 ppm (hexylamine and dihexylamine) with a relative integration of 6. Furthermore, a urea resonance was observed at $\delta$ = 4.37 ppm with an integration of 1, indicating that the desired primary and secondary additions had occurred. **(Figure 4.11)** This was confirmed by heteronuclear single quantum correlation 2D NMR spectroscopy (HSQC 2D NMR), which showed a correlation between the proton resonance at $\delta$ = 3.13 ppm and the carbon resonance at $\delta$ = 40 ppm of the methylene next to the secondary urea and between the proton resonance at $\delta$ = 3.08 ppm and the carbon resonance at $\delta$ = 47 ppm of the methylene next to the primary urea. **(Figure 4.12)**

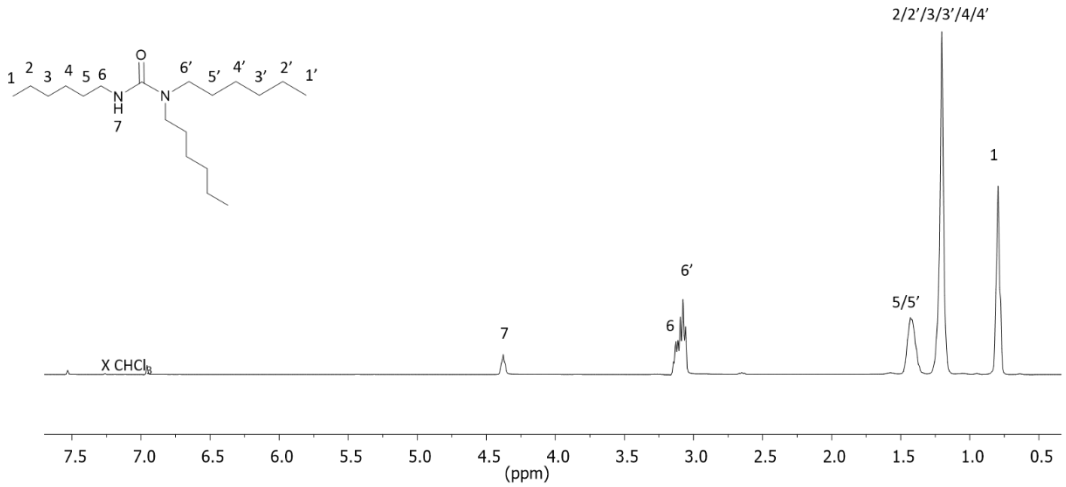


**Figure 4.11 $^{1}$H NMR spectrum of the 1,1,3-trihexylurea obtained by the sequential charging of hexylamine and dihexylamine to CDI (400 MHz, 298 K, $CDCl_3$).**

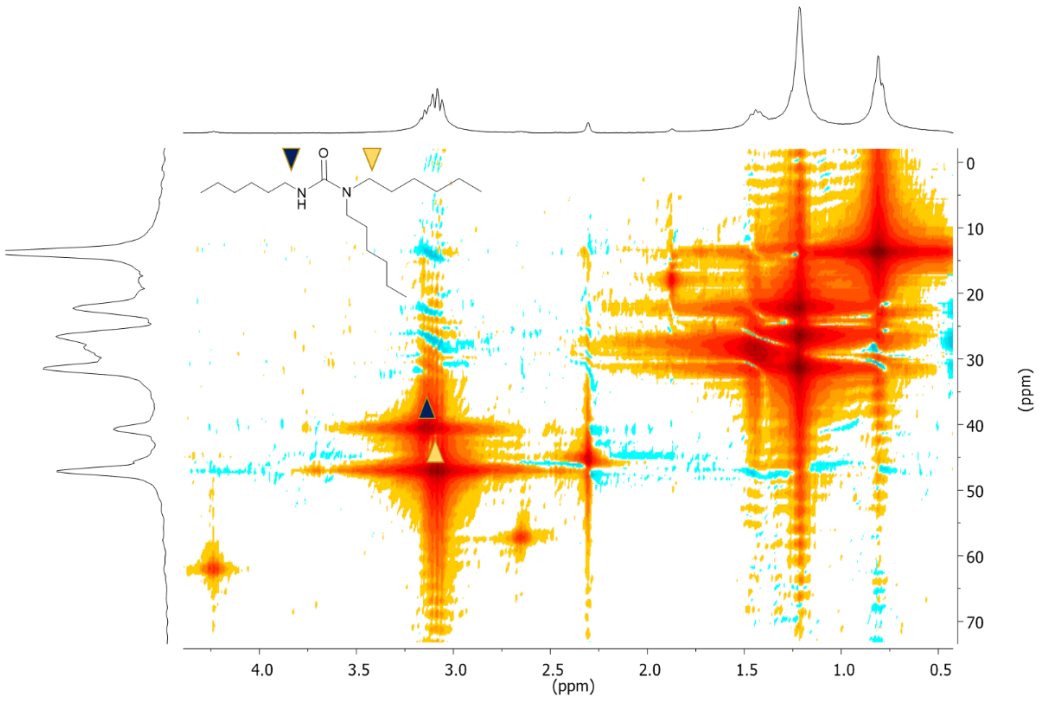


**Figure 4.12 HSQC 2D NMR spectrum of 1,1,3-trihexylurea obtained by the sequential charging of hexylamine and dihexylamine to CDI (400 MHz, 298 K, $CDCl_3$).**

The use of BHMTA for the synthesis of CDI-HCTAs involves the reaction of CDI with only the primary amines even in the presence of a secondary amine. To investigate

this, a further experiment was conducted in which hexylamine and dihexylamine were added to CDI concurrently, at -78 ˚C and then the reaction was allowed to warm to room temperature. **(Scheme 4.11)**

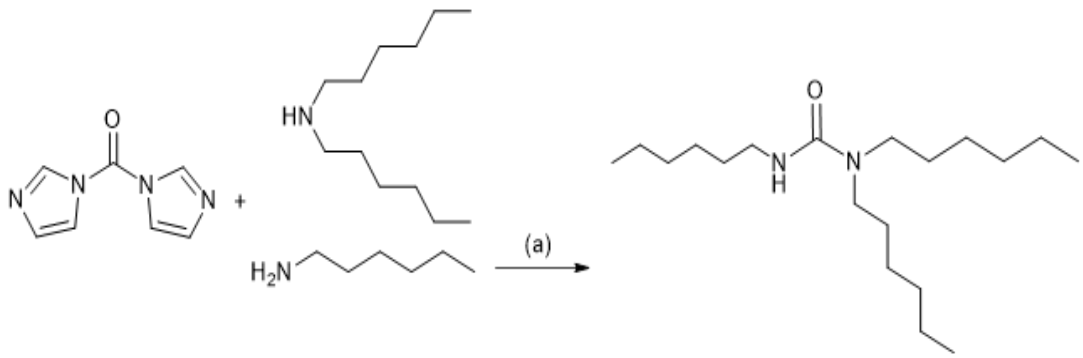


(a) -78 °C to room temperature, toluene, 2 h. hexylamine and dihexylamine charged concurrently, 20% yield.

**Scheme 4.11 The synthesis of 1,1,3-trihexylurea obtained by the concurrent charging of hexylamine and dihexylamine to CDI.**

This experiment also yielded 1,1,3-trihexylurea, as was yielded in the sequential charging of hexylamine and dihexylamine, as confirmed by $^{1}$H NMR spectroscopy. The formation of a proton resonance at $\delta$ = 3.17 ppm (hexylamine) for the methylene next to the primary urea and $\delta$ = 3.11 ppm (dihexylamine) for the methylene next to the secondary urea, with a relative integration ratio of 2:4. This was further complimented by $^{13}$C NMR spectroscopy that showed a single carbonyl resonance at $\delta$ = 158 ppm. **(Figure 4.13)** In addition, HSQC 2D NMR spectroscopy confirmed that the proton resonance at $\delta$ = 3.11 ppm correlated to the carbon resonance at $\delta$ = 47 ppm for the methylene next to the secondary urea and the proton resonance at $\delta$ = 3.17 ppm correlated to the carbon resonance at $\delta$ = 41 ppm of the methylene next to the primary urea. **(Figure 4.14)** This set of experiments confirmed a promising basis by which CDI-HCTAs could be produced from CDI and showed that CDI can, through the one-pot, temperature-controlled sequential synthesis, react preferentially towards primary amines over secondary amines when the temperature is maintained at -78 °C. Whilst these reactions show the successful isolation of the desired product, the reaction yield was *c.a*. 20%, which suggests that side reactions have occurred but have been washed out in the work up. These side

reactions are likely to be multiple additions of the primary amine or the single addition of the secondary amine to CDI.

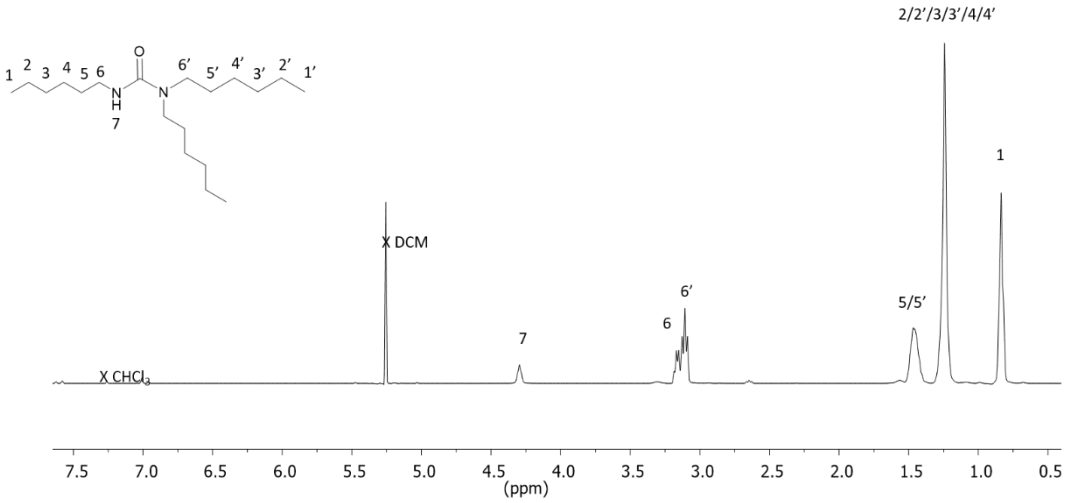


**Figure 4.13 $^{1}$H NMR spectrum of 1,1,3-trihexylurea obtained by the concurrent charging of hexylamine and dihexylamine to CDI (400 MHz, 298 K, $CDCl_3$).**

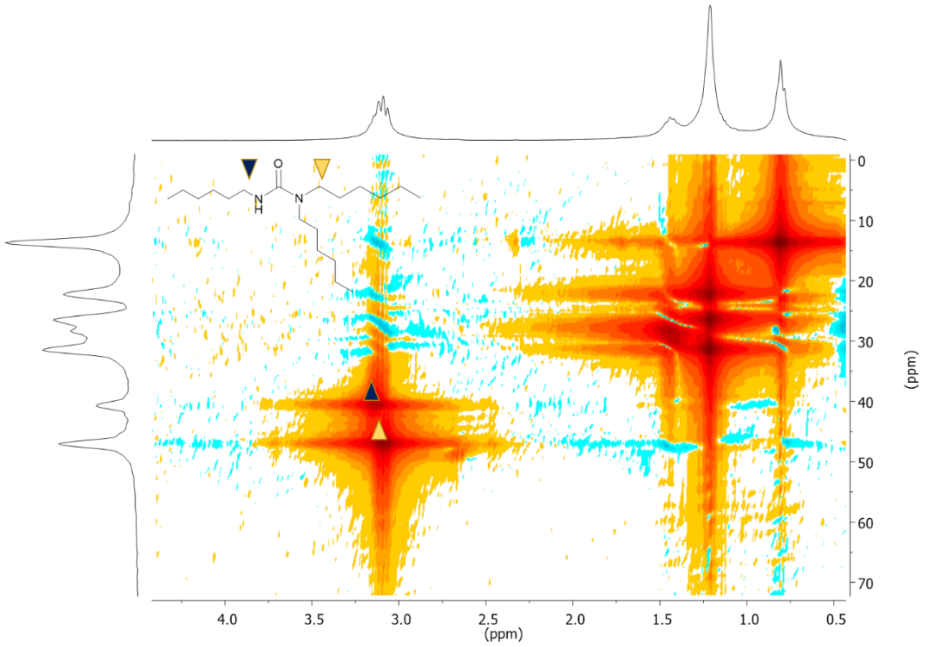


**Figure 4.14 HSQC 2D NMR spectrum of 1,1,3-trihexylurea obtained by the concurrent charging of hexylamine and dihexylamine to CDI (400 MHz, 298 K, $CDCl_3$).**

#### 4.2.2.2 Synthesis of aromatic hyperbranched chain terminating agents from 1,1'-carbonyldiimidazole

Following the preliminary one-pot, temperature-controlled sequential addition reactions of amines with CDI, experiments were designed to observe whether a similar selectivity would occur when BHMTA and CDI were combined. The initial experiments were carried out under the same conditions as discussed previously but they all yielded insoluble gels. It is hypothesised that these gels consisted of extremely high molecular weight, extensively branched polymers but no suitable solvent could be found to dissolve the gels to enable $^{1}$H NMR spectroscopy or SEC analysis to be carried out to confirm this hypothesis.

These initial experiments confirmed that the branching of CDI with BHMTA was too efficient for the divergent (core first) approach to hyperbranched polymer synthesis to produce controlled polyureas. The convergent (branch first) approach was then investigated. Rannard and Davis.[27,28], have reported that a species of CDI with one side being an alcohol rather than an imidazole can react sequentially with two primary amines and one secondary amine on BHMTA to form a branched urethane. This process is very efficient in allowing the formation of branched structures as the alcohol acts as a ''chain capper'' that prevents further branching reactions occurring, whilst the remainder of the reaction mixture, an imidazole urea, propagates the hyperbranching reaction. An experiment was conducted using a chosen stoichiometric molar ratio of 1:2:1 of BHMTA:CDI:BnOH at -78 °C. **(Scheme 4.12)**

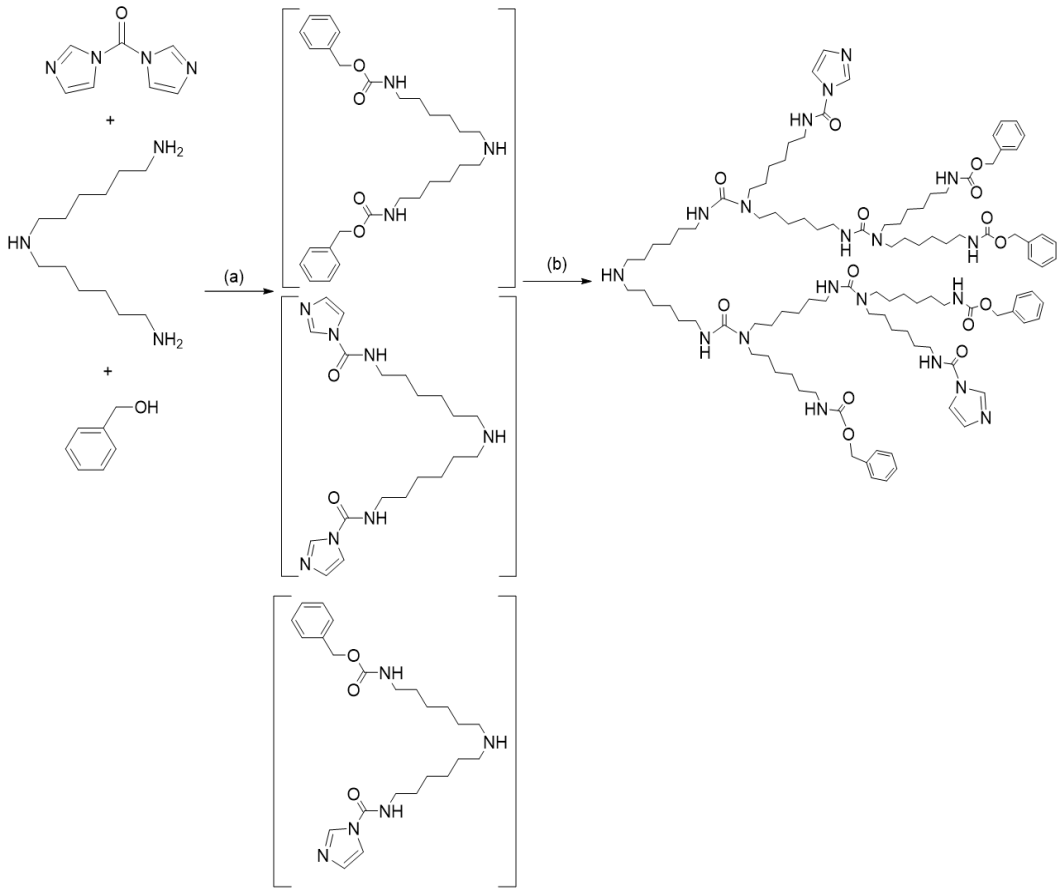


(a) -78 °C, 2 h; (b) room temperature, 5 h, 21% yield.

**Scheme 4.12 The one-pot, temperature-controlled sequential synthesis of a CDI-AHCTA from CDI, BHMTA and BnOH.**

This experiment was also successfully conducted at -20 °C. The resulting CDI-HCTA with aromatic chain ends (CDI-AHCTA) was confirmed by SEC analysis that revealed a $M_w$ of 14,000 g mol$^{-1}$, $M_n$ of 7,000 g mol$^{-1}$, $Đ_M$ of 1.94 with a Mark-Houwink parameter (*a*) of 0.43. for the CDI-AHCTA produced at -78 °C and a $M_w$ of 32,000 g mol$^{-1}$, $M_n$ of 6,000 g mol$^{-1}$, $Đ_M$ of 5.08, and *a* of 0.36 for the CDI-AHCTA produced at -20 °C. The reduction in the *a* parameter from 0.57 to 0.36 shows that, at the higher temperature, the branching was more extensive. **(Figure 4.15)** The CDI-AHCTA produced at -78 °C had a relatively narrow distribution with lower molecular weight shoulders, whereas the CDI-AHTA produced at -20 °C had a much broader distribution with several lower and higher molecular weight shoulders that are indicative of different generational structures. Further reactions conducted at 0 °C and at ambient temperature produced CDI-AHCTAs with evidence of gelation,

indicating extensive uncontrolled branching had occurred. All further branching experiments were conducted at -20 °C. **(Table 4.2)**. F. Xiang *et al*. have shown that a chemically similar linear polymer synthesised from CBC blocked hexamethylene diisocyanate and *N,N'*-dimethyl-1,6-diaminohexane had a Mark-Houwink *a* value of 0.68, which is indicative of a linear polymer in a theta solvent. This shows that the hyperbranched polymers produced above don't inherently have a low Mark-Houwink *a* value but are extensively branched.[19]

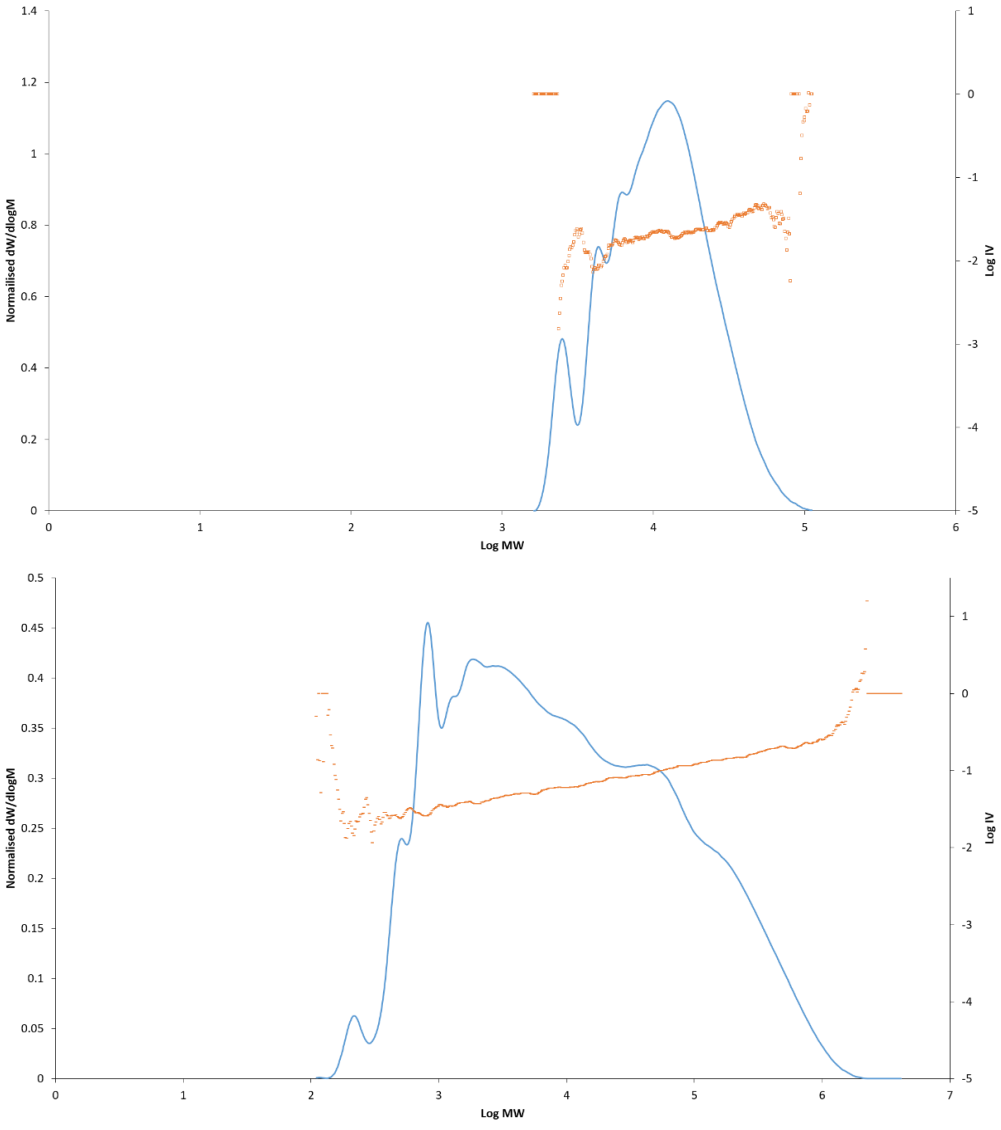


**Figure 4.15 SEC chromatograms and Mark-Houwink plots of the CDI-AHCTA convergently synthesised from CDI, BHMTA and BnOH at -78 °C (*top*) and -20 °C (*bottom*) in DMF against PMMA standards.**

**Table 4.2 Temperature optimisation data for the CDI-AHCTA convergently synthesised from CDI, BHMTA and BnOH.**

| Temperature (°C) | $M_w$ (g mol$^{-1}$)[a] | $M_n$ (g mol$^{-1}$)[a] | $Đ_M$[a] | $a$[a] |
|---|---|---|---|---|
| **-78** | 7,000 | 4,000 | 1.73 | 0.57 |
| **-78** | 14,000 | 7,000 | 1.94 | 0.43 |
| **-20** | 32,000 | 6,000 | 5.08 | 0.36 |
| **0** | No data | No data | No data | No data |
| **ambient** | No data | No data | No data | No data |

a) Determined by SEC analysis in DMF against PMMA standards.

Diffusion Ordered NMR Spectroscopy (DOSY) was utilised to verify whether the aromatic chain ends were attached to the aliphatic branched network. This was confirmed by both the aromatic proton signals and the aliphatic branching proton signals having the same diffusion value. Despite exposure to air and water after an organic work-up, these CDI-AHCTAs became gels over time. It is considered that this is because the residual imidazole chain ends of the hyperbranched structures continued to combine *via* the secondary amine focal point.

A second approach to quench all the remaining imidazole chain ends was used where the alcohol charge at the beginning of the experiment was increased. It was predicted that this would reduce chain propagation by increasing the concentration of benzyl urethane and decreasing the concentration of the imidazole urea. To achieve this, the alcohol charge was increased from a molar ratio of 1.05 to 1.20. The results showed that increasing the alcohol charge in this way did result in a decreased molecular weight and decreased polydispersity of the CDI-AHCTAs, however, after 48 h these CDI-AHCTAs also gelled indicating the continued existence of imidazole chain ends. **(Table 4.3)**

**Table 4.3 Alcohol charge optimisation data for the branching reactions of CDI-AHCTA convergently synthesised from CDI, BHMTA and BnOH.**

| Reaction Time at RT (h) | Reaction Temp. (°C) | CDI | BnOH | BHMTA | $M_w$ (g mol$^{-1}$)[a] | $M_n$ (g mol$^{-1}$)[a] | $Đ_M$[a] |
|---|---|---|---|---|---|---|---|
| **2** | -20 | 1.06 | 1.00 | 0.5 | 32,000 | 6,000 | 5.08 |
| **24** | -20 | 1.06 | 1.05 | 0.5 | 95,000 | 7,000 | 13.36 |
| **48** | -20 | 1.06 | 1.05 | 0.5 | No data | No data | No data |
| **24** | -20 | 1.06 | 1.10 | 0.5 | 41,000 | 6,000 | 6.60 |
| **48** | -20 | 1.06 | 1.10 | 0.5 | No data | No data | No data |
| **24** | -20 | 1.06 | 1.15 | 0.5 | 23,000 | 5,000 | 4.82 |
| **48** | -20 | 1.06 | 1.15 | 0.5 | No data | No data | No data |
| **24** | -20 | 1.06 | 1.20 | 0.5 | 9,000 | 4,000 | 2.36 |
| **48** | -20 | 1.06 | 1.20 | 0.5 | No data | No data | No data |

a) Determined by SEC analysis in DMF against PMMA standards.

As such the process was expanded to add a further step whereby a 100 times molar excess of methanol was added, once polymerisation had completed, to quench any remaining imidazole chain ends. **(Scheme 4.13)** Methanol was chosen as it is a small alcohol, only one carbon chain in length, and is a volatile solvent so it could easily be removed once the reaction was quenched.

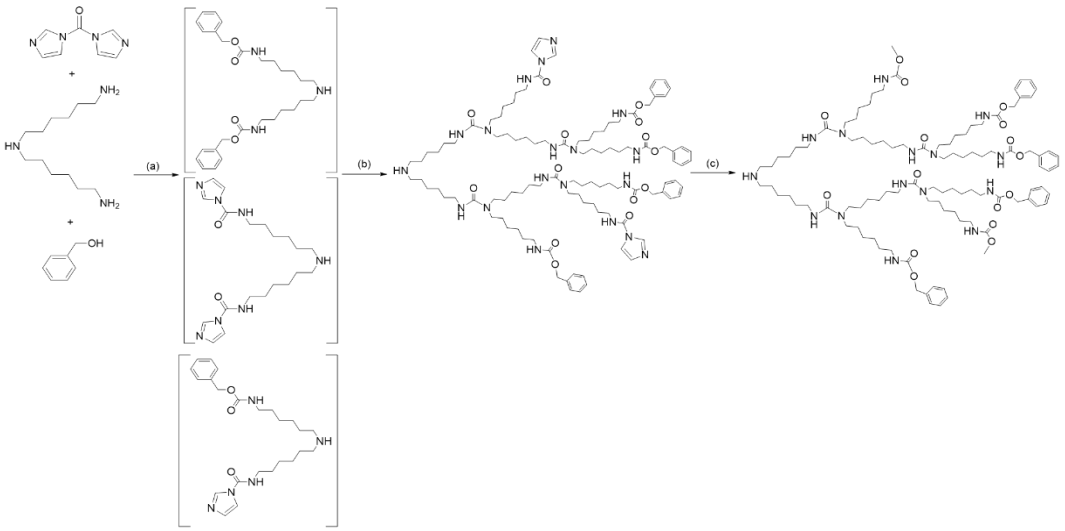


(a) -20 °C, 3 h; (b) room temperature, 5 h, (c) methanol, 48 h, 30 °C, 22% yield.

**Scheme 4.13 The one-pot, temperature-controlled sequential synthesis of a CDI-AHCTA from CDI, BHMTA and BnOH after menthol quenching.**

A further series of experiments were then run to ascertain the optimal quenching time. Time points were collected 2 h, 5 h, 15 h and 24 h after the reaction mixture reached room temperature. At 2 h no CDI-AHCTA was present indicating that the polymerisation wasn't as efficient as initially predicted. After 5 h the CDI-AHCTA had a $M_w$ of 4,000 g mol$^{-1}$, a $M_n$ of 2,000 g mol$^{-1}$ and a $Đ_M$ of 1.63, which indicates that the branching reaction had proceeded in a controlled manner. After 15 h and 24 h the CDI-AHCTA had a $M_w$ of 17,000 g mol$^{-1}$, $M_n$ of 4,000 g mol$^{-1}$ and a $Đ_M$ of 4.25 and $M_w$ of 25,000 g mol$^{-1}$, $M_n$ of 4,000 g mol$^{-1}$ and $Đ_M$ of 6.10 respectively, which indicated that increasingly uncontrolled branching was occurring. Based on these results, it was decided that in further experiments the reaction mixture would be maintained for 3 h at -20 °C and a further 5 h at room temperature before quenching with a 100 times molar excess of methanol. **(Table 4.4)**

**Table 4.4 Temperature optimisation data for the branching reactions of a CDI-AHCTA convergently synthesised from CDI, BHMTA and BnOH.**

| Time at RT (h) | $M_w$ (g mol$^{-1}$)[a] | $M_n$ (g mol$^{-1}$)[a] | $Đ_M$[a] |
|---|---|---|---|
| **2** | No data | No data | No data |
| **5** | 4,000 | 2,000 | 1.63 |
| **15** | 17,000 | 4,000 | 4.25 |
| **24** | 25,000 | 4,000 | 6.10 |

a) Determined by SEC analysis in DMF against PMMA standards.

However, complete termination of the branching reaction had still not been achieved as the molecular weight continued to increase even after precipitation, as a work up, and eventually gelled over time. Further reactions were conducted to produce a fully alcohol-terminated CDI-AHCTA. SEC analysis showed that after 24 h in methanol at room temperature the CDI-AHCTA still gelled but after 48 h in methanol at room temperature its molecular weight rose as shown by the increase in the high molecular weight distribution. **(Figures 4.16 and 4.17)** After 24 h in methanol at 30 °C its chain ends were mostly capped as shown by the minimal change in the higher molecular weight region and after 48 h in methanol at 30 °C no change was seen in the molecular weight of the CDI-AHCTA. As such this method was chosen to fully quench the branching reactions that occur and the molecular weight of the CDI-AHCTA

remained stable throughout the one-month testing period. **(Figures 4.18 and 4.19)** The slight fluctuations in molecular weight values arose because of instrument error.

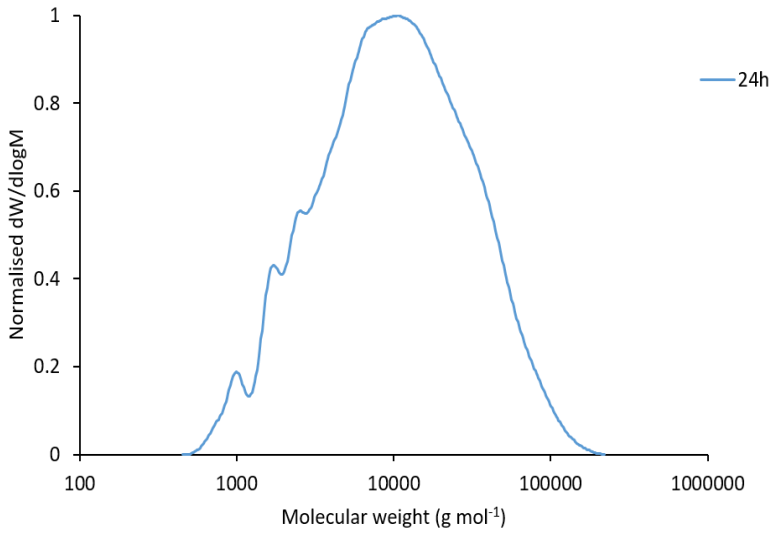


**Figure 4.16 SEC chromatogram of a CDI-AHCTA convergently synthesised from CDI, BHMTA and BnOH in DMF for 24 h at room temperature in methanol against PMMA standards.**

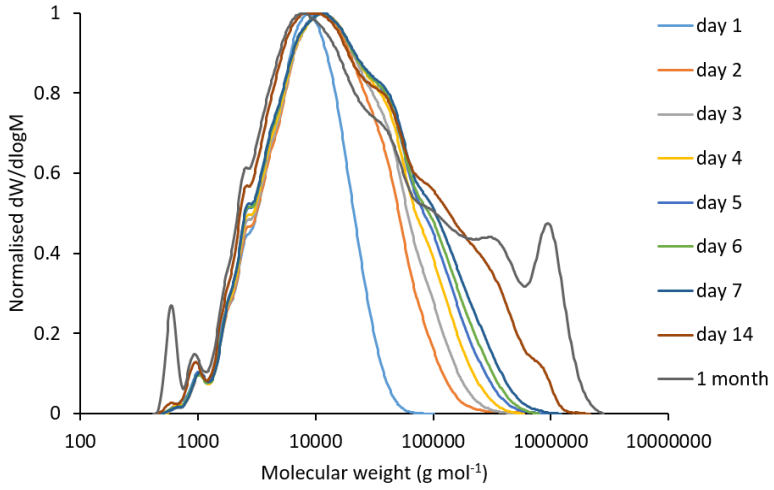


**Figure 4.17 SEC chromatogram of a CDI-AHCTA convergently synthesised from CDI, BHMTA and BnOH in DMF for 48 h at room temperature in methanol against PMMA standards.**

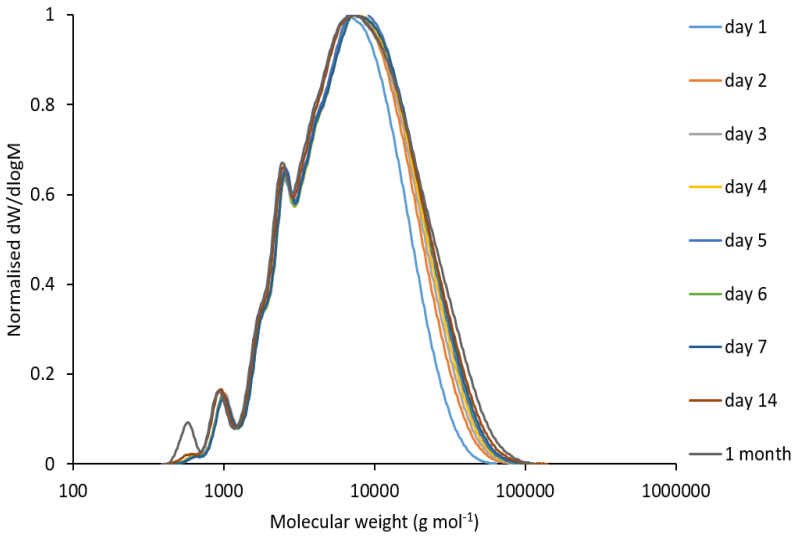


**Figure 4.18 SEC chromatogram of a CDI-AHCTA convergently synthesised from CDI, BHMTA and BnOH in DMF for 24 h at 30 °C in methanol against PMMA standards.**

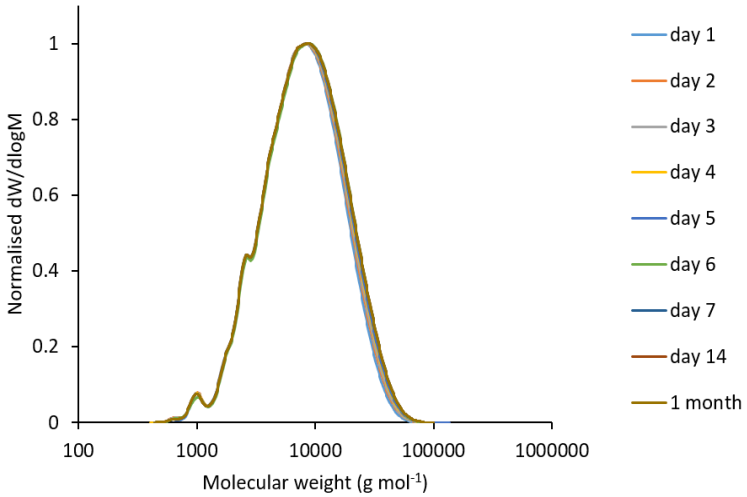


**Figure 4.19 SEC chromatogram of a CDI-AHCTA convergently synthesised from CDI, BHMTA and BnOH in DMF for 48 h at 30 °C in methanol against PMMA standards.**

After the successful quenching of the branching reaction, the CDI-AHCTA was washed with brine and water to remove any remaining imidazole and then dried. SEC analysis confirmed the material had a Mark-Houwink *a* parameter of 0.27 indicating a highly branched structure. **(Table 4.5 and Figure 4.20)**

**Table 4.5 SEC analysis for hyperbranched a CDI-AHCTA convergently synthesised from CDI, BHMTA and BnOH.**

| Detection method | $M_w$ (g mol$^{-1}$)[a] | $M_n$ (g mol$^{-1}$)[a] | $Đ_M$[a] | $a$[a] |
|---|---|---|---|---|
| **Light scattering** | 7,713 | 4,383 | 1.76 | 0.27 |
| **Viscometry** | 7,704 | 4,531 | 1.70 | No data |

a) Determined by SEC analysis in DMF against PMMA standards.

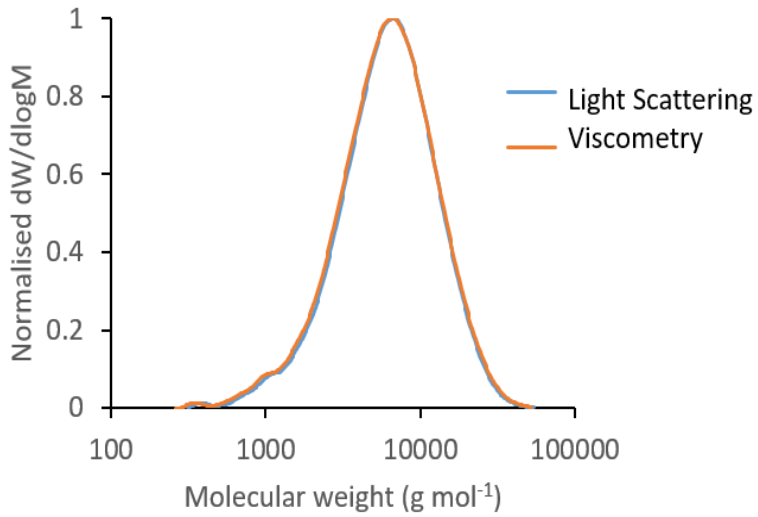


**Figure 4.20 SEC chromatograms of a CDI-AHCTA convergently synthesised from CDI, BHMTA and BnOH in DMF against PMMA standards.**

The final composition of the CDI-AHCTA was confirmed by $^1$H NMR spectroscopy. The resonances for the branching methylenes appeared between $\delta$ = 1.75 ppm and 1.00 ppm followed by the resonances for the methylenes next to the urea between $\delta$ = 3.40 – 3.00 ppm. The resonances for the methanol chain ends were between $\delta$ = 3.60 – 3.40 ppm and for the benzyl chain ends at $\delta$ = 7.38 and 5.08 ppm. The amine focal point resonance was at $\delta$ = 7.19 ppm and the chain urea resonances were between $\delta$ = 6.50 – 5.75 ppm. There is a residual amount of BnOH that remained at $\delta$ = 7.40 ppm, 4.60 ppm and 5.10 ppm. In addition, $^{13}$CNMR spectroscopy further complimented these results and showed multiple resonances relating to the mid chain carbonyls and the methanol and benzyl carbamate chain ends between $\delta$ = 160 ppm and 150 ppm. **(Figure 4.21)** DOSY spectroscopy confirmed the

attachment of the aromatic chain ends to the aliphatic branch structure as the diffusion coefficients of both proton resonances are of the same value. **(Figure 4.22)**

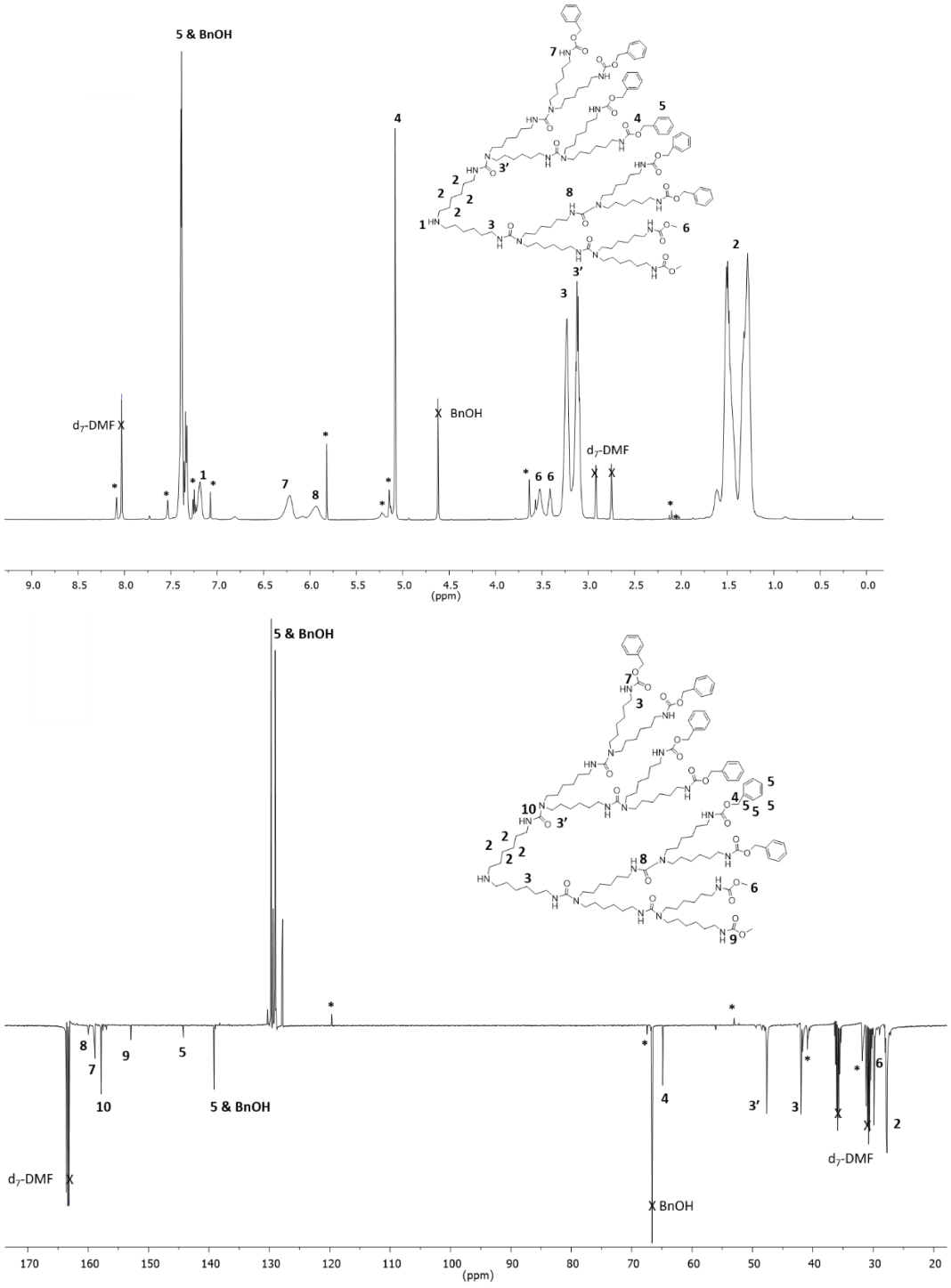


**Figure 4.21 $^{1}$H NMR and $^{13}$C HNMR spectra of a CDI-AHCTA convergently synthesised from CDI, BHMTA and BnOH (400 MHz and 125 MHz, 298 K, DMF-*d*$_7$).**

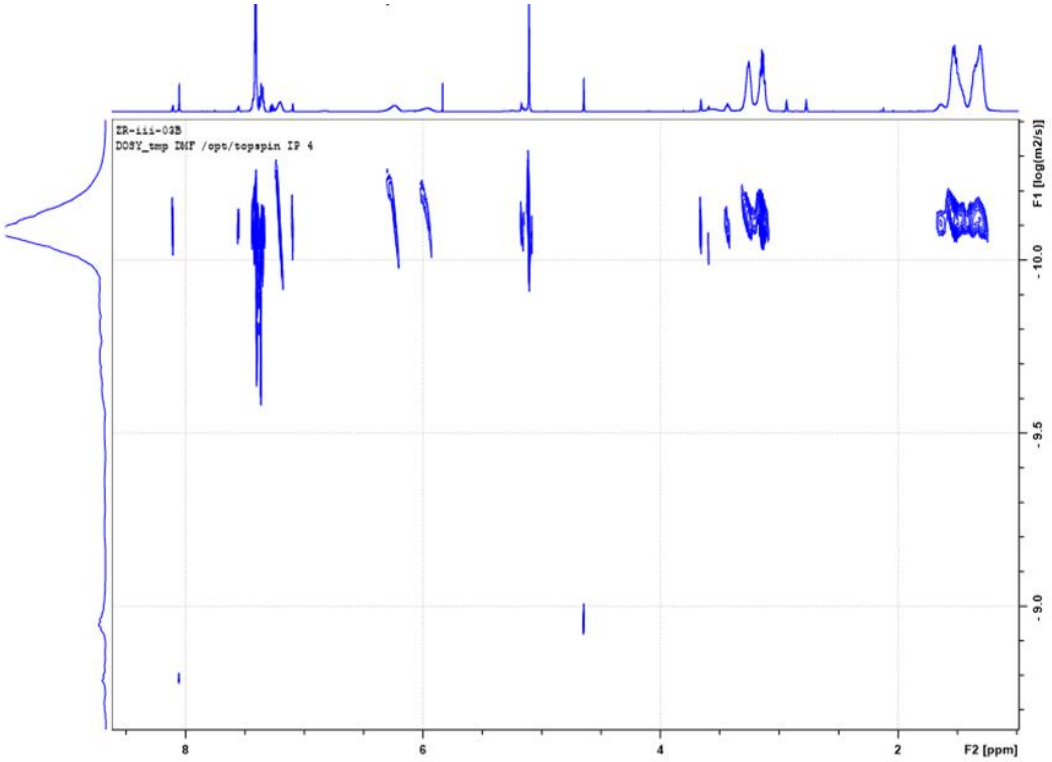


**Figure 4.22 DOSY spectrum of a CDI-AHCTA convergently synthesised from CDI, BHMTA and BnOH (400 MHz, 298 K, DMF-$d_7$).**

In addition to the above, a thermogravimetric analysis (TGA) of the CDI-AHCTA showed sequential generational degradation as temperature increased. **(Table 4.6 and Figure 4.23)** The first step loss of 19% at 264 °C indicated the loss of its aromatic chain ends, followed by subsequent mass losses of 42% at 355 °C and 28% at 483 °C that indicated its third generation and second generation respectively. The final drop between the trend line and the x-axis is the 11% mass loss for its core or first generation.

**Table 4.6 TGA mass loss data for a CDI-AHCTA convergently synthesised from CDI, BHMTA and BnOH.**

| Onset (°C) | Mass loss (mg) | Mass loss (%) |
|---|---|---|
| *264.7* | 1.14 | 19 |
| *355.0* | 2.45 | 42 |
| *483.0* | 1.65 | 28 |

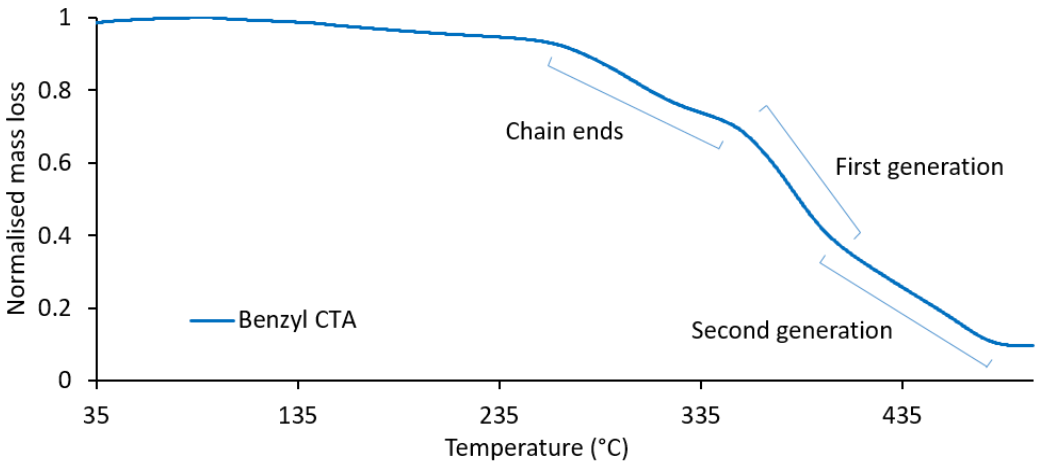


**Figure 4.23 TGA mass loss curve of a CDI-AHCTA convergently synthesised from CDI, BHMTA and BnOH.**

To gain further understanding of the distribution of molecular weights shown in the SEC analysis of the CDI-AHCTA, electron spray ionisation mass spectrometry (ESI-MS) was conducted. As expected, given the uncontrolled nature of the hyperbranching mechanism, a wide range of species was detected. Species were observed between 700 m/z and 3000 m/z that were significantly lower than the molecular weight value obtained by SEC analysis at 8,000 g $mol^{-1}$. **(Figure 4.24)**. No species over 3000 m/z were observed as they were too large to fly because of the vast number of aromatic chain ends that extensively ionised. It is considered that this CDI-AHCTA has a non-polar branched network with highly-polar, aromatic chain ends and therefore often self-assembles or forms micelles along the column of the SEC machine, thus resulting in an increase of the hydrodynamic radius in solution. However, the major peaks give an indication of the lower molecular weight species that are present in the CDI-AHCTA. Because of the larger number of chain ends on the hyperbranched polymers the potential for multiple ionisations is likely. With that in mind, the doubly ionised peak distribution at 1,305.8714 m/z suggests a three-generation species with two methyl chain ends and six benzyl chain ends. This data begins the process of understanding the composition and structure of such hyperbranched polymers, but further work needs to be carried out to understand their ionisation characteristics.

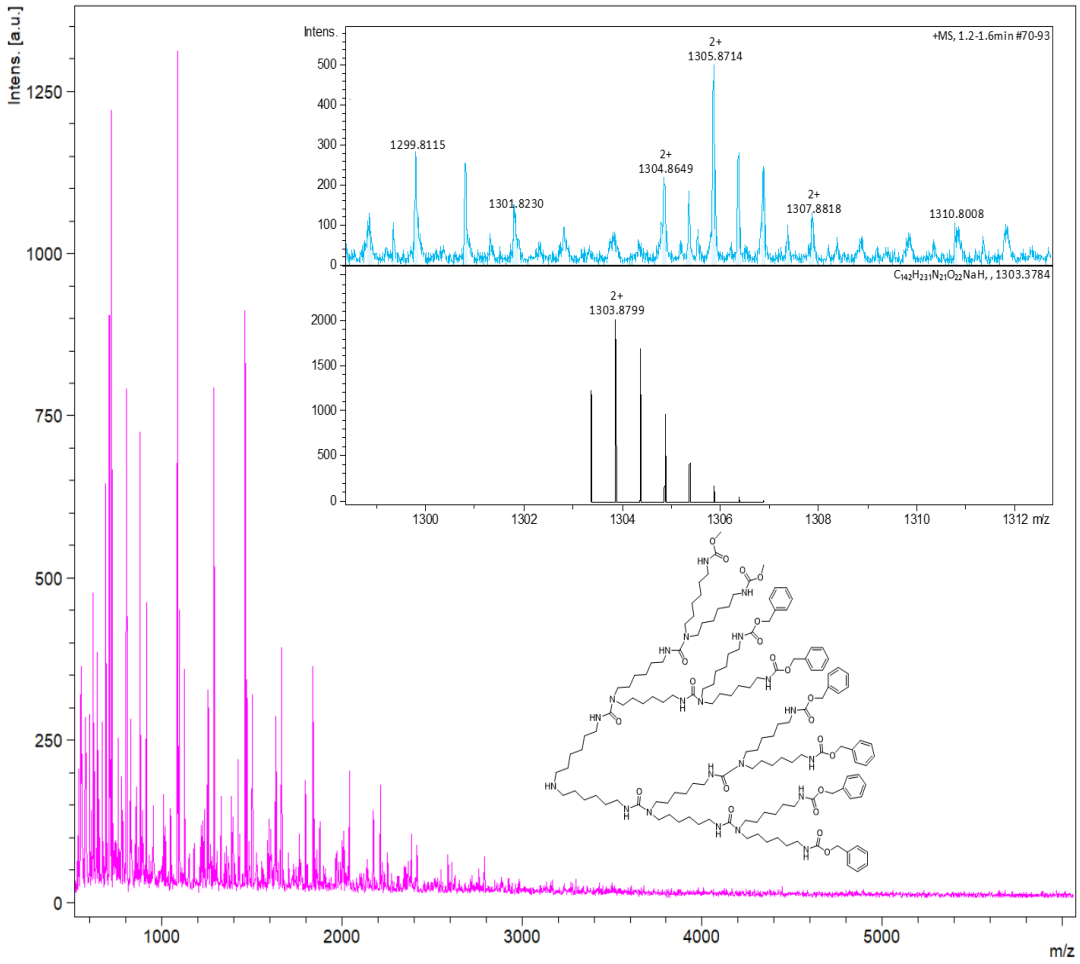


**Figure 4.24 ESI-MS spectrum of a CDI-AHCTA convergently synthesised from CDI, BHMTA and BnOH (50:50 MeOH/THF, positive mode).**

### 4.2.2.3 Synthesis of fluorinated hyperbranched chain terminating agents from 1,1'-carbonyldiimidazole

As described above the CDI-AHCTA served as a model for a more complex HCTA with fluorinated chain ends (CDI-FHCTA). It was hypothesised that such a hyperbranched structure would possess many fluorinated chain ends, which would alter the surface properties of the CDI-FHCTA. The conversion from aromatic to fluorinated chain ends was carried out under the same conditions as when BnOH was introduced. The fluorinated compound used was DuPont™ Capstone®, which is a $C_6$ perfluoro with a $C_2$ ethyl unit terminated by an alcohol. The stability of the resulting CDI-FHCTA was tested over one month, to see if all the chain ends were quenched with either methanol or Capstone®. This was confirmed by no observable change in the higher molecular weight distribution obtained by SEC analysis. **(Figure 4.25)**

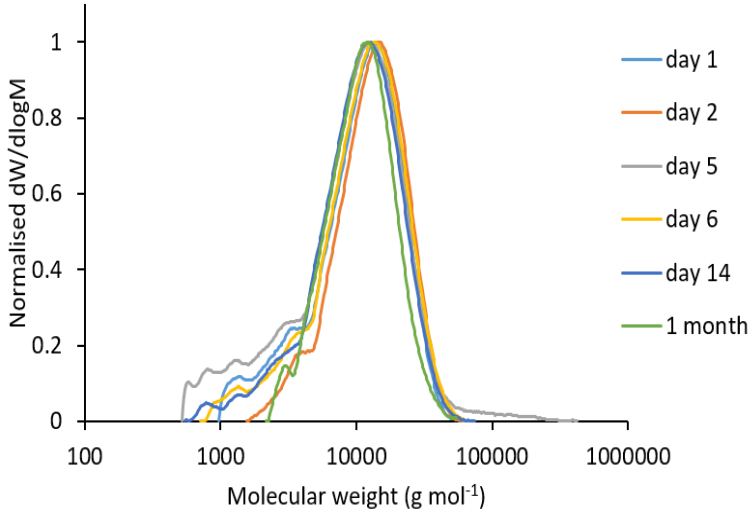


**Figure 4.25 SEC chromatograms of a CDI-FHCTA convergently synthesised from CDI, BHMTA and Capstone® in DMF against PMMA standards.**

The incorporation of Capstone® into the hyperbranched structure was confirmed by $^{19}$F NMR spectroscopy that showed the retention of six fluorine resonances. **(Figure 4.26)**

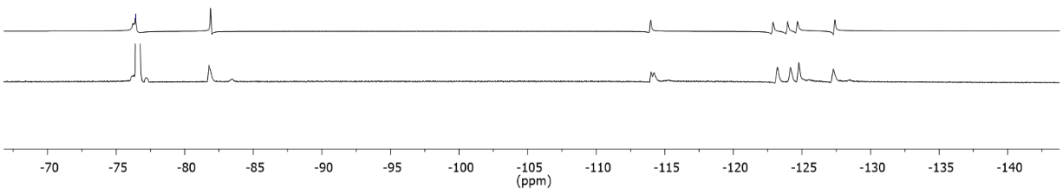


**Figure 4.26 $^{19}$F NMR spectra for Capstone® (top) and CDI-FHCTA convergently synthesised from CDI, BHMTA and Capstone® (bottom) (282 MHz, 298 K, DMSO-$d_6$, 0.01 v/v% trifluoroacetic acid standard).**

The final composition of the CDI-FHCTA was confirmed by $^{1}$H NMR spectroscopy. Branching methylene resonances were observed between $\delta$ = 1.75 ppm and 1.00 ppm followed by the resonances of the methylenes next to the urea at $\delta$ = 3.40 - 3.00 ppm. The resonances of the methanol chain ends were at $\delta$ = 4.00 - 3.40 ppm and those of the Capstone® chain ends at $\delta$ = 4.35 ppm and 2.67 ppm. The amine focal point was at $\delta$ = 7.23 ppm and the chain urea resonances were observed between $\delta$ = 6.55 ppm and 5.55 ppm. There was a residual amount of Capstone® that remained at $\delta$ = 5.10 ppm and 2.50 ppm. In addition, the $^{13}$C NMR spectroscopy further complimented this and showed resonances relating to the mid chain carbonyls and the methanol and Capstone® chain ends between $\delta$ = 160 and 150 ppm. **(Figure 4.27)**.

As for the CDI-AHCTA, $^{1}$H DOSY spectroscopy confirmed the attachment of the fluorinated chain ends to the aliphatic branch structure as the diffusion coefficients of both proton resonances were of the same value **(Figure 4.28)**. Further to this, $^{19}$F DOSY spectroscopy showed two diffusions indicating different fluorinated species, which confirmed the attachment of Capstone® to the CDI-FHCTA, but also a residual amount of the Capstone® starting material remaining in the mixture.

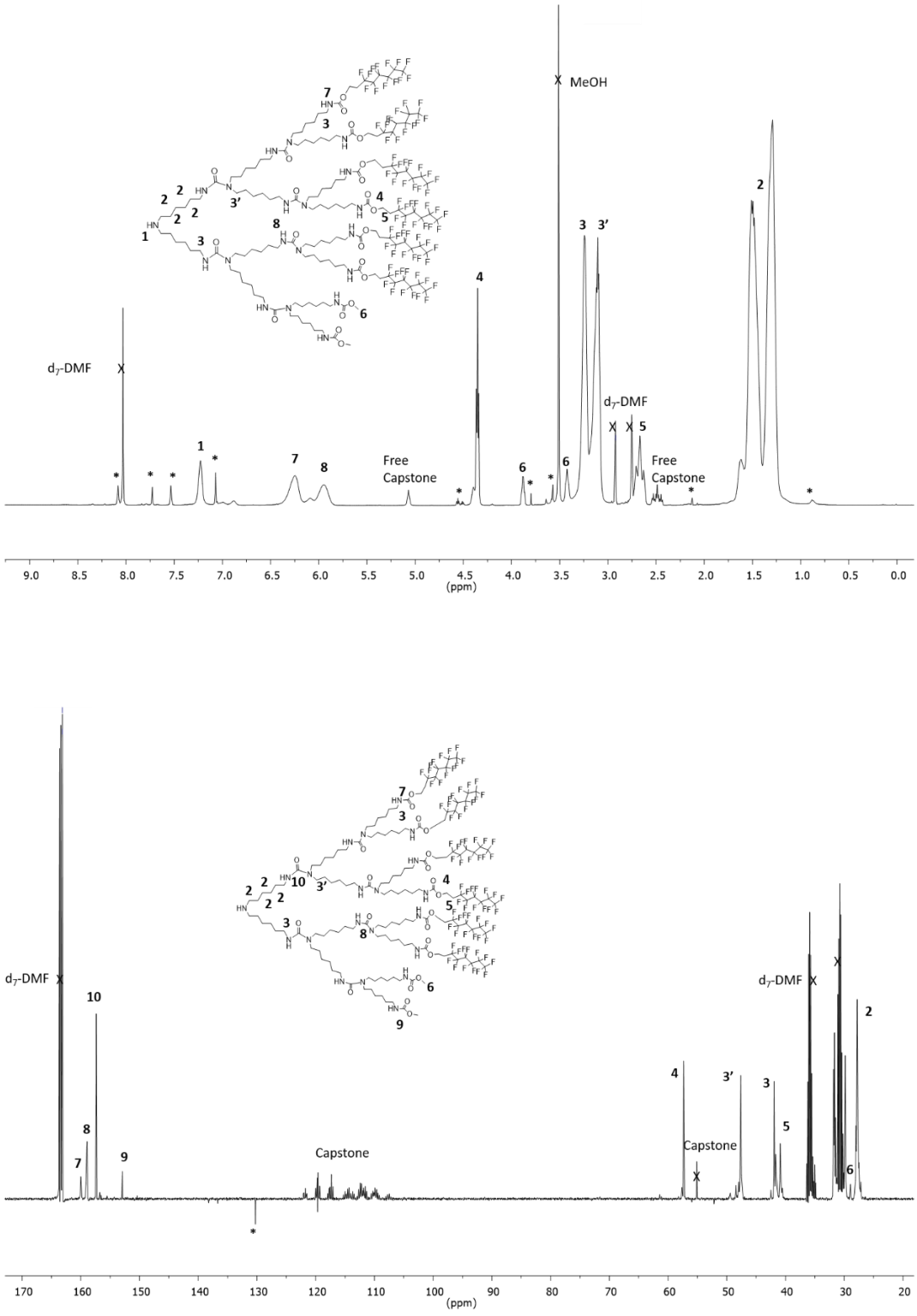


**Figure 4.27 $^{1}$H NMR (top) and $^{13}$C NMR (bottom) spectra of a CDI-FHCTA convergently synthesised from CDI, BHMTA and Capstone® (400 MHz and 125 MHz, 298 K, DMF-$d_7$).**

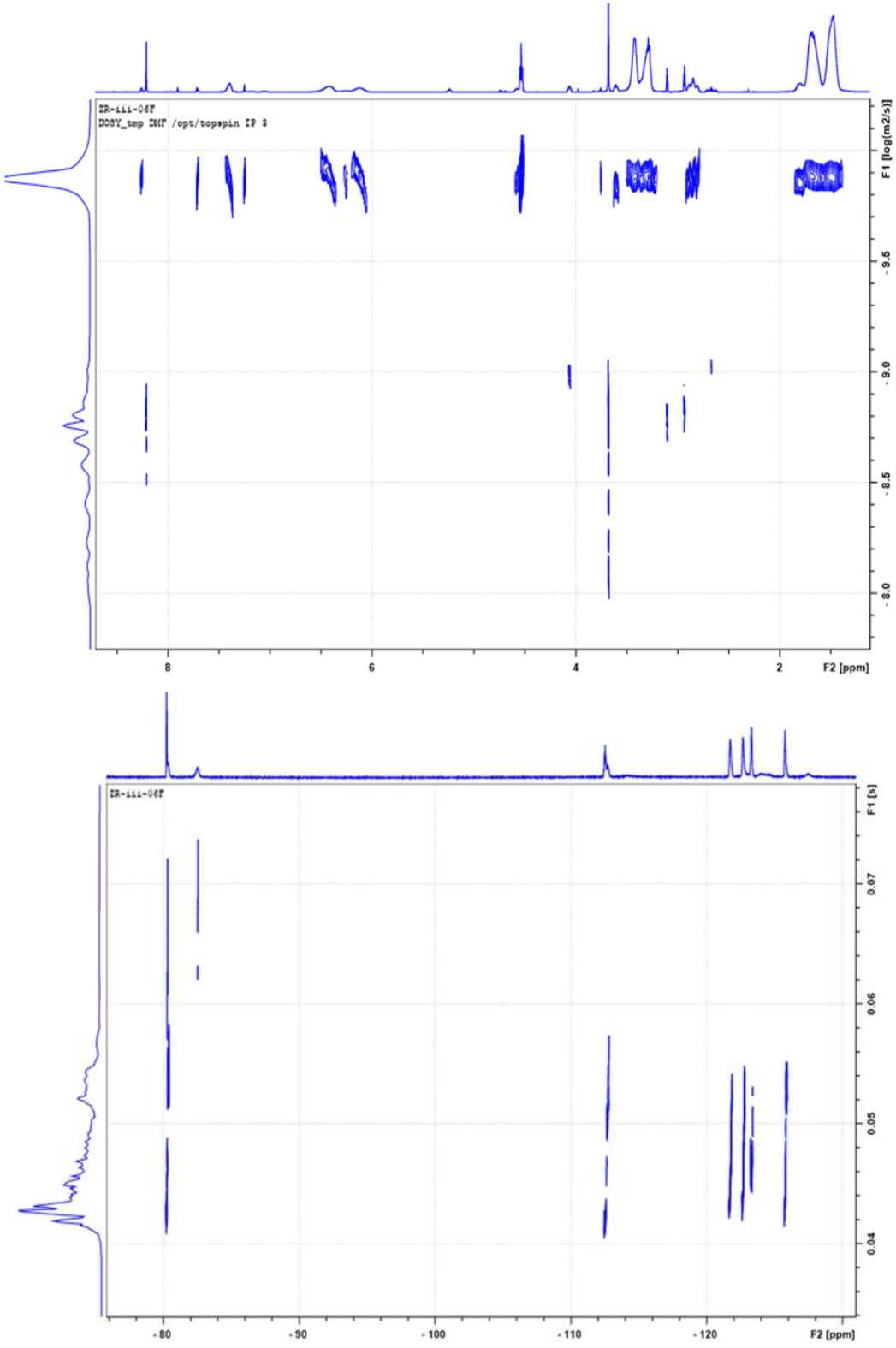


**Figure 4.28 $^{1}$H (top) and $^{19}$F (bottom) DOSY spectra of CDI-FHCTA convergently synthesised from CDI, BHMTA and Capstone® (400 MHz and 376 MHz, 298 K, DMSO-*d*$_6$).**

TGA of the CDI-FHCTA showed the same trend as that observed for the CDI-AHCTA. The first mass loss of 39% at 271 °C indicated the loss of the fluorinated chain ends, followed by further mass losses of 31% at 352 °C and 16% at 455 °C, which indicated the third generation and the second generation respectively. The final mass loss between the trend line and the x-axis is the 14% mass loss for the core of the CDI-FHCTA or first generation. **(Table 4.7)**. The difference between the first step drops in the TGA curves shows that the fluorinated chain ends of the CDI-FHCTA have a higher mass than the aromatic chain ends of the CDI-AHCTA. Such a result corresponds with the differing molecular weights of BnOH and Capstone® respectively. **(Figure 4.29)**

**Table 4.7 TGA mass loss data for CDI-FHCTA convergently synthesised from CDI, BHMTA and Capstone®.**

| Onset (°C) | Mass loss (mg) | Mass loss (%) |
|---|---|---|
| **271.8** | 2.72 | 39 |
| **352.0** | 2.16 | 31 |
| **455.7** | 1.11 | 16 |

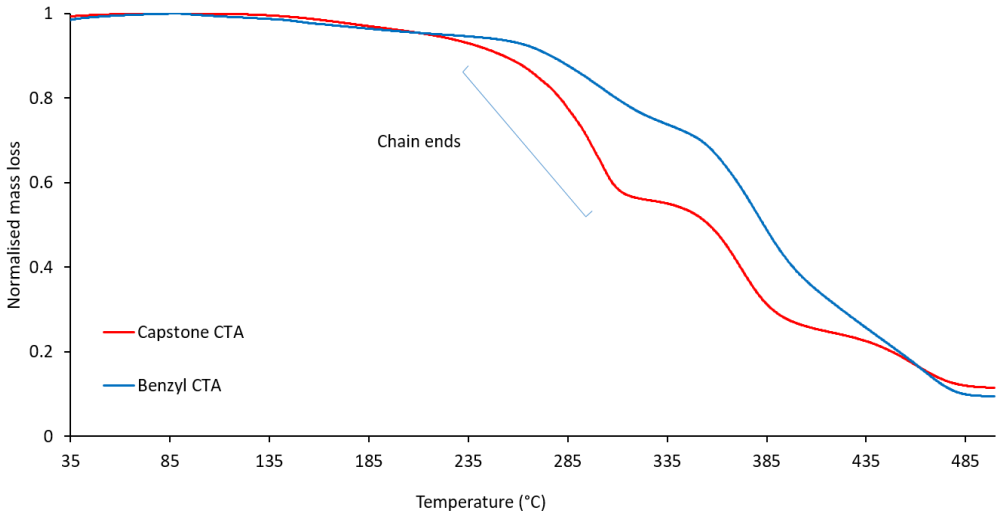


**Figure 4.29 TGA curves of a CDI-AHCTA convergently synthesised from CDI, BHMTA and BnOH (blue) and a CDI-FHCTA convergently synthesised from CDI, BHMTA and Capstone® (red).**

ESI-MS spectrometry was conducted to understand the distinct species within the CDI-FHCTA. As expected, a wide range of species were detected given the uncontrolled nature of the hyperbranching mechanism. The mass/charge ratios were observed to be significantly lower at 600 – 4000 m/z than the values obtained by SEC analysis ($M_w$ 14,000 g $mol^{-1}$), as was observed for the CDI-AHCTA. Species greater than 4000 m/z were not observed as they were too large to fly because of the vast number of fluorinated chain ends that extensively ionised. As was the case for the CDI-AHCTA, the CDI-FHCTA has a non-polar branched network and highly polar chain ends and therefore often self-assembles or forms micelles along the column of the SEC machine, thus resulting in an increase of the hydrodynamic radius in solution. However, the major distributions give some indication of the lower molecular weight species that are present in the CDI-FHCTA. However, the singly ionised peak distribution at 2,058.7242 m/z suggests a three-generation species with two methyl chain ends and six Capstone® chain ends. This data begins the process of understanding the composition and structure of such hyperbranched polymers, but further work needs to be carried out to understand their ionisation characteristics. **(Figure 4.30)**

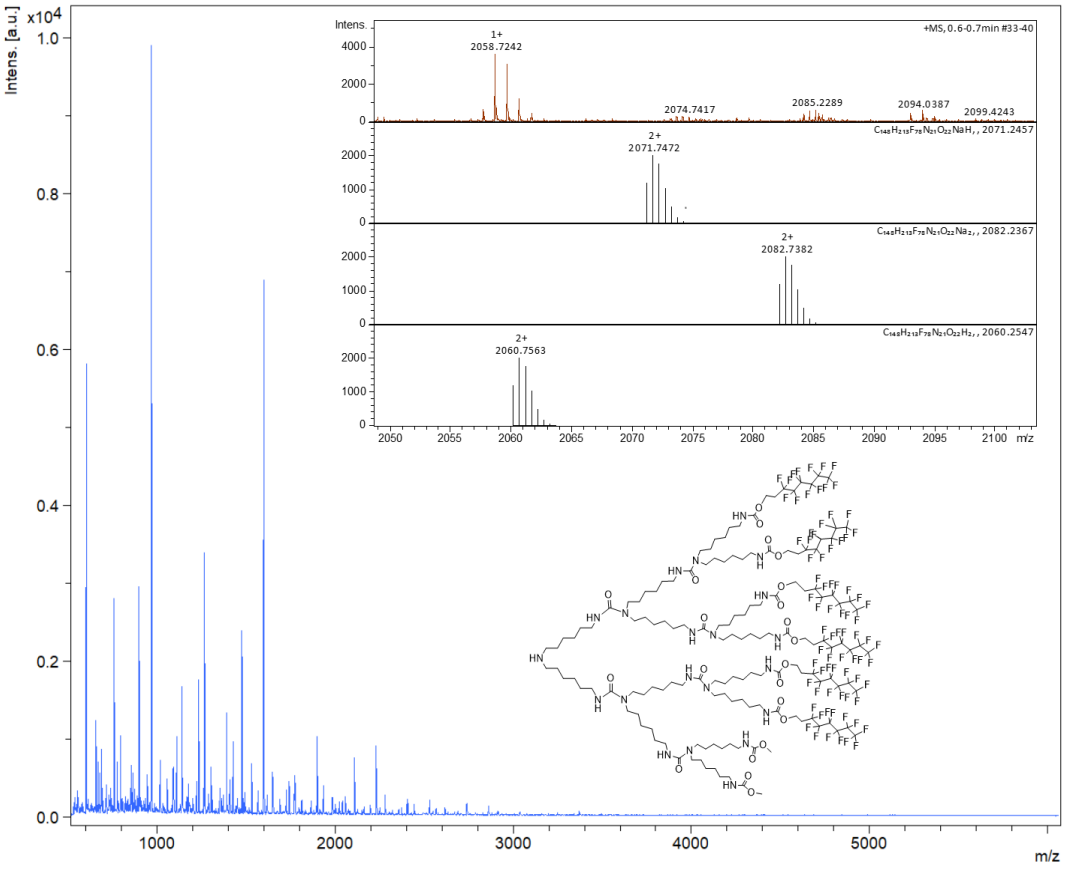


**Figure 4.30 ESI-MS spectrum of a CDI-FHCTA convergently synthesised from CDI, BHMTA and Capstone® (50:50 MeOH/THF, positive mode).**

## 4.3 Conclusions

To conclude, CBC has been shown to react in a one-pot, temperature-controlled sequential synthesis towards primary amines even in the presence of secondary amines, which allows for the formation of an $AB_2$ monomer utilising a one-pot process. This $AB_2$ monomer then self-condensed to form a hyperbranched polyurea. Post-polymerisation modification was then exemplified with BnOH to induce aromatic chain ends. This method opened up the way to a range of CBC-AHCTAs that are candidates for further coupling reactions.

It was also demonstrated that CDI can react preferentially, in a one-pot, temperature-controlled sequential synthesis with primary amines in the presence of secondary amines at -20 °C and is a cheap and readily available precursor compared to CBC and a viable alternative for the formation of HCTAs. Initial experiments were conducted using a model system with aromatic chain ends and then the methodology was transferred further to incorporate fluorinated chain ends. The one-pot, temperature-controlled, sequential synthesis proved to be a highly efficient method of synthesising an HCTAs from CDI and BHMTA, as evidenced by the substantial number of chain ends, the imidazole ones of which were subsequently quenched by a 100-molar excess of methanol thereby terminating any unreacted chain ends. It is expected that it should be possible to attach the CDI-HCTAs to a host material, *via* the secondary amine focal point, and that such CDI-HCTAs should induce hydrophobic and lipophobic surface characteristics.

## 4.4 References


1. F. Xiang, L. Asri, O. Ivashenko, P. Rudolf and T. Loontjens, *Langmuir*, 2015, **31**, 2761-2769.

2. J. Yin, J. Wildeman and T. Loontjens, *J. Polym. Sci., Part A: Polym. Chem.*, 2015, **53**, 2036-2049.

3. T. Emrick, H.-T. Chang and J. M. J. Fréchet, *Macromolecules*, 1999, **32**, 6380-6382.

4. M. Smet, Y. Fu, X. Zhang, E. H. Schacht and W. Dehaen, *Macromol. Rapid Commun.*, 2005, **26**, 1458-1463.

5. C. Sivakumar and A. S. Nasar, *Eur. Polym. J.*, 2009, **45**, 2329–2337.

6. Y. H. Kim, *J. Polym. Sci., Part A: Polym. Chem.*, 1998, **36**, 1685-1698.

7. M. Jikei and M. A. Kakimoto, *J. Polym. Sci., Part A: Polym. Chem.*, 2004, **42**, 1293-1309.

8. C. R. Yates and W. Hayes, *Eur. Polym. J.*, 2004, **40**, 1257-1281.

9. B. Voit, *J. Polym. Sci., Part A: Polym. Chem.*, 2000, **38**, 2505-2525.

10. B. Voit, *J. Polym. Sci., Part A: Polym. Chem.*, 2005, **43**, 2679-2699.

11. J. W. Bartels, P. M. Imbesi, J. A. Finlay, C. Fidge, J. Ma, J. E. Seppala, A. M. Nystrom, M. E. Mackay, J. A. Callow, M. E. Callow and K. L. Wooley, *Appl. Mater. Interfaces*, 2011, **3**, 2118-2129.

12. M. Vanjinathan, A. Raghavan and A. S. Nasar, *J. Polym. Sci., Part A: Polym. Chem.*, 2007, **45**, 2959-2977.

13. T. Shanmugam and A. S. Nasar, *Macromol. Chem. Phys.*, 2008, **209**, 651-665.

14. H. R. Meyer, *Kunstst. Plast.*, 1956, **3**, 160-162.

15. O. Persenaire, M. Alexandre, P. Degée and P. Dubois, *Macromol. Mater. Eng.*, 2008, **293**, 581-588.

16. S. Maier, T. Loontjens, B. Scholtens and R. Mülhaupt, *Macromolecules*, 2003, **36**, 4727-4734.

17. S. Maier, T. Loontjens, B. Scholtens and R. Mülhaupt, *Angew. Chem. Int. Ed.*, 2003, **42**, 5094-5097.

18. T. Loontjens, *J. Polym. Sci., Part A: Polym. Chem.*, 2003, **41**, 3198-3205.

19. F. Xiang, T. Loontjens, E. Geladé and J. Vorenkamp, *Macromol. Chem. Phys.*, 2012, **213**, 1841-1850.

20. F. Xiang, M. Stuart, J. Vorenkamp, S. Roest, H. Timmer-Bosscha, M. C. Stuart, R. Fokkink and T. Loontjens, *Macromolecules*, 2013, **46**, 4418-4425.

21. W. J. Feast, S. P. Rannard and A. Stoddart, *Macromolecules*, 2003, **36**, 9704-9706.

22. H. Bonnard, L. Ferruccio, J.-P. Senet and P.-Y. L. Roy, *USA Pat.,* 6,699,988, 2004.

23. H. A. Staab, *Liebigs Ann. Chem.*, 1957, **609**, 75-83.

24. H. A. Staab, *Liebigs Ann. Chem.*, 1957, **609**, 83-88.

25. H. A. Staab, *Angew. Chem. Int. Ed.*, 1962, **1**, 351-367.

26. W. Otting and H. A. Staab, *Liebigs Ann. Chem.*, 1959, **622**, 23-30.

27. S. P. Rannard and N. J. Davis, *Org. Lett.*, 2000, **2**, 2117-2120.

28. S. P. Rannard and N. J. Davis, *Org. Lett.*, 1999, **1**, 933-936.

# Chapter 5

# The Use and Potential Application of Fluorinated Hyperbranched Chain Terminating Agents

## 5.1 Introduction

Thermoplastic polyurethanes (TPUs) allow the manufacture of a very diverse range of materials because of their easily modifiable structure, which fundamentally consists of hard and soft segments. Different percentages of hard segment can be used in the TPU composition with resulting changes in material properties.

When the hard segment percentage (%HS) in a TPU is reduced to very low levels, such as 10%HS, the polymer is predominately made of soft segments, which makes the TPU extra soft. This softness is measured on one of three Shore scales: Shore 00 for extra soft materials; Shore A for soft materials; and Shore D for hard materials **(Figure 5.1[1]).[2]**


**Figure 5.1 Shore 00, Shore A and Shore D scales for measuring hardness of materials.**

When the %HS is kept low, TPUs become viscous, especially when their soft segment is also inherently viscous such as with polycarbonates.[3] As a result, such TPUs are not amenable to processing by the extrusion moulding technique because they coat the machine. In addition, it has been observed that such TPUs are highly sensitive to the inevitable fluctuations in processing temperatures of the extrusion moulding technique and this often results in deviances in the final material plaque.[4] To circumvent this problem, plasticisers are often used to make TPUs more suitable for

extrusion moulding but this is not ideal as plasticisers are known to be toxic in a wide variety of applications.[5]

TPUs that are extra soft, non-tacky, plasticiser-free and suitable for extrusion moulding have begun to be produced *via* the introduction of linear crystalline chain ends (LCCEs). Currently the technology is centred on using highly crystalline, well-defined, low molecular weight, polyethylene monoalcohols, which are covalently bonded to the chain ends of the TPU. LCCEs have also been shown to significantly alter the surface properties of the final TPU, in loadings less than 2-3 wt%, without altering its mechanical properties. The key advantages of using LCCEs in TPU synthesis are:

- a significant reduction in tackiness;
- improved suitability for extrusion moulding; and
- a widened processing window.

This reduces the deviances in the output material and results in the formation of more uniform plaques. It has also been noted that fluorinated LCCEs reduce the surface tension of TPUs and they have been observed to be hydrophobic.[6,7]

LCCEs are incorporated into TPUs after the traditional TPU synthesis has been conducted, forming covalent bonds between the TPU and the LCCE. This is particularly important as TPUs that rely on physical interactions fail after short lifetimes and result in a reduction in material performance.[8] In forming TPUs, the hard and soft segments react with an excess diisocyanate, leaving free isocyanate groups on the chain ends. As an LCCE is a monoalcohol it is only able to act as a chain terminator as opposed to a diol that is a chain extender. It is added to and reacts with the free isocyanate groups to cap the chain ends of the TPU. **(Scheme 5.1)**[9,10] LCCEs are expensive and only allow for limited additional functionality, because of the single chain end whereas hyperbranched polymers offer an abundance of chain ends that can be functionalised according to the desired application.

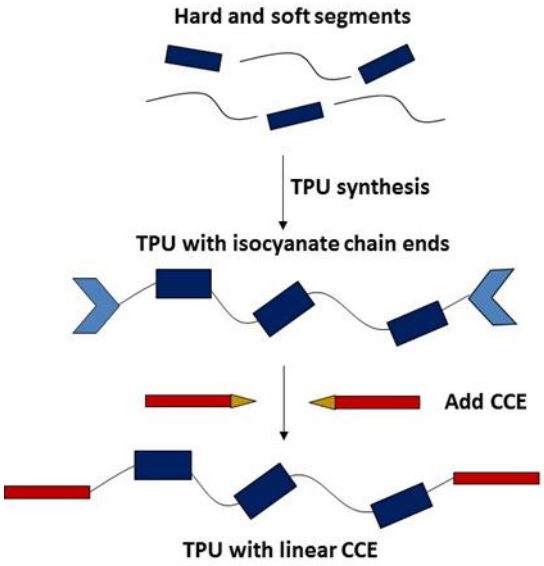


**Scheme 5.1 Incorporation of linear crystalline chain ends into a TPU.**

It is hypothesised that the hyperbranched chain-terminating agents synthesised from 1,1'-carbonyldiimidazole (CDI-HCTAs) synthesised and characterised in chapter 4 should be capable of functioning in a comparable way to LCCEs and when. attached to the TPUs should be mobile and migrate to the surface. It is also projected that such HCTAs will selectively alter the surface properties of a TPU, dependant on its functionality, whilst maintaining its existing mechanical properties.[11,12] However, it is essential to minimise concentration of the HCTAs, so that the effect on the existing mechanical properties of the TPU will be negligible. An analysis of the effect of fluorinated CDI-HCTAs (CDI-FHCTAs) on the surface properties of the TPUs will be performed, as fluorinated molecules have previously been reported to lower the surface energy of polymers.[13]

## 5.2 Results and Discussion

### 5.2.1 The incorporation of hyperbranched chain terminating agents into thermoplastic polyurethane elastomers

The use of CDI-HCTAs functionalised with aromatic and fluorinated chain ends, which consist of a secondary amine focal point and aliphatic branching points was investigated. It was anticipated that the secondary amine focal point of the HCTAs would allow coupling reactions with isocyanate chain ends on the TPUs and would form covalent attachments between the HCTAs and the TPU.

An aromatic TPU without HCTAs, with a known softness of 80-85 Shore A, which is the typical softness of a shoe heel, was produced as a control material. Typically, such TPUs are made in the melt and in bulk on an industrial scale, however, to research the concept a 10-g scale TPU was synthesised in DMF. The TPU had a %HS of 40%, which consisted of methylene diphenyl diisocyanate (MDI) and 1,4-butanediol (BDO) and a soft segment of a poly(ε-caprolactone) (PCL) diol with a molecular weight of 2,000 g mol$^{-1}$ (2K-PCL) as determined by SEC analysis. The required MDI:BDO:2K-PCL ratio was calculated according to equation **(5.1)**, where $M$ = molar mass. The composition of the TPU remained constant throughout all the following experiments.

$$\frac{(M_{\mathrm{MDI}}+M_{\mathrm{BDO}})}{(M_{\mathrm{MDI}}+M_{\mathrm{BDO}}+M_{2K\ PCL})}x100 = \%HS \qquad (5.1)$$

The control experiment yielded a TPU with the following characteristics: $M_w$ of 25,300 g mol$^{-1}$ and $Đ_M$ of 1.86. **(Figure 5.2)** The molecular weight shown in the SEC analysis was lower than expected. It is considered that the lower molecular weight is a result of changing the polymerisation conditions from bulk to solvent in DMF, but as all the TPUs that were synthesised had similar molecular weight values (within error) then for the purposes of comparing TPUs with and without HCTAs this is considered acceptable. Diffusion Ordered NMR spectroscopy (DOSY) of the TPU

without HCTAs produced a reference chart for confirming whether the HCTAs had attached to the TPU **(Figures 5.3 and 5.4)**

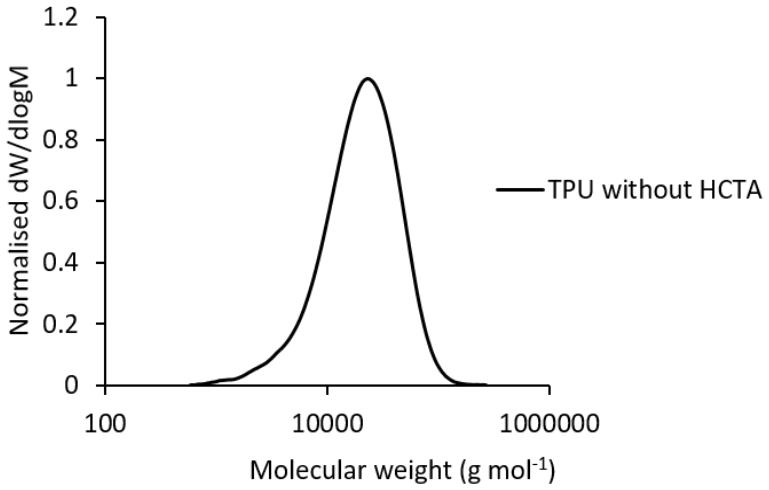


**Figure 5.2 SEC analysis of a TPU without HCTAs in DMF against PMMA standards.**

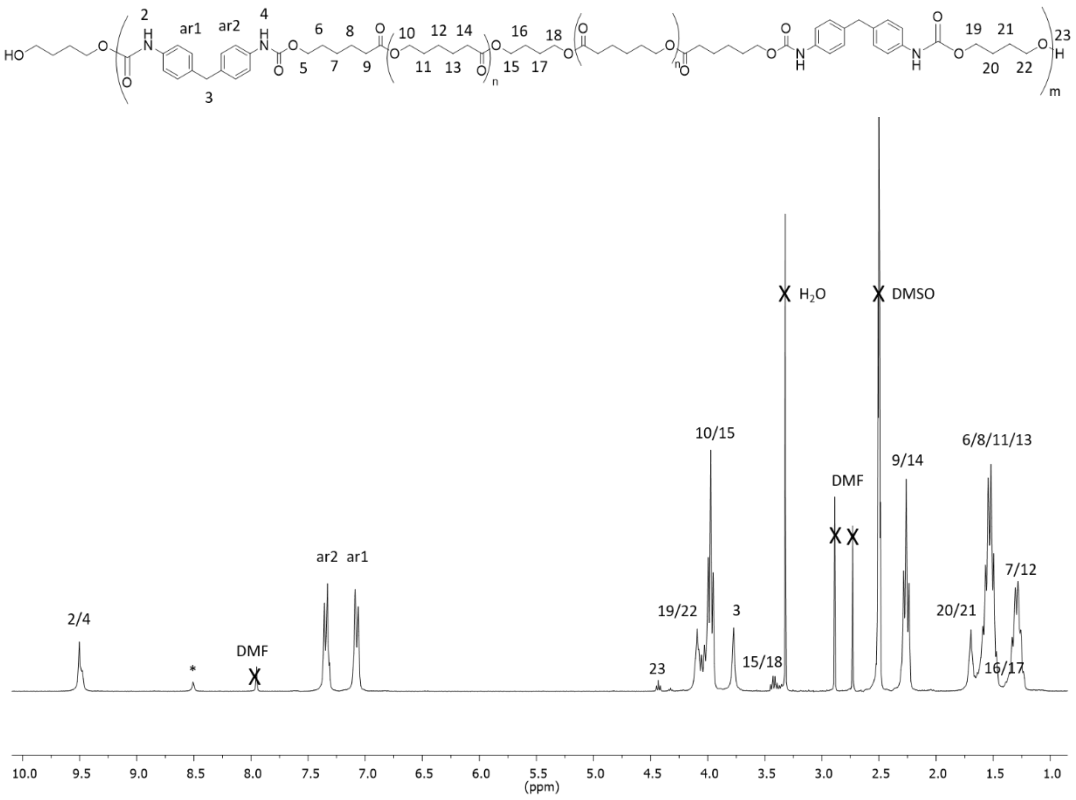


**Figure 5.3 $^{1}$H NMR spectrum of a TPU without HCTAs (400 MHz, 298 K, DMSO-$d_6$).**

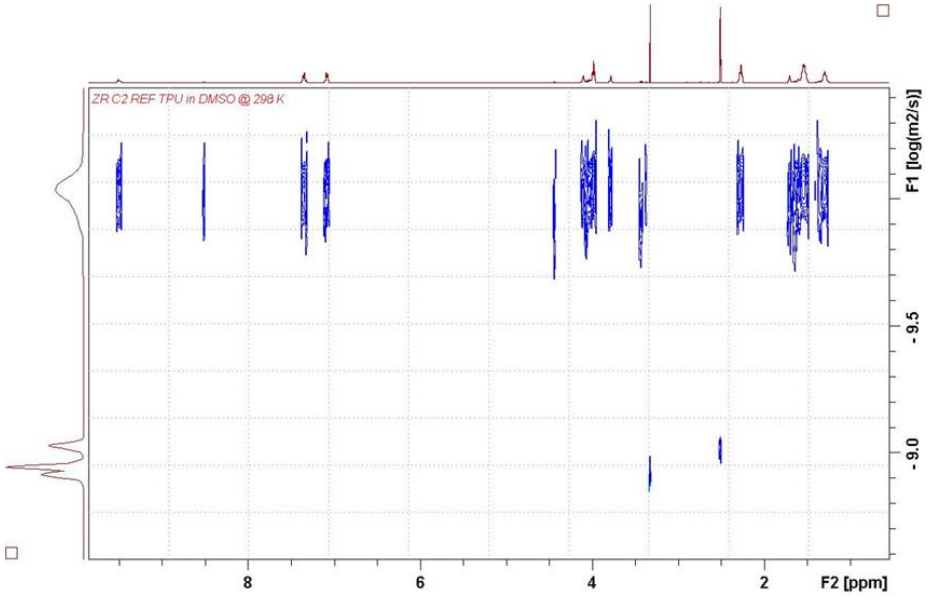


**Figure 5.4 DOSY spectrum of a TPU without HCTAs (400 MHz, 298 K, DMSO-$d_6$).**

#### 5.2.1.1 Aromatic hyperbranched chain terminating agents

A control TPU with benzyl alcohol (BnOH) aromatic HCTAs (AHCTA-TPU) was produced to assess the hypothesis that HCTAs can be attached to a TPU. BnOH is an inexpensive, strongly nucleophilic molecule that also provides an aromatic handle; which is important for the NMR spectroscopy experiments that were used to confirm the attachment of the aromatic HCTAs (AHCTAs) to the AHCTA-TPU. These AHCTAs were incorporated into the AHCTA-TPU at different wt%s *via* the secondary amine functionality present at their focal point and were covalently attached by reaction with the free isocyanate chain ends. The resulting AHCTA-TPUs were subsequently used as control materials when analysing the surface properties of TPUs with fluorinated HCTAs (FHCTA-TPUs). After the optimisation of this system it was projected that the transfer from an aromatic to a fluorinated alcohol would produce HCTAs with fluorinated chain ends (FHCTAs). **(Scheme 5.2)**

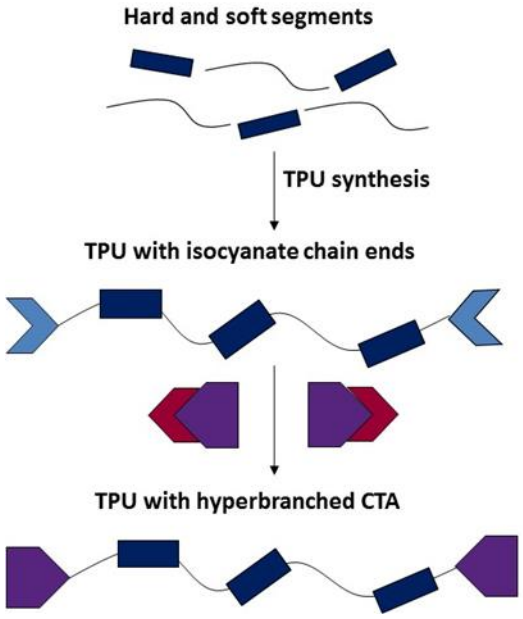


**Scheme 5.2 Attachment of HCTAs to a TPU.**

The synthesis of the AHCTA-TPUs was conducted in a comparable manner to the control experiment (TPU without HCTAs) with the added steps of monitoring the free isocyanate and the addition of the AHCTAs. After standard TPU synthesis (reaction of the hard and soft segments) Fourier transform infrared (FT-IR) spectroscopy was

utilised to calculate the percentage isocyanate (NCO%) of the TPU chain ends. The areas under the NCO peak at *c.a.ν̃* = 2,300 $cm^{-1}$ and under the CH peak at *c.a.ν̃* = 2,900 $cm^{-1}$ were measured and the NCO% was calculated according to equation **(5.2)**.

$$\frac{Area\ under\ NCO\ peak}{Area\ under\ CH\ peak} x\ factor = NCO\% \qquad (5.2)$$

Values of 0.2-0.3% indicated that the polymerisation had proceeded but sufficient NCO groups remained to react with the AHCTAs. It should be noted that the NCO% calculation was not used as a quantitative measurement of free NCO groups, but instead was an *in-situ* measurement that offered an indication of the progress of the reaction. TPUs were loaded with 3, 4 and 5 wt% of AHCTAs. The AHCTA-TPUs obtained had a $M_w$ between 16,000 g $mol^{-1}$ and 38,000 g $mol^{-1}$ with increasing $Đ_M$ values between 1.82 and 2.05. **(Table 5.1 and Figure 5.5)** By contrast to the AHCTA chromatographs, the AHCTA-TPU chromatographs appear to be monomodal because of the linear TPU that the AHCTAs have been attached to. It was also observed that by adding 5 wt% of AHCTA the $M_w$ has doubled when compared to 0, 3 and 4 wt%. The increase in $M_w$ observed when increasing the wt% of AHCTA is mainly a consequence of the size of the end group, which increases the hydrodynamic volume of the AHCTA-TPU in the DMF solution. This result is to be expected following the SEC and electron spray ionisation mass spectrometry (ESI-MS) analysis of the AHCTAs in chapter 4, which showed significantly larger SEC molecular weight values compared with the lower *m/z* values obtained by the ESI-MS analysis. This suggests self-assembly or micellisation in the SEC instruments column.[14] The 5 wt% AHCTA-TPU data suggests that the system reaches a greater level of self-assembly because of the SEC measurement process at this concentration of AHCTA. Further the data also suggests that the increased amount of AHCTA contributes to a larger $M_w$ for the 5 wt% AHCTA-TPU, however, no clear trend was observed across the various wt% AHCTA loadings.

**Table 5.1 SEC data for TPUs with AHCTAs.**

| Polymer | wt% AHCTA | $M_w$ (g mol$^{-1}$) | $Đ_M$ |
|---|---|---|---|
| TPU without HCTAs | 0 | 25,300 | 1.86 |
| 3 wt% AHCTA-TPU | 3 | 16,100 | 1.82 |
| 4 wt% AHCTA-TPU | 4 | 17,300 | 1.83 |
| 5 wt% AHCTA-TPU | 5 | 38,500 | 2.05 |

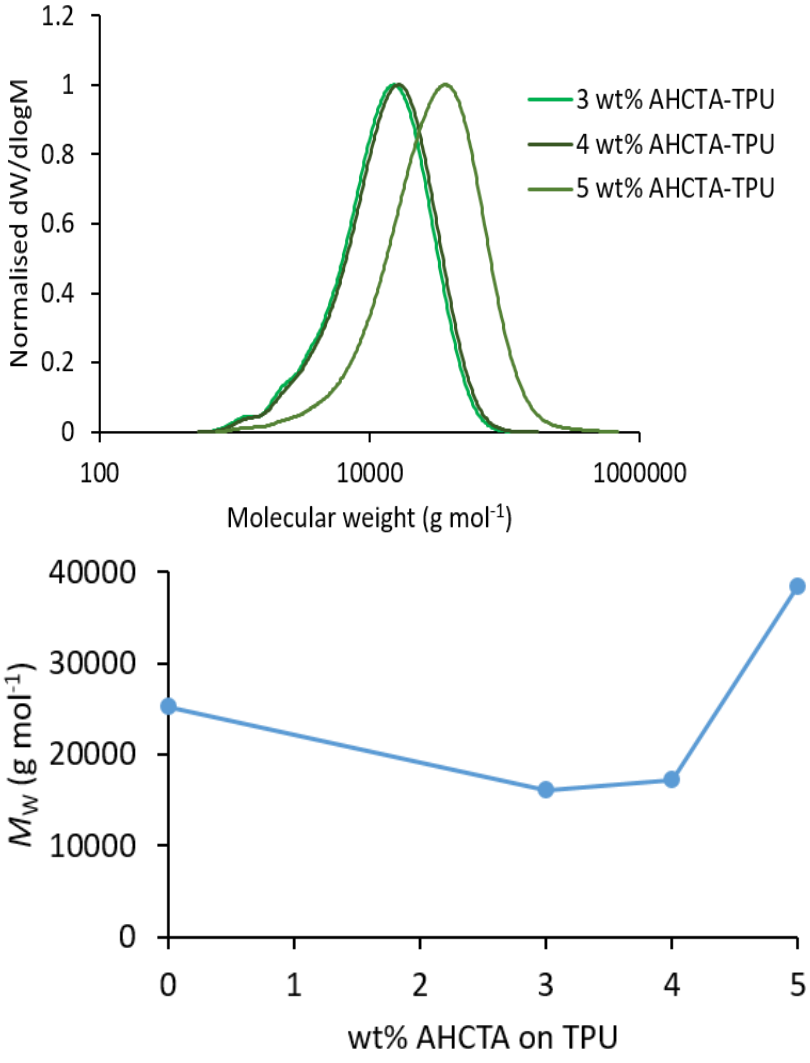


**Figure 5.5 SEC chromatograms (top) of TPUs with 3, 4 and 5 wt% AHCTAs in DMF against PMMA standards and a chart (bottom) showing the change in molecular weight with increasing wt%.**

To confirm the attachment of the AHCTAs, $^{1}$H NMR spectroscopy and DOSY spectroscopy were conducted on each of the AHCTA-TPUs. The resonances in the aromatic region of the $^{1}$H NMR spectrum are predominately associated with the MDI methines located in the TPU as well as the BnOH in the AHCTAs, therefore the resonance of the methylene in the AHCTAs at $\delta$ = 4.98 ppm was used to confirm attachment. **(Figure 5.6)** DOSY spectroscopy provided a further indication of attachment and showed that the methylene in the BnOH of the AHCTAs exhibited the same diffusion coefficient as the TPUs, which was consistent across all wt%s. This DOSY spectrum was complimented by a further DOSY experiment on a mixture of the TPU without HCTAs and AHCTA in a similar ratio to the 3wt.% AHCTA-TPU. Multiple diffusion coefficients were observed. First, a coefficient that corresponded to the TPU only. This had signature peaks for the urethane NH at 9.00 ppm and 8.50 ppm, two aromatic peaks corresponding to the MDI at 7.50 ppm and 7.00 ppm followed by aliphatic regions *c.a.* 4.00 ppm and between 2.00-0.00 ppm corresponding to the methylene's next to urethane and ester groups and the BDO chain extender and PCL chains respectively. The second corresponded to the AHCTA. It had signature peaks with an aromatic region between 7.50 ppm and 7.00 ppm, a peak at 5.00 ppm corresponding to the methylene on benzyl alcohol chain ends and aliphatic regions between 4.00-3.00 ppm and 2.00-0.00 ppm corresponding to the extensive branch network. **(Figure 5.7)**

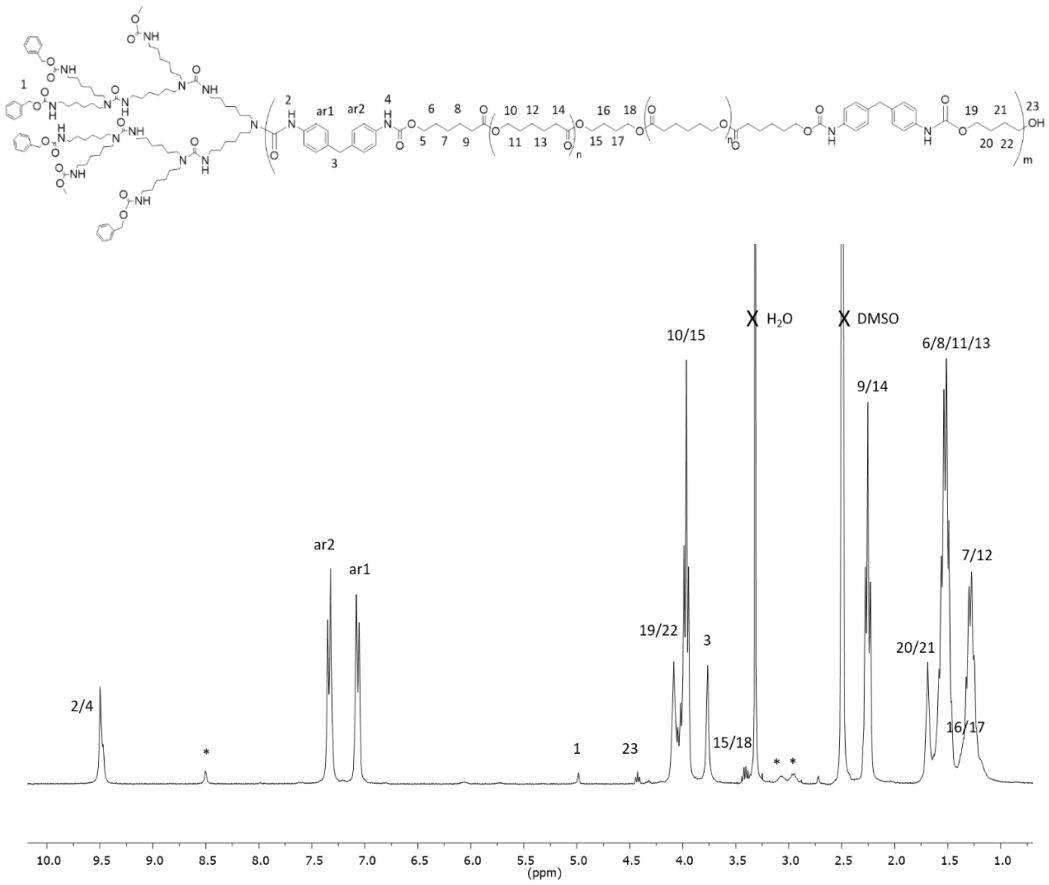


**Figure 5.6 $^{1}$H NMR spectrum of a 5 wt% AHCTA-TPU (400 MHz, 298 K, DMSO-$d_6$).**

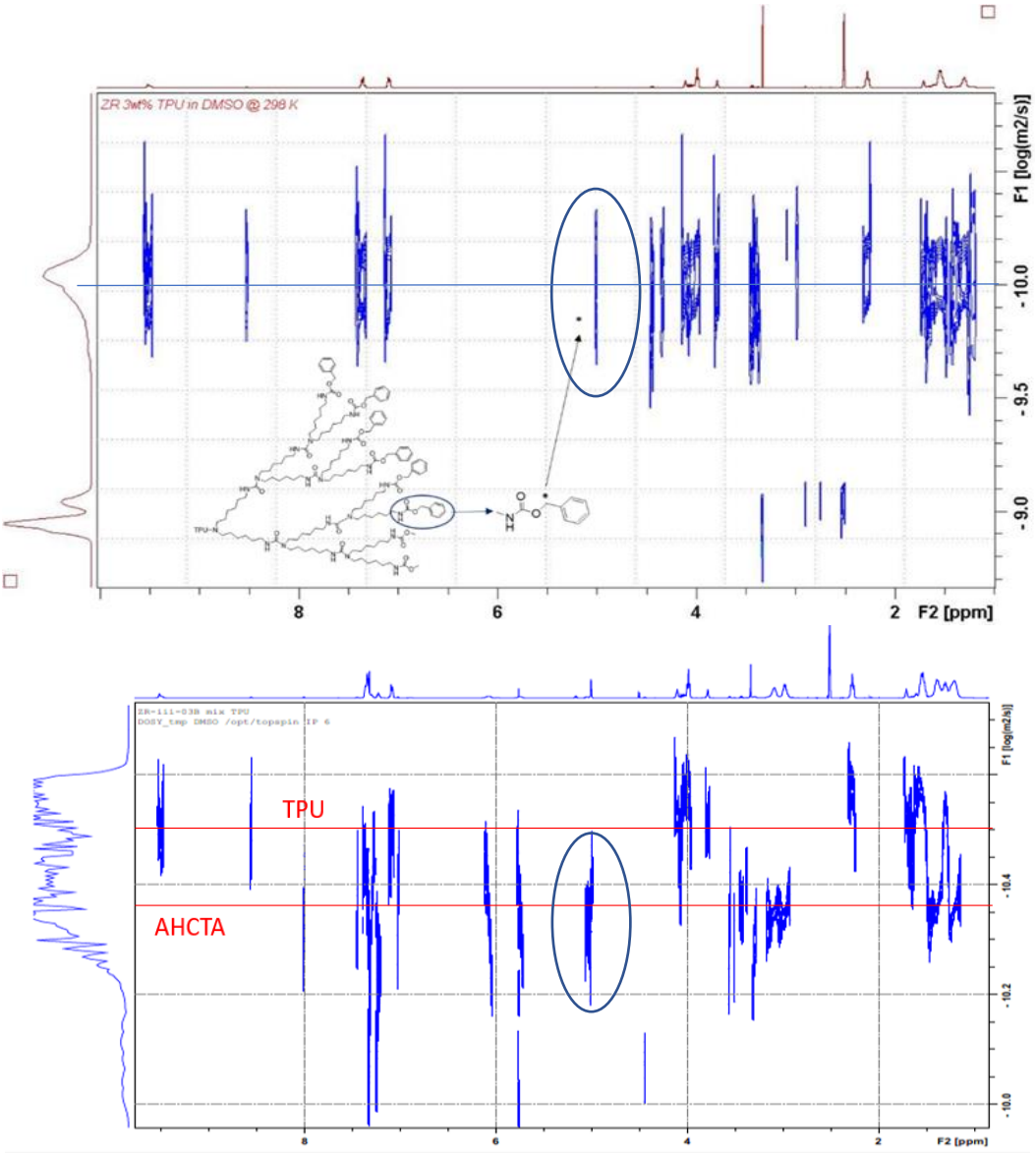


**Figure 5.7 DOSY spectrum of a TPU with 3 wt% AHCTAs (top), DOSY spectrum of a mixture of TPU without HCTAs with 3 wt% AHCTA in solution (bottom) (400 MHz, 298 K, DMSO-$d_6$).**

#### 5.2.1.2 Fluorinated hyperbranched chain terminating agents

Following the synthesis of AHCTA-TPUs with 0, 3, 4, and 5 wt% AHCTAs and the confirmation of the attachment of the AHCTAs by $^{1}$H NMR and DOSY spectroscopy, the incorporation of fluorinated CTAs (FHCTAs) into TPUs was now targeted.

The synthesis of the TPUs with FHCTAs (FHCTA-TPUs) was conducted in the same manner as for the AHCTA-TPUs. The FHCTA-TPUs were loaded with 1, 2, 3, 4 and 5 wt% FHCTAs and each yielded FHCTA-TPUs with molecular weights between 16,000 g mol$^{-1}$ and 30,000 g mol$^{-1}$ with increasing dispersity values from 1.79 to 1.84. **(Table 5.2 and Figure 5.8)** By contrast to the FHCTA chromatographs, the FHCTA-TPU chromatographs appear to be monomodal because of the linear TPU that the FHCTAs have been attached to. It was also observed that by adding 5 wt% of FHCTA the $M_w$ has doubled when compared to 0, 1, 2, 3 and 4 wt%. The increase of molecular weight observed when increasing the wt% is mainly a consequence of the size of the end group, which increases the hydrodynamic volume of the FHCTA-TPU in the DMF solution. This result is to be expected following the SEC and ESI-MS analysis of the FHCTAs in chapter 4, which showed significantly larger SEC molecular weight values compared with the lower m/z values obtained by the ESI-MS analysis. This suggests self-assembly or micellisation in the SEC instruments column.[14] As observed with the AHCTA TPUs, the 5 wt% FHCTA-TPU data suggests that the system reaches a greater level of self-assembly because of the SEC measurement process at this concentration of FHCTA. Further the data also suggests that the increased amount of FHCTA contributes to a larger $M_w$ between 0 and 5 wt% FHCTA-TPU. With the added benefit of 1,2 wt% FHCTA samples an increasing trend is observed over the 0, to 5 wt% FHCTA range of loadings.

**Table 5.2 SEC date for the TPUs with FHCTAs.**

| Polymer | wt% FHCTA | $M_w$ (g mol$^{-1}$) | $Đ_M$ |
|---|---|---|---|
| TPU without HCTAs | 0 | 25,300 | 1.86 |
| 1 wt% FHCTA-TPU | 1 | 16,900 | 1.79 |
| 2 wt% FHCTA-TPU | 2 | 18,200 | 1.80 |
| 3 wt% FHCTA-TPU | 3 | 22,500 | 1.82 |
| 4 wt% FHCTA-TPU | 4 | 18,700 | 1.83 |
| 5 wt% FHCTA-TPU | 5 | 30,700 | 1.84 |

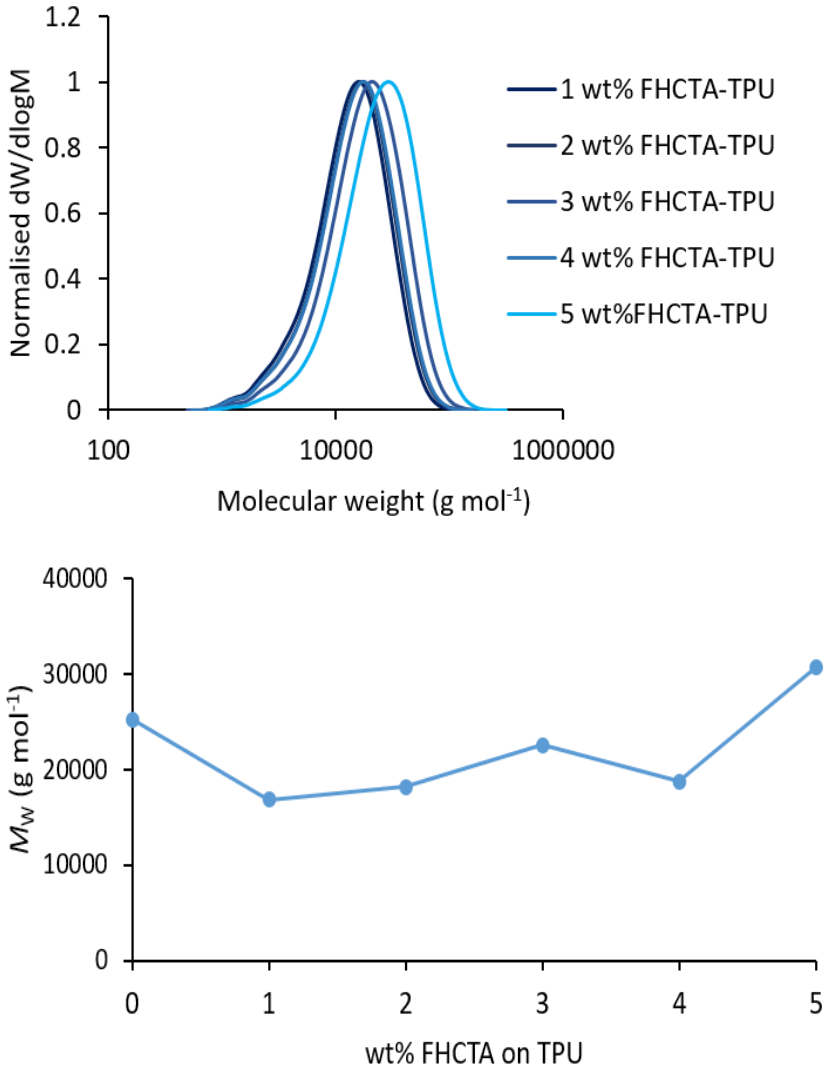


**Figure 5.8 SEC chromatograms (top) of TPUs with 1, 2, 3, 4 and 5 wt% AHCTAs in DMF against PMMA standards and a chart (bottom) showing the change in molecular weight with increasing wt%.**

It should be noted that the reaction solution went from clear to cloudy upon addition of the clear FHCTA solution indicating slight incompatibility of the FHCTAs and the TPU in the DMF. The FHCTAs act as compatibility agents, which attach a considerable number of fluorinated functionalities to the FHCTA-TPU.

To confirm the attachment of the FHCTAs, $^{1}$H NMR and $^{1}$H and $^{19}$F DOSY spectroscopy was conducted on each of the FHCTA-TPUs. $^{1}$H NMR spectroscopy showed evidence of the resonance for the methylene in Capstone® next to the urethane group on the FHCTAs at $\delta$ = 4.20 ppm, which was used to confirm attachment, but it was difficult to fully differentiate between overlapping peaks that did not appear in the heteronuclear single quantum correlation 2D NMR spectroscopy (HSQC 2D NMR) experiments. Attachment of the CTA to the TPU was hypothesised following the successful characterisation of the BHTCA-TPU model system that was easier to observe than the attachment of the FHCTA to the TPU. **(Figure 5.9)** $^{1}$H DOSY spectroscopy was used to further confirm that the attachment was successful as the resonance for the methylene in Capstone® next to the urethane group on the FHCTAs exhibited the same diffusion coefficient as the TPU, which was consistent across all wt%s. However again this peak was difficult to differentiate between overlapping signals. This DOSY spectrum was complimented by a further DOSY experiment of a mixture of TPU without HCTAs and FHCTA in a similar ratio to the 5wt.% FHCTA-TPU. Multiple diffusion coefficients were observed. First, a coefficient that corresponded to the TPU only. This had signature peaks for the urethane NH at 9.00 ppm and 8.50 ppm, two aromatic peaks corresponding to the MDI at 7.50 ppm and 7.00 ppm followed by aliphatic peaks at *c.a*. 4.00 ppm and between 2.00-0.00 ppm corresponding to the methylenes next to urethane and ester groups and the methylenes on the BDO chain extender and PCL chains respectively. The second corresponds to the FHCTA. It had signature peaks with a peak at 4.20 ppm corresponding to the methylene on the Capstone® chain ends and aliphatic peaks at *c.a.* 3.00 ppm and 2.00-0.00 ppm, corresponding to the extensive branch network. Finally, $^{19}$F DOSY spectroscopy confirmed a fluorine species with 6 fluorine resonances with the same diffusion coefficient which gives further evidence to successful attachment of the CTA to the TPU. **(Figure 5.10)**

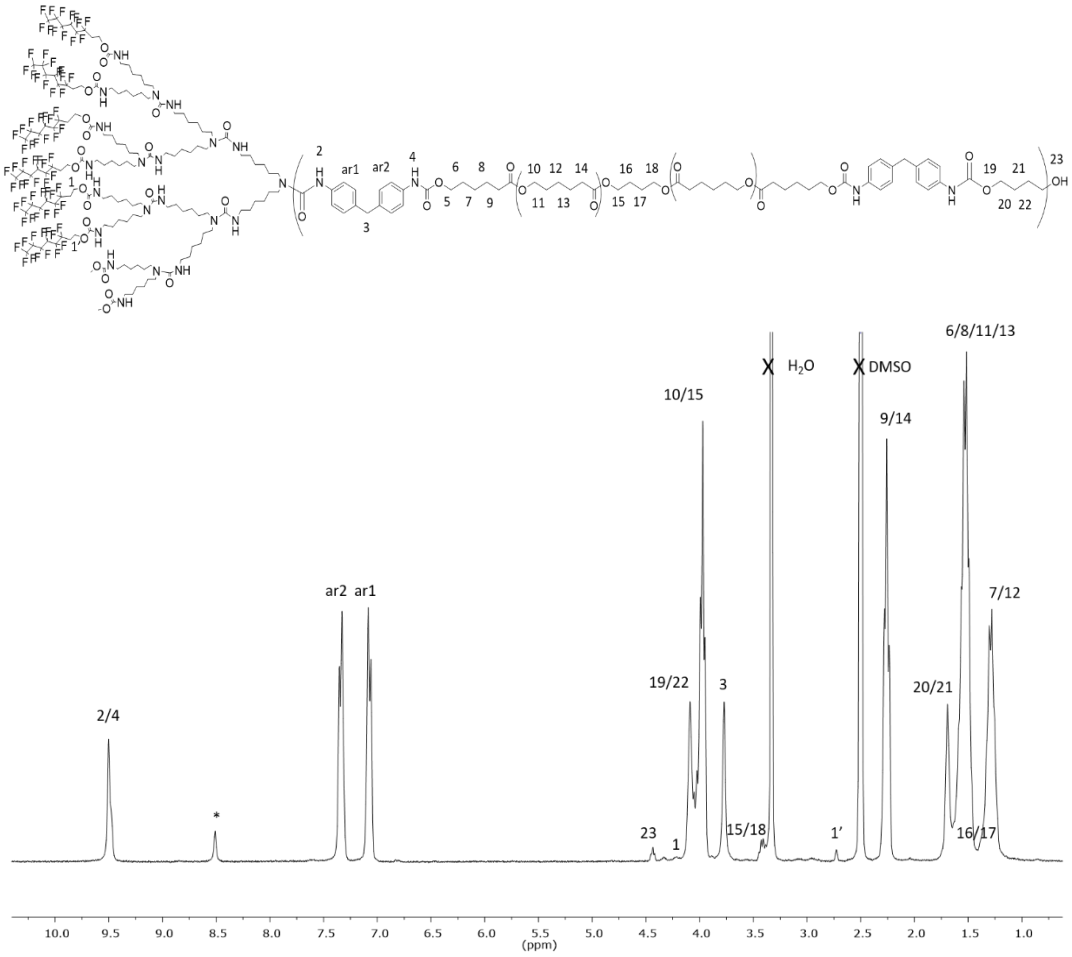


**Figure 5.9 $^{1}$H NMR spectrum of a 5 wt% FHCTA-TPU (400 MHz, 298 K, DMSO-$d_6$).**

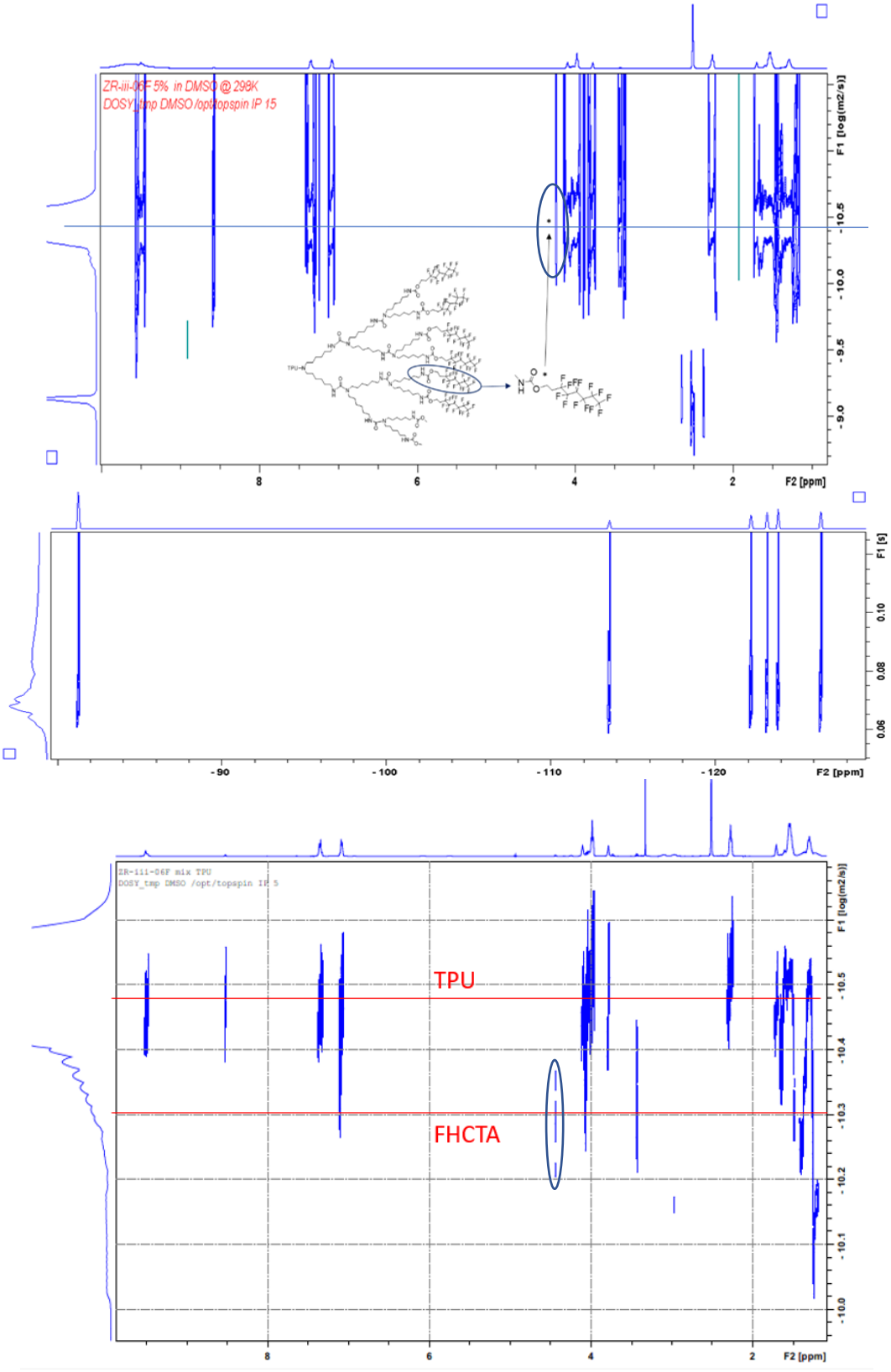


**Figure 5.10 $^{1}$H (top) and $^{19}$F (middle) DOSY spectra of a TPU with 5 wt% FHCTA, DOSY spectrum of a mixture of TPU without HCTAs with 5 wt% FHCTA in solution (bottom) (400 MHz and 376 MHz, 298 K, DMSO-$d_6$).**

Capstone® is a highly-fluorinated alcohol, which offers a fluorine handle to further probe the attachment of the FHCTAs. $^{19}$F NMR spectroscopy confirmed that all five fluorinated FHCTA-TPUs had retained the six fluorine environments that were previously observed on Capstone® and the FHCTAs. **(Figure 5.11)**

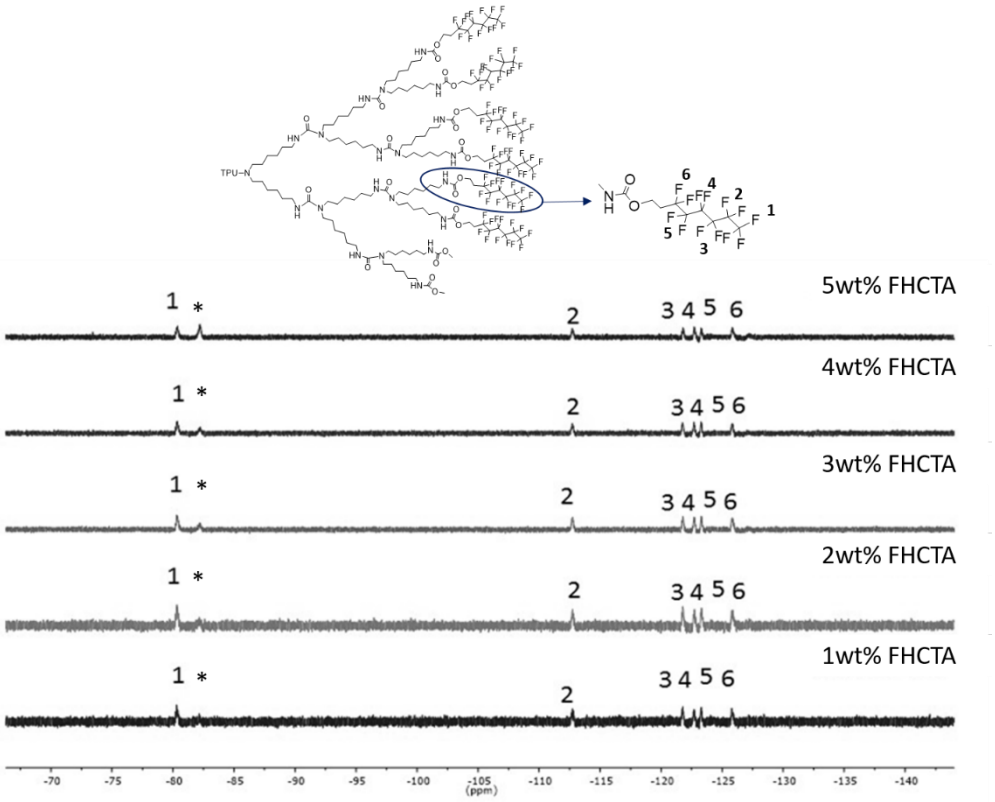


**Figure 5.11 $^{19}$F NMR spectra of Capstone®, FHCTAs TPUs with 1, 2, 3, 4 and 5 wt% FHCTAs (376 MHz, 298 K, DMSO-$d_6$ + 0.01% v/v $CF_3COOH$).**

### 5.2.2 Elastomers with hyperbranched chain terminating agents

Thermogravimetric analysis (TGA) of a TPU without HCTAs, the AHCTA-TPUs and the FHCTA-TPUs was conducted to compare their thermal degradation. The TPU without HCTA showed an onset of degradation at 245 °C for the hard segment and then a second degradation inflection at 360 °C for the soft segment. The onset of degradation for the 5 wt% AHCTA-TPU was at 235 °C and for the 5 wt% FHCTA-TPU was at 215 °C. These degradation profiles are in contrast to the stepwise mass loss of the HCTAs by themselves because of the loss of their branches with onsets of degradation at 110°C and 150°C for the AHCTA and the FHCTA respectively. This result suggests that the 5 wt% AHCTA-TPU had a greater propensity for its chains to

stack as a consequence of its ability to create π-π interactions with its chain ends. This resulted in a greater amount of heat energy to melt and consequently degrade it when compared to the 5 wt% FHCTA-TPU. This is shown by the steeper gradient for the degradation of the 5 wt% HCTA-TPUs compared with the TPU without HCTAs and the deviations in the degradation curves. **(Figure 5.12)**

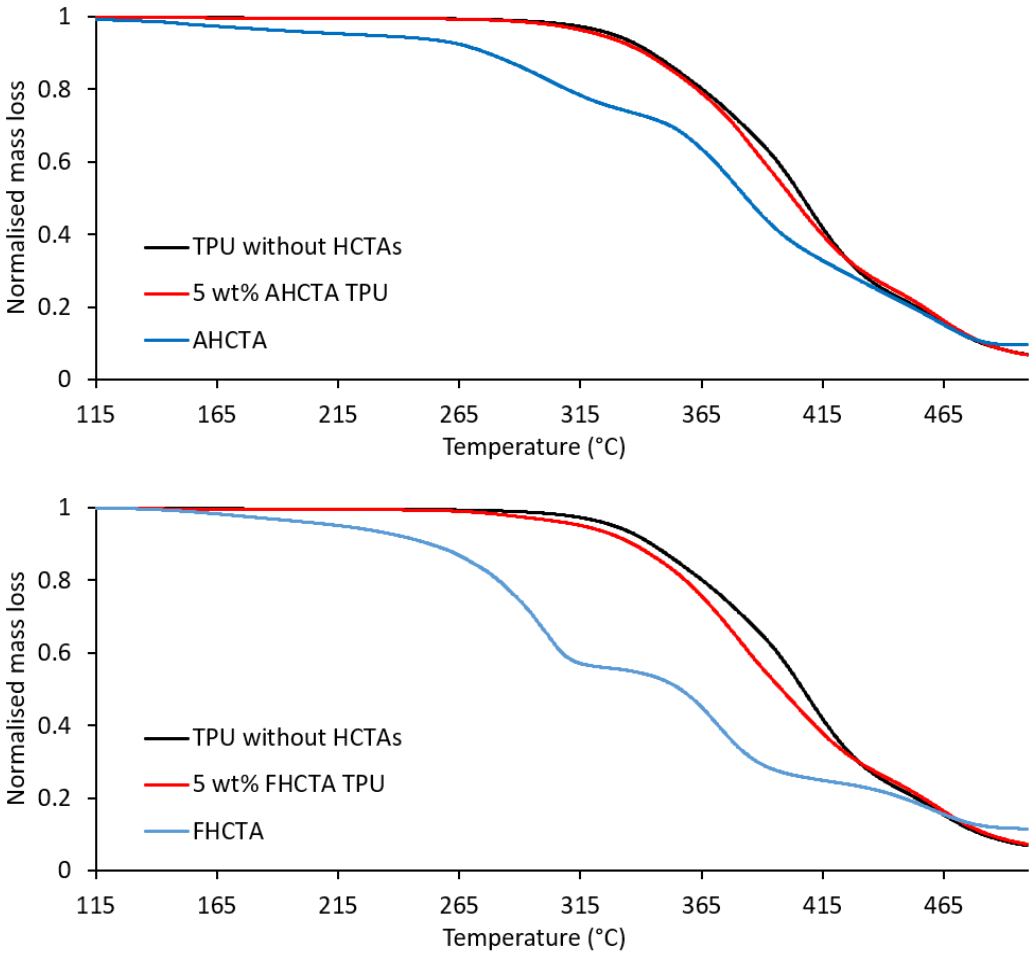


**Figure 5.12 TGA thermograms of a TPU without HCTAs (*both*), a TPU with 5 wt% AHCTAs (*top*) and a TPU with 5 wt% FHCTAs (*bottom*).**

Differential scanning calorimetry (DSC) analysis of the TPU without HCTAs and the various wt% AHCTA-TPUs and FHCTA-TPUs showed glass transition ($T_g$), crystallisation ($T_c$) and melt ($T_m$) onset temperatures as set out in **(Table 5.3)**. It was observed that both the 5 wt% AHCTA-TPU and FHCTA-TPU did not crystallise. It is considered that this is because of the higher wt% of the HCTA in the TPUs, which is a

sufficiently high concentration to affect its thermal properties and hinder crystallisation **(Figure 5.13)**

**Table 5.3 Glass transition, crystallisation and melt onset temperatures of a TPUs without HCTAs, TPUs with 3, 4 and 5 wt% AHCTAs and TPUs with 1, 2, 3, 4 and 5 wt% FHCTAs.**

| Polymer | $T_g$ onset (°C) | $T_c$ onset (°C) | $T_m$ onset (°C) |
|---|---|---|---|
| TPU without HCTAs | -53 | -13 | 36 |
| 3 wt% AHCTA-TPU | -58 | -20 | 39 |
| 4 wt% AHCTA-TPU | -55 | -18 | 38 |
| 5 wt% AHCTA-TPU | -55 | No data | 34 |
| 1 wt% FHCTA-TPU | -57 | -18 | 38 |
| 2 wt% FHCTA-TPU | -58 | -19 | 37 |
| 3 wt% FHCTA-TPU | -57 | -17 | 35 |
| 4 wt% FHCTA-TPU | -56 | -17 | 37 |

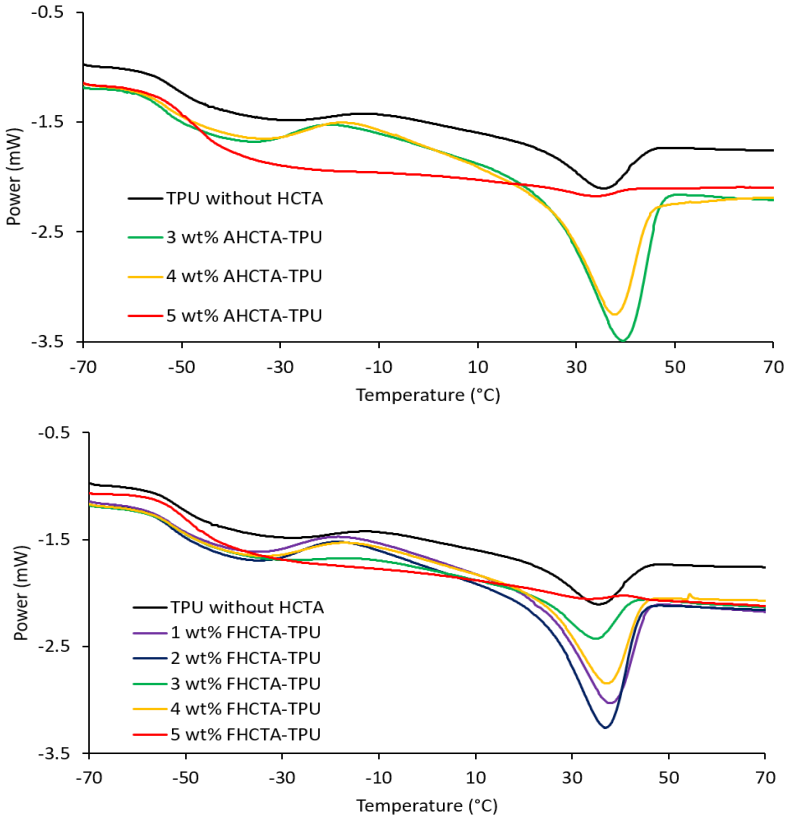


**Figure 5.13 DSC thermograms (second heating run) of a TPU without HCTAs (*both*), TPUs with 3, 4 and 5 wt% AHCTAs (*top*) and TPUs with 1, 2, 3, 4 and 5 wt% FHCTAs (*bottom*).**

### 5.2.3 Static contact angle analysis of the surface properties of thermoplastic polyurethane elastomers with hyperbranched chain terminating agents

To study the effect of the HCTAs on the surface properties of the TPUs, solutions of the TPU without HCTAs, the AHCTA-TPUs and the FHCTA-TPUs were made at all wt% in DMF and used to make thin films, which were spin coated onto glass coverslips. The thin films were placed in an oven overnight at 65 °C to remove the residual DMF and were then left at room temperature for seven days. Static contact angle measurements in water and hexadecane were conducted on each film. This process was repeated ten times and the error for each angle between samples was calculated using standard deviation.

It was observed that the static water contact angles for the TPU without HCTAs averaged 51 ° for both the left and right angles. These values served as a baseline for the AHCTA-TPUs and the FHCTA-TPUs. For the 3, and 4 wt% AHCTA-TPUs it was observed that the average contact angles were relatively stable considering the standard deviation of each contact angle average. This observed plateau suggests that the initial presence of HCTAs in the TPU made a significant difference to the hydrophobicity of its surface, which allowed a high concentration of aromatic functionality to migrate to the surface. However, at 5 wt% there was a significant increase in contact angle average, with a lower standard deviation, that indicates a more stable surface with a higher hydrophobicity. **(Table 5.4, Figures 5.14 and 5.15)** This plateau was also observed for the FHCTA-TPUs at the 1, 2, 3, and 4 wt% but at a higher contact angle average indicating that they were significantly more hydrophobic than the AHCTA-TPUs; differing by *c.a*. 30 °. Again, at 5 wt% there was a significant increase in contact angle average, with a lower standard deviation, that again indicates a more stable surface with a higher hydrophobicity. This increased hydrophobicity of the FHCTA-TPUs is because of the highly electronegative fluorine atoms that polarise the $CF_2$ bonds. Consequently, this means the FHCTA-TPUs have low intermolecular forces and hence low surface tension.[15,16] Finally, it should be noted that the reduction in values for both the 4 wt% AHCTA-TPU and FHCTA-TPU are because the HCTAs did not fully migrate to the surface of the TPUs during the annealing time. These results showed that both the AHCTAs and FHCTAs selectively

modified the surface of the TPUs to different degrees of hydrophobicity depending on the functionality of the HCTAs.

**Table 5.4 Left and right static water contact angle data of a TPU without HCTAs, TPUs with 3, 4 and 5 wt% AHCTAs and TPUs with 1, 2, 3, 4 and 5 wt% FHCTAs.**

| Polymer | wt% HCTA | θ Left ( ° ) | θ Right ( ° ) |
|---|---|---|---|
| TPU without HCTAs | 0 | 50.5 ± 4.1 | 51.1 ± 7.3 |
| 3 wt% AHCTA-TPU | 3 | 55.2 ± 5.3 | 57.8 ± 2.5 |
| 4 wt% AHCTA-TPU | 4 | 54.8 ± 6.9 | 53.7 ± 4.8 |
| 5 wt% AHCTA-TPU | 5 | 70.3 ± 0.3 | 70.9 ± 2.0 |
| 1 wt% FHCTA-TPU | 1 | 80.3 ± 30.3 | 85.1 ± 26.0 |
| 2 wt% FHCTA-TPU | 2 | 91.1 ± 13.5 | 88.3 ± 16.2 |
| 3 wt% FHCTA-TPU | 3 | 97.8 ± 13.5 | 99.9 ± 14.4 |
| 4 wt% FHCTA-TPU | 4 | 88.2 ± 14.5 | 89.1 ± 9.6 |
| 5 wt% FHCTA-TPU | 5 | 111.2 ± 1.5 | 110.3 ± 1.0 |

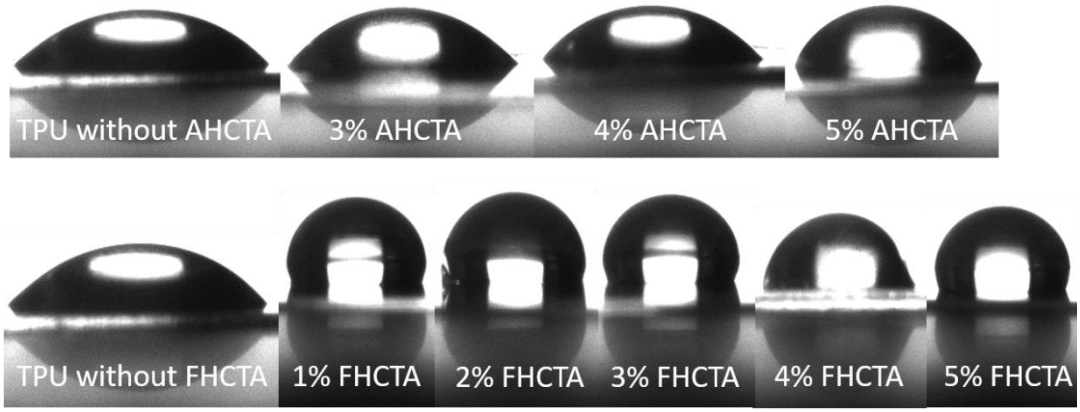


**Figure 5.14 Static water contact angle images of a TPU without HCTAs (*both*), TPUs with 3, 4 and 5 wt% AHCTAs (*top*) and TPUs with 1, 2, 3, 4 and 5 wt% FHCTAs (*bottom*).**

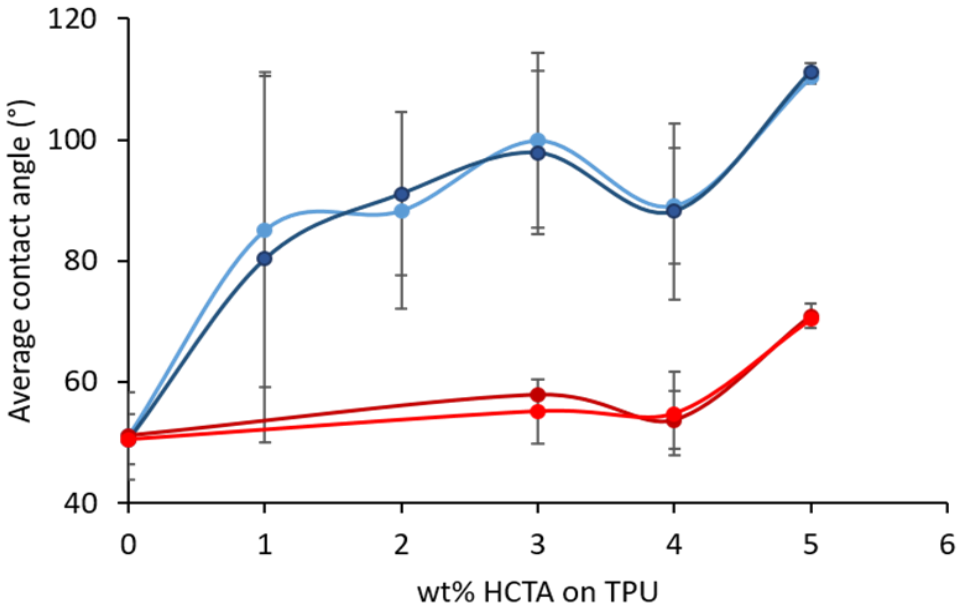


**Figure 5.15 Chart of the left and right static water contact angles of a TPU without HCTAs (*both*), TPUs with 3, 4 and 5 wt% AHCTAs (*red*) and TPUs with 1, 2, 3, 4 and 5 wt% FHCTAs (*blue*).**

The same analysis was conducted with hexadecane to observe whether the lipophobic effect of the HCTAs on the surface of the TPUs would lead to similar trend. The TPU without HCTAs and the 3, 4 and 5 wt% AHCTA-TPUs all resulted in complete wetting of the surface. Whilst this was expected for the TPU without HCTAs, it was hypothesised that the 3, 4 and 5 wt% AHCTA-TPUs would show repulsion to the aliphatic solvent because of the BnOH aromatic chain ends. Such repulsion did not occur and it is considered that this was because the AHCTAs had not fully migrated to the surface of the TPUs. The 1, 2, 3, 4 and 5 wt% FHCTA-TPUs had contact angles averaging 64 ° with no observed difference, within error, between the different wt%s. These results were lower than initially hypothesised and again it is considered that this was because the FHCTAs had not fully migrated to the surface of the TPUs. **(Table 5.5, Figures 5.16 and 5.17)** These results further confirmed, alongside the water contact angle analysis, that the FHCTAs were selectively modifying the surface of the TPUs but there was no significant advantage seen by increasing the wt% of the FHCTAs.

**Table 5.5 Left and right static hexadecane contact angle data of a TPU without HCTAs, TPUs with 3, 4 and 5 wt% AHCTAs and TPUs with 1, 2, 3, 4 and 5 wt% FHCTAs.**

| Polymer | wt% CTA | θ Left ( ° ) | θ Right ( ° ) |
|---|---|---|---|
| TPU without HCTAs | 0 | 0.0 ± 0.0 | 0.0 ± 0.0 |
| 3 wt% AHCTA-TPU | 3 | 0.0 ± 0.0 | 0.0 ± 0.0 |
| 4 wt% AHCTA-TPU | 4 | 0.0 ± 0.0 | 0.0 ± 0.0 |
| 5 wt% AHCTA-TPU | 5 | 0.0 ± 0.0 | 0.0 ± 0.0 |
| 1 wt% FHCTA-TPU | 1 | 58.9 ± 2.9 | 60.1 ± 3.5 |
| 2 wt% FHCTA-TPU | 2 | 65.5 ± 3.7 | 66.8 ± 3.8 |
| 3 wt% FHCTA-TPU | 3 | 65.7 ± 3.4 | 66.8 ± 2.9 |
| 4 wt% FHCTA-TPU | 4 | 63.9 ± 3.5 | 65.4 ± 3.8 |
| 5 wt% FHCTA-TPU | 5 | 61.6 ± 1.7 | 62.5 ± 2.4 |


**Figure 5.16 Static hexadecane contact angle images of a TPU without HCTAs and TPUs with 1, 2, 3, 4 and 5 wt% FHCTAs.**

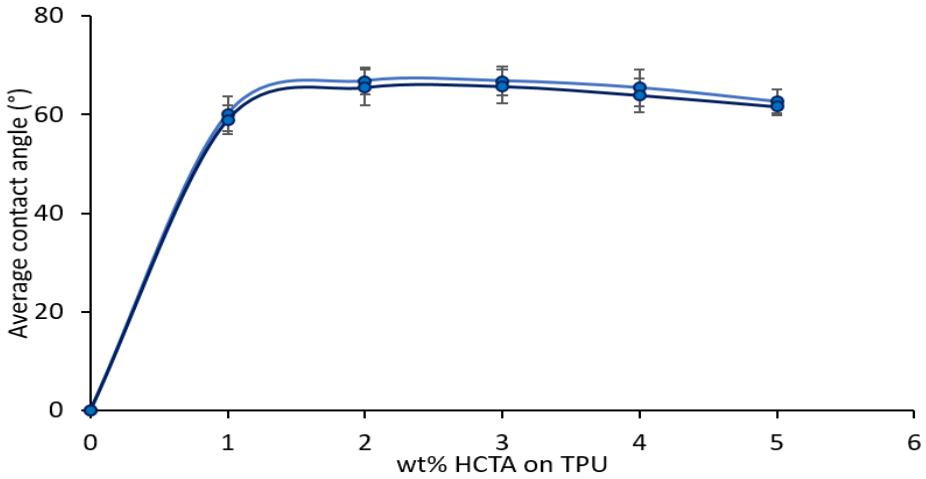


**Figure 5.17 Chart of the left and right static hexadecane contact angles of a TPU without HCTAs and TPUs with 1, 2, 3, 4 and 5 wt% FHCTAs.**

These initial results showed that the FHCTAs had affected the surface properties of the TPUs, but they did not fully migrate to the surface of the TPUs as it was noted that the contact angles were not sustained for longer than a minute after measurement. Thus, a second batch of thin films were cast for all the TPUs in water and hexadecane with a longer annealing time where the samples were placed in an oven at 65 °C for seven days and then left on at room temperature for a further ten days. It was expected that this time lapse would allow a more complete migration of the FHCTAs to the surface of the TPUs. **(Tables 5.6 and 5.7 and Figures 5.18, 5.19, 5.20 and 5.21)**

**Table 5.6 Left and right static water contact angle data after a prolonged annealing time of a TPU without HCTAs, TPUs with 3, 4 and 5 wt% AHCTAs and TPUs with 1, 2, 3, 4 and 5 wt% FHCTAs.**

| Polymer | wt% HCTA | θ Left ( ° ) | θ Right ( ° ) |
|---|---|---|---|
| TPU without HCTAs | 0 | 47.2 ± 3.2 | 48.9 ± 5.1 |
| 3 wt% AHCTA-TPU | 3 | 71.0 ± 3.2 | 70.1 ± 3.3 |
| 4 wt% AHCTA-TPU | 4 | 70.5 ± 3.8 | 70.4 ± 2.2 |
| 5 wt% AHCTA-TPU | 5 | 66.7 ± 2.3 | 67.6 ± 1.5 |
| 1 wt% FHCTA-TPU | 1 | 104.7 ± 4.6 | 104.9 ± 4.6 |
| 2 wt% FHCTA-TPU | 2 | 108.8 ± 2.9 | 109.1 ± 3.1 |
| 3 wt% FHCTA-TPU | 3 | 108.7 ± 2.8 | 109.4 ± 3.0 |
| 4 wt% FHCTA-TPU | 4 | 107.8 ± 5.4 | 108.2 ± 5.6 |
| 5 wt% FHCTA-TPU | 5 | 107.6 ± 5.3 | 108.3 ± 5.1 |

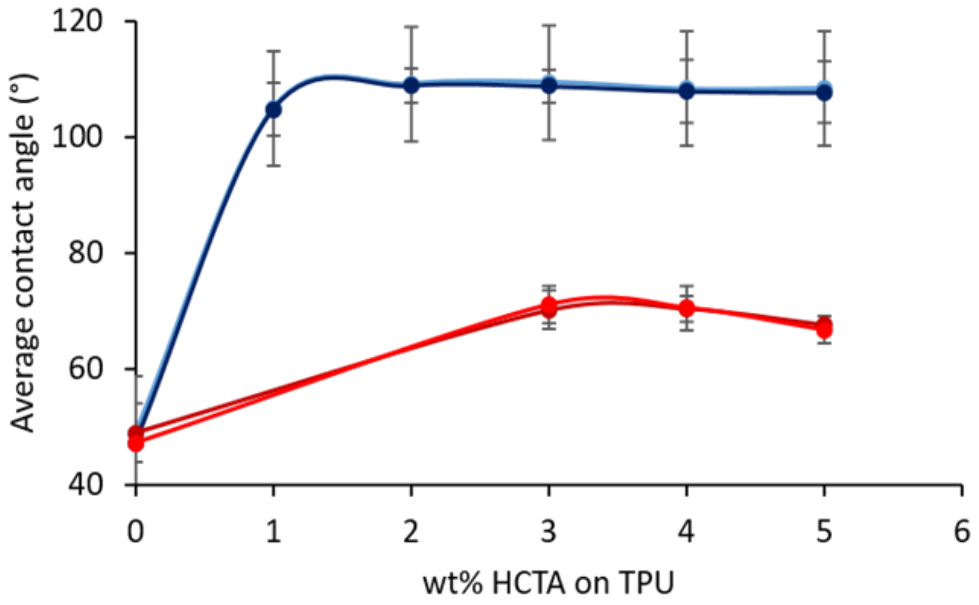


**Figure 5.18 Chart of the left and right static water contact angles after a prolonged annealing time of a TPU without HCTAs (*both*), TPUs with 3, 4 and 5 wt% AHCTAs (*red*) and TPUs with 1, 2, 3, 4 and 5 wt% FHCTAs (*blue*).**

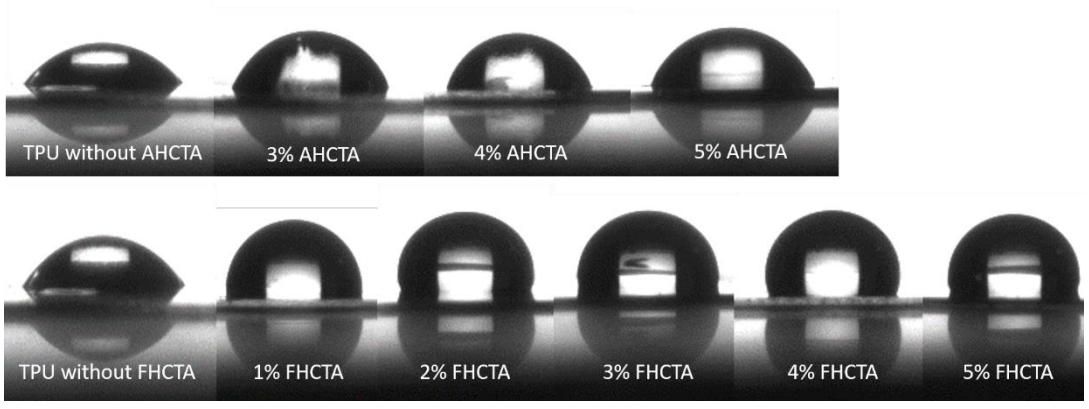


**Figure 5.19 Static water contact angle images of a TPU without HCTAs (*both*), TPUs with 3, 4 and 5 wt% AHCTAs (*top*) and TPUs with 1, 2, 3, 4 and 5 wt% FHCTAs (*bottom*).**

**Table 5.7 Left and right static hexadecane contact angle data after a prolonged annealing time of a TPUs without CTAs, TPUs with 3, 4 and 5 wt% AHCTAs and TPUs with 1, 2, 3, 4 and 5 wt% FHCTAs.**

| Polymer | wt% HCTA | θ Left ( ° ) | θ Right ( ° ) |
|---|---|---|---|
| TPU without HCTAs | 0 | 0.0 ± 0.0 | 0.0 ± 0.0 |
| 3 wt% AHCTA-TPU | 3 | 7.9 ± 2.0 | 7.9 ± 2.0 |
| 4 wt% AHCTA-TPU | 4 | 9.6 ± 2.2 | 9.6 ± 2.2 |
| 5 wt% AHCTA-TPU | 5 | 12.9 ± 0.5 | 12.9 ± 0.5 |
| 1 wt% FHCTA-TPU | 1 | 52.9 ± 2.9 | 53.7 ± 3.2 |
| 2 wt% FHCTA-TPU | 2 | 65.2 ± 4.9 | 64.8 ± 2.9 |
| 3 wt% FHCTA-TPU | 3 | 67.5 ± 2.9 | 68.4 ± 2.8 |
| 4 wt% FHCTA-TPU | 4 | 67.9 ± 1.3 | 68.8 ± 1.2 |
| 5 wt% FHCTA-TPU | 5 | 70.1 ± 2.0 | 70.8 ± 2.3 |

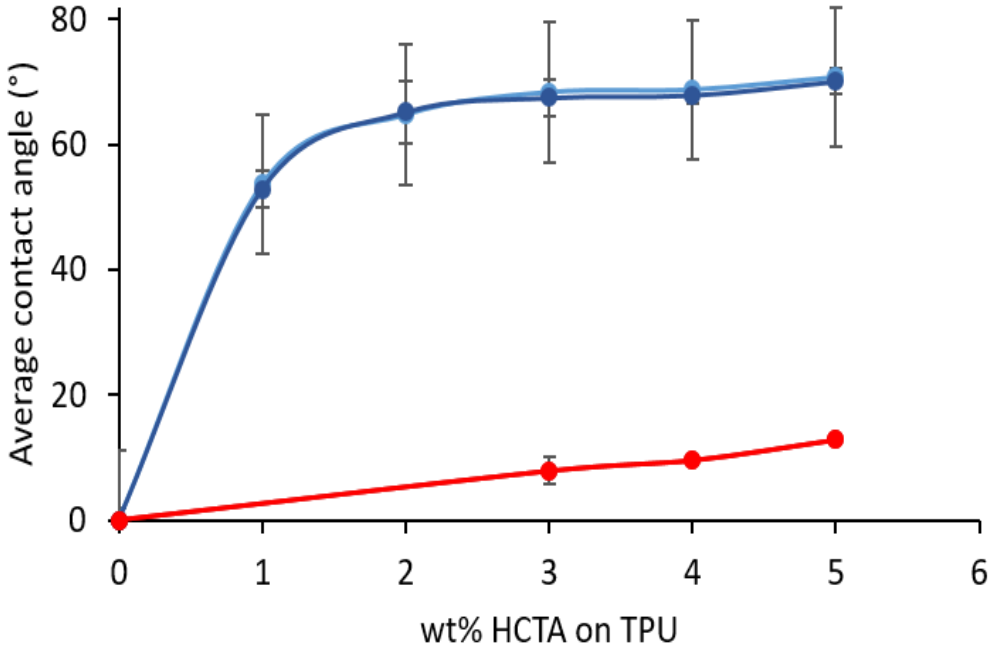


**Figure 5.20 Chart of the left and right static hexadecane contact angles after a prolonged annealing time of a TPU without HCTAs (both), TPUs with 3, 4 and 5 wt% AHCTAs (red) and TPUs with 1, 2, 3, 4 and 5 wt% FHCTAs (blue).**

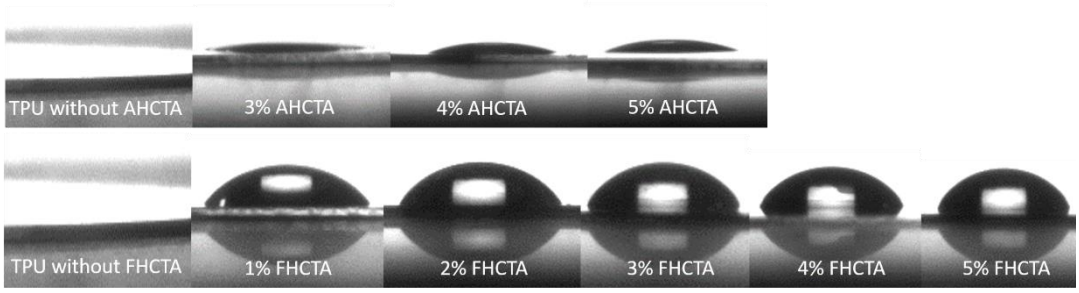


**Figure 5.21 Static hexadecane contact angle images of a TPU without HCTAs (*both*), TPUs with 3, 4 and 5 wt% AHCTAs (*top*) and TPUs with 1, 2, 3, 4 and 5 wt% FHCTAs (*bottom*).**

As expected, it was observed that the water and hexadecane contact angles significantly increased across the complete test set. For the AHCTA-TPUs, the water contact angles averaged 70 ° and the hexadecane contact angles averaged 10 ° (because these contact angles were less than 20 ° the circle method of measurement had to be used) and for the FHCTA-TPUs the water contact angles averaged 106 ° and the hexadecane contact angles averaged 65 °. For both AHCTA-TPUs and FHCTA-TPUs a steady increase of hexadecane contact angles showed a steady increase as the wt% was increased. It should also be noted that for both the AHCTA-TPUs and the FHCTA-TPUs the water and hexadecane contact angles were maintained for 15 minutes after the measurement was conducted, which indicated that the surface coverage of the HCTAs was more uniform than in the previous experiments conducted with a shorter annealing time.

### 5.2.4 Potential applications of hyperbranched chain terminating agents

Chapters 4 and 5 have presented two novel products. First, hyperbranched polymers (HBPs) derived from commercially available precursor which is easily modifiable. Secondly, the attachment of the HBPs to the chain end of the TPU. They present a new technology, which has the potential to help solve problems in the following areas:

- surface modification without disruption of mechanical properties– stain or water resistance;
- extrusion moulding additives to aid the production of ultra-soft TPUs;

- compatibility agents for fluorine and silicon functional polymers;
- tailor chain ends to desired applications e.g. anti-microbial, biocidal, oleophobic, click-reaction precursors;
- physical properties – abrasion resistance, viscosity modifiers, surfactants;
- drug delivery by self-assembly for hydrophobic drugs;
- performance coatings -use focal point to anchor the HBP to the surface and through reactive end groups to grow a coated surface.

## 5.3 Conclusions

This research shows the versatility of the HCTA technology to introduce a high degree of desired functionality to TPUs and to overcome current incompatibility issues associated with the introduction of a high fluorine content to existing TPUs. This HCTA technology provides a simple but effective method to selectively modify the surface properties of TPUs without changing their existing mechanical properties.

It has been demonstrated that the HCTAs derived from 1,1'-carbonyldiimidazole from chapter 4, with a secondary amine focal point and aromatic or fluorinated chain ends, can be covalently attached as HCTAs to TPUs with a range of loadings from 1 to 5 wt%, *via* free isocyanate groups.

Furthermore, it has been demonstrated that the HCTAs on the TPUs, are mobile and can migrate to the surface of the material and change the surface properties of the TPUs. This allows the concurrent formation of both hydrophobic and lipophobic TPUs, particularly with the FHCTA-TPUs. Materials that are simultaneously hydrophobic and lipophobic are ideal candidates for stain resistant coatings as they can repel water and oil-based stains and thereby resist colouration.

## 5.4 References


1. http://www.advancedseals.com/wp-content/uploads/2013/07/shore-hardness-chart.jpg, Accessed 02/07/2016.

2. H. J. Qi, K. Joyce and M. C. Boyce, *Rubber Chem. Technol.*, 2003, **76**, 419-435.

3. A. T. Miller, D. L. Safranski, K. E. Smith, R. E. Guldberg and K. Gall, *J. Mech. Behav. Biomed. Mat.*. 2016, **54**, 268–282.

4. U. G. Makal, unpublished work.

5. J. L. Wilkinson, P. S. Hooda, J. Barker, S. Barton and J. Swinden, *Crit. Rev. Env. Sci. Technol.*, 2016, **46**, 336-381.

6. U. G. Makal, B. W. Steinmetz, Q. Lu and R. W. Day, *USA Pat.,* 9,546,242, 2017.

7. R. W. Day, H. Zhang, U. G. Makal, R. Woofter and K. Smith, *WO Pat.,* 172460, 2016.

8. S. T. Milner, *Science (New York, N.Y.)*, 1991, **251**, 905-914.

9. U. G. Makal, B. W. Steinmetz, Q. Lu and R. W. Day, *WO Pat.,* 189993, 2014.

10. K. J. Wynne, B. Duan, S. Grunzinger, U. G. Makal, P. Kurt and J. Wynne, *USA Pat.,* 7,771,793, 2010.

11. F. Xiang, L. Asri, O. Ivashenko, P. Rudolf and T. Loontjens, *Langmuir*, 2015, **31**, 2761-2769.

12. L. v. Ravenstein, W. Ming, R. D. v. d. Grampel, R. v. d. Linde, G. d. With, T. Loontjens, P. C. Thüne and J. W. Niemantsverdriet, *Macromolecules*, 2004, **37**, 408-413.

13. M. K. Bernett and W. A. Zisman, *J. Phys. Chem.*, 1962, **66**, 1207-1208.

14. F. Xiang, M. Stuart, J. Vorenkamp, S. Roest, H. Timmer-Bosscha, M. C. Stuart, R. Fokkink and T. Loontjens, *Macromolecules*, 2013, **46**, 4418-4425.

15. D. O'Hagan, *Chem. Soc. Rev.*, 2008, **37**, 308-319.

16. J. L. Kiplinger, T. G. Richmond and C. E. Osterberg, *Chem. Rev.*, 1994, **94**, 373-431.

# Chapter 6

# Summary of Findings and Conclusions

## 6.1 Summary of findings and general conclusion

This thesis has explored and exploited the diverse and versatile nature of TPU synthesis to target two specific applications; biomaterials and stain resistant coatings.

First, by using their segmented structure to tune their thermal, mechanical and degradative properties a structure-function relationship was formed. Careful selection of non-toxic and degradable reagents and a metal-free catalyst make them desirable candidates for use as biomaterials.

Secondly hyperbranched polymers (HBPs) synthesised with aromatic and fluorinated chain ends were covalently attached to TPUs to selectively alter their surface properties and functionality, without affecting their other existing properties, which makes them ideal candidates for use as stain resistant coatings.

This research highlights the varied range of applications of TPUs. They stem from a simple three component system of a diol, polyol and a diisocyanate and have unique, flexible properties which can be easily tuned and tailored.

## 6.2 Conclusions from chapters 2-3

Cyclic dipeptides of tyrosine and glutamic acid in the hard segment of polyurethanes offer a viable and versatile route for incorporating bio-based chain extenders into TPUEs. The %HS of such TPUEs has a significant effect on their thermal, mechanical and degradative properties with a higher %HS resulting in a tougher, less elastic material. The addition of DKPs with ester and amide links with aromatic functionality allows finer tuning of such properties. The choice of DKP has a significant effect on the rate of degradation with additional ester links producing a more controlled and uniform breakdown. Conversely, additional amide links result in a faster degradation of the soft segment, but the hard segment does not degrade, resulting in premature material failure. By blending the ester and amide linked DKPs further control can be achieved. This research enables further understanding of the structure-function relationship of TPUEs and provides a solid platform for understanding how they can be tuned and tailored to a desired application by modifying their hard segment structure and content.

## 6.3 Conclusions from chapters 4-5

CDI is a feasible and inexpensive precursor for the formation of HCTAs *via* a one-pot, temperature-controlled, sequential synthesis. At -20 °C and below, it preferentially reacts with primary amines even in the presence of secondary amines and is efficient in forming HBPs with BHMTA. When attached to the chain ends of TPUs, these HBPs are mobile and migrate to the surface of the TPUs and change their surface properties. Functionalisation can be achieved by the further addition of aromatic or fluorinated chain ends. This technology can create simultaneously hydrophobic and lipophobic TPUs, which are desirable for stain resistant applications and is a simple but effective method to selectively modify TPU surfaces without affecting their remaining specific properties.

# Chapter 7

# Experimental Methods

## 7.1 Materials

*S*-Pyroglutamic acid, acetic anhydride, phosphorus pentoxide ($P_2O_5$), 1,8-diazabicyclo[5.4.0]undec-7-ene (DBU), 4-(chloromethyl)benzyl alcohol, methyl 4-cyanobenzoate, lithium aluminium hydride ($LiAlH_4$), 1-ethyl-3-(3-dimethylaminopropyl) carbodiimide (EDC), *N*-hydroxysuccinimide (NHS), 4-dimethylaminopyridine (DMAP), 4-(aminomethyl)benzoic acid, ε-caprolactam (CLM, subsequently dried over $P_2O_5$), *N,N*-diisopropylethylamine (DIPEA), 1,1'-carbonyldiimidazole (CDI), bis(hexamethylene)triamine (BHMTA), hexylamine, dihexylamine, *m*-cresol, thionyl chloride, tin(II) ethyl hexanoate, ($Sn(oct)_2$), benzyl alcohol and methylene diphenyl diisocyanate (MDI) were purchased from Sigma Aldrich. Dimethylsulfoxide (DMSO, dried over activated 3 Å molecular sieves) and *N,N*-dimethylformamide (DMF), toluene, methanol, dichloromethane, chloroform, triethylamine ($NEt_3$), concentrated sulfuric acid ($H_2SO_4$), tetrahydrofuran (THF), pyridine, sodium chloride, magnesium sulfate, sodium sulfate, sodium hydrogen carbonate ($NaHCO_3$), trifluoracetic acid, 1,4-butanediol (BDO), hexane, sodium hydroxide, ethyl acetate, isopropanol and calcium chloride were purchased from Fisher Scientific. *L*-Tyrosine and 1,4-benzenedimethanol were purchased from Alfa Aesar. Triphosgene and 4,4'-methylenebis(cyclohexyl isocyanate) ($H_{12}$MDI, purified by distillation) were purchased from Tokyo Chemical Industry (TCI) UK Ltd. Deuterated dimethylsulfoxide ($(CD_3)_2SO$) and deuterated chloroform ($CDCl_3$) were purchased from Apollo Scientific Ltd. Deuterated dimethylformamide ($(CD_3)_2NOCD$) was purchased from Cambridge Isotope Laboratories. Poly(ε-caprolactone) (PCL) with a $M_w$ of 2,000 g mol$^{-1}$ (2K-PCL, dried over $P_2O_5$ in chapter 2 only) was gifted from Perstorp UK Ltd (Chapter 2) and Lubrizol Corporation (Chapter 5). Capstone 62L was gifted from DuPont. Bicat 8106M was sourced from Shepard Chemical Company. All chemicals were used as purchased unless stated otherwise.

## 7.2 Instrumental methods

### 7.2.1 Nuclear magnetic resonance spectroscopy

One-dimensional $^{1}H$, $^{13}C$ and $^{19}F$ nuclear magnetic resonance (NMR) spectroscopy and two-dimensional $^{1}H$ and $^{13}C$ heteronuclear single quantum correlation 2D NMR spectroscopy (HSQC 2D NMR) and $^{1}H$ and $^{19}F$ diffusion ordered NMR spectroscopy (DOSY) spectra were obtained on either a Bruker DPX-250, DPX-300, DPX-400 or DPX-500 spectrometers (250, 300, 400 and 500 MHz) at 298 K. All chemical shifts were reported as $\delta$ in parts per million (ppm) and referenced to the residual solvent signal: ($CDCl_3$: $^{1}H$, $\delta$ = 7.26 ppm; $^{13}C$, $\delta$ = 77.16 ppm; $(CD_3)_2SO$: $^{1}H$, $\delta$ = 2.50 ppm; $^{13}C$, $\delta$ = 39.52 ppm; $(CD_3)_2NOCD$: $^{1}H$, $\delta$ = 8.03, 2.92, 2.75 ppm; $^{13}C$, $\delta$ = 163.15, 34.89, 29.76 ppm) or to an internal standard ($CF_3COOH$ $^{19}F$: $\delta$ = -76.55 ppm). The resonance multiplicities are denoted as s (singlet), d (doublet), t (triplet), q (quartet) or m (multiplet).

### 7.2.2 Size exclusion chromatography

Size exclusion chromatography (SEC) was used to determine the molecular weights and molecular weight distributions (dispersities, $Đ_M$) of all synthesised polymers. SEC and absolute molecular weight SEC analyses were conducted in *N,N*-dimethylformamide (DMF) at 50 °C with 5 mM $NH_4BF_4$ salt, using a Varian PL-GPC50 gel permeation chromatograph system equipped with a guard column and two PLgel 5 µM mixed C columns in series with differential refractive index (RI), viscometer, dual angle (15° and 90°) light scatter and ultraviolet (UV) detectors at a flow rate of 1.0 mL $min^{-1}$. The system was calibrated against Varian Polymer Laboratories Easi-Vial linear poly(methyl methacrylate) (PMMA) standards and a universal PMMA standard (Peak molecular weight: 73,150 g $mol^{-1}$, $Đ_M$: 1.02, refractive index increment: 0.069 mL/g, inherent viscosity: 0.2670 dL/g) and was analysed using the software package Cirrus v2.2 (RI) v3.3 (triple). Each analyte sample was filtered through a polytetrafluoroethylene (PTFE) membrane with 0.22 µm pore size before injection.

### 7.2.3 Thermal analysis

Differential scanning calorimetry (DSC) and thermogravimetric analysis (TGA) were obtained using a Mettler Toledo DSC1 star and a TGA/DSC star system and was analysed by the software package STARe v13. DSC heating and cooling cycles were run in triplicate in series between -80 and 100 °C under a nitrogen atmosphere at a heating rate of +/- 5 °C $min^{-1}$ (chapter 3) or +/- 10 °C $min^{-1}$ (chapters 4 and 5) in a closed 40 µL aluminium crucible with a hole in the lid. The onset of degradation was determined at the inflexion point in the heating curve. The melting point ($T_m$) was determined from the midpoint in the first heat cycle of the DSC and the glass transition temperature ($T_g$) was determined from the midpoint in the second heat cycle of DSC.

### 7.2.4 Dynamic mechanical analysis

Molten polymers were compression moulded using a PTFE mould into cuboids and allowed to cool to ambient temperature and were annealed for 7 days in an incubator at 25 °C before being subjected to dynamic mechanical analysis (DMA).

DMA was obtained using a Mettler Toledo DMA 1 Star System and was analysed by the software package STARe v13. All DMA samples were analysed in tension mode under a preload of 1 N with an oscillating frequency of 5.0 and 0.5 Hz with a displacement of 20 µm across a temperature range from -80 through to 200 °C at a heating rate of 5 °C $min^{-1}$. Glass transitions ($T_g$) were determined by the peak maximum of the tan $\delta$ thermogram. The loss modulus (E'') and storage modulus (E') moduli at 37 °C were determined by a temperature against E' or E'' thermogram. The system was calibrated against Indium metal (temperature) and PMMA (moduli).

### 7.2.5 Tensile analysis

Molten polymer samples were compression moulded into ''dog-bones'' using a PTFE mould and allowed to cool to ambient temperature and were placed in an incubator for 7 days at 25 °C to anneal prior to tensile analysis.

Tensile data was obtained at ambient temperature by axially loading ''dog bones'' in a Tensiometric M100-1CT system with a load cell capacity of 1 kN and crosshead speed of 5 mm $min^{-1}$ with a premeasured grip-to-grip separation. All values reported were obtained from an average of 6 repeat ''dog bones'' and the results were recorded using winTest v4.3.2 software.

### 7.2.6 Mass spectrometry

Mass spectrometry (MS) was used to obtain molecular weights of small molecules including precursors, chain extenders, proof-of-concept selectivity reaction products and hyperbranched polymers. Mass spectrometry was conducted on a Bruker UHR-Q-TOF MaXis with electron spray ionisation (ESI) (+ or -) in 50:50 methanol:water for low resolution MS spectra and 50:50 methanol: THF for high resolution MS spectra. Analysis was carried out through direct infusion at 2 µL $min^{-1}$ using a syringe pump with a scan range of 50 - 3000 m/z and a spectra rate of 1 - 10 Hz or on a Varian 4000 gas chromatograph (GC), 3800 oven, ion trap MS, CP8400 autosampler, Factor Four VF-5MS capillary column, 1177 split/splitless used in splitless mode with a scan range of 20 - 1000 m/z, injector temp: 240 °C, injection volume 1 µL, He as carrier gas, 1 mL $min^{-1}$ constant flow, methane as CI reactant gas. The gradient started at 50 °C, held for 5 minutes, ramped to 300 °C in 10 minutes and then hold for 15 minutes with a scan range of 20 – 1,000 m/z. Calibration was done with sodium formate (10 mM).

### 7.2.7 Static contact angle analysis

The thin films from chapter 3 were dissolved in a minimal volume of DMF and layered as a thin film on a heated glass slide at 65 °C for 8 h and then allowed to cool to ambient temperature overnight. The thin films were placed in an incubator for 7 days at 25 °C to anneal prior to static contact angle analysis.

The first batch of thin films in chapter 5 were obtained by dissolving each polymer in DMF at 5 wt.% concentration and spin coated using a WS-650Mz-23NPPB Spin Processor at 2000 rpm for 60 seconds onto glass cover slips. The thin films with a thickness of 300-500 nm (determined by interferometry) were placed in an oven at

65 °C overnight to remove residual solvent and placed in ambient conditions for 7 days to allow migration of the chain terminating agents to the surface of the polymer network before being subjected to static contact angle analysis.

The second batch of thin films in chapter 5 were obtained by the same spin coating method as the first batch and were placed in an oven at 65 °C for 7 days to remove residual solvent and then placed in ambient conditions for 10 days to allow more complete migration of the chain terminating agents to the surface of the polymer network before being subjected to static contact angle analysis.

Static contact angle measurements were obtained using a KRUSS DSA10 drop shape analyser and were processed using the software package DSA3. A 100 µL droplet of deionised water or hexadecane was deposited onto the surface of the thin film and a measurement was taken immediately (unless stated otherwise) after deposition and analysed using a sessile drop type according to a polynomial (tangent 2) computational method (unless stated otherwise).

### 7.2.8 Hydrolytic degradation analysis

Accelerated hydrolytic degradation analyses were carried out under the previously reported conditions of D. W. Hutmacher and co-workers.[1] Molten polymers were compression moulded into small discs (Ø 1 cm, *c.a.* 1 mm thickness) using a PTFE mould and allowed to cool to ambient temperature. The polymer discs were placed into individual screw top vials containing 20 mL of 5 M KOH aqueous solution and placed in an incubator heated to 37 ˚C and stirred at 60 rpm. Each polymer disc was measured after being removed from the degradation medium and left to dry at ambient temperature for 1 h before being weighed at predetermined time points using an analytical balance. This process was performed in triplicate.

## 7.3 Experimental for Chapter 2

### 7.3.1 Synthesis of (3*S*,6*S*)-3,6-bis(4-hydroxybenzyl)piperazine-2,5-dione (TDKP)

The previously reported method for the cyclisation of *L*-phenylalanine was applied to the cyclisation of *L*-tyrosine.[2] *L*-Tyrosine (10 g, 0.055 mol) was suspended in a *m*-cresol (20 mL) and heated to 200 °C at which point $P_2O_5$ (0.75 g, 5.3 $x$ $10^{-3}$ mol) was charged to remove the water by-product. The cyclisation reaction was monitored by crude $^1$H NMR spectroscopy: isolating a sample reaction mixture every 2 h and washing the sample with a 50:50 water: methanol solvent (2 $x$ 2 mL) mixture and collecting the solid by vacuum filtration prior to analysis. After 8 h, $^1$H NMR spectroscopy confirmed the cyclisation was complete and the reaction mixture was cooled to ambient temperature, filtered by vacuum filtration and washed with a 50:50 water: methanol solvent mixture (3 $x$ 10 mL). The beige solid was dried over $P_2O_5$ overnight; yield 8.5 g, 85%.

Melting point: 276 – 296 °C,$^1$H NMR (300 MHz, DMSO-$d_6$): $\delta$ 9.24 (s, 2H), 7.94 (s, 2H), 6.90 (d, $^3J_{HH}$ = 8.4 Hz, 2H), 6.60 (d, $^3J_{HH}$ = 8.4 Hz, 2H), 3.30 (m, 2H), 2.91 (dd, $^3J_{HH}$ = 13.6 Hz $^2J_{HH}$ = 3.2 Hz, 2H), 2.59 (dd, $^3J_{HH}$ = 13.7 Hz $^2J_{HH}$ = 4.7 Hz, 2H), $^{13}$C NMR (75 MHz, DMSO-$d_6$): $\delta$ 167.01 (s, C=O), 156.02 (s, arCH$_2$-OH), 131.05 (s, arCH), 125.77 (s, arCH$_2$-CH$_2$), 114.75 (s, arCH), 54.78 (s, CH), 36.94 (s, CH$_2$); CHN calculated for $C_{18}H_{18}N_2O_4$: calculated C, 66.25: H, 5.56: N, 8.58. Found C, 65.97: H, 5.53: N, 8.52; ESI-MS: [M]- calculated 325.12, found 325.12. FT-IR: $\nu$ (cm$^{-1}$) = 3,500 (O-H), 3,300 (N-H), 3,000 (C-H), 1,650 (C=O), 1,600 (N-H), 1,450 (C-H), 1,400 (C=C). Product analysis agreed with E. Kolehmainen and co-workers.[3]

### 7.3.2 Synthesis of 1,7-diazatricyclo[7.3.0.0]dodecane-2,6,8,12-tetrone (PDKP)

The previously reported method from Parrish and Mathias was adapted for the synthesis of pyroglutamic diketopiperazine.[4] Acetic anhydride (67.65 mL, 0.72 mol) and pyridine (12.55 mL, 0.16 mol) were heated to 110 °C. *S*-Pyroglutamic acid (15.10 g, 0.12 mol) was added to the solvent mixture when the temperature reached

110 °C. Pyroglutamic diketopiperazine began to precipitate from solution after 5 minutes as a white solid and heating continued for a further 1 h. The reaction mixture was cooled to ambient temperature and the product was collected by vacuum filtration and washed with cold methanol (3 $x$ 10 mL). The resulting white solid wash then washed with methanol and collected by filtration. This was then repeated with water. The white powder was dried over $P_2O_5$ overnight; yield 11.17 g, 43%.

Melting point: 236 - 292 °C,$^1$H NMR (300 MHz, DMSO-$d_6$): $\delta$ 4.85 (t, $^3J_{HH}$ = 8.5 Hz, 2H), 2.65-2.35 (m, 4H), 2.30-2.05 (m, 4H); $^{13}$C NMR (75 MHz, DMSO-$d_6$): $\delta$ 172.47 (s, C=O-$CH_2$), 165.50 (s, C=O, CH), 58.16 (s, CH), 31.02 (s, $CH_2$), 18.64 (s, $CH_2$); CHN calculated for $C_{10}H_{10}N_2O_4$: C, 54.05: H, 4.54: N, 12.61. Found C, 54.00: H, 4.51: N, 12.63; GC-MS: [M]+ calculated 222, found 222. FT-IR: $\nu$ (cm$^{-1}$) = 3,000 (C-H), 1,650 (C=O), 1,450 (C-H), 1,250 (C-O). Product analysis was in accordance with Parrish and Mathias.[4]

### 7.3.3 Synthesis of 3,3'-((2*S*,5*S*)-3,6-dioxopiperazine-2,5-diyl) dipropionic acid (Glutamic acid diketopiperazine, GDKP)

The previously reported method from Parrish and Mathias was adapted for the synthesis of glutamic diketopiperazine.[4] Pyroglutamic diketopiperazine (3.00 g, 0.13 mol) was dissolved in cold concentrated sulfuric acid (10 mL). The reaction was cooled and distilled water (50 mL) was added dropwise over 15 minutes. The precipitate was collected by vacuum filtration and recrystallised from water and the resulting white powder was dried over $P_2O_5$ overnight; yield 2.66 g, 89%

Melting point: 244 - 283 °C,$^1$H NMR (300 MHz, DMSO-$d_6$): $\delta$ 12.15 (s, 2H), 8.20 (s, 2H), 3.88 (t, $^3J_{HH}$ = 5.3 Hz, 2H), 2.41-2.20 (m, 4H), 2.04-1.76 (m, 4H); $^{13}$C NMR (75 MHz, DMSO-$d_6$): $\delta$ 174.07 (s, C=O-OH), 168.11 (s, C=O-NH), 53.48 (s, CH), 29.05 (s, $CH_2$), 27.98 (s, $CH_2$); CHN calculated for $C_{10}H_{14}N_2O_6$: C, 46.51: H, 5.46: N, 10.85. Found C, 46.51: H, 5.50: N, 10.93; ESI-MS: [M+Na]+ 281.08 calculated, found 281.08. FT-IR: $\nu$ (cm$^{-1}$) = 3,300 (O-H), 3,200 (N-H), 3,000 (C-H), 1,700 (C=O), 1,650 (C=O), 1,600 (N-H), 1,450 (C-H), 1,250 (C-O). Product analysis was in accordance with Parrish and Mathias.[4]

### 7.3.4 Synthesis of 4-(chloromethyl)benzyl alcohol

The previously reported method from G. C. George and co-workers was used to synthesis of 4-(chloromethyl)benzyl alcohol.[5] 1,4-benzenedimethanol (1.00 g, 7.2 $x$ $10^{-3}$ mol) was suspended in chloroform (100 mL) and the suspension was cooled to 0 °C. Thionyl chloride (0.50 mL, 8.0 $x$ $10^{-3}$ mol) was charged dropwise over 10 minutes with rapid stirring. The suspension cleared and the reaction mixture was warmed to room temperature and was stirred overnight. The reaction mixture was neutralised by $NaHCO_3$ and the solid removed by vacuum filtration and the solvent removed by *in vacuo*. The white solid was recrystallised in hexane and then sublimed at 40 °C under high vacuum; yield 1.07 g, 94%.

Melting point: 58 - 62 °C,$^1$H NMR (300 MHz, DMSO-$d_6$): $\delta$ 7.39 (d,$^3J_{HH}$ = 8.2 Hz, 2H), 7.31 (d,$^3J_{HH}$ = 8.1 Hz, 2H),5.22 (t, $^3J_{HH}$ = 5.6 Hz, 1H), 4.75 (s, 2H), 4.47 (d, $^3J_{HH}$ = 5.4 Hz, 2H); $^{13}$C NMR (75 MHz, DMSO-$d_6$): $\delta$ 164.36 (s, Ar); 128.69 (s, Ar), 128.64 (s, Ar), 126.58 (s, Ar), 62.50 (s, $CH_2$), 46.15 (s, $CH_2$). CHNCl calculated for $C_8H_9ClO$: C, 61.36: H, 5.79: Cl, 22.64. Found C, 60.92: H, 5.56: Cl, 22.60; GC-MS: [M]+ calculated 156, found 156. FT-IR: $\nu$ (cm$^{-1}$) = 3,300 (O-H), 3,000 (C-H), 1,450 (C-H), 1,400 (C=C), 700 (C-Cl). Product analysis agreed with G. C. George and co-workers.[5]

### 7.3.5 Synthesis of bis4-hydroxymethylbenzyl-3,3'-((2S,5*S*)-3,6-dioxopiperazine-2,5-diyl)dipropionate (Glutamic acid diketopiperazine with aromatic ester, GDKPAE)

Glutamic acid diketopiperazine (1.50 g, 0.012 mol), 4-(chloromethyl)benzyl alcohol (1.83 g, 0.023 mol), triethylamine (2.18 mL, 0.58 mol) and dry DMF were heated at 80 °C with a $N_2$ blanket overnight. The reaction mixture was cooled to room temperature and the solid was collected by vacuum filtration and the solvent removed *in vacuo*. The resulting solid was washed with water and filtered *in vacuo*. The white solid was recrystallised in 50:50 methanol: water to yield a white powder; yield 1.30 g, 47%

Melting point: 159 - 168 °C, $^1$H NMR (300 MHz, DMSO-$d_6$): $\delta$ 8.23 (s, 2H), 7.31 (m, 8H), 5.19 (t, $^3J_{HH}$ = 5.5 Hz, 2H), 5.06 (4H, s), 4.49 (d, $^3J_{HH}$ = 4.6 Hz, 4H), 3.90 (t, $^3J_{HH}$ =

5.5 Hz, 2H), 2.60-2.25 (m, 4H), 2.10-1.79- (m, 4H); $^{13}$C NMR (100 MHz, DMSO-$d_6$): $\delta$ 172.58 (s, C=O-OH), 168.09 (s, C=O-NH), 142.72 (s, Ar), 134.75 (s, Ar), 128.00 (s, Ar), 126.73 (s, Ar), 65.85 (s, $CH_2$), 62.70 (s, $CH_2$), 53.60 (s, CH), 29.53 (s, $CH_2$), 28.23 (s, $CH_2$); CHN calculated for $C_{26}H_{30}N_2O_8$: C, 62.64: H, 6.07: N, 5.62. Found C, 62.77: H, 6.17: N, 5.49. ESI-MS: [M+Na]+ calculated 521.19, found 521.19. FT-IR: $\nu$ (cm$^{-1}$) = 3,600 (O-H), 3,200 (N-H), 3,000 (C-H), 1,700 (C=O), 1,650 (C=O), 1,600 (N-H), 1,450 (C-H), 1,400 (C=C).

### 7.3.6 Synthesis of methyl 4-(aminomethyl)benzoate intermediate

4-(aminomethyl)benzoic acid (5.00 g, 0.033 mol) was suspended in methanol (100 mL) and cooled to 0 °C. Thionyl chloride (2.40 mL, 0.17 mol) was added dropwise over 10 minutes and then the reaction was warmed to room temperature and stirred overnight. The solvent was removed *in vacuo* and the white solid was recrystallised from methanol to yield a shiny white powder. Yield 5.40 g, 98%

$^1$H NMR (300 MHz, DMSO-$d_6$): $\delta$ 8.55 (s, 2H), 7.99 (d, $^3J_{HH}$ = 8.0 Hz, 2H), 7.64 (d, $^3J_{HH}$ = 8.1 Hz, 2H), 4.10 (s, 2H), 3.85 (s, 3H); $^{13}$C NMR (75 MHz, DMSO-$d_6$): $\delta$ 165.83 (s, C=O), 139.34 (s, Ar), 129.37 (s, Ar), 129.44 (s, Ar), 129.22 (s, Ar), 52.46 (s, $CH_2$), 39.85 (s, $CH_3$); ESI-MS: [M]+ calculated 166.09, found 166.09. FT-IR: $\nu$ (cm$^{-1}$) = 3,200 (N-H), 3,000 (C-H), 1,700 (C=O), 1,600 (N-H), 1,450 (C-H), 1,400 (C=C).

### 7.3.7 Synthesis of 4-(aminomethyl)benzyl alcohol

Methyl 4-cyanobenzoate (10.00 g, 0.062 mol) was dissolved in THF (30 mL) and cooled to 0 °C. $LiAlH_4$ (11.77 g, 0.62 mol) was gradually added over 30 minutes. The reaction mixture was refluxed for 3 days and then cooled to 0 °C. $H_2O$ (50 mL) was added dropwise over 30 minutes followed by 1 M NaOH solution (50 mL). The resulting slurry was removed by vacuum filtration and the organic phase was dried over $MgSO_4$ and the solvent removed *in vacuo*. The resulting yellow solid was recrystallised in ethyl acetate and the resulting solid sublimed at 80 °C under vacuum to yield a white solid; yield 6.12 g, 85%

Melting point: 107 - 120 °C,$^{1}$H NMR (300 MHz, DMSO-$d_6$): $\delta$ 7.27 (d, $^{3}J_{HH}$ = 8.1 Hz, 2H), 7.23 (d, $^{3}J_{HH}$ = 8.0 Hz, 2H), 4.47 (s, 2H), 4.10 (bs, 1H), 3.68 (s, 2H), 3.10 (bs, 2H); $^{13}$C NMR (75 MHz, DMSO-$d_6$): $\delta$ 142.49 (s, Ar), 140.35 (s, Ar), 126.71 (s, Ar), 126.26 (s, Ar), 62.79 (s, $CH_2$), 45.44 (s, $CH_2$); CHN calculated for $C_8H_{11}NO$: C, 70.04: H, 8.08: N, 10.21. Found C, 70.07: H, 8.05: N, 10.01. ESI-MS: [M]+ calculated 138.09, found 138.09. FT-IR: $\nu$ (cm$^{-1}$) = 3,400 (O-H), 3,300 (N-H), 3,000 (C-H), 1,600 (N-H), 1,450 (C-H), 1,400 (C=C), 1,300 (C-N).

### 7.3.8 Synthesis of 3,3'-((2*S*,5*S*)-3,6-dioxopiperazine-2,5-diyl)bisN-4-hydroxymethylbenzyl propanamide (Glutamic acid diketopiperazine with aromatic amide, GDKPAA)

The reaction mixture of glutamic acid diketopiperazine (0.50 g, 1.94 $x$ 10$^{-3}$ mol), NHS (0.67 g, 5.81 $x$ 10$^{-3}$ mol), DMAP (0.05 g, 3.87 $x$ 10$^{-4}$ mol) and dry DMF and was stirred at room temperature for 1 h under a $N_2$ blanket. EDC (1.11 g, 5.81 $x$ 10$^{-3}$ mol) was added and the reaction mixture was stirred for 30 minutes after which point 4-(aminomethyl)benzyl alcohol (0.80 g, 5.81 $x$ 10$^{-3}$ mol) was added. The reaction mixture was stirred at room temperature overnight. The mixture was filtered and the solvent removed *in vacuo.* The resulting white solid was washed in water and filtered under vacuum. The white solid was recrystallised in 50:50 methanol: water to yield a white powder; yield 0.48 g, 50%

Melting point: 205 – 234 °C, $^{1}$H NMR (250 MHz, DMSO-$d_6$): $\delta$ 8.30 (t, $^{3}J_{HH}$ = 5.5 Hz, 2H), 8.14 (d, $^{3}J_{HH}$ = 1.67 Hz, 2H), 7.24 (d, $^{3}J_{HH}$ = 8.2 Hz, 4H), 7.17 (d, $^{3}J_{HH}$ = 8.2 Hz, 4H), 5.12 (t, $^{3}J_{HH}$ = 5.7 Hz, 2H), 4.45 (d, $^{3}J_{HH}$ = 5.7 Hz, 2H), 4.22 (d, $^{3}J_{HH}$ = 5.9 Hz, 2H), 3.86 (m, 2H), 2.23 (m, 4H) 1.93 (m, 4H); $^{13}$C NMR (75 MHz, DMSO-$d_6$): $\delta$ 171.73 (s, C=O-NH-$CH_2$), 168.03 (s, C=O-NH-CH), 141.32 (s, Ar), 138.19 (s, Ar), 127.33 (s, Ar), 126.75 (s, Ar), 62.99 (s, $CH_2$), 53.96 (s, CH), 42.19 (s, $CH_2$), 31.12 (s, $CH_2$), 29.43 (s, $CH_2$); CHN calculated for $C_{26}H_{32}N_4O_6$: C, 62.89: H, 6.50: N, 11.28. Found C, 61.32: H, 6.66: N, 11.85. ESI-MS: [M+Na]+ calculated 519.22, found 519.22. FT-IR: $\nu$ (cm$^{-1}$) = 3,600 (O-H), 3,200 (N-H), 3,000 (C-H), 1,690 (C=O), 1,650 (C=O), 1,600 (N-H), 1,450 (C-H), 1,400 (C=C).

### 7.3.9 General synthesis of a GDKPAE-TPUE

All polymerisations were carried out in oven baked glassware with a magnetic stirrer bar, under a nitrogen blanket. This method is based on the synthesis and analysis of a GDKPAE-TPUE30. 2K-PCL (0.50 g, 2.50 $x$ $10^{-4}$ mol) was charged to a vial and subsequently stirred and heated at 100 °C for 1 h under a $N_2$ blanket after which the reaction was cooled to 80 °C. At 60 °C a solution of 5% DBU (1.98 µL, 1.30 $x$ $10^{-5}$ mol), $H_{12}$MDI (149 µL, 5.67 $x$ $10^{-4}$ mol) in dry DMSO (1 mL) was added to the reaction mixture and was heated for 30 minutes. The reaction temperature was increased to 80 °C and the prepolymer solution was added to the GDKPAE (158 mg, 3.18 $x$ $10^{-4}$ mol) dissolved in 200% w/v solution of dry DMSO (300 µL) and the reaction mixture was heated for 1-2 h until completion which was monitored by FT-IR indicated by the disappearance of the NCO peak (2200 $cm^{-1}$). The remaining DMSO was removed under high vacuum for 7 days at 50 °C. Yield 0.38 g, 76%.

$^1$H NMR (300 MHz, DMSO-$d_6$): $\delta$ 8.25 (s, 2H), 7.34 (m, 8H), 7.17 (s, 1H), 6.95 (s, 1H), 5.20 (s, 1H), 5.14 (s, 1H), 5.06 (m, 4H), 4.98 - 4.47 (m, 15% reacted in the TPUE, 15% residual unreacted monomer, 4H), 3.97 (m, 28H), 3.89 (m, 4H), 2.43 (m, 4H), 2.26 (m, 29H), 1.91 (m, 4H), 1.79-1.69 (m, 5H), 1.55 (m, 78H), 1.26 (m, 36H), 1.12-0.86 (m, 16H). $^{13}$C NMR (100 MHz, DMF-$d_7$): $\delta$ 174.04 (s, C=O-OH), 173.47 (s, C=O), 169.08 (s, C=O-NH), 129.23 (s, Ar), 129.06 (s, Ar), 128.93 (s, Ar), 126.65 (s, Ar), 64.78 (s, $CH_2$), 64.57 (s, $CH_2$, reacted GDKPAE), 63.38 (s, $CH_2$, unreacted GDKPAE), 56.83 (s, CHNHC=O), 54.89 (s, CH), 51.42 (s, $CH_2$), 34.68 (s, $CH_2$), 33.94 (s, $CH_2$), 33.26 (s, CH), 29.62 (s, $CH_2$), 29.32 (s, $CH_2$), 28.92 (s, $CH_2$), 26.36 (s, $CH_2$), 26.30 (s, $CH_2$), 25.62 (s, $CH_2$), 25.54 (s, $CH_2$). $M_w$ 30,400 g $mol^{-1}$, $M_n$ 11,100 g $mol^{-1}$, $Đ_M$ = 2.75 (RI detection, DMF SEC). FT-IR: $\nu$ ($cm^{-1}$) = 3,600 (O-H), 3,300 (N-H), 3,000 (C-H), 1,700 (C=O), 1,650 (C=O), 1,600 (N-H), 1,500 (C-H), 1,400 (C=C), 1,300 (C-N), 1,100 (C-O).

### 7.3.10 General synthesis of a GDKPAA-TPUE

All polymerisations were carried out in oven baked glassware with a magnetic stirrer bar, under a nitrogen blanket. This method is based on the synthesis and analysis of a GDKPAA-TPUE30. 2K-PCL (0.50 g, 2.50 $x$ $10^{-4}$ mol) was charged to a vial and

subsequently stirred and heated at 100 °C for 1 h under a $N_2$ blanket after which the reaction was cooled to 80 °C. At 60 °C a solution of 5% DBU (1.98 µL, 1.30 $x$ $10^{-5}$ mol), $H_{12}$MDI (239 µL, 8.58 $x$ $10^{-4}$ mol) in dry DMSO (1 mL) was added to the reaction mixture and was heated for 30 minutes. The reaction temperature was increased to 80 °C and the pre-polymer solution was added to the GDKPAA (303 mg, 6.08 $x$ $10^{-4}$ mol) dissolved in 200% w/v solution of dry DMSO (606 µL) and the reaction mixture was heated for 1-2 h until completion which was monitored by FT-IR indicated by the disappearance of the NCO peak (2200 $cm^{-1}$). The remaining DMSO was removed under high vacuum for 7 days at 50 °C. Yield 0.42 g, 84%.

$^1$H NMR (300 MHz, DMSO-$d_6$): $\delta$ 8.31 (s, 2H), 8.18 (s, 2H), 7.23 (m, 8H), 6.93 (s, 2H), 5.11 (s, 1H), 5.04 (s, 1H), 4.96 - 4.46 (m, 13% reacted in the TPUE, 17% residual unreacted monomer, 4H), 4.23 (m, 4H), 3.99 (m, 32H), 3.87 (m, 2H), 2.27 (m, 36H), 2.15 (m, 4H), 1.90 (m, 4H), 1.76 (m, 5H), 1.52 (m, 89H), 1.31 (m, 43H), 1.17-0.73 (m, 16H). $^{13}$C NMR (75 MHz, DMF-$d_7$): $\delta$ 174.02 (s, C=O), 173.96 (s, C=O-NH-$CH_2$), 165.41 (s, C=O-NH-CH), 129.69 (s, Ar), 128.95(s, Ar), 128.49 (s, Ar), 127.61 (s, Ar), 64.74 (s, $CH_2$), 64.53 (s, $CH_2$, reacted GDKPAA), 63.67 (s, $CH_2$, unreacted GDKPAA), 56.73 (s, CHNHC=O), 55.33 (s, CH), 34.83 (s, $CH_2$), 34.63 (s, $CH_2$), 33.92 (s, $CH_2$), 33.25 (s, CH), 29.52 (s, $CH_2$), 29.27 (s, $CH_2$), 29.89 (s, $CH_2$), 26.31 (s, $CH_2$), 26.25 (s, $CH_2$), 25.57 (s, $CH_2$) 25.49 (s, $CH_2$). $M_w$ 31,000 g $mol^{-1}$, $M_n$ 10,100 g $mol^{-1}$, $Đ_M$ = 3.07 RI detection, DMF SEC). FT-IR: $\tilde{\nu}$ ($cm^{-1}$) = 3,600 (O-H), 3,300 (N-H), 3,000 (C-H), 1,690 (C=O), 1,650 (C=O), 1,600 (N-H), 1,500 (C-H), 1,400 (C=C), 1,300 (C-N), 1,100 (C-O).

### 7.3.11 General synthesis of a GDKPAE/GDKPAA-TPUE

All polymerisations were carried out in oven baked glassware with a magnetic stirrer bar, under a nitrogen blanket. This method is based on the synthesis and analysis of a GDKPAE/GDKPAA-TPUE30. 2K- PCL (0.50 g, 2.50 $x$ $10^{-4}$ mol) was charged to a vial and subsequently stirred and heated at 100 °C for 1 h under a $N_2$ blanket after which the reaction was cooled to 80 °C. At 60 °C a solution of 5% DBU (1.98 µL, 1.30 $x$ $10^{-5}$ mol), $H_{12}$MDI (382 µL, 1.37 $x$ $10^{-3}$ mol) in dry DMSO (1 mL) was added to the reaction mixture and was heated for 30 minutes. The reaction temperature was

increased to 80 °C and the pre-polymer solution was added to the GDKPAE and GDKPAA (556 mg, 1.12 $x$ $10^{-3}$ mol) dissolved in 200% w/v solution of dry DMSO (1100 µL) and the reaction mixture was heated for 1-2 h until completion which was monitored by FT-IR indicated by the disappearance of the NCO signal (2200 $cm^{-1}$). The remaining DMSO was removed under high vacuum for 7 days at 50 °C. Yield 0.44 g, 88%.

$^{1}$H NMR (300 MHz, DMSO-$d_6$): $\delta$ 8.35 (s, 2H), 8.19 (s, 2H), 8.03 (s, 2H), 7.45-7.00 (m, 16H), 7.14 (s, 2H), 6.91 (s, 2H), 5.15 (s, 2H), 5.27 - 4.10 (m, 18% reacted in the TPUE, 12% residual unreacted monomer, 10% GDKPAE, 8% GDKPAA, 10H), 3.98 (m, 36H), 3.88 (m, 4H), 2.45 – 2.01 (m, 8H), 2.26 (m, 39H), 2.03 – 1.85 (m, 8H), 1.75 (m, 5H), 1.55 (m, 98H), 1.29 (m, 46H), 1.20 - 0.73 (m, 20H). $^{13}$C NMR (75 MHz, DMSO-$d_6$): $\delta$ 174.03 (s, C=O), 171.32 (s, C=O-NH-$CH_2$), 170.91 (s, C=O), 168.99 (s, C=O-NH-CH), 128.68 (s, Ar), 128.33 (s, Ar), 127.79 (s, Ar), 127.52 (s, Ar), 64.76 (s, $CH_2$), 64.55 (s, $CH_2$,reacted GDKPAE), 64.54 (s, $CH_2$, reacted GDKPAA), 63.44 (s, $CH_2$, unreacted GDKPAE), 64.35 (s, $CH_2$, unreacted GDKPAA), 57.03 (s, CHNHC=O), 54.83 (s, CH), 34.71 (s, $CH_2$), 34.65 (s, $CH_2$), 33.37 (s, $CH_2$), 33.23 (s, CH), ), 29.51 (s, $CH_2$), 29.29 (s, $CH_2$), 29.05(s, $CH_2$), 26.33 (s, $CH_2$), 26.27 (s, $CH_2$), 25.59 (s, $CH_2$) 25.51 (s, $CH_2$). $M_w$ 16,000 g $mol^{-1}$, $M_n$ 6,200 g $mol^{-}$1, $Đ_M$ = 2.58 (RI detection, DMF SEC). FT-IR: $\nu$ ($cm^{-1}$) = 3,600 (O-H), 3,300 (N-H), 3,000 (C-H), 1,700 (C=O), 1,690 (C=O), 1,650 (C=O), 1,600 (N-H), 1,500 (C-H), 1,400 (C=C), 1,300 (C-N), 1,100 (C-O).

## 7.4 Experimental for Chapter 4

### 7.4.1 Synthesis of carbonylbiscaprolactam

The synthesis of carbonylbiscaprolactam (CBC) was modified from the previously reported method by H. Bonnard *et al.*[6] To a 250 mL oven-baked Schlenk flask fitted with a flea stirrer, *ε*-caprolactam (2.50 g, 3.67 $x$ $10^{-3}$ mol) and toluene (10 mL) were charged under $N_2$ and stirred until the ε-caprolactam had dissolved. Once a solution was formed, *N,N*-diisopropylethylamine (3.87 mL, 3.67 $x$ $10^{-3}$ mol) was charged and then the reaction solution was cooled to 0 °C. A solution of triphosgene (1.14 g, 1.68 $x$ $10^{-3}$ mol) in toluene (5 mL) was charged dropwise over 15 minutes. The reaction mixture was stirred under $N_2$, at 0 °C, for 30 minutes and then warmed to room temperature and was stirred for a further 30 minutes. The reaction mixture was then heated at 40 °C for 5 h at which point the reaction mixture was cooled to room temperature and the solid was collected by vacuum filtration. The solvent was removed *in vacuo* and the resulting white solid was recrystallised from isopropanol to yield a white powder. Yield 1.79 g, 63%.

Melting point: 113 - 115 °C, $^{1}$H NMR (400 MHz, $CDCl_3$): $\delta$ 3.80 (bs, 4H) 2.55 (bs, 4H) 1.78 (bs, 8H) 1.69 (bs, 4H). $^{13}$C NMR (101 MHz, $CDCl_3$): $\delta$ 176.15 (s, C=O), 156.50 (s, C=O), 47.03 (s, $CH_2$), 38.70 (s, $CH_2$), 29.27 (s, $CH_2$), 28.14 (s, $CH_2$), 22.37 (s, $CH_2$); CHN calculated for $C_{13}H_{20}N_2O_4$: C, 61.88: H, 7.99: N, 11.10. Found C, 61.80: H, 8.07: N, 10.99. ESI-MS: [M+Na]+ calculated 275.12, found 275.14. FT-IR: $\nu$ ($cm^{-1}$) = 3,000 (C-H), 1,700 (C=O), 1,500 (C-H). Product analysis was consistent with H. Bonnard *et al.*[6]

### 7.4.2 Synthesis of *N*-hexyl-2-oxoazepane-1-carboxamide

The synthesis of *N*-hexyl-2-oxoazepane-1-carboxamide was modified from the previously reported method by S. Maier *et al.*[7] Hexylamine (50 µL, 3.97 $x$ $10^{-4}$ mol) was charged to a solution of CBC (0.10 g, 3.97 $x$ $10^{-4}$ mol) and toluene (200 µL) under $N_2$ and was heated at 80 °C for 6 h. The reaction mixture was cooled to room temperature and toluene (10 mL) was charged. The organic phase was washed with saturated calcium chloride solution (3 $x$ 10 mL) followed by water (3 $x$ 10 mL) and

dried over $Na_2SO_4$. The solvent was removed *in vacuo* to yield a colourless liquid. Yield 0.09 g, 94%.

$^1$H NMR (400 MHz, $CDCl_3$): $\delta$ 9.25 (s, 1H) 3.96 (s, 2H), 3.27 (q, $^3J_{HH}$ = 6.5 Hz, 2H), 2.69 (m, 2H), 1.70 (m, 6H), 1.53 (q, $^3J_{HH}$ = 7.0 Hz, 2H), 1.29 (m, 6H), 0.87 (t, $^3J_{HH}$ = 6.2 Hz, 3H). $^{13}$C NMR (101 MHz, $CDCl_3$): $\delta$ 179.36 (s, C=O), 154.74 (s, C=O), 40.72 (s, $CH_2$), 37.44 (s, $CH_2$), 36.39 (s, $CH_2$), 31.65 (s, $CH_2$), 29.49 (s, $CH_2$), 28.67 (s, $CH_2$), 27.69 (s, $CH_2$), 26.43 (s, $CH_2$), 25.40 (s, $CH_2$), 22.94 (s, $CH_2$), 22.37 (s, $CH_3$); CHN calculated for $C_{13}H_{24}N_2O_2$: C, 64.97: H, 10.07: N, 11.66. Found C, 64.96: H, 810.16: N, 10.97. ESI-MS: [M+Na]+ calculated 263.17, found 263.17. FT-IR: $\nu$ (cm$^{-1}$) = 3,300 (N-H), 3,000 (C-H), 1,650 (C=O), 1,600 (N-H), 1,500 (C-H). Product analysis was consistent with S. Maier *et al.*[7]

### 7.4.3 The reaction between CBC and BHMTA at 80 °C

The synthesis of *N*,*N*'-(azanediylbis(hexane-6,1-diyl))bis (2-oxoazepane-1-carboxamide) was modified from the previously reported method of F. Xiang *et al*.[8] A solution of CBC (300 mg, 1.19 $x$ 10$^{-3}$ mol), BHMTA (178 mg, 5.9 $x$ 10$^{-4}$ mol) and toluene (400 µL) was formed under $N_2$. The reaction mixture was heated at 80 °C for 6 h. The reaction mixture was cooled and toluene (10 mL) was charged. The organic phase was washed with saturated calcium chloride solution (3 $x$ 5 mL) followed by water (3 $x$ 5 mL) and dried over $Na_2SO_4$. The solvent was removed *in vacuo* to yield a colourless liquid. Yield 0.04g, 14%.

$^1$H NMR (400 MHz, $CDCl_3$): $\delta$ 9.20 (s, 2H) 3.92 (m, 4H), 3.21 (q, $^3J_{HH}$ = 6.4 Hz, 4H), 2.64 (m, 4H), 2.50 (t, $^3J_{HH}$ = 7.2Hz, 4H), 2.25 (s, 1H), 1.70 (m, 12H), 1.55-1.35 (m, 8H), 1.35-1.20 (m, 8H). $^{13}$C NMR (101 MHz, $CDCl_3$): $\delta$ 171.59 (s, C=O), 155.13 (s, C=O), 49.52 (s, $CH_2$), 40.72 (s, $CH_2$), 38.76 (s, $CH_2$), 37.44 (s, $CH_2$), 29.46 (s, $CH_2$), 29.06 (s, $CH_2$), 28.67 (s, $CH_2$), 27.43 (s, $CH_2$), 26.45 (s, $CH_2$), 25.38 (s, $CH_2$), 22.48 (s, $CH_2$); ESI-MS: [M]+ calculated 494.37, found 494.37. FT-IR: $\nu$ (cm$^{-1}$) = 3,300 (N-H), 3,000 (C-H), 1,650 (C=O), 1,600 (N-H), 1,500 (C-H). Product analysis consistent with F. Xiang *et al*.[8]

### 7.4.4 Synthesis of hyperbranched *N*,*N*'-(azanediylbishexane-6,1-diyl)bis(2-oxoazepane-1-carboxamide)

The synthesis of *N*,*N*'-(azanediylbis(hexane-6,1-diyl))bis(2-oxoazepane-1-carboxamide) was modified from previous reports from F. Xiang *et al*.[9] A solution of CBC (316 mg, 1.28 $x$ $10^{-3}$ mol), BHMTA (135 mg, 6.27 $x$ $10^{-4}$ mol) and DMF (6.25 mL) was formed under $N_2$. The reaction mixture was heated at 80 °C for 12 h at which point the temperature was elevated to 145 °C for a further 6 h. The reaction mixture was cooled and precipitated into ethyl acetate and dried under vacuum to yield a yellow waxy liquid. Yield 0.50g, 13%.

$^1$H NMR (400 MHz, DMSO-$d_6$): $\delta$ 9.15 (s, 2H), 7.40 (m, 1H), 3.89 (m, 4H), 3.26-2.88 (m, 8H), 2.68 (s, 1H), 2.29 (m, 4H), 1.65 (m, 12H), 1.58-1.07 (m, 8H). $^{13}$C NMR (101 MHz, DMSO-$d_6$): $\delta$ 176.62 (s, C=O), 176.87 (s, C=O), 158.81 (s, C=O), 154.67 (s, C=O), 41.43 (s, NHC=ONCH$_2$), 35.83, (s, C=OCH$_2$CH$_2$), 29.98 (s, C=OOCH$_3$), 46.82 (s, CH$_2$), 46.35 (s, CH$_2$), (s, 39.13 (s, CH$_2$), 38.57 (s, CH$_2$),36.71 (s, CH$_2$), 29.81 (s, CH$_2$), 29.39 (s, CH$_2$), 29.06 (s, CH$_2$), 28.69 (s, CH$_2$).28.47 (s, CH$_2$), 28.39 (s, CH$_2$), $M_w$ = 7,100 g mol$^{-1}$, $M_n$ = 2,900 g mol$^{-1}$, $Đ_M$ = 2.50 (RI detection, DMF SEC). Product analysis consistent with F. Xiang *et al*.[9] FT-IR: $\nu$ (cm$^{-1}$) = 3,300 (N-H), 3,000 (C-H), 1,650 (C=O), 1,600 (N-H), 1,500 (C-H).

### 7.4.5 Synthesis of hyperbranched *N*,*N*'-(azanediylbishexane-6,1-diyl)bis(2-oxoazepane-1-carboxamide) with aromatic chain ends

The synthesis of hyperbranched *N*,*N*'-(azanediylbis(hexane-6,1-diyl))bis(2-oxoazepane-1-carboxamide) with benzyl chain ends was modified from previous reports from F. Xiang *et al*.[9] A solution of CBC (506 mg, 2.00 $x$ $10^{-3}$ mol), BHMTA (216 mg, 1.00 $x$ $10^{-4}$ mol) and DMF (6.25 mL) was formed under $N_2$. The reaction mixture was heated at 80 °C for 12 h at which point the temperature was elevated to 145 °C for a further 6h. The reaction temperature was reduced to 125 °C and a solution of benzyl alcohol (0.248 mL, 2.4 $x$ $10^{-3}$ mol), tin(II) 2-ethylhexanoate (0.040 mL, 9.87 $x$ $10^{-3}$ mol) in DMF (2 mL) was charged. The reaction mixture was heated at 125 °C for 70 h. The reaction mixture was cooled and precipitated into a

50:50 ethyl acetate and hexane solvent mixture and dried under vacuum to yield a yellow waxy liquid. Yield 0.30g 10%.

$^{1}$H NMR (400 MHz, DMSO-$d_6$): $\delta$ 9.15 (s, 2H), 7.45 (m, 1H), 7.30 (m, 4H), 5.00 (s, 2H), 3.88 (m, 4H), 3.23-2.92 (m, 8H), 2.90 (s, 1H), 2.25 (m, 4H), 1.65 (m, 12H), 1.50-1.10 (m, 8H ). $^{13}$C NMR (101 MHz, DMSO-$d_6$): $\delta$ 176.92 (s, C=O), 176.87 (s, C=O), 158.81 (s, C=O), 154.67 (s, C=O), 142.68 (s, Ar), 137.39 (s, Ar), 127.70 (s, Ar), 126.61 (s, Ar), 65.52 (s, $CH_2$), 49.94 (s, $CH_2$), 46.35 (s, $CH_2$), (s, 39.43 (s, $CH_2$), 38.57 (s, $CH_2$), 36.71 (s, $CH_2$), 30.41 (s, $CH_2$), 30.10 (s, $CH_2$), 29.89 (s, $CH_2$), 28.59 (s, $CH_2$).28.59 (s, $CH_2$), 27.73 (s, $CH_2$), $M_w$ = 7,400 g mol$^{-1}$, $M_n$ = 3,000 g mol$^{-1}$, $Đ_M$ = 2.51 (RI detection, DMF SEC). FT-IR: $\nu$ (cm$^{-1}$) = 3,300 (N-H), 3,000 (C-H), 1,650 (C=O), 1,600 (N-H), 1,500 (C-H), 1,400 (C=C). Product analysis was consistent with F. Xiang *et al*.[9]

### 7.4.6 The reaction between CDI and hexylamine at room temperature

This synthesis method was modified from a previous report from H. A. Staab.[10] A mixture of CDI (500 mg, 3.08 $x$ 10$^{-3}$ mol) in hexylamine (407 µL, 3.08 $x$ 10$^{-3}$ mol) was formed. The reaction mixture was stirred at room temperature for 30 minutes. The reaction mixture was dissolved in $CH_2Cl_2$ and washed with saturated brine (3 $x$ 10 mL) followed by water (3 $x$ 10 mL) and dried over $Na_2SO_4$. The solvent was removed *in vacuo* to yield a white solid. Yield 0.30 g, 50%.

$^{1}$H NMR (400 MHz, $CDCl_3$) (Single addition): $\delta$ 9.16 (s, 1H), 8.58 (s, 1H) 8.44 (s, 1H), 7.77 (s, 1H), 3.37 (s, 2H), 1.69 (bs, 2H), 1.49 (bs, 6H), 1.09 (bs, 3H). (Double addition): $\delta$ 5.57 (s, 1H), 3.62 (s, 2H), 1.69 (bs, 2H), 1.49 (bs, 6H), 1.09 (bs, 3H). $^{13}$C NMR (101 MHz, $CDCl_3$): $\delta$ 151.1 (s, C=O), 149.0 (s, C=O), 136.1 (s, CH), 131.7 (s, CH), 118.4 (s, CH), 40.8 (s, $CH_2$), 40.2 (s, $CH_2$), 31.3 (s, $CH_2$), 31.2 (s, $CH_2$), 29.8 (s, $CH_2$), 29.2 (s, $CH_2$), 26.3 (s, $CH_2$), 22.5 (s, $CH_2$), 13.8 (s, $CH_3$). ESI-MS: double addition [M+Na]+: calculated 251.19, found 251.21. FT-IR: $\nu$ (cm$^{-1}$) = 3,300 (N-H), 3,000 (C-H), 1,650 (C=O), 1,600 (N-H), 1,500 (C-H). Product analysis was consisted with H. A. Staab.[10]

### 7.4.7 Synthesis of *N,N*-dihexyl-1H-imidazole-1-carboxamide

The synthesis of *N,N*-dihexyl-1H-imidazole-1-carboxamide was modified from previous reports from H. A. Staab.[11] A mixture of CDI (500 mg, 3.08 $x$ $10^{-3}$ mol) in dihexylamine (717 µL, 3.08 $x$ $10^{-3}$ mol) was formed. The reaction mixture was stirred at room temperature for 30 minutes. The reaction mixture was dissolved in $CH_2Cl_2$ and washed with saturated brine (3 $x$ 10 mL) followed by water (3 $x$ 10 mL) and dried over $Na_2SO_4$. The solvent was removed *in vacuo* to yield a colourless liquid. Yield 0.22 g, 25%.

$^1$H NMR (400 MHz, $CDCl_3$): $\delta$ 8.05 (s, 1H) 7.39 (s, 1H), 7.26 (s, 1H), 3.53 (bs, 4H), 1.79 (bs, 4H), 1.45 (bs, 12H), 1.05 (t, 6H). $^{13}$C NMR (101 MHz, $CDCl_3$): $\delta$ 151.8 (s, C=O), 136.6 (s, CH), 129.6 (s, CH), 118.2 (s, CH), 48.7 (s, $CH_2$), 31.6 (s, $CH_2$), 28.1 (s, $CH_2$), 26.6 (s, $CH_2$), 23.1 (s, $CH_2$), 14.2 (s, $CH_3$). CHN calculated for $C_{16}H_{29}N_3O$: C, 68.77: H, 10.46: N, 15.04. Found C, 68.46: H, 10.70: N, 14.85. ESI-MS: [M] +, calculated 280.24, found 280.24. FT-IR: $\nu$ ($cm^{-1}$) = 3,300 (N-H), 3,000 (C-H), 1,650 (C=O), 1,600 (N-H), 1,500 (C-H). Product analysis was consistent with H. A. Staab.[11]

### 7.4.8 Synthesis of 1,1,3-trihexylurea (sequential addition method with *N*-hexyl-1H-imidazole-1-carboxamide intermediate)

A solution of hexylamine (653 µL, 4.94 $x$ $10^{-3}$ mol) and toluene (5 mL) was charged dropwise, under $N_2$, to suspension of CDI (817 mg, 5.04 $x$ $10^{-3}$ mol) and toluene (50 mL) cooled to -78 °C. The reaction mixture was stirred at -78 °C for 2 h at which point a solution of dihexylamine (1,152 µL, 4.94 $x$ $10^{-3}$ mol) in toluene (5 mL) was charged dropwise to the mixture. The reaction mixture was warmed to room temperature and stirred for a further 2 h. The solvent was removed *in vacuo* and the resulting white solid was dissolved in $CH_2Cl_2$ and washed with saturated brine (3 $x$ 10 mL) followed by water (3 $x$ 10 mL) and dried over $Na_2SO_4$. The solvent was removed *in vacuo* to yield a colourless liquid. Yield 0.16 g, 10%.

$^1$H NMR (400 MHz, $CDCl_3$): $\delta$ 4.37 (s, 1H), 3.13 (t, 6H, $^3J_{HH}$ = 6.5Hz), 3.08 (t, 6H, $^3J_{HH}$ = 7.4 Hz), 1.43 (bs, 6H), 1.20 (bs, 18H), 0.80 (t, $^3J_{HH}$ = 7.6 Hz, 9H). $^{13}$C NMR (101 MHz, $CDCl_3$): $\delta$ 157.4 (s, C=O), 53.4 (s, $CH_2$), 49.3 (s, $CH_2$), 47.1 (s, $CH_2$), 40.7

(s, $CH_2$), 31.5 (s, $CH_2$), 31.3 (s, $CH_2$), 30.2 (s, $CH_2$), 29.4 (s, $CH_2$), 28.4 (s, $CH_2$), 26.5 (s, $CH_2$), 22.4 (s, $CH_2$), 13.8 (s, $CH_3$). CHN calculated for $C_{19}H_{40}N_2O$: C, 73.02: H, 12.90: N, 8.96. Found C, 72.49: H, 13.03: N, 8.77. ESI-MS: [M+Na] +: calculated 335.30, found 335.30. FT-IR: $\nu$ ($cm^{-1}$) = 3,300 (N-H), 3,000 (C-H), 1,650 (C=O), 1,600 (N-H), 1,500 (C-H).

### 7.4.9 Synthesis of 1,1,3-trihexylurea (all-in-one method)

A solution of hexylamine (653 µL, 4.94 $x$ $10^{-3}$ mol), dihexylamine (1152 µL, 4.94 $x$ $10^{-3}$ mol) and toluene (5 mL) was charged dropwise, under $N_2$, to solution of CDI (817 mg, 5.04 $x$ $10^{-3}$ mol) and toluene (10 mL) cooled to -78 °C. The reaction mixture was stirred at -78 °C for 2 h and then allowed to warm to room temperature and stir for a further 2 h. The solvent was removed *in vacuo* and the resulting white solid was dissolved in $CH_2Cl_2$ and washed with saturated brine (3 $x$ 10 mL) followed by water (3 $x$ 10 mL) and dried over $Na_2SO_4$. The solvent was removed *in vacuo* to yield a colourless liquid. Yield 0.30 g, 20 %.

$^1$H NMR (400 MHz, $CDCl_3$): $\delta$ 4.30 (s, 1H), 3.17 (t, $^3J_{HH}$ = 6 .5 Hz, 2H), 3.11 (t, $^3J_{HH}$ = 7.3 Hz, 4H), 1.47 (bs, 6H), 1.24 (bs, 18H), 0.84 (bs, 9H). $^{13}$C NMR (125 MHz, $CDCl_3$): $\delta$ 157.7 (C=O), 53.5 ($CH_2$), 49.2 ($CH_2$), 47.4 ($CH_2$), 40.9 ($CH_2$), 31.7 ($CH_2$), 31.6 ($CH_2$), 30.4 ($CH_2$), 29.5 ($CH_2$), 28.7 ($CH_2$), 26.7 ($CH_2$), 22.6 ($CH_2$), 14.4 ($CH_3$). CHN calculated for $C_{19}H_{40}N_2O$: C, 73.02: H, 12.90: N, 8.96. Found C, 72.65: H, 13.14: N, 9.49. ESI-MS: [M] -: calculated 311.30, found 311.31. FT-IR: $\nu$ ($cm^{-1}$) = 3,300 (N-H), 3,000 (C-H), 1,650 (C=O), 1,600 (N-H), 1,500 (C-H).

### 7.4.10 Synthesis of hyperbranched *N*,*N*'-(azanediylbishexane-6,1-diyl)bis(1*H*-imidazole-1-carboxamide) with aromatic chain ends

CDI (1.05 g, 6.52 $x$ $10^{-3}$ mol) was suspended in toluene (20 mL) under $N_2$. The suspension was cooled to -20 °C and solutions of bis(hexamethylene)triamine (644 mg, 2.99 $x$ $10^{-3}$ mol) in toluene (20 mL) and benzyl alcohol (673 µL, 6.47 $x$ $10^{-3}$ mol) in toluene (20 mL) were charged to the reaction mixture. The reaction was stirred at -20 °C for 3 h and was warmed to room temperature and was stirred for a further 5 h. The hyperbranching reaction was quenched with methanol

(25 mL) and the reaction mixture was heated at 30 °C for 48 h. The solvent was removed *in vacuo* and the viscous liquid was subsequently dissolved in dichloromethane and washed with brine (3 $x$ 20 mL) and water (3 $x$ 20 mL) and the organic phase was dried with $MgSO_4$ and the solvent was removed *in vacuo*. Yield 0.226 g, 21%.

$^1$H NMR (400 MHz, DMF-$d_7$): $\delta$ 7.38 (m, 4H), 7.19 (s, 1H), 6.22 (s, 1H), 5.93 (s, 1H), 5.08 (s, 2H), 3.52 (s, 3H), 3.41 (s, 3H), 3.23 (m, 4H), 3.12 (m, 4H), 1.61 (s, 1H), 1.51 (m, 8H), 1.28 (m, 8H). $^{13}$C NMR (101 MHz, DMF-$d_7$): $\delta$ 159.93 (s, C=O), 158.89 (s, C=O), 157.83 (s, C=O), 152.92 (s, C=O), 144.24 (s, Ar), 139.15 (s, Ar), 129.70 (s, Ar), 127.01 (s, Ar), 64.88 (s, $CH_2$), 47.63 (s, NHC=ONCH$_2$), 41.97 (s, NHC=ONCH$_2$), 31.82 (s, C=OOCH$_3$), 29.86 (s, $CH_2$), 28.01 (s, $CH_2$), 27.84 (s, $CH_2$), 27.73 (s, $CH_2$). $M_w$ = 7,700 g mol$^{-1}$, $Đ_M$ = 1.76 (RI detection, DMF SEC) FT-IR: $\nu$ (cm$^{-1}$) = 3,300 (N-H), 3,000 (C-H), 1,650 (C=O), 1,600 (N-H), 1,500 (C-H), 1,400 (C=C).

### 7.4.11 Synthesis of hyperbranched *N,N'*-(azanediylbishexane-6,1-diyl)bis(1*H*-imidazole-1-carboxamide) with fluorinated chain ends

1,1'-carbonyldiimidazole (1.05 g, 6.52 $x$ 10$^{-3}$ mol) was suspended in toluene (20 mL) under $N_2$. The suspension was cooled to -20 °C and solutions of bis(hexamethylene)triamine (644 mg, 2.99x10$^{-3}$ mol) in toluene (20 mL) and Capstone® (1,386 µL, 6.47 $x$ 10$^{-3}$ mol) in toluene (20 mL) were charged to the reaction mixture. The reaction was stirred at -20 °C for 3 h and was warmed to room temperature and was stirred for a further 5 h. The hyperbranching reaction was quenched with methanol (25 mL) and the reaction mixture was heated at 30 °C for 48 h. The solvent was removed *in vacuo* and subsequently dissolved in dichloromethane and washed with brine (3 $x$ 20 mL) and water (3 $x$ 20 mL) and the organic phase was dried with $MgSO_4$ and the solvent was removed *in vacuo*. Yield 0.230 g, (22%).

$^1$H NMR (400 MHz, DMF-$d_7$): $\delta$ 7.23 (s, 1H), 6.25 (s, 1H), 5.95 (s, 1H), 4.35 (m, 2H), 3.88 (s, 3H), 3.42 (s, 3H), 3.24 (m, 4H), 3.10 (m, 4H), 2.67 (m, 2H), 1.62 (s, 1H), 1.48 (m, 8H), 1.29 (m, 8H). $^{19}$F NMR (376 MHz, DMSO-$d_6$): $\delta$ -80.76, -114.32, -123.20, -

124.16, -124.76, -127.24. $^{13}$C NMR (101 MHz, DMF-$d_7$): $\delta$ 159.99 (s, C=O), 158.71 (s, C=O), 157.37 (s, C=O), 152.94 (s, C=O), 121.30 (m, $CF_2$), 119.15 (m, $CF_2$), 113.98 (m, $CF_2$), 112.19 (m, $CF_2$), 110.01 (m, $CF_2$), 107.62 (m, $CF_3$), 57.22 (s, NHC=O$CH_2CH_2CF_2$), 47.63 (s, NHC=ON$CH_2$), 41.93 (s, NHC=ON$CH_2$), 40.91, (s, C=O$CH_2CH_2CF_3$), 28.95 (s, C=OO$CH_3$), 28.18 (s, $CH_2$), 28.01 (s, $CH_2$), 27.80 (s, $CH_2$), 27.72 (s, $CH_2$). $M_w$ = 15,000 g mol$^{-1}$ $Đ_M$ = 1.86 (RI detection, DMF SEC). FT-IR: $\nu$ (cm$^{-1}$) = 3,300 (N-H), 3,000 (C-H), 1,650 (C=O), 1,600 (N-H), 1,500 (C-H), 1,100 (C-F).

## 7.5 Experimental for Chapter 5

### 7.5.1 General synthesis of aromatic TPUs

Molten PCL with a $M_W$ of 2,000 g mol$^{-1}$ (2KPCL, 5.98 g, 2.99 $x$ 10$^{-3}$ mol), 1,4-butane diol (0.86 g, 9.54 $x$ 10$^{-3}$ mol), a 1% solution of Bicat 8106M in PCL (0.02 g, 1.00 $x$ 10$^{-5}$ mol) and DMF (20 mL) were charged and heated at 80 °C until the reaction mixture became a solution. Methylene diphenyl diisocyanate (3.14 g, 0.125 mol) was charged to the mixture and the reaction mixture was heated at 80 °C for 5 h. The reaction mixture was cooled to room temperature and precipitated in to diethyl ether. The white solid was collected by vacuum filtration and dried in a vacuum desiccator for 1 week. Yield 8.47 g, 85%.

$^1$H NMR (300 MHz, DMSO-$d_6$): $\delta$ 9.50 (s, 4H), 7.33 (d, $^3J_{HH}$ = 7.2 Hz, 8H), 7.09 (d, $^3J_{HH}$ = 7.2 Hz, 8H), 4.43 (t, $^3J_{HH}$ = 5.1 Hz, 2H), 4.09 (m, 4H), 3.97 (t, $^3J_{HH}$ = 6.5 Hz, 14H), 3.77 (s, 4H), 3.41 (m, 4H), 2.26 (t, $^3J_{HH}$ = 7.1 Hz, 6H), 1.70 (m, 4H), 1.52 (m, 34H), 1.31 (m, 16H). $^{13}$C NMR (101 MHz, DMSO-$d_6$): $\delta$ 172.74 (s, C=O), 153.48 (s, C=O), 137.01 (s, Ar), 135.43 (s, Ar), 128.82 (s, Ar), 118.29 (s, Ar), 63.84 (s, $ArCH_2Ar$), 63.48 (s, $O{=}COCH_2$), 60.52 (s, $OCO\underline{C}H_2CH_2CH_2CH_2$) 60.30 (s, $CH_2CH_2CH_2\underline{C}H_2OH$), 33.40 (s, $CH_2\underline{C}H_2\underline{C}H_2CH_2$), 28.23 (s, $CH_2$), 27.80 (s, $CH_2$), 24.89 (s, $CH_2$), 24.08 (s, $CH_2$). $M_w$ = 25,300 g mol$^{-1}$, $Đ_M$ = 1.86 (RI detection, DMF SEC). FT-IR: $\nu$ (cm$^{-1}$) = 3,300 (N-H), 3,000 (C-H), 1,700 (C=O), 1,600 (N-H), 1,500 (C-H), 1,400 (C=C).

### 7.5.2 General synthesis of aromatic TPUs with hyperbranched aromatic chain terminating agents

This method was based on the synthesis and analysis of an aromatic TPU with 5% hyperbranched aromatic chain terminating agents. Molten PCL with a $M_W$ of 2,000 g mol$^{-1}$ (2KPCL, 5.98 g, 2.99 $x$ 10$^{-3}$ mol), BDO (0.86 g, 9.54 $x$ 10$^{-3}$ mol), a 1% solution of Bicat 8106M in PCL (0.02 g, 1.00 $x$ 10$^{-5}$ mol) and DMF (20 mL) were charged and heated at 80 °C until the reaction mixture became a solution. Methylene diphenyl diisocyanate (3.14 g, 0.125 mol) was charged to the mixture and the reaction mixture was heated at 80 °C for 5 h. FT-IR was used to determine the percentage of free isocyanate chain ends (0.2-0.3%) at which point the hyperbranched polymer (0.50 g)

was charged in DMF (1 mL). The reaction was heated overnight at 80 °C. The reaction mixture was cooled to room temperature and precipitated in to diethyl ether. The white solid was collected by vacuum filtration and dried in a vacuum desiccator for 1 week. Yield 9.47 g, 95%.

$^{1}$H NMR (300 MHz, DMSO-$d_6$): $\delta$ 9.50 (s, 3H), 7.32 (d, $^{3}J_{HH}$ = 7.2 Hz, 8H), 7.08 (d, $^{3}J_{HH}$ = 7.2 Hz, 8H), 5.00 (s, 2H, 5% capped chain ends), 4.43 (t, $^{3}J_{HH}$ = 5.1 Hz, 1H), 5.00 (s, 2H), 4.09 (m, 5H), 3.97 (t, $^{3}J_{HH}$ = 6.5 Hz, 15H), 3.77 (s, 4H), 3.41 (m, 2H), 2.25 (t, $^{3}J_{HH}$ = 7.1 Hz, 15H), 1.69 (m, 5H), 1.51 (m, 31H), 1.28 (m, 18H). $^{13}$C NMR (101 MHz, DMSO-$d_6$): $\delta$ 172.16 (s, C=O), 161.72 (s, C=O), 153.65 (s, C=O), 137.08 (s, Ar), 135.42 (s, Ar), 128.80 (s, Ar), 118.28 (s, Ar), 63.72 (s, $ArCH_2Ar$), 63.66 (s, $O{=}COCH_2$), 60.34 (s, $OCO\underline{C}H_2CH_2CH_2CH_2$) 63.29 (s, $CH_2CH_2CH_2\underline{C}H_2OH$), 33.34 (s, $CH_2\underline{C}H_2\underline{C}H_2CH_2$), 27.78 (s, $CH_2$), 25.24 (s, $CH_2$), 24.87 (s, $CH_2$), 24.14 (s, $CH_2$). $M_w$ = 16,100 g mol$^{-1}$, $Đ_M$ = 1.82 (RI detection, DMF SEC) FT-IR: $\nu$ (cm$^{-1}$) = 3,300 (N-H), 3,000 (C-H), 1,700 (C=O), 1,600 (N-H), 1,500 (C-H), 1,400 (C=C).

### 7.5.3 General synthesis of aromatic TPUs with hyperbranched fluorinated chain terminating agents

This method was based on the synthesis and analysis of an aromatic TPU with 5% hyperbranched fluorinated chain terminating agents. Molten PCL with a $M_W$ of 2,000 g mol$^{-1}$ (2KPCL, 5.98 g, 2.99 $x$ 10$^{-3}$ mol), BDO (0.86 g, 9.54 $x$ 10$^{-3}$ mol), a 1% solution of Bicat 8106M in PCL (0.02 g, 1.00 $x$ 10$^{-5}$ mol) and DMF (20 mL) were charged and heated at 80 °C until the reaction mixture became a solution. Methylene diphenyl diisocyanate (3.14 g, 0.125 mol) was charged to the mixture and the reaction mixture was heated at 80 °C for 5 h. FT-IR was used to determine the percentage of free isocyanate chain ends (0.2-0.3%) at which point the hyperbranched polymer (0.50 g) was charged in DMF (1 mL). The reaction was heated overnight at 80 °C. The reaction mixture was cooled to room temperature and precipitated in to diethyl ether. The white solid was collected by vacuum filtration and dried in a vacuum desiccator for 1 week. Yield 9.58 g, 96%.

$^{1}$H NMR (300 MHz, DMSO-$d_6$): $\delta$ 9.50 (s, 3H), 7.35 (d, $^{3}J_{HH}$ = 7.2 Hz, 8H), 7.08 (d, $^{3}J_{HH}$ = 7.5 Hz, 8H), 4.44 (t, $^{3}J_{HH}$ = 5.1 Hz, 1H), 4.23 (s, 2H, 5% capped chain ends), 4.09 (m, 5H), 3.97 (t, $^{3}J_{HH}$ = 6.5 Hz, 14H), 3.77 (s, 4H), 3.43 (m, 2H), 2.26 (t, $^{3}J_{HH}$ = 7.1 Hz, 13H), 1.69 (m, 5H), 1.52 (m, 28H), 1.28 (m, 14H). $^{13}$C NMR (101 MHz, DMSO-$d_6$): $\delta$ 172.75 (s, C=O), 153.75 (s, C=O), 137.10 (s, Ar), 135.44 (s, Ar), 128.83 (s, Ar), 118.32 (s, Ar), 63.68 (s, $ArCH_2Ar$), 63.49 (s, $O{=}COCH_2$), 60.27 (s, $OCO\underline{C}H_2CH_2CH_2CH_2$) 60.30 (s, $CH_2CH_2CH_2\underline{C}H_2OH$), 33.36 (s, $CH_2\underline{C}H_2\underline{C}H_2CH_2$), 27.80 (s, $CH_2$), 25.26(s, $CH_2$), 24.89 (s, $CH_2$), 24.09 (s, $CH_2$). $^{19}$F NMR (376 MHz, DMSO-$d_6$): $\delta$ -80.74, -114.15, -123.18, -123.85, -124.58, -127.18. $M_w$ = 22,500 g mol$^{-1}$ $Đ_M$ = 1.82 (RI detection). FT-IR: $\nu$ (cm$^{-1}$) = 3,300 (N-H), 3,000 (C-H), 1,700 (C=O), 1,600 (N-H), 1,500 (C-H), 1,400 (C=C), 1,000 (C-F).

## 7.6 References


1. C. X. Lam, M. M. Savalani, S. H. Teoh and D. W. Hutmacher, *Biomed Mater*, 2008, **3**, 034108.

2. J. J. Stevenson and D. Moye-Sherman, *USA Pat.,* 7,709,639, 2010.

3. Nonappa, K. Ahonen, M. Lahtinen and E. Kolehmainen, *Green Chem.*, 2011, **13**, 1203-1209.

4. D. A. Parrish and L. J. Mathias, *J. Org. Chem.*, 2002, **67**, 1820-1826.

5. M. E. Pierce, G. D. Harris, Q. Islam, L. A. Radesca, L. Storace, R. E. Waltermire, E. Wat, P. K. Jadhav and G. C. Emmett, *J. Org. Chem.*, 1996, **61**, 444-450.

6. H. Bonnard, L. Ferruccio, J.-P. Senet and P.-Y. L. Roy, *USA Pat.,* 6,699,988, 2004.

7. S. Maier, T. Loontjens, B. Scholtens and R. Mülhaupt, *Angew. Chem. Int. Ed.*, 2003, **42**, 5094-5097.

8. F. Xiang, T. Loontjens, E. Geladé and J. Vorenkamp, *Macromol. Chem. Phys.*, 2012, **213**, 1841-1850.

9. F. Xiang, M. Stuart, J. Vorenkamp, S. Roest, H. Timmer-Bosscha, M. C. Stuart, R. Fokkink and T. Loontjens, *Macromolecules*, 2013, **46**, 4418-4425.

10. H. A. Staab, *Liebigs Ann. Chem.*, 1957, **609**, 75-83.

11. H. A. Staab, *Liebigs Ann. Chem.*, 1957, **609**, 83-88.